MICHIGAN STATE UNIVERSITY LIBRARIES
3 1293 00786 8205

LIBRARY
Michigan State
University

This is to certify that the

dissertation entitled

Solvolysis of a Single Lignocellulose Particle by Anhydrous Hydrogen Fluoride Vapor: Reaction Rate Studies, Sugar Yield Studies, and Development of a Detailed Kinetic and Heat Transport Model

presented by

Gregory L. Rorrer

has been accepted towards fulfillment
of the requirements for

Ph.D. degree in Chemical Engineering

Major professor

Date July 7, 1989

MSU is an Affirmative Action/Equal Opportunity Institution

O-12771

PLACE IN RETURN BOX to remove this checkout from your record.
TO AVOID FINES return on or before date due.

DATE DUE	DATE DUE	DATE DUE

MSU Is An Affirmative Action/Equal Opportunity Institution

c:\circ\datedue.pm3-p.1



SOLVOLYSIS OF A SINGLE LIGNOCELLUOSE PARTICLE BY ANHYDROUS HYDROGEN FLUORIDE VAPOR: REACTION RATE STUDIES, SUGAR YIELD STUDIES, AND DEVELOPMENT OF A DETAILED KINETIC AND HEAT TRANSPORT MODEL

VOLUME I

By

Gregory Lawrence Rorrer

A DISSERTATION

Submitted to
Michigan State University
in partial fulfillment of the requirements
for the degree of

DOCTOR OF PHILOSOPHY

Department of Chemical Engineering

1989

ABSTRACT

SOLVOLYSIS OF A SINGLE LIGNOCELLULOSE PARTICLE BY ANHYDROUS HYDROGEN FLUORIDE VAPOR: REACTION RATE STUDIES, SUGAR YIELD STUDIES, AND DEVELOPMENT OF A DETAILED KINETIC HEAT TRANSPORT MODEL

By

Gregory Lawrence Rorrer

The reaction of a single, dry wood chip (Bigtooth Aspen, 15 mg, 1.0 cm/side x 0.4 mm) with anhydrous HF vapor (b.p. 19.54 °C) was studied using two laboratory reactors. The first reactor measured the sugar yield and temperature within the HF-reacting wood chip as a function of time (0 - 20 min), HF-N_2 gas-stream flowrate (0.1 - 0.4 g/cm^2-min), HF partial pressure (P_{HF} = 0 - 1.0 atm), and temperature (T_g = 30 - 90 °C). The second reactor gravimetrically measured the HF vapor adsorption onto a single wood chip.

The equilibrium HF loading increased with increasing P_{HF} and decreased with increasing T_g. At P_{HF} = 1.0 atm, the HF loading was 1.5 g HF/g-wood at 30 °C and 0.4 g HF/g-wood at 60 °C.

The solvolysis of a single wood chip by HF vapor at 1.0 atm was complete within 3 minutes at 30 °C and 6 minutes at 60 °C. The reaction products, sugar fluorides and "reversion" oligosaccharides (water-soluble, D.P. 2 - 10 via HPLC) resided on the intact lignin framework. After mild posthydrolysis of the water-soluble products, the glucose yield averaged 0.52 g/g-wood (85% theoretical), and the xylose yield averaged 0.16 g/g-wood (76%); 3% glucan and 5% xylan remained

in the lignin. Glucose recoveries from prehydrolyzed wood, filter paper, and filter paper/lignin wafers all averaged 94%.

The intrinsic glucose yield vs. time profile was S-shaped, decreased with decreasing HF partial pressure, and decreased with increasing temperature. Adsorbed HF was the limiting reagent; the minimum HF loading was 0.4 g HF/g-wood. The HF-reacting chip temperature rose rapidly (20 °C above T_g within 15 seconds) and then decreased back to T_g within 2 minutes. These data pointed to three adsorption/reaction processes: 1) exothermic physical adsorption of HF vapor onto lignocellulose; 2) solvation of paracrystalline cellulose via displacement of OH...OH hydrogen bonds with HO...HF hydrogen bonds, and 3) cleavage of HF-solvated cellulose chains to glucosyl fluoride.

A detailed kinetic and heat transport model was developed. Predictions for the sugar yield and temperature distribution in the HF-reacting lignocellulose chip as a function of time and HF vapor conditions agreed well with the complimentary experimental data.

Copyright by

GREGORY LAWRENCE RORRER

1989

This dissertation is dedicated to my parents, who instilled in me the importance of education.

ACKNOWLEDGEMENTS

I would like to thank Dr. Martin C. Hawley, my thesis advisor, for the guidance, encouragement, and unwaivering support that he has extended to me over the past five and one-half years. He helped greatly in building my confidence, and provided me with a unique environment for intellectual growth. I would also like to thank Dr. Derek T. A. Lamport of the MSU-DOE Plant Research Laboratory for allowing me to carry out my dissertation research in his laboratory over the past five years. The intellectual stimulation in his laboratory was superb. The days in his laboratory were sometimes trying but never dull. A special thanks goes to my wife Kristin, who always supported me, and even assisted me in finalizing this dissertation.

Finally, I wish to thank the National Science Foundation and the State of Michigan Research Excellence/Economic Development Fund for the Graduate Research Assistantship, and the Union Carbide Corporation for the Graduate Tuition Fellowship.

TABLE OF CONTENTS

List of Tables xi

List of Figures xiv

List of Notation xxii

Chapter 1. General Introduction 1

Chapter 2. Literature Review 5

Introduction 5
I. Liquid-phase HF Solvolysis 6
A. Early Work and Historical Perspective 6
B. Reaction Chemistry, Kinetics, and HF Removal 7
II. Vapor-phase HF Solvolysis 15
A. Early Process Development Studies 17
B. Recent Process Development Studies 18

Chapter 3. Rationale, Objectives, and Scope of Research Program 26

I. Rationale and Problem Definition 26
A. Overview of Vapor-Phase HF Solvolysis of Lignocellulose 26
B. Needed Chemical Reaction Engineering Research 31
II. Research Objectives and Scope 33
A. Overall Research Objectives 33
B. Overview of Research Program and Dissertation 36

Chapter 4. Experimental Design 41

Introduction 41
I. HF Properties and Lignocellulose Substrate Preparation 41
A. Anhydrous Hydrogen Fluoride: Selected Liquid and Vapor properties 41
B. Lignocellulose Sample Preparation, Composition, and Properties 48

II. Vapor-phase HF Solvolysis Experiment 66
A. Vapor-Phase HF Solvolysis Apparatus and Reaction Procedure 67
B. Reaction Product Recovery and Sugar Analysis 85
III. Gravimetric HF Adsorption Experiment 90
IV. Miscellaneous Experimental Design 100

Chapter 5. Preliminary Gravimetric HF Adsorption Experiments 103

Introduction 103
I. HF Adsorption Data and Heat of Adsorption Data for the Vapor-Phase HF Solvolysis of Bigtooth Aspen Wood 104
A. Equilibrium HF Adsorption Isotherms 104
B. Comments on HF Desorption 112
C. Heat of Adsorption 113
D. Comparison to Literature Data 118
II. HF Adsorption/Desorption Data for the Vapor-Phase HF Solvolysis of Prehydrolyzed Wood 120
A. HF Adsorption/Desorption Experiment 122
B. Equilibrium HF Loading vs. 100% HF Vapor Temperature 123
C. HF Desorption 123
III. Pore-Condensation of Nonideal HF Vapor into the Microporous Volume of Wood 130

Chapter 6. Reaction Rate and Sugar Yield Experiments 137

Introduction 137
I. Physical Observations of Wood and Filter Paper Wafers Before and After Reaction with HF Vapor 140
II. Reaction Rate and Sugar Yield Data from the Vapor-Phase HF of Bigtooth Aspen Wood and Pure Cellulose 144
A. Minimization of Mass-Transfer Resistances 144
B. Effect of Gas-Stream HF Partial Pressure on the Glucose Yield vs. Time Profile 149
C. Effect of Gas-Stream Temperature on the Glucose Yield vs. Time Profile 153
D. Effect of 100% HF Vapor Temperature and Equilibrium HF Loading on Maximum Glucose Yield 156
E. Effect of Gas-Stream HF Partial Pressure and Temperature on the Xylose Yield vs. Time Profile 164
III. Reaction Rate and Sugar Yield Data from the Vapor-Phase HF Solvolysis of Prehydrolyzed Wood 168
A. Effect of 100% HF Vapor Stream Flowrate and Temperature on the Glucose Yield vs. Time Profile 170

B. Effect of 100% HF Vapor Temperature and Equilibrium HF Loading on Maximum Glucose Yield 175
C. Comparison of the Rate Processes of Liquid- and Vapor-Phase HF Solvolysis of Lignocellulose 180
IV. Sugar Yield Comparisons and Total Product Recovery Data from the Vapor-Phase HF Solvolysis of Four Lignocelulosic Substrates 181
A. Sugar Yield Comparisons: Water-Soluble Products 181
B. Total Product Recovery Comparisons 184
C. Possible Sources of Sugar Yield Loss 190
V. HF-catalyzed Glucosyl Fluoride Repolymerization and Reversion Oligosaccharide Profiling 204
A. Reversion Chemistry 204
B. HPLC Oligosaccharide Profiling 205
C. Modification of the Oligosaccharide Product Distribution by in situ Methanolysis 218

Chapter 7. Particle Temperature Measurements 226

Introduction 226
I. Experimental Design 227
A. Sampling Probe Modification 227
B. Computer Data Acquisition 232
C. Post-Run Processing of Data 234
D. HF Vapor Stream Temperature Measurement 237
II. Effect of 100% HF Vapor Stream Temperature on the Particle Temperature vs. Time Profile 240
III. Effect of 100% HF Vapor Flowrate on the Particle Temperature vs. Time Profile 245
Recommended Future Studies 246

Chapter 8. Model Development I: Material Balance and Kinetic Model 249

Introduction 249
I. The Lignocellulosic Matrix 250
II. Micrographs of the HF-reacted Lignocellulosic Matrix 255
III. The Intrinsic Adsorption/Reaction Scheme 259
A. Background and Cellulose Hydrolysis Chemistry 259
B. Formulation of the Intrinsic Adsorption/Reaction Scheme 262
IV. Differential Material Balance and Kinetic Model 270
A. Formulation of Rate Equations and Development of the Differential Material Balance and Kinetic Model 270
B. The Simplified Differential Material Balance and Kinetic Model 277

V. Kinetic Parameter Estimation 286
A. Overview 286
B. Final Algorithm 288
C. Final Parameter Estimates 292

Chapter 9. Model Development II: Energy Balance and Heat Transport Model 299

Introduction 299
I. The Modes of Energy Generation and Transport 300
II. Mathematical Formulation of the Differential Energy Balance and Heat Transport Model 302

Chapter 10. Model Predictions and Comparison to Experimental Data 311

Introduction 311
I. Combination of the Differential Material and Energy Balance Equations 312
II. Numerical Solution Procedure 319
III. Model Predictions and Comparison to Experimental Data 321
A. Comparison of Model Predictions to Data over a Limited Range of Process Variables 321
B. A Discussion of the Differences between Model Predictions and Data 331
IV. Extended Model Predictions 334
A. Energy Release 334
B. Nonisothermal Effectiveness Factor 337

Chapter 11. Summary and Conclusions 340

Introduction 340
I. Summary of Major Results and Conclusions 342
II. Significance 350
III. Overview of Suggested Future Work 351

Appendices

A. List of References 355
B. HF Saccharification Bibliography 366
C. HF Safety 371
D. Computer Programs 376

LIST OF TABLES

3.1.	Process advantages and disadvantages of the vapor-phase HF solvolysis of lignocellulose.	30
3.2.	Summary of experimental research program.	35
4.1.	Selected anhydrous HF liquid properties.	43
4.2.	Selected anhydrous, 100% HF vapor properties at 1.0 atm.	45
4.3.	Detailed composition of Trembling Aspen wood.	50
4.4.	Estimated composition of Bigtooth Aspen wood.	51
4.5.	Estimated composition of prehydrolyzed Bigtooth Aspen wood.	57
4.6.	Volumetric properties of dry Bigtooth Aspen wood and dry prehydrolyzed Bigtooth Aspen wood (literature and estimated).	64
4.7.	Selected thermal properties of dry Aspen wood and dry prehydrolyzed aspen wood.	65
4.8.	Range of reactor conditions for the vapor-phase HF. solvolysis apparatus.	76
4.9.	Typical retention times and response factors for monosaccharide analysis via HPLC.	91
5.1.	Summary of the estimated contributions to the total HF loading on Bigtooth Aspen wood by 100% HF vapor at 30 °C and 1.0 atm.	110

5.2. Calculated heat of adsorption, $\Delta H_A(\theta_e)$, vs. equilibrium HF loading (θ_e) for the adsorption of HF vapor onto dry Bigtooth Aspen wood. 116

5.3. Equilibrium HF loading (θ_e) vs. 100% HF vapor stream temperature (T_g) at 1.0 atm for the vapor-phase HF solvolysis of prehydrolyzed wood (see Figure 5.8). 126

6.1. Summary of maximum average glucose and xylose yields obtained from the vapor-phase HF solvolysis of Bigtooth Aspen wood as a function of 100% HF vapor temperature (T_g) at 1.0 atm and equilibrium HF loading (θ_e) (water-soluble products after posthydrolysis); see Figure 6.7. 158

6.2. Summary of maximum average glucose yields obtained from the vapor-phase HF solvolysis of filter paper as a function of 100% HF vapor temperature (T_g) at 1.0 atm (after posthydrolysis of water-soluble products). 159

6.3. Summary of maximum average glucose yields obtained from the vapor-phase HF solvolysis of prehydrolyzed wood as function of 100% HF vapor temperature (T_g) at 1.0 atm and equilibrium HF loading (θ_e) at 1.0 atm (after posthydrolysis of water-soluble products); see Figure 6.14. 178

6.4. Comparison of maximum average glucose yields obtained from the solvolysis of Bigtooth Aspen wood, prehydrolyzed Bigtooth Aspen wood, filter paper, and filter paper/"milled-wood" lignin (MWL) composite wafers by an anhydrous HF vapor stream at 30-31 °C and 1.0 atm (after posthydrolysis of water-soluble products). 182

6.5. Comparison of the maximum average glucose and xylose yields obtained from the liquid-phase and vapor-phase HF solvolysis of Bigtooth Aspen wood (after posthydrolysis of water-soluble products). 185

6.6. Comparison of total average measured product recoveries obtained from solvolysis of Bigtooth Aspen wood, prehydrolyzed Bigtooth Aspen wood, filter paper, and filter paper/"milled-wood" lignin (MWL) composite wafers by an anhydrous HF vapor stream at 30-31 °C and 1.0 atm (after posthydrolysis of water-soluble products). 186

6.7.

6.8.

6.9.

6.10.

8.1.

10.1.

10.2.

10.3.

10.4.

C.1.

6.7. Total product recovery from Bigtooth Aspen wood: vapor-phase HF solvolysis (dry and methanol-absorbed wood) vs. two-step sulfuric acid hydrolysis. 189

6.8. Composition of the water-insoluble solid residue obtained from the solvolysis of Bigtooth Aspen wood by 100% HF vapor at 1.0 atm, 30-31 °C. 201

6.9. Incremental improvement of maximum average glucose and xylose yield from the vapor-phase HF solvolysis of Bigtooth Aspen wood. 203

6.10. Glucose yields before and after posthydrolysis of the water-soluble reaction products obtained from the solvolysis of dry, prehdyrolyzed wood by a 100% HF vapor stream at 1.0 atm and temperatures of 31 °C, 41 °C, and 52 °C. See also Figures 6.21 to 6.23. 217

8.1. Estimation of kinetic parameters posed by the differential material balance and kinetic model (nonisothermal method). 293

10.1. Range of process parameters selected for comparison of model to data. 322

10.2. Physical property input data for combined material and energy balance model. 323

10.3. Kinetic and adsorption parameters for combined material and energy balance model. 324

10.4. Model calculations for cumulative heat release. 336

C-1. HF toxicity. 371

LIST OF FIGURES

2.1.	Defaye's (1983) mechanism for the HF-solvolysis of cellulose.	9
3.1.	Vapor-phase HF solvolysis of lignocellulose: basic concept.	27
3.2.	Vapor-phase HF solvolysis of lignocellulose: process concept for wood-to-ethanol via HF vapor.	28
3.3.	Vapor-phase HF solvolysis of a single lignocellulose wafer: four basic features.	34
4.1.	Thermal conductivity (k_g) of nonideal HF vapor as a function of temperature (T_g) and HF partial pressure.	47
4.2.	Photographs of the four types of lignocellulosic wafers used in this study: Bigtooth Aspen wood, prehydrolyzed Bigtooth Aspen wood, pure cellulose (filter paper), and the filter paper/"milled-wood" lignin composite.	49
4.3.	Schematics of the cellulose and hemicellulose polymer chains.	52
4.4.	Sugars from hardwood hemicellulose.	53
4.5.	Xylose yield vs. time profile for Bigtooth Aspen wood prehydrolysis in 2 N trifluoroacetic acid (TFA) at 100 °C.	55
4.6.	UV spectrum of "milled-wood" lignin (MWL) isolated from Bigtooth Aspen wood.	60
4.7.	Vapor-phase HF solvolysis apparatus: flow diagram.	68
4.8.	Calibration of the Monel mass-flow transducer/controller (Matheson model 8205, HF-MFC) for HF vapor flow.	69

4.9. Vapor-phase HF solvolysis apparatus: reactor detail (front cross-sectional view). 70

4.10. Vapor-phase HF solvolysis apparatus: reactor and sampling mechanism detail (side cross-sectional view). 71

4.11. Vapor-phase HF solvolysis apparatus: photographs of sampling mechanism operation (top view). 72

4.11. (cont'd.). 73

4.11. (cont'd.). 74

4.12. Flowsheet: vapor-phase HF solvolysis and product recovery protocol. 75

4.13. Schematic of the High-Performance Liquid Chromatograph (HPLC) for carbohydrate analysis. 88

4.14. HPLC chromatogram of the water-soluble sugar products (after posthydrolysis) obtained from the vapor-phase HF solvolysis of Bigtooth Aspen wood. 92

4.15. HPLC chromatogram of the water-soluble sugar products (after posthydrolysis) obtained from the vapor-phase HF solvolysis of prehydrolyzed Bigtooth Aspen wood. 93

4.16. HPLC chromatogram of the water-soluble sugar products (after posthydrolysis) obtained from the vapor-phase HF solvolysis of pure cellulose (filter paper). 94

4.17. Gravimetric HF adsorption apparatus: (a) flow diagram; (b) reactor detail. 95

5.1a. Equilibrium HF adsorption isotherms on dry Bigtooth Aspen wood: T_g = 30 °C, 40 °C, 50 °C. 106

5.1b. Equilibrium HF adsorption isotherms on dry Bigtooth Aspen wood: T_g = 60 °C, 70 °C, 80 °C. 107

5.2. Clausius-Clapeyron plots ($\log_{10}P_{HF}$ vs. $1/T_g$) at fixed HF loading (θ_e). 114

5.3. Heat of adsorption, $-\Delta H_A(\theta_e)$, vs. HF loading (θ_e). 117

5.4. Literature comparison: equilibrium HF sorption isotherms on prehydrolyzed spruce wood at 30 °C, 40 °C, 60 °C, and 70 °C. Data of Franz et al. (1987). 119

5.5. Literature comparison: heat of desorption from HF-adsorbed, prehydrolyzed spruce wood. Data of Franz et al. (1987). 121

5.6. HF adsorption/desorption data for the solvolysis of a single prehydrolyzed wood chip by a 100% HF vapor stream at 1.0 atm. (a) HF adsorption/desorption profile, $\theta_{HF}(t)$; (b) 100% HF vapor stream temperature vs. time profile, $T_g(t)$, used to set the HF adsorption/desorption profile. 124

5.7. HF adsorption vs. reaction time profile, $\theta_{HF}(t)$, for the solvolysis of a single prehydrolyzed wood chip by an anhydrous, 100% HF vapor stream at T_g = 31 °C and 1.0 atm. 125

5.8. Equilibrium HF loading on prehydrolyzed wood (θ_e) vs. 100% HF vapor stream temperature (T_g). 127

5.9. Selected HF desorption profiles: (a) 100% HF vapor stream temperature vs. time profile, $T_g(t)$, used to set the HF desorption profile; (b) HF loading vs. desorption time profile, $\theta_{HF}(t)$, set by $T_g(t)$. 129

5.10. Maximum micropore radius (r_k) for capillary condensation of nonideal HF vapor: effect of nonideal HF vapor partial pressure (P_{HF}) and temperature (T_g). 135

6.1. Photographs of single lignocellulose wafers before and after reaction with HF vapor. 141

6.1. **(cont'd.).** 142

6.2. Vapor-phase HF solvolysis of a single Bigtooth Aspen wood chip (2L = 0.4 mm): effect of 100% HF vapor velocity (G_{HF}, g HF/cm^2-min) on the glucose production rate. 146

6.3. Vapor-phase HF solvolysis of a single Bigtooth Aspen wood chip: effect of chip thickness (2L = 0.4 mm vs. 0.2 mm) on the glucose yield vs. time profile at G = 0.3 g/cm^2-min. 148

6.4. Vapor-phase HF solvolysis of a single Bigtooth Aspen wood chip (2L = 0.4 mm): effect of gas-phase HF mole fraction, y_{HF} on the glucose yield vs. time profile at 1.0 atm and T_g = 30 °C. 150

6.5. Vapor-phase HF solvolysis of a single Bigtooth Aspen wood chip (2L = 0.4 mm): effect of 100% HF vapor stream temperature (T_g) on the glucose yield vs. time profile. (a) 30 °C, 40 °C, 50 °C; (b) 67 °C, 80 °C. 154

6.6. Vapor-phase HF solvolysis of a single, pure cellulose wafer (Whatman filter paper No. 3): effect of 100% HF vapor stream temperature on the glucose yield vs. time profile (T_g = 27 °C, 50 °C, 77 °C). 155

6.7. Vapor-phase HF solvolysis of Bigtooth Aspen wood: effect of 100% HF vapor temperature (T_g) on the maximum average glucose yield obtained from the water-soluble products (after posthydrolysis). 157

6.8. Vapor-phase HF solvolysis of a single Bigtooth Aspen wood chip (2L = 0.4 mm): effect of HF-N_2 gas-stream temperature (T_g) on the glucose yield vs. time profile at a reduced mole fraction of HF in the gas phase (y_{HF} = 0.64, P_{HF} = 0.64 atm). 163

6.9. Vapor-phase HF solvolysis of a single Bigtooth Aspen wood chip (2L = 0.4 mm): effect of gas-stream HF mole fraction, y_{HF} (or HF partial pressure, P_{HF}) on the xylose yield vs. time profile at T_g = 30 °C. 165

6.10. Vapor-phase HF solvolysis of a single Bigtooth Aspen wood chip (2L = 0.4 mm): effect of 100% HF vapor stream temperature (T_g) on the xylose yield vs. time profile. (a) 30 °C, 40 °C, 50 °C; (b) 67 °C, 80 °C. 167

6.11. Vapor-phase HF solvolysis of a single prehydrolyzed wood chip (2L = 0.4 mm): effect of 100% HF vapor stream flowrate on the glucose production rate at T_g = 31 °C. 171

6.12. Vapor-phase HF solvolysis of a single prehydrolyzed wood chip (2L = 0.4 mm): effect of 100% HF vapor stream flowrate on the glucose yield vs. time profile at T_g = 31 °C. 172

6.13a. Vapor-phase HF solvolysis of a single prehydrolyzed wood chip (2L = 0.4 mm): effect of 100% HF vapor stream temperature (T_g) on the glucose yield vs. time profile (T_g = 31 °C, 52 °C, 68 °C). 173

6.13b. Vapor-phase HF solvolysis of a single prehydrolyzed wood chip (2L = 0.4 mm): effect of 100% HF vapor stream temperature (T_g) on the glucose yield vs. time profile (T_g = 41 °C, 60 °C). 174

6.14. Vapor-phase HF solvolysis of prehydrolyzed wood: effect of 100% HF vapor temperature (T_g) on the maximum average glucose yield attainable from the water-soluble products (after posthydrolysis). 176

6.15. Vapor-phase HF solvolysis of prehydrolyzed wood: effect of equilibrium HF loading (θ_e) on the maximum average glucose yield obtained from the water-soluble reaction products (after posthydrolysis). 177

6.16. Vapor-phase HF solvolysis of a single prehydrolyzed wood chip (2L = 0.4 mm): glucan, xylan, solid residue, and total product recovery as a function of reaction time. 187

6.17. Hypothetical mechanism for HF-catalyzed, Friedel-Crafts alkylation of glucosyl fluoride onto lignin. 194

6.18. Comparison of glucose yield vs. time profiles obtained from the solvolysis of a single pure cellulose (filter paper) wafer and a single pure cellulose/"milled-wood" lignin (MWL) composite wafer by a 100% HF vapor stream at T_g = 30-31 °C. 197

6.19. In situ reactions of glucosyl fluoride in HF. 206

6.20. Solvolysis of a single, dry, pure cellulose wafer (Whatman filter paper No. 3) by a 100% HF vapor stream at T_g = 30 °C: HPLC-oligosaccharide profiles before posthydrolysis as a function of reaction time. 208

6.20. (cont'd.). 209

6.21. Solvolysis of a single, dry, prehydrolyzed wood chip (2L = 0.4 mm) by a 100% HF vapor stream at T_g = 31 °C: HPLC oligosaccharide profiles before posthydrolysis as a function of reaction time. 212

6.22. Solvolysis of a single, dry, prehydrolyzed wood chip (2L = 0.4 mm) by a 100% HF vapor stream at T_g = 41 °C: HPLC oligosaccharide profiles before posthydrolysis as a function of reaction time. 213

6.23. Solvolysis of a single, dry, prehydrolyzed wood chip (2L = 0.4 mm) by a 100% HF vapor stream at T_g = 52 °C: HPLC oligosaccharide profiles before posthydrolysis as a function of reaction time. 214

6.24. Solvolysis of a single, methanol-absorbed pure cellulose wafer by a 100% HF vapor stream at T_g = 30 °C: HPLC oligosaccharide profiles before posthydrolysis as a function of reaction time. 220

6.24. **(cont'd.).** 221

6.25. Comparison of HPLC-oligosaccharide profiles obtained from the vapor-phase HF solvolysis of pure cellulose and methanol-absorbed pure cellulose (see Figures 6.20 and 6.24). 223

6.26. Solvolysis of a single, dry cellulose (filter paper) wafer and a single, methanol-absorbed filter paper wafer by a 100% HF vapor stream at T_g = 30 °C: comparison of the glucose (glucose + 1-O-methyl glucose) yields before posthydrolysis as a function of reaction time. 224

7.1. Modification of the Teflon sampling probe for particle temperature measurement studies. 228

7.2. The thermocouple microprobe/wood chip assembly. 231

7.3. Retrofitted computer data acquisition system for particle temperature measurement. 233

7.4. Processing of the raw particle temperature vs. time data file. 235

7.5. Calibration of the computer data acquisition system for linear voltage offset. 238

7.6. Correction and smoothing of the particle temperature vs. reaction time profile. 239

7.7. 100% HF vapor stream temperature (T_g) vs. reaction time (t). 241

7.8. Vapor-phase HF solvolysis of a single prehydrolyzed wood chip (L = 0.4 mm): effect of 100% HF vapor stream temperature (T_g) on the centerline particle temperature vs. reaction time profile. 243

7.9. Vapor-phase HF solvolysis of a single prehydrolyzed wood chip (L = 0.4 mm): effect of 100% HF vapor stream flowrate on the center particle temperature vs. time profile at T_g = 31 °C. 247

8.1. Schematics of: (a) a single wood wafer aligned perpendicular to the HF vapor stream; (b) the lignocellulosic matrix cross-section. 251

8.2. Exploded view of the secondary cell wall of the lignocellulosic matrix of wood. 253

8.3. Lignocelluose composite microstructure. 254

8.4. Two-dimensional schematic of the hydrogen-bonding network within the crystalline cellulose microfibril. 256

8.5. Light microphotographs (200 x) of the lignocellulosic matrix cross-section before and after reaction with HF vapor. 257

8.5. **(cont'd.).** 258

8.6. Schematic representation of the sequential adsorption and reaction processes presumed to occur during the vapor-phase HF solvolysis of crystalline cellulose. 263

8.7. Summary of the intrinsic adsorption/reaction scheme proposed for the vapor-phase HF solvolysis of crystalline cellulose. 265

8.8. Composite illustration of the adsorption and reaction processes proposed to occur during the vapor-phase HF solvolysis of the cellulose microfibril. 268

8.9. Fraction of glucan units completely HF-complexed, $(1 - Z_1)$, as a function of the total fraction of -OH groups on glucan HF-complexed, $f(1 - Z_1)$. 283

8.10. Parameter estimation scheme 1: minimization of the sum of squared residuals, s_1^2 (see Table 8.1). (a) s_1^2 vs. k_{1o}; (b) k_{1o} vs. E_1. 295

8.11.

8.12.

10.1.

10.2.

10.3.

10.4.

10.5.

8.11. Parameter estimation scheme 2: minimization of the sum of squared residuals, s_2^2 (see Table 8.1). (a) s_2^2 vs. k_{2o}; (b) k_{2o} vs. E_2. 296

8.12. Least-squares fit of glucose yield vs. time data to parameter estimation scheme 2 (see kinetic parameter estimates in Table 8.1). 297

10.1. Particle temperature vs. reaction time profiles for the solvolysis of a single prehydrolyzed wood (lignocellulose) chip by a 100% HF vapor stream at 1.0 atm: data and model predictions compared. (a) T_g = 52 °C; (b) T_g = 60 °C; (c) T_g = 68 °C. 326

10.2. Global glucose yield vs. reaction time profiles, $Y_g(t)$ vs. t, for the solvolysis of a single prehydrolyzed wood (lignocellulose) chip by a 100% HF vapor stream at 1.0 atm: data and model predictions compared. (a) T_g = 52 °C; (b) T_g = 60 °C; (c) T_g = 68 °C. 327

10.3. Model predictions for global gravimetric uptake of HF vapor onto a single, HF-reacting lignocellulose chip (2L = 0.4 mm), $\theta_{HF}(t)$, as a function of reaction time and 100% HF vapor temperature, T_g, at 1.0 atm. 328

10.4. Thermal properties of the HF-reacting prehydrolyzed wood chip: model predictions for (a) the effective thermal conductivity, $k_e(L,t)$, and (b) the effective thermal diffusivity, $\alpha_e(L,t)$, at the chip centerline (2L = 0.4 mm). 330

10.5. Model predictions for the nonisothermal effectiveness factor, $\eta(t)$, in the HF-reacting lignocellulose chip (2L = 0.4 mm) as a function of reaction time (t) and 100% HF vapor stream temperature (T_g). 338

LIST OF NOTATION

a	empirical constant in equation [5-4]
A_I	chromatographic peak area for internal standard; see equation [4-14] (μV-sec)
A_s	chromatographic peak area for a given sugar; see equation [4-14] (μV-sec)
a_o	empirical constant in equation [5-6]
a_1	empirical constant in equation [5-6]
a_2	empirical constant in equation [5-6]
a_3	empirical constant in equation [5-6]
A_x	cross-sectional area of reactor (cm^2)
b_o	empirical constant in equation [8-47]
b_1	empirical constant in equation [8-47]
b_2	empirical constant in equation [8-47]
b_3	empirical constant in equation [8-47]
C	conversion factor; see equation [4-14]
$C_{p,g}$	heat capacity of 100% HF vapor (cal/g ^oC)
$C_{p,G3}$	heat capacity of glucosyl fluoride/lignin reaction product (no adsorbed HF; cal/g ^oC)
$C_{p,HF,ads}$	heat capacity of adsorbed HF (cal/g ^oC)
$C_{p,HF,l}$	heat capacity of anhydrous liquid HF (cal/g ^oC)

$C_{p,LC}$	heat capacity of dry lignocellulose (cal/g °C)
E_u	internal energy of the HF-reacting lignocellulose wafer (cal/g)
E_1	activation energy for k_1 (kcal/mol)
E_2	activation energy for k_2 (kcal/mol)
f	association factor for HF vapor; see equation [5-8]
F_{HF}	molar flowrate of HF vapor; see equation [4-10b] (mol HF/min)
F_{MFC}	flowrate of HF vapor as measured by the mass-flow controller; see equation [4-10a]
F_{N2}	molar flowrate of N_2 gas (mol N_2/min)
G	superfacial mass velocity of HF-N_2 gas stream (g/cm^2-min)
G_{HF}	superfacial mass velocity of 100% HF vapor stream; see equation [4-11] (g HF/cm^2-min)
$[G_o]$	total concentration of glucan in the lignocellulosic matrix; see equation [8-17] (mol glucan/g-lignocellulose)
$[G_o']$	maximum theoretical glucose yield as a function of θ_e; see equation [6-5a] and [6-6] (mol glucose/g-lignocellulose)
$[G_1]$	concentration of glucan in crystalline cellulose within the HF-reacting lignocellulosic matrix; see equation [8-18] (mol/g-lignocellulose)
$[G_2]$	concentration of completely HF-complexed glucan units; see equation [8-19] (mol/g-lignocellulose)
$[G_{3\text{-}F}]$	concentration of glucosyl fluoride or solvolytically-cleaved ß-1,4-O-glycosidic linkages (mol/g-lignocellulose)
h	film heat transfer coefficient for the convection from the HF-reacting lignocellulose particle surface to the surrounding HF vapor stream (cal/cm^2-sec °C)
H_o	empirical constant in equation [5-4] (205 cal/g-HF adsorbed)

$\Delta H_A(\theta_e)$ enthalpy (heat) of the adsorption of HF vapor onto lignocellulose as a function of θ_e (cal/g HF adsorbed)

$\Delta H_{HF,1-6}$ enthalpy of formation of the vapor-phase, hydrogen-bonded HF hexamer (cal/mol H-bond formed)

$\Delta H_R(T)$ enthalpy of reaction for solvolytic cleavage of the ß-1,4-O-glycosidic linkage of a completely HF-complexed glucan unit (cal/mol glucan)

$\Delta H_v(T)$ enthalpy of vaporization of HF liquid (cal/g HF)

k_e effective thermal conductivity of the HF-reacting lignocellulose chip; see equation [9-13] (cal/cm-sec °C)

k_g thermal conductivity of 100% HF vapor (cal/cm-sec °C)

$k_{HF,ads}$ thermal conductivity of adsorbed HF (cal/cm-sec °C)

$k_{HF,l}$ thermal conductivity of liquid HF (cal/cm-sec °C)

k_{LC} thermal conductivity of lignocellulose; see equation [4-9] (cal/cm-sec °C)

k_s thermal conductivity of the solid phase of the HF-reacting lignocelllulose chip; see equation [9-11] (cal/cm-sec °C)

k_1 rate constant for the disruption of OH...OH hydrogen bonds in crystalline cellulose by stronger HO...HF hydrogen bonds (g/g-sec)

k_{1o} k_1 evaluated at reference temperature T_o (g/g-sec)

k_2 rate constant for solvolytic cleavage of the ß-1,4-O-glycosidic linkage of a completely HF-complexed glucan unit (g/g-sec)

k_{2o} k_2 evaluated at reference temperature T_o (g/g/-sec)

K_1 adsorption constant for monolayer adsorption of HF onto -OH groups on glucan; $K_1 = k_{a1}/k_{d1}$

K_2 adsorption constant for monolayer adsorption of HF onto -O- linkages in glucan; $K_2 = k_{a2}/k_{d2}$

K equilibrium constant for vapor-phase HF monomer/hexamer equilibrium; see equations [5-9] and [5-10a]

$K_{t,s}$	posthydrolysis loss-correction factor; see equation [4-13]
L	half-thickness of lignocellulose wafer (cm or mm; typically 0.2 mm)
m	moisture content of lignocellulose (mg water/mg dry lignocellulose)
m_{FP}	mass of dried filter paper (mg)
$m_{HF,g}$	mass flowrate of HF vapor (g HF/min)
m_{LC}	mass of dried lignocellulose (mg)
m_{MWL}	mass of dry milled-wood lignin (mg)
M_w	molecular weight (g/mol)
$M_{w,HF}$	molecular weight of the HF monomer (20.01 g/mol)
[MWL]	concentration of "milled-wood" lignin in the "milled-wood" lignin/filter paper composite wafer (g MWL/g composite)
n	number of trials
Nu	Nusselt number for film heat transfer from HF-reacting lignocellulose chip surface to the surrounding HF vapor stream; see equations [9-17] and [9-20]
P_{HF}	HF partial pressure of HF-N_2 gas stream if all HF molecules are monomeric (atm)
P'_{HF}	HF partial pressure of nonideal HF vapor (atm)
$P^{\bullet}_{HF}$	HF vapor pressure; see equation [4-1] (atm)
$P_{HF,1}$	partial pressure of monomeric HF in the nonideal, hydrogen-bonded, oligomeric HF vapor mixture (atm)
$P_{HF,6}$	partial pressure of the hydrogen-bonded HF hexamer in the nonideal, oligomeric HF mixture (atm)
Pr	Prandtl number for a 100% HF vapor stream; see [9-19]
P_T	total system pressure in reactor; always 1.0 atm

$q(t)$	rate of heat release from the HF-reacting lignocellulose chip to the surrounding HF vapor stream; see equation [10-26] (cal/g-wood sec)
$Q(t)$	cumulative heat release from the HF-reacting lignocellulose chip to the surrounding HF vapor stream; see equation [10-27] (cal/g-wood)
Q_{iso}	total isothermal heat release from the HF-reacting lignocellulose chip (cal/g-wood)
r_k	maximum micropore for capillary condensation; see equation [5-7] (A)
R	thermodynamic gas constant (1.987 cal/mol or 0.08206 L-atm/mol K)
Re	Reynold's number for HF vapor flowing over a single lignocellulose chip; see equations [6-1] and [9-18]
$R_{F,I}$	detector response factor for the internal standard; see equation [4-14] (μV-sec/μmol)
$R_{F,s}$	detector response factor for a given sugar; see equation [4-14] (μV-sec/μmol)
s_1^2	sum of squared residuals for parameter estimation scheme 1; see equation [8-59]
s_2^2	summ of squared residual for parameter estimation scheme 2; see equation [8-63]
$[S_o]$	total concentration of -OH group HF-adsorption sites; see equation [8-6]
$[S_t]$	total concentration of -OH group and -O- linkage HF-adsorption sites on glucan; see equation [8-9]
$[S_1]$	concentration of -OH group HF-adsorption sites on glucan not yet complexed with HF; see equation [8-7]
$[S_2]$	concentration of -OH group HF-adsorption sites on glucan complexed with HF
$[S_3]$	concentration of HF-adsorbed -O- linkages in glucan; see equation [8-8]
t	reaction time (min or sec)

T	particle temperature of the HF-reacting lignocellulose chip (^oC)
T_g	HF-N_2 gas stream temperature (^oC)
$v_{HF,l}$	molar volume of HF liquid (cm^3/mol HF)
$\hat{V}_g$	molar volume of HF vapor (L/mol HF)
V_p	total void volume of lignocellulose (cm^3/g)
$V_{p,\mu}(r)$	cumulative microvoid pore volume at micropore radius r (cm^3/g)
w_{HF}	weight fraction of adsorbed HF on the HF-adsorbed/reacted lignocellulose chip
w_I	mass of internal standard in the reaction-quench vial (mg)
w_o	mass of dry lignocellulose sample before reaction (mg)
w_s	mass of lignocellulose sample plus adsorbed HF (mg)
x	distance along the thickness axis of the lignocellulose chip (cm)
X_1	normalized $[G_1]$; $X_1 = [G_1]/[G_o]$
X_2	normalized $[G_2]$; $X_2 = [G_2]/[G_o]$
X_3	normalized $[G_3]$; $X_2 = [G_3]/[G_o]$
$[X_o]$	maximum theoretical xylose yield as a function of θ_e; see equation [6-5b] and [(mol xylose/g-wood)
y_{HF}	mole fraction of HF in the HF-N_2 gas stream; see equation [6-2]
Y_o	stoichiometry factor when adsorbed HF is the limiting reagent; see equation [10-16]
Y_s	sugar yield in the water-soluble reaction products after posthydrolysis; see equation [4-14] (e.g. g sugar/g-wood)
Y_g	glucose yield (g glucose/g-lignocellulose, or mol glucose/g-lignocellulose)
$Y_{g,ex}$	normalized glucose yield obtained by experiment using $Y_{g,max}$

$Y_{g,max}$ maximum average glucose yield obtained by experiment (g glucose/g-lignocellulose)

Y_x glucose yield (g xylose/g-lignocellulose, or mol xylose/g-lignocellulose)

z face length of lignocellulose wafer (typically 1.0 cm)

Z_1 normalized $[S_1]$; $Z_1 = [S_1]/[S_o]$

Z_2 normalized $[S_2]$; $Z_2 = [S_2]/[S_o]$

Greek:

α_e effective thermal diffusivity of the HF-reacting lignocellulose chip (cm^2/sec)

χ_{HF} fugasity coefficient for nonideal HF vapor; see equation [5-15]

χ_{HF}^* fugasity coefficient for nonideal, saturated HF vapor

ϵ void fraction of lignocellulose; see equation [4-6]

$\gamma_{HF,l}$ surface tension of liquid HF; see equation [4-3] (dyne/cm)

$\eta_1(t)$ nonisothermal effectiveness factor for glucosyl fluoride production; see equation [10-29]

$\eta_2(t)$ nonisothermal effectiveness factor for gravimetric HF uptake; see equation [10-30]

θ expermentally determined HF loading; see equation [4-15] (g HF adsorbed/g-lignocellulose)

θ_e equilibrium HF loading (g HF adsorbed/g-lignocellulose)

$\theta_{e,p-c}$ equilibrium HF loading due to capillary condensation in cell wall microvoids; see equation [5-16] (g HF/g-lignocellulose)

θ_{min} minimum HF loading for complete solvolysis of cellulose; see equations [6-4] and [6-7] (g HF/g-lignocellulose)

$\theta_{HF}(t)$ gravimetric uptake of HF vapor onto lignocellulose; see equations [8-50] and [8-51] (g HF adsorbed/g-lignocellulose)

θ_1	fractional coverage of HF-adsorbed -OH sites on glucan; see equation [8-16]
θ_2	fractional coverage of HF-adsorbed -O- sites on glucan; see equation [8-29]
μ_g	100% HF vapor viscosity (g/cm-sec)
$\rho_{HF,l}$	density of anhydrous HF liquid; see equation [4-2] (g/cm^3)
$\rho_{HF,g}$	density of HF vapor; see equation [4-4b] (g/L)
ρ_{LC}	bulk density of lignocellulose (g/cm^3)
ρ_{LC}'	density of the lignocellulose solid; no void (g/cm^3)

Abbreviations:

D.P.	degree of polymerization
GC/MS	gas chromatography/mass spectrometry
HF	anhydrous Hydrogen Fluoride
HMF	5-hydroxymethyl-2-furfuraldehyde
HPLC	high-performance liquid chromatography
MWL	milled-wood lignin
slpm	standard liters per minute
TFA	trifluoroacetic acid

Chapter 1. General Introduction

I. Chemicals from Biomass

The steadily-decreasing supply of nonrenewable petroleum resources provides an incentive for chemical engineers to develop efficient processes to produce useful chemicals and liquid fuels from renewable natural resources. Lignocellulosic biomass, e.g. wood or agricultural residues, is an abundant, low-value, renewable raw material which can serve as a chemical feedstock for the production of useful chemicals and liquid fuels. Lignocellulose is actually a biopolymer composite of three chemical raw materials: cellulose, a glucan polymer (50%); hemicellulose, a polymer of pentose sugars (25%); and lignin, a phenylpropanoid polymer (25%).

Processes for the production of useful chemicals and fuels from lignocellulose generally fall into two categories: thermochemical and biochemical. Thermochemical processes pyrolyze, gasify, or liquefy lignocellulose to synthesis gas, light hydrocarbons, char, levoglucosan-rich tars, or deoxygenated oils, depending on processing conditions. These intermediate products can then be catalytically upgraded to methanol (from synthesis gas) or hydrocarbon-based chemicals and fuels. Biochemical processes hydrolyze the cellulose and hemicellulose fractions to glucose and xylose, and then ferment the sugars to useful chemical products, including, alcohols, ketones, and organic acids.

II. Lignocellulose Hydrolysis Processes

A fairly selective route for converting lignocellulose to useful chemical products is hydrolysis of the cellulose fraction to glucose, followed by the fermentation of glucose to (for example) ethanol. The residual lignin can also be processed, depending on the quality of the lignin, to a spectrum of useful chemicals, including phenols or adhesives for wood-based composite materials (Hawley et al., 1986).

At the present time, the production of useful chemicals and liquid fuels from lignocellulose by hydrolysis and fermentation is not economically attractive. The major reason is the inefficiency of the cellulose hydrolysis step.

In general, enzyme-catalyzed and mineral-acid catalyzed and cellulose hydrolysis processes are inefficient in one or more respects (Hawley et al., 1983). In enzymatic processes, cellulose is usually hydrolyzed to cellobiose by cellulase, which is in turn hydrolyzed to glucose to ß-glucosidase (e.g. from Trichoderma reesei). Enzyme-catalyzed lignocellulose hydrolysis processes require a cumbersome enzyme production system, extensive lignocellulose pretreatment to open up the pore structure for enzyme diffusion, long reaction/residence times, and a dilute aqueous reaction media. Enzymatic processes also suffer from low glucose yields (without pretreatment) and low enzyme recovery, but offer a reactive lignin byproduct. Dilute-acid cellulose hydrolysis processes require only small amounts of acid catalyst, but operate at high reaction temperatures (e.g. 230 °C), and thus suffer from low glucose yields (about 50%) due to acid-catalyzed dehydration of the glucose product to hydroxymethylfurfural (HMF) at these high temperatures. Concentrated-acid

cellulose hydrolysis processes operate at near-ambient reaction temperatures and offer a concentrated reaction system and high glucose yields, but suffer from high acid consumption, difficult acid recovery, and a condensed lignin byproduct.

To summarize, enzymatically-catalyzed and mineral-acid catalyzed cellulose hydrolysis processes lack the high glucose yields, efficient processing conditions, and low catalyst consumption necessary for economically-attractive, large-scale processing of lignocellulose to fermentable sugars and residual lignin.

The process technology for cellulose hydrolysis must improve significantly before the production of fermentable sugars and residual lignin from lignocellulosic biomass can be economically viable. For concentrated acid-hydrolysis processes in particular, the two major requirements for efficient lignocellulose hydrolysis are 1) high yields of fermentable sugars under favorable hydrolysis conditions, and 2) simple, efficient, and near 100% recovery and recycle of the acid catalyst in concentrated form.

This dissertation focuses on a chemical reaction engineering analysis of the solvolysis of lignocellulose by anhydrous Hydrogen Fluoride (HF) vapor, a novel and potentially efficient concentrated-acid process. The vapor-phase HF solvolysis of lignocellulose offers both high glucose yields and efficient HF recovery/recycle and thus may satisfy the two basic criteria for an efficient concentrated-acid process. However, despite these advantages, the technology for the vapor-phase HF solvolysis of lignocellulose is not well developed, especially when compared to the more well-established enzyme-catalyzed and mineral-acid catalyzed lignocellulose

hydrolysis processes.

In chapter 2, the available literature for both the liquid- and vapor-phase HF solvolysis of lignocellulose is summarized and reviewed. In chapter 3, the rationale, scope and objectives for the research program contained in this dissertation are defined. Also in chapter 3, the research program described in chapters 4 to 10 is overviewed.

Chapter 2. Literature Review

Introduction

In general, the HF-solvolysis of lignocellulose is not as well-studied as enzyme and mineral-acid catalyzed lignocellulose hydrolysis processes. However, the available body of literature on the HF-solvolysis of lignocellulose has grown steadily, especially since the oil crisis of the late 1970's, when this process was reconsidered as a technology to produce ethanol (a liquid fuel) from wood or other renewable lignocellulosic materials.

This chapter presents a literature review of both the liquid and vapor-phase HF solvolysis of lignocellulose. For liquid-phase process, most references focus on reaction chemistry, reaction kinetics, and HF removal. For the vapor-phase process, most references focus on empirical process development.

Until this disseratation, no kinetic or fundamental chemical reaction engineering studies were reported for the vapor-phase HF solvolysis of lignocellulose.

A complete "HF-Saccharification Bibliography," which lists all available literature references for both the liquid- and vapor-phase HF solvolysis of lignocellulose, is provided in Appendix B. An adequately informative review of the "HF-saccharification of lignocellulosic materials," which summarizes (as of 1984) process development studies, process economic studies, sugar yields and HF lignin, HF losses, and liquid-phase reaction kinetics, is provided by Hawley et al. (1986).

Literature reviews on the properties of anhydrous HF and wood are reserved for chapters 4 and 8 respectively.

I. Liquid-Phase HF Solvolysis

A. Early Work and Historical Perspective

Gore (1869) first noted that anhydrous HF liquid immediately dissolved cellulose to a "glutinous mass." Helferich et al. (1929, 1930, 1932) noted that cellulose rapidly dissolved in anhydrous HF liquid to yield water-soluble "reversion" polyglucans, which upon boiling in dilute acid, were recovered as reducing sugars. These observations were confirmed by Fredenhagen and Cadenbach (1933), Rogovin and Pogosov (1959) and Sharkov et al. (1972). Clark (1962) and Sachs et al. (1963) used aqueous hydrofluoric acid (70% to 90% HF by weight) to dissolve cellulosic materials from wood in order to estimate the lignin composition in wood.

As previously mentioned, research on the liquid-phase HF solvolysis of lignocellulose was revived around 1979 as the result of the oil crisis of the late 1970's. Since 1979, the liquid-phase HF solvolysis of pure cellulose and lignocellulose has been studied by Bentsen (1981), Defaye et al. (1982, 1983), Franz et al. (1987), Hardt and Lamport (1982a, 1982b), Hawley et al. (1983, 1986), Ishii and Hiroi (1986), Lamport et al. (1981), Mort and Parker (1982), Murray (1985), Papadopoulos and Defaye (1986), Selke et al. (1982, 1983), Saddler et al. (1985), and Smith et al. (1983).

A considerable body of literature also exists on the reactions of sugars, sugar derivatives, and oligosaccharides with liquid HF. An early review of the reactions of proteins, carbohydrates, and related substances in liquid HF is provided by Lenard (1969). An excellent review of the selectivity of cleavage of various O-glycosidic linkages of polysaccharides in liquid HF as a function of temperature ranging from -40 °C to 23 °C is provided by Mort et al. (1988, 1989).

B. Reaction Chemistry, Kinetics, and HF-Removal

HF solvolysis of cellulose to glucosyl fluoride. In general, anhydrous HF liquid at temperatures of 0 °C or greater rapidly dissolves cellulose fibers by solvating the hydrogen-bonded cellulose chains in the paracrystalline cellulose microfibril. Once the cellulose is dissolved in HF solution, the β-1,4-O-glycosidic linkages joining the glucan units which constitute the cellulose chain are solvolytically cleaved to yield α-D-glucosyl fluoride in HF solution.

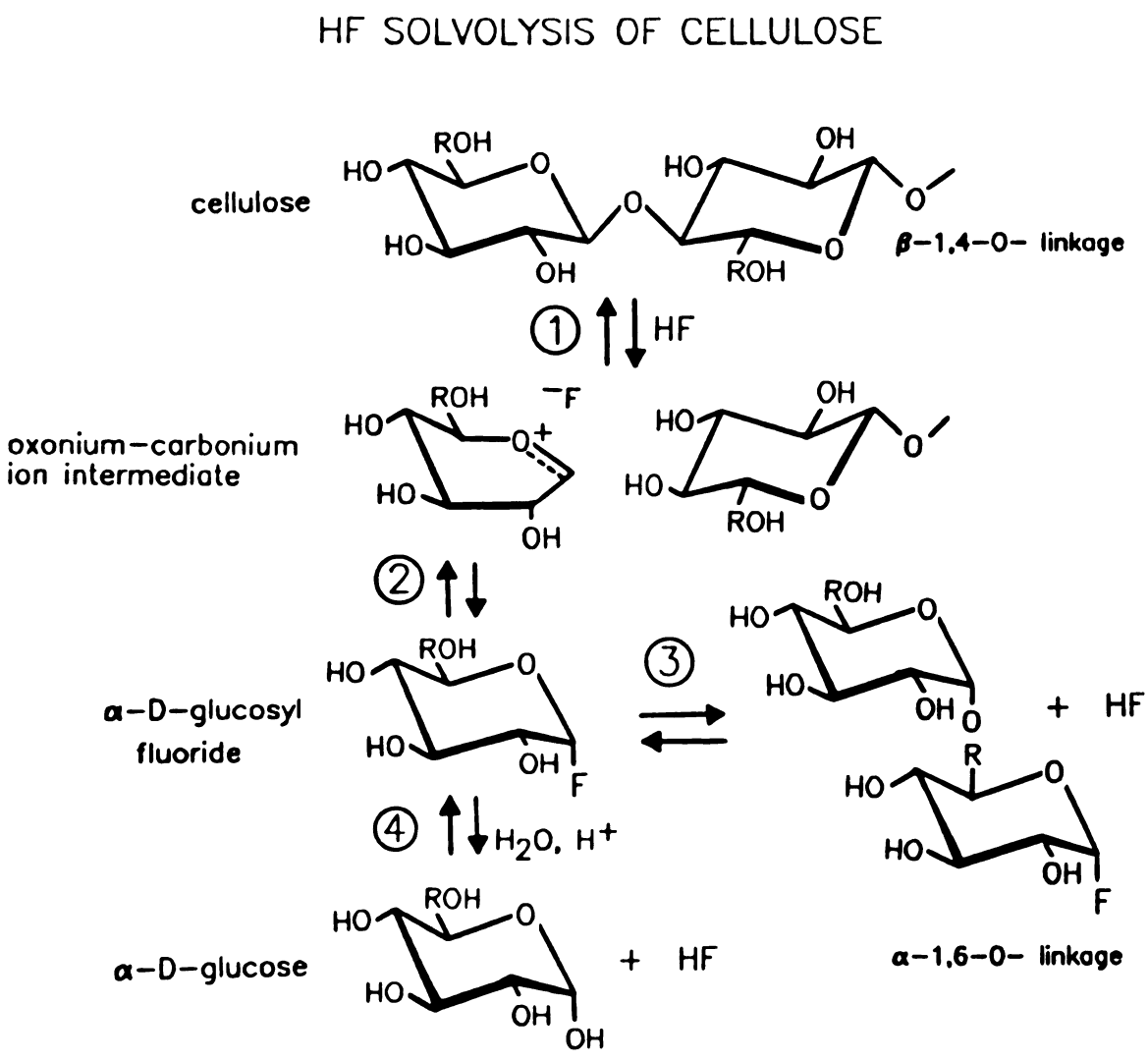
Aqueous hydrofluoric acid of concentrations of less than 80% (wt.) HF does not completely dissolve cellulose from wood at near-ambient temperatures (Fredenhagen and Cadenbach, 1933; Rogovin and Pogosov, 1958; Clark, 1962).

Fredenhagen and Cadenbach (1933) first discovered glucosyl fluoride in the liquid HF/cellulose reaction mixture by in situ solution conductivity measurements. Later, Hardt and Lamport (1982a, 1982b) and Mort and Parker (1982) captured the glucosyl fluoride intermediate by rapid quenching of the liquid HF/cellulose reaction mixture (1 h reaction at 0 °C, 10:1 ratio of HF to cellulose by weight) in a calcium carbonate/dichloroethane slurry cooled in a Dewar flask filled with liquid

N_2. The glucosyl fluoride intermediate was purifed by paper chromatrography and identifed exclusively as α-D-glucopyranosyl fluoride by GC/MS. The solvolysis of cellulose to α-D-glucosyl fluoride at 0 °C proceeded smoothly to completion within 1 h, and HF-catalyzed dehydration of glucosyl fluoride to 1,6-anhydro-ß-D-glucose (levoglucosan) was negligible.

Defaye et al. (1982, 1983) identified glucosyl fluoride in the liquid HF/cellulose reaction mixture in situ by ^{13}C NMR spectroscopy. Defaye proposed that at temperatures of 0 °C and greater, crystalline cellulose dissolves in liquid HF, due to the strong tendency of HF to form hydrogen bonds with cellulose. The solvolytic cleavage of cellulose to glucosyl fluoride in HF solution proceeds by an oxonium/carbonium ion intermediate analogous to the hydronium-ion catalyzed hydrolysis of cellulose to glucose. The glucosyl fluoride intermediate can then repolymerize to oligosaccharides in concentration and temperature-dependent equilibrium. Defaye's mechanism for the HF-solvolysis of cellulose is presented in Figure 2.1.

Hydrolysis of Glucosyl Fluoride. Glucosyl fluoride is stable in water at pH 7. However, glucosyl fluoride readily hydrolyzes to glucose and free HF in acidic solution at ambient conditions (Barnett, 1969). If small amounts of water are in concentrated HF (< 10% wt. H_2O in HF), glucosyl fluoride in HF solution hydrolyzes to glucose (Franz et al., 1987; Fredenhagen and Cadenbach, 1933; Hardt and Lamport, 1982a, 1982b; Mort and Parker, 1982).



① Solvolytic cleavage of the β–1,4–O–glycosidic bond

② Formation of α–D–glucosyl fluoride

③ Repolymerization to oligosaccharides (dimer shown)

④ Hydrolysis

Figure 2.1. Defaye's (1983) mechanism for the HF-solvolysis of cellulose.

HF-Catalyzed Glucosyl Fluoride Repolymerization (Reversion). Cellulose rapidly dissolves in anhydrous HF at temperatures of 0 °C and greater. The HF-dissolved cellulose is then solvolytically cleaved to glucosyl fluoride in HF solution. Under certain conditions, glucosyl fluoride in HF solution can repolymerize to oligosaccharides in concentration and temperature-dependent equilibrium. This repolymerization occurs when the fluoride on glucosyl fluoride attacks free -OH groups on other saccharide structures. The condensation creates an ether bond, or O-glycosidic linkage between glucan units, and regenerates HF. These "reversion" oligosaccharides range from 2 to 20 glucose residues in size, possess randomized O-glycosidic linkages, and are water-soluble.

In previous work, the molecular weight distribution and glycosidic linkage composition of the reversion oligosaccharides were characterized by optical rotation (Rogovin and Pogosov, 1959), gel-filtration chromatography (Franz et al., 1987; Hardt and Lamport, 1982a; Lamport et al., 1981; Mort and Parker, 1982), ^{13}C NMR spectroscopy (Defaye et al., 1982, 1983; Franz et al., 1987), and Hakomori methylation/gas-liquid chromatography (Defaye et al., 1982, 1983; Franz et al., 1987; Mort and Parker, 1982).

In general, the extent of reversion (e.g. the average D.P. of the reversion oligosaccharides) increases with increasing reaction temperature and increasi cellulose cocentration in HF liquid. For example, Hardt and Lamport (1982a), Mort and Parker (1982) reported that at 0 °C and initial HF to cellulose ratio of 10:1 by weight, the equilibrium oligosaccharides ranged from 1 to 6 glucose residues

in size (monomer to trimer primarily) with the α-1,6 O-glycosidic linkage between glucose residues predominating. However, when HF removed was removed from the reaction mixture by vacuum evaporation at 100 °C, the oligosaccharide product distribution shifted to an average of 6 glucose residues in size, and the sugar-oligomers still were water-soluble. Defaye et al. (1982, 1983) and Franz et al. (1987) also reported that HF removal by evaporation increased the average D.P. and also increased amount of branching within the reversion oligosaccharide structures.

Finally, a low concentration of water (<10% wt.) in liquid HF shifted the oligosaccharide product distribution back toward glucose, because the hydrolysis of glucosyl fluoride to glucose by the water competed with the repolymerization of glucosyl fluoride to oligosaccharides (Mort and Parker, 1982; Franz et al., 1987).

Prolonged exposure of glucose in concentrated HF solution resulted in dehydration of the glucose to 1,6-anhydroglucose (levoglucosan). Specifically, Kraska and Micheel (1976) reported that a 6% (wt.) solution of glucose in anhydrous, liquid HF at 20 °C for 3 days yielded reversion oligosaccharide structures (average D.P. 8-12) consisting of glucose residues and levoglucosan in approximately a 5:1 ratio.

In Situ Derivatizations of Glucosyl Fluoride. Inhibition of glucosyl fluoride reversion in HF solution by a competitive in situ methanolysis of glucosyl fluoride to 1-O-methyl glucose (α and β anomers) was studied by Franz et al. (1987) and Ishii and Hiroi (1986) as a means to control the reversion oligosaccharide product

distribution. In general, the in situ methanolysis did not completely block reversion unless the reaction mixture was very dilute, e.g. a 1% solution of glucose in liquid HF. However, in situ methanolysis did reduce the extent of reversion. Franz et al. (1987) also studied the condensation of glucosyl fluoride with sorbitol (a six-carbon polyhydroxyalchol) in liquid HF as a function of sorbitol concentration.

Posthydrolysis. The effect of acid concentration (0.005 to 0.05 N), temperature (90 to 160 °C), and sugar concentration (0.5% to 10% wt.) on the posthydrolysis of reversion oligosaccharides generated was studied by Hardt and Lamport (1982a). The water-soluble reversion oligosaccharides were readily hydrolyzed to glucose by dilute acid at mild conditions, e. g. 0.01 N H_2SO_4 at 140 °C for 60 min. The recovery of glucose from the reversion oligosaccharides was near 100% provided the sugar solution was diluted substantially in water (<10% wt.), so that acid-catalyzed dehydration of glucose to HMF was negligible. At high sugar concentrations (e.g. 10% wt.) about 5 to 10% of the glucose dehydrated to HMF.

Posthydrolysis of water-soluble reversion oligosaccharides with a mixture of glucosyl-hydrolase enyzmes (e.g. α-amylase, amyloglucosidase) has been accomplished with varying success (Bentsen, 1982; Ishii and Hiroi, 1986; Yu et al., 1984).

Glucose Yields and Reaction Kinetics. Sharkov et al. (1972) claimed that the minimum HF to wood ratio for complete solvolysis of cellulose materials in pine was 3:1 by weight. Defaye et al. (1983) and Selke et al. (1982, 1983) reported that

glucose yields in excess of 90% of theoretical were obtained from wood and near quantitative yields were obtained from pure cellulose following liquid-phase HF solvolysis and dilute-acid posthydrolysis of water-soluble reaction products. Similar high yields of glucose and xylose from the liquid-phase HF solvolysis of barley straw were reported by Bentsen (1981).

The reaction kinetics of liquid-phase HF solvolysis of wood and pure cellulose were studied by Selke et al. (1983) and Selke (1983) on a laboratory scale using a well-stirred batch reactor retrofitted within a KEL-F vacuum distillation apparatus. Glucose and xylose yields (in the water-soluble reaction products after posthydrolysis) were determined as a function of reaction time (0 to 60 min), temperature (-12 to 23 °C) and water concentration in liquid HF (0 to 6.4% wt.) at fixed HF to lignocellulose ratio of (typically) 10:1 or 40:1 by weight (e. g., 1 g lignocellulose to 40 mL HF). Wood chips of 0.05 cm thickness were sufficient to minimize internal mass-transfer resistances. Typical reaction conditions and results: anhydrous HF reacted with Bigtooth Aspen wood (0.05 cm) at 0 °C for 30 to 60 min yielded (after posthydrolysis) 0.56 g glucose/g dry wood (91% of theoretical yield) and 0.18 g xylose/g dry wood (85% of theoretical yield).

The reaction kinetics were reasonably described by a psuedo first-order rate model, provided an artifical delay time was used to account for solubilization of cellulose in HF liquid. At 4 °C, the first-order rate constant was 0.179 min^{-1}, and the activation energy ranged from 12 to 34 kcal/mole and was dependent on water concentration in liquid HF. A more sophisticated two-step rate model accounted

for the rate of cellulose solublization in liquid HF.

A microapparatus for liquid-phase HF solvolysis of milligram quantities of lignocellulosic material is described by Sanger and Lamport (1983), whereas a larger KEL-F vacuum distillation apparatus modified for liquid-phase HF solvolysis of gram quantities of lignocellulosic material at controlled reaction temperatures and reaction times is described by Mort (1983) and Mort et al. (1989).

HF Evacuation and Fluoride Retention. Following liquid-phase HF solvolysis of lignocellulose, volitile HF in the reaction mixture can be removed from the nonvolitile reaction products (glucosyl fluoride, reversion oligosaccharides, HF lignin) by vacuum evaporation at elevated temperature. Early studies by Fredenhagen and Cadenbach (1933) claimed +99% HF recovery from HF/pine wood reaction mixtures by vacuum/flue evaporation at 100 °C. Recently, Lamport et al. (1981), Hardt and Lamport (1982a), Selke et al. (1982), and Smith et al. (1983) studied the vacuum evaporation of HF from the liquid HF/Bigtooth Aspen wood reaction mixture (10:1 HF to wood by weight) at 100 °C by measuring the fluoride retention in the HF-desorbed reaction products. Optimal conditions: evacuation of HF liquid (5 % wt. H_2O) at 100 °C for 2 h resulted in fluoride retention of 4 mg/g dry wood in the water-soluble sugar fraction and 1 mg/g dry wood in the water-insoluble lignin residue. Total fluoride retention was 5 mg HF/g dry wood (0.5%). Supposedly, HF loss was due to formation of fluoride salts with ash (0.3% wt.) in Bigtooth Aspen wood.

HF lignin. Clark (1962) showed that HF-insoluble residue from the reaction of liquid HF and wood had a Klason lignin content of about 95%. A small portion of the lignin was HF-soluble. Smith et al. (1983), Defaye et al. (1983), and Papadopoulos and Defaye (1986) all concurred by alkaline nitrobenzene oxidation experiments that the "HF lignin" was condensed onto itself (autocondensed). Defaye et al. (1983) and Papadapoulos and Defaye (1986) also showed by IR spectroscopy that the aryl-alkyl ether linkages in HF lignin remained essentially intact. Furthmores, Papadopoulos and Defaye (1986) showed that a small portion of carbohydrate remained in the HF lignin residue even after prolonged treatment with liquid HF at 0 °C and 23 °C. Clark (1962) and later Lamport and Hardt (1982b) further demonstrated that HF lignin was not fluorinated.

Lignin is the major byproduct of the HF-solvolysis of lignocellulose. However, characterization of HF lignin, and evaluation of its technical and economic potential as a chemical feedstock for production of useful chemicals, is beyond the scope of this disseration and is reserved for future study.

II. Vapor-Phase HF Solvolysis

Although both liquid and vapor-phase HF saccharification of lignocellulose share the same reaction chemistry, their rate processes are different. In the liquid-phase process, the cellulose fraction dissolves in liquid HF and is then solvolytically cleaved to glucosyl fluoride in HF solution. The lignin residue is essentially insoluble in HF. The volitile HF is separated from the nonvolitile sugar

and lignin reaction products by vacuum evaporation or spray drying at elevated temperature (e.g. 60 to 80 °C).

However, in the vapor-phase process, HF vapor (b.p. 19.54 °C) physically adsorbs onto the lignocellulosic matrix. The adsorbed HF then solvolytically cleaves cellulose to glucosyl fluoride. The glucosyl fluoride resides on the intact and porous residual lignin matrix. The HF adsorbed on the HF-reacted lignocellulose is desorbed by passing a hot, inert gas stream (e.g. air at 80 °C) over the HF-adsorbed/reacted solid.

From a process standpoint, the vapor-phase HF solvolysis of lignocellulose has three major advantages over liquid-phase HF solvolysis. First, since HF vapor adsorbs on the lignocellulose (as opposed to the cellulose fraction dissolving in liquid HF), less HF is required for processing: a 0.5:1 (wt.) HF to wood ratio is required for the vapor-phase process, whereas a 3:1 (wt.) HF to wood ration is required for the liquid-phase process. This reduces the amount of HF recycling through the process. Second, the adsorbed HF is more simply desorbed and recovered from the solid reaction products. Third, the vapor-phase process offers more flexible processing conditions. For example, the reaction temperature is not constrained by the normal boiling point of HF (19.54 °C), and the reaction rate is easily controlled by diluting the HF vapor in an inert gas such as air. For these reasons, most bench and pilot-scale studies on the HF-solvolysis of lignocellulose have focused on the vapor-phase process.

A. Early Process Development Studies (1930-1972)

The reaction of HF vapor with lignocellulose was first studied by Fredenhagen and Cadenbach (1933) in a crude, unsafe, non-instrumented, and poorly-controlled semi batch reactor. Specifically, pine wood slivers were added to a silver bottle with stoppered inlet and outlets, and then HF vapor at room temperature was introduced into the bottle and allowed to adsorb and react with the wood. The HF vapor not adsorbed on the wood trickled out of the bottle through the outlet port. The vessel was cooled in an ice bath to dissipate the exothermic heat of adsorption; otherwise, the temperature of the reaction mixture in the vessel increased to 90 °C, and further HF adsorption occurred very slowly. Occasionally, the stopper was removed and the reaction contents were mixed with a nickel wire. The vessel and contents were also periodically weighed. The reaction was complete within 15 to 30 min. The maximum water-soluble carbohydrate yield was dependent on the quantity of HF adsorbed, with the optimum of 95% yield obtained at an HF loading of 1 g HF to 1 g wood (1:1 ratio of HF to wood by weight). The reaction products looked like a dark, spongy, and crumbly mass which retained the overall structure of the original wood slivers. The adsorbed HF could be removed by vacuum evaporation under slow heating to 100 °C. Similar studies by Sharkov et al. (1972) verified Fredenhagen and Cadenbach's observations.

Based upon Fredenhagen and Cadenbach's pioneering experiments just described, several early German patents were issued for the vapor-phase HF solvolysis of lignocellulose (I.G. Farbenindustrie, 1932, 1933a, 1933b). The final process concept, credited to inventors Pfleiderer and Koch, is nicely summarized by Selke (1983) and Smith et al. (1983) will not be repeated here. Smith et al.'s (1983) includes an annotated schematic of Pfleiderer's and Koch's process.

The first pilot-scale studies of the vapor-phase HF solvolysis of lignocellulose were carried out by Hoch and Bohunek, as described by Luers (1937, 1938). These studies are also nicely summarized by Selke (1983) and Smith et al. (1983) and will not be repeated here.

B. Recent Process Development Studies (1979-1989)

Here, three recent bench and pilot-scale processes for the vapor-phase HF solvolysis of lignocellulose are highlighted. These processes are 1) the Canertech process (Winnipeg, Canada), 2) the Biotechnical Institute of Denmark process (Kolding, Denmark), and 3) the Hoechst A. G. process (Frankfurt, West Germany).

In general, all three processes claimed both high glucose yields (90% of theoretical) and high HF recovery (+99% by weight) - the two crucial areas for technical and economic viability. However, due to the proprietary nature of the technology, detailed process data and configurations were not well documented. Furthermore, all of the process developement work was empirical, and so a chemical reaction engineering analysis was not performed on any of the chemical

reactor configurations developed for HF vapor/lignocellulose contacting, reaction, and HF desorption.

Canertech Process. The most ambitious pilot-scale studies of the vapor-phase HF solvolysis of lignocellulose were conducted by Ostrovski et al. (1984, 1985) at Canertech, Inc. of Canada, under a project funded by the Canada Department of Energy, Mines, and Resources (EM&R). Despite the rudimentary state of the technology (as of 1983), the Canadian researchers claimed that vapor-phase HF solvolysis of lignocellulose showed technical and economic promise relative to existing lignocellulose hydrolysis processes. In mid-1983, the Canertech group built a pilot-scale facility for the vapor-phase HF solvolysis of poplar wood located in the Hydraulics Laboratory of the University of Manitoba.

The heart of the Canertech process was a semi-batch, fixed-bed reactor of 20 kg wood chip capacity that operated in two stages. In stage one, HF vapor at ambient temperature and pressure was passed through a bed of poplar chips (Populus tremuloides, air dried to 5% moisture content, chipped to 2.5 cm mesh) until the adsorbed loading was 0.5 kg HF per 1 kg wood. The adsorbed HF was allowed to react with the cellulosic material in the wood for a given reaction time. In stage two, the adsorbed HF was desorbed by passing a hot air stream (typically 80 °C) through the HF-reacted wood chips. The desorbed HF (in air) was recycled to a fresh bed of wood chips. During HF-adsorption, reaction, and HF-desorption, the weight change of the reactor was measured by load cell as a function of time in order to determine the loading of adsorbed HF in the bed. The gas-phase HF

concentration and temperature profile down the length of the bed were also monitored continuously as a function of time. Materials of construction, which included plain-carbon steel, copper and polyethylene all proved suitable for anhydrous HF vapor service under the process conditions studied.

The HF-desorbed reaction products (reversion oligomers and HF lignin) were posthydrolyzed directly in dilute H_2SO_4 (0.5% wt.) at 140 °C for 30 min. After pH adjustment, the glucose and xylose product solution was filtered from the HF lignin residue and fermented to ethanol.

Although detailed process data are not available, Ostrovski et al. (1984, 1985) claimed that maximum glucose yields of around 90% of theoretical, maximum xylose yields of around 75% of theoretical, and +99% by weight of the HF vapor adsorbed on the wood chips during the adsorption/reaction stage could be desorbed and recycled to a fresh bed of wood chips. Residual fluoride in the HF-desorbed reaction products was about 1% by weight. Furthermore, Ostrovski claimed that following posthydrolysis, an aqueous sugar (glucose + xylose) concentration of 15% (wt.) was obtained, which upon fermentation could yield up to 400 L of ethanol per 1000 kg of wood originally charged to the process.

In 1987, Canertech, Inc. and Canada EM&R (after interim management by Allose Manitoba, Ltd.) handed their vapor-phase HF solvolysis process over to W.L. Wardrop and Associates Engineering Inc. of Winnepeg, Manitoba for continued process development (Husain, 1987; Wayne Gilraine, personal communication, Feb. 1988). The two year project, funded at $943,000 (Canadian) per year, focused on

development of 1) a continuous, 2 kg capacity vapor-phase HF solvolysis reactor and HF recovery system, 2) a continuous posthydrolysis reactor, and 3) a 40 L fermentation unit capable of fermenting both xylose and glucose to ethanol simultaneously. Since the process technology is proprietary, no technical details have been released.

Biotechnical Institute of Denmark Process. Bentsen (1982) at the Biotechnical Institute of Denmark verified the technical feasibilty of the vapor-phase HF solvolysis of lignocellulose on the bench scale using a semi-batch reactor. Specifically, in Bentsen's experiments, ground, dry (2-3% moisture) barley straw was loaded into a Monel-clad batch reactor (500 g capacity), and HF vapor was introduced to the reactor under partial vacuum until about 35-40% by weight of HF was adsorbed and the HF partial pressure in the reactor reached 1.0 atm. During HF adsorption, the outside of the vessel was maintained at 10 to 20 °C, presumably to remove the exothermic heat of adsorption, and the contents of the reactor were mechanically agitated by a Z-mixer. At room temperature the reaction was complete within 1 h. An inert stream of perchloroethylene (C_2Cl_4) carrier gas at 80-100 °C was passed through the HF-adsorbed reaction products in the reactor, and after 1 h of desorption, 98.7% of the adsorbed HF was desorbed and recovered. After repeated extraction of the HF-desorbed solid reaction products with hot water, a 10% solution (by weight) of sugar-oligomers was obtained.

Later, Reffstrup and Kau (1985) at the Biotechnical Institute of Denmark developed a continuous pilot-scale process for the solvolysis of barley straw by HF

vapor. In this process, 0.4 kg of anhdyrous HF vapor (optimum) at ambient temperature and reduced pressure was loaded per 1 kg of dried barley straw (test reactor capacity about 2 kg straw per hour). The HF-adsorbed barley straw was then compressed and heated to 80 to 100 °C. Within 1 minute, the porous, HF-adsorbed lignocellulose particles collapsed to a plasticlike, black, dense fluid (1.4 g/cm^3) which readily transferred heat to drive the solvolysis to completion. The HF in the reaction mixture was desorbed by milling the HF-reacted materials under a stream of hot air. The milling enhanced the rate of HF desorption by increasing the surface area of the HF-reacted material so that mass-transfer resistances were reduced. The desorbed HF was then condensed and recycled. By this desorption process, 99% (by weight) of the HF loaded on the barley straw was recovered and recycled. Total residence time of the process was 10 min, and the end product was a free-flowing dark powder of about 1% wt. residual flouride content. After posthydrolysis of the HF-desorbed reaction products in 1.5% wt. H_2SO_4 at 140 °C for 30 min, glucose yields of 80% of theoretical and xylose yields of 60% of theoretical were obtained.

Hoechst A. G. Process. Franz et al. (1982, 1987) developed a bench-scale process for the solvolysis of prehydrolyzed (hemicellulose free) wood by HF vapor. In the Hoechst process, an HF vapor-air mixture at 25 °C to 50 °C was introduced into a rotating cylindrical vessel loaded with prehydrolyzed spruce wood chips (10% wt. moisture; capacity not specified). HF vapor was allowed to adsorb onto the wood chips until the HF loading was between 0.4 and 0.8 kg HF per 1 kg

lignocellulose. The HF/air flow was then stopped, and the reaction was allowed to proceed to completion, typically 30 to 60 min.

The desorption of HF from the reaction products was accomplished within the reaction vessel in two steps. This two-step HF desorption was designed to enhance the process efficiency of HF recycle. In step one, hot air at 60 to 80 °C was passed through the reaction vessel until the HF concentration in the desorbed gas stream was below the gas-stream HF concentration required for adsorption with a fresh bed of wood chips (primary HF recycle). This HF/air gas-stream was recycled directly. In step two, the residual HF still adsorbed on the reaction products was desorbed at a higher temperature, if necessary, in a fluidzed-bed dryer. The desorbed HF was then condensed, vaporized, and mixed with air in order to re-establish the initial gas-stream HF concentration required for HF adsorption (secondary recycle). By this method of HF desorption and recovery, +99% by weight of HF used for adsorption and reaction was efficiently recycled, and the HF-desorbed reaction products had a residual fluoride content of about 1% by weight.

The HF-desorbed reaction products were washed in hot water to dissolve the water-soluble sugar oligomers, and then filtered from the residual lignin. The water-soluble reaction products were then posthydrolyzed in 2% (wt.) H_2SO_4 at 140 °C for 1 h. After posthydolysis, the overall glucose recovery from prehydrolyzed wood was in excess of 90% of maximum theoretical.

Franz et al. (1982, 1987) also determined the equilibrium HF sorption isotherms and the heat of desorption. These data are reviewed in detail in chapter

5 of this dissertation.

Process Design and Economics Studies. Preliminary process design studies for both the liquid- and vapor-phase HF solvolysis of lignocellulose are described by Downey et al. (1983), Hawley et al. (1986) and Selke (1982). Further process design studies for the liquid-phase HF solvolysis of lignocellulose and other acid-catalyzed lignocellulose hydrolysis processes (e.g. dilute/concentrated H_2SO_4, concentrated-liquid HCl, gas-phase HCl) are described by Wright and Powers (1985, 1986).

In general, on the basis of the cost of glucose or ethanol produced by the process, the HF-solvolysis technology was very competitive, and was in fact superior (on paper) to all existing enzyme-catalyzed, aqueous mineral-acid catalyzed, and concentrated halogen-acid catalyzed lignocellulose hydrolysis processes. Major process advantages included efficient lignocellulose feedstock utilization (high glucose yields and a potentially reactive lignin byproduct), potential for simple and highly efficient HF recovery and recycle, and production of concentrated sugar solution (e.g. 10 to 15% by weight) for fermentation. Major process disadvantages included high economic sensitivity to recovery and recycle of expensive HF, and the handling of the highly toxic and corrosive HF in a large-scale process. The major process advantages and disadvantages are highlighted in Table 3.1 (chapter 3).

Final Comments. All of the vapor-phase HF solvolysis processes described in this literature review were developed empirically without first performing a fundamental chemical reaction engineering analysis of the reaction of lignocellulose with HF vapor. Whether this hampered process development is hard to say, but I feel that it is simpler and more cost-effective to first study the vapor-phase process on a laboratory-scale under carefully-controlled conditions so that the intrinsic merits of this process can be readily assessed relative to the more well-established enzyme and aqueous mineral-acid catalyzed lignocellulose hydrolysis processes. Therefore, the research program in this dissertation is directed toward developing a lasting and readily available database, theoretical framework, and chemical reaction engineering analysis of the vapor-phase HF solvolysis of lignocellulose. In chapter 3, I will describe the rationale, objectives, and scope of this research program.

Chapter 3. Rationale, Objectives, and Scope of Research Program

In this chapter, I describe the rationale, objectives, and scope of the research presented in this dissertation.

I. Rationale and Problem Definition

A. Overview of the Vapor-Phase HF Solvolysis of Lignocellulose

Biomass conversion processes produce useful chemicals or fuels from renewable plant resources. In chapter 2, I reviewed the available literature on the "vapor-phase HF solvolysis of lignocellulose", a novel and potentially efficient biomass conversion process which produces fermentable sugars and residual lignin from wood or agricultural residues. The sugar products, glucose and xylose, are value-added chemical intermediates which can be fermented or catalytically processed to a spectrum of useful organic chemicals or liquid fuels, for example, alcohols (e.g. ethanol), ketones, or organic acids.

The basic concept of the vapor-phase HF solvolysis of lignocellulose is shown in Figure 3.1. A more realistic process concept for wood-to-ethanol via HF vapor is shown in Figure 3.2. The production of glucose and residual lignin from lignocellulose by vapor-phase HF solvolysis is carried out in several stages:

1) Diffusion of HF vapor into the lignocellulose particle
2) Physical adsorption of HF vapor onto the lignocellulosic matrix
3) Solvolysis of the glucan polymer cellulose to the monomer glucosyl fluoride by adsorbed HF

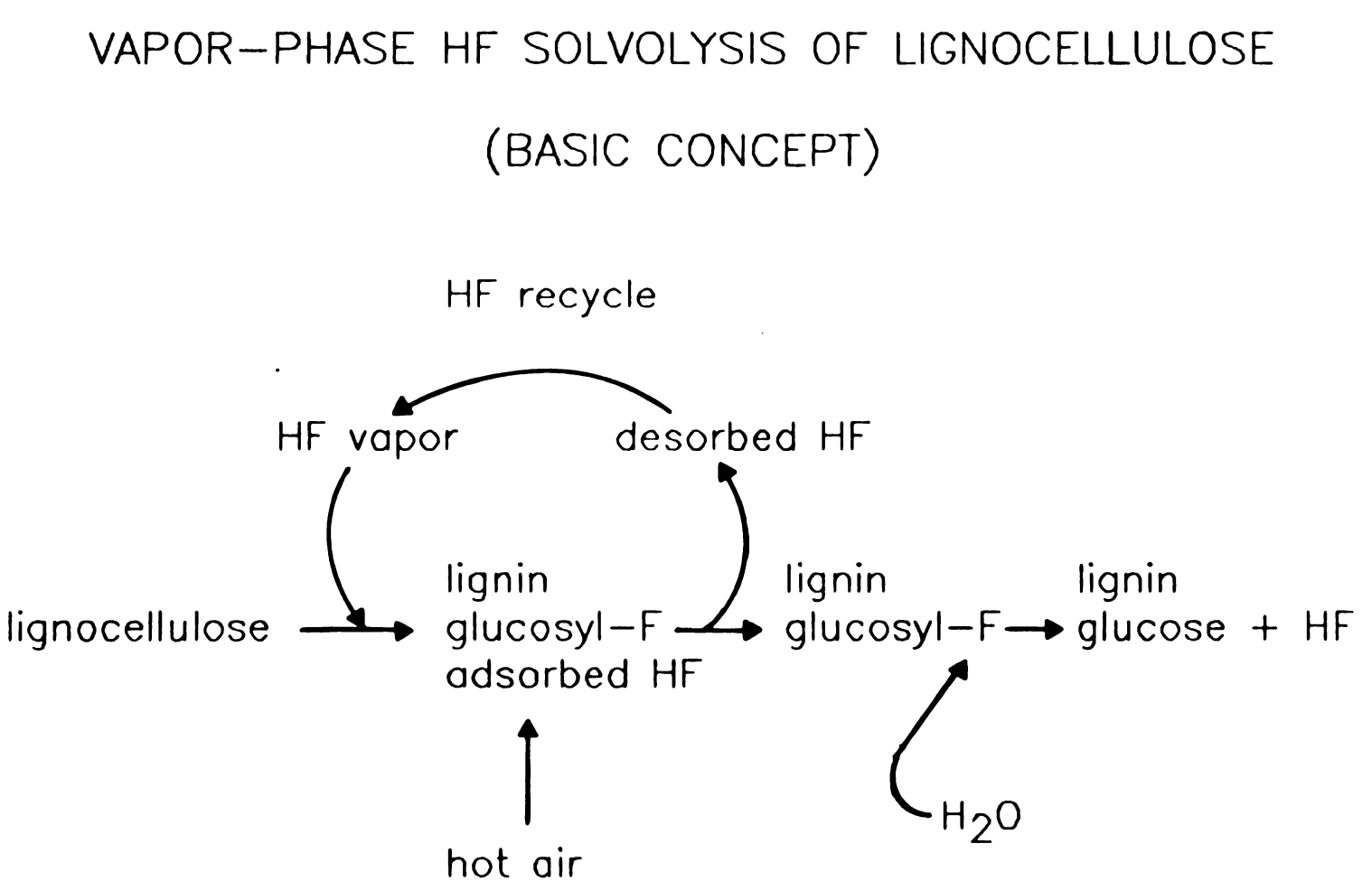


Figure 3.1. Vapor-phase HF solvolysis of lignocellulose: basic concept.

VAPOR-PHASE HF SOLVOLYSIS OF LIGNOCELLULOSE

PROCESS CONCEPT FOR WOOD-TO-ETHANOL VIA HF VAPOR

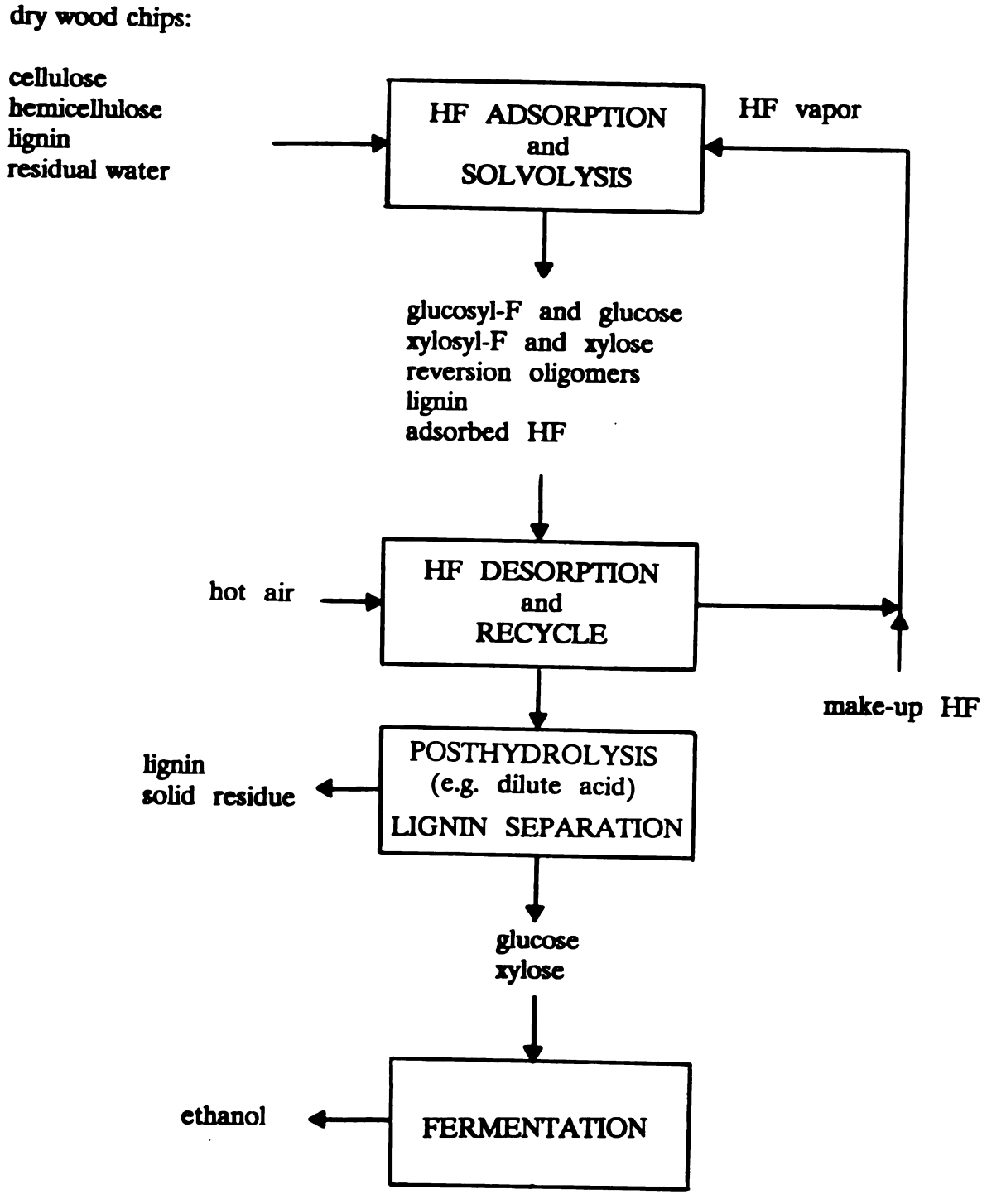


Figure 3.2. Vapor-phase HF solvolysis of lignocellulose: process concept for wood-to-ethanol via HF vapor.

4) Secondary reactions of glucosyl fluoride, including:

   In situ repolymerization (reversion) of glucosyl fluoride to water-soluble oligomers and regeneration of HF

   In situ hydrolysis of glucosyl fluoride to glucose by water in the solid and regeneration of HF

5) Desorption of adsorbed HF by passing a hot, inert diluent gas over the HF-adsorbed/reacted solid

6) Separation of free sugars and sugar-oligomers from residual lignin

7) Posthydrolysis of water-soluble sugar-oligomers to glucose

The process advantages and disadvantages of the vapor-phase HF solvolysis of lignocellulose are contrasted in Table 3.1. Do the advantages outweigh the disadvantages? I will not address this question directly. However, disadvantages 1 and 2 can be minimized by careful equipment design and materials selection. Disadvantages 3 and 4 are really opportunities for future research and may be successfully resolved.

The vapor-phase HF solvolysis process also has two primary advantages over the liquid-phase process. First, much less HF is required in the reactor for lignocellulose solvolysis. Typically, a 3 to 1 ratio of HF to wood (by weight) is required for liquid-phase HF solvolysis (Sharkov et al., 1972), a whereas 0.5 to 1 ratio is required for vapor-phase HF solvolysis (Luers, 1938; Bentsen, 1982; Franz et al.,1982; Ostrovski et al., 1985). Second, the HF is more readily separated from the reaction products. In the vapor-phase process, the HF adsorbed on the HF-reacted solid is removed simply by desorption. However, for the liquid-phase process, the sugar products are in HF solution, and so the HF must be separated

Table 3.1. Process advantages and disadvantages of the vapor-phase HF solvolysis of lignocellulose.

Advantages	Disadvantages
1. Minimal substrate pretreatment (chipping and drying)	1. HF is extremely toxic
2. Production of sugar and sugar-oligomer products in solid form	2. HF is corrosive
3. High yields of fermentable sugars in concentrated solution after posthydrolysis (+90% glucose, (+80% xylose)	3. HF is relatively expensive ($0.6875/lb, [a]), which makes HF recovery/recycle very sensitive to process economics
4. Rapid reaction rates at near-ambient processing conditions	4. Sugar fluorides repolymerize to oligosaccharides during HF solvolysis and desorption; therefore, a posthydrolysis step is required to recover fermentable sugars
5. Simple and +99% recovery/recycle of HF used for processing	

Notes:

[a] Chemical Marketing Reporter, May 8, 1989.

from the sugars by (for example) spray drying (Wright and Power, 1986).

B. Needed Chemical Reaction Engineering Research

As detailed in Literature Review (chapter 2), previous work claims that the vapor-phase HF solvolysis of lignocellulose is a technically-feasible process for the production of fermentable sugars from wood. However, the available literature data on the vapor-phase HF solvolysis of lignocellulose is sparse, incomplete, and lacks technical documentation.

Early papers were rudimentary and lacked careful experimental design (Fedenhagen and Cadenbach, 1933; Luers, 1938; Sharkov et al., 1972). Most of recent papers were stetchy as well (Franz et al., 1982; Ostrovski et al., 1984, 1985; Reffstrup and Kau, 1985). Each of these recent papers described the empirical development of a specific process concept for HF vapor/ lignocellulose contacting, reaction, and HF-desorption. These reports did not provide any detailed process data or analysis necessary for an objective technical evaluation of the process. Furthermore, much of the empirical process-development work was propietary, and was conducted by corporate or private research laboratories in foreign countries.

In summary, no consistent and intrinsic set of process data and models exist for the vapor-phase HF solvolysis of lignocellulose. However, this information is obviously vital for process development, improvement, and analysis.

The solvolysis of lignocellulose by anhydrous HF vapor is fundamentally a chemical reaction engineering problem. Research by the chemical reaction engineering approach is needed in three key areas of the overall process:

1) HF-adsorption/reaction, 2) sugar fluoride reversion/posthydrolysis, and 3) HF-desorption/recycle.

HF-Adsorption/Reaction. The adsorption of HF vapor onto lignocellulose, and the subsequent solvolysis of cellulose to glucosyl fluoride by the adsorbed HF, is the heart of the process. Research on the HF-adsorption/reaction stage is needed to determine HF loading requirements, energy release, cellulose conversion, and sugar yield as a function of processing conditions. This information is in turn used to develop, design, and optimize a chemical reactor for efficient HF vapor/wood contacting and reaction.

Sugar Fluoride Repolymerization/Posthydrolysis. During vapor-phase HF solvolysis of lignocellulose, glucosyl fluoride products can repolymerize to sugar-oligomers. A dilute-acid posthydrolysis step at mild conditions is required to convert the sugar-oligomers back to fermentable glucose. This posthydrolysis step increases process complexity, requires chemical and energy input, and can degrade sugars. Research on HF-catalyzed glucosyl fluoride repolymerization is needed to develop processing stategies to block reversion or control the sugar-oligomer distribution. With this information, posthydrolysis can be eliminated or optimized.

HF-Desorption/Recycle. The desorption and recycle of expensive HF from the HF-adsorbed/reacted solid is crucial to process economics (Hawley et al., 1986). Research is needed to determine the rate of HF desorption, the efficiency of HF desorption, the energy requirements for HF adsorption, and the fluoride retention in the HF-reacted solid as a function of processing conditions.

II. Research Objectives and Scope

A. Overall Research Objectives

A fundamental study of the vapor-phase HF solvolysis of lignocellulose begins with a chemical reaction engineering analysis on the HF vapor/single wood chip reaction system. This reaction system has four basic features, as shown in Figure 3.3.

In this dissertation, I will study the vapor-phase HF solvolysis of a single, dry, lignocellulose wafer. Specifically, this investigation will focus on a chemical reaction engineering analysis of the adsorption and reaction steps of the process under conditions where gas-phase mass-transfer resistances are minimized. This analysis is "intrinsic", and is thus independent of a particular reactor or process configuration.

The major research objectives of this dissertation are to

1) Verify and document the intrinsic feasibility of the vapor-phase HF solvolysis of lignocellulose for the production of fermentable sugars from and residual lignin from wood

2) Study the adsorption and reaction processes of the vapor-phase HF solvolysis of a single lignocellulose chip by (a) gravimetric HF adsorption experiments, (b) reaction rate/sugar yield experiments, and (c) particle temperature measurements (see Table 3.2)

3) Determine maximum sugar yields and minimum HF loading requirements

4) Develop a detailed kinetic and heat transport model for the vapor-phase HF solvolysis of lignocellulose under conditions where gas-phase mass-transfer resistances are minimized

RESEARCH OBJECTIVE

Study the reaction of HF vapor with a single wood wafer

- **HF adsorption measurements**
- **Reaction rate and sugar yield experiments**
- **Particle temperature measurements**
- **Development of a detailed kinetic and heat transport model** (under conditions where mass-transfer resistances are minimized)

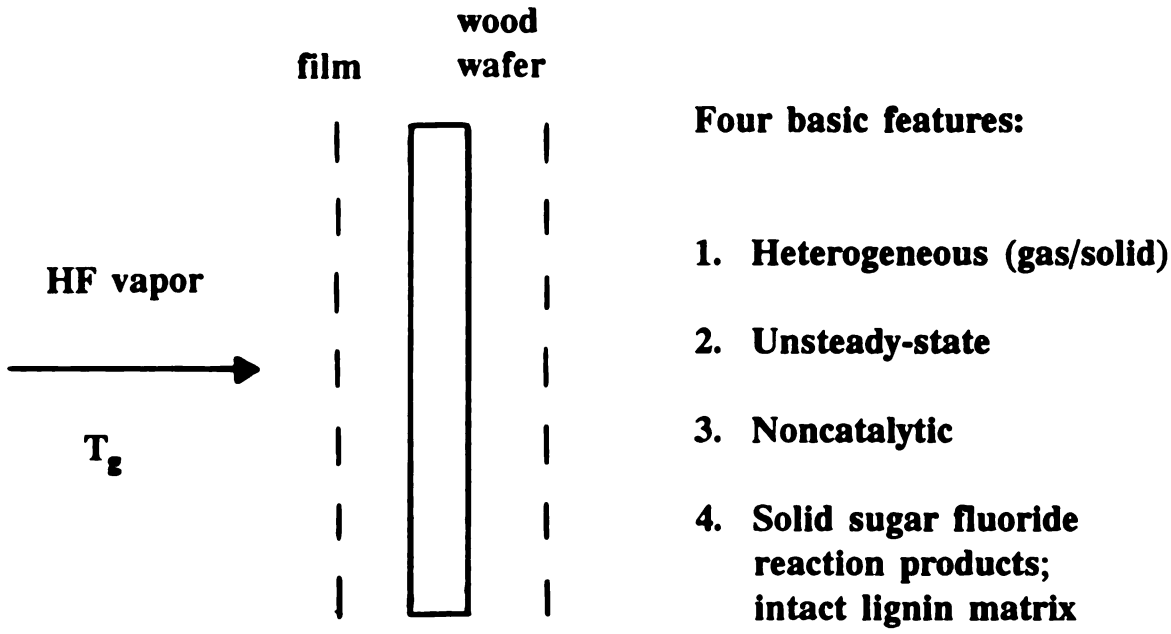


Figure 3.3. Vapor-phase HF solvolysis of a single lignocellulose wafer: four basic features.

Table 3.2. Summary of experimental research program.

Experiment	Process Data
gravimetric HF adsorption on wood and prehydrol. wood (chapter 5)	Equilibrium HF loading as a function of HF vapor conditions, e.g. HF partial pressure (0 to 1.0 atm) and temperature (30 °C to 80 °C) HF loading requirements for maximum cellulose conversion and sugar yield Physical model for HF adsorption
vapor-phase HF solvolysis: sugar yield vs. time (after posthydrolysis) (chapter 6)	Cellulose conversion and sugar production as a function of reaction time and HF vapor conditions, e.g. flowrate, HF partial pressure (0 to 1.0 atm), temperature (30 to 90 °C) Minimization of gas-phase mass-transfer resistances to sugar production rate HF loading requirements for maximum cellulose conversion and sugar yield Comparison of sugar yields and overall product recovery from Bigtooth Aspen wood, prehydrolyzed Bigtooth Aspen wood, pure cellulose, and pure cellulose/lignin composites Physical model for coupled HF adsorption and cellulose solvolysis
vapor-phase HF solvolysis: HPLC-oligosaccharide profiling (before posthydrolysis) (chapter 6)	Determine the extent of glucosyl repolymerization as a function of reaction time and HF vapor conditions
particle temperature measurement (chapter 7)	Particle temperature in the center of a single HF-reacting lignocellulose chip as a function of reaction time and 100% HF vapor conditions Determine the extent of heat-transfer resistances Physical model for energy release and accumulation

Although the above research objectives limit the scope of this dissertation, several exploratory areas are also investigated. These exploratory investigations strengthen the main research program and also develop avenues for future research. These exploratory areas are overviewed next.

First, the research program does not focus on mass-transfer effects. However, screening experiments are conducted in order to minimize gas-phase mass-transfer resistances. Second, the research program does not focus on HF-desorption or glucosyl fluoride repolymerization. However, limited HF-desorption and glucosyl fluoride repolymerization experiments are performed. Third, since the HF vapor/wood reaction is anhydrous (or nearly so), the effect of substrate water content on HF adsorption/desorption, reaction rate, and sugar yield is not investigated. However, limited experiments are conducted to explore the effect of substrate methanol content on the reversion oligosacchride product distribution.

Finally, the residual "HF lignin" is not characterized, nor is it compared to residual lignins from other acid-hydrolysis processes. However, in many of the sugar yield experiments, the solid residue is gravimetrically determined, and the residual carbohydrate in the residue is also determined. In addition, the possibility of HF-catalyzed glucosyl fluoride condensation onto lignin is investigated.

B. Overview of Research Program and Disseration

The research program defined by the research objectives is contained in chapters 4 to 10 of this dissertation. Chapters 4 to 7 detail the experimental design and experimental research program, which includes gravimetric HF adsorption

studies, reaction rate studies, and sugar yield studies. Chapters 8 to 10 develop and verify a detailed kinetic and heat transport model for the solvolysis of a single lignocellulose particle by anhydrous HF vapor. The research program and dissertation contents are overviewed next.

Chapter 4. The experimental design is described in chapter 4. Specifically, the reaction of a single lignocellulose chip by an anhydrous HF vapor stream is studied with the aid of two carefully-controlled, milligram-scale laboratory experiments. The first experiment measures the gravimetric uptake of HF vapor onto a single lignocellulose chip as a function of time and HF vapor stream conditions. The second experiment measures the cellulose conversion and sugar product yield in a single HF-reacting lignocellulose chip as a function of reaction time and HF vapor stream conditions. The glucose yield in the water-soluble reaction products after posthydrolysis quantifies the glucosyl fluoride production and cellulose conversion in the HF-reacting lignocellulose chip. Analytical techniques include High Performance Liquid Chromography (HPLC) for analysis of sugars and oligosaccharides in the water-soluble reaction products both before and after posthydrolysis.

Chapter 5. Preliminary gravimetric HF adsorption experiments are described in chapter 5. Specifically, equilibrium HF adsorption data (HF loading data) for Bigtooth Aspen wood are presented as a function of HF-N_2 gas stream HF partial pressure (0 to 1.0 atm) and temperature (30 °C to 80 °C; n.b.p. HF is 19.54 °C). Much of these data were previously obtained by Mohring (1987). From these data,

the heat of adsorption as a function of HF loading is estimated. HF adsorption/desorption data for the reaction of a single "prehydrolyzed" (hemicellulose-free) wood chip with a 100% HF vapor stream at 1.0 atm are also presented as a function of time and 100% HF vapor temperature.

Chapter 6. Reaction rate and sugar yield experiments are described in chapter 6. This chapter is the heart of the dissertation. Specifically, glucose and xylose yield vs. reaction time data from the vapor-phase HF solvolysis of single Bigtooth Aspen wood chips are presented as a function of HF vapor flowrate, chip thickness (0.2 and 0.4 mm), HF-N_2 gas-stream HF partial pressure (0.4 to 1.0 atm), temperature (30 °C to 90 °C), and HF loading (0.2 to 1.5 g HF/g-wood). Glucose yield vs. time data from the vapor-phase HF solvolysis of "prehydrolyzed" wood chips are also presented as a function of 100% HF vapor stream flowrate, temperature, and HF loading. Most of these data are obtained under conditions where gas-phase mass-transfer resistances were minimized. Similar experiments with pure cellulose (filter paper) wafers and filter paper/"milled-wood" lignin composite wafers are also presented.

Maximum sugar yield and overall product recovery data from the vapor-phase HF solvolysis of Bigtooth Aspen wood, prehydrolyzed Bigtooth Aspen wood, pure cellulose (filter paper), and pure cellulose/"milled-wood" lignin composite wafers are also compared.

Finally, glucosyl fluoride repolymerization in the HF-reacting lignocellulose chip is analyzed by HPLC-oligosaccharide profiling of the water-soluble reaction

products before posthydrolysis as a function of reaction time, HF vapor temperature, and substrate methanol content.

Chapter 7. Preliminary particle temperature measurements are described in chapter 7. Specifically, the center of the HF-reacting "prehydrolyzed" wood chip is measured as a function of reaction time (0 to 6 min), 100% HF vapor stream temperature (31 °C to 68 °C) and 100% HF vapor stream flowrate. These experiments gauge the significance of unsteady-state heat transport in the HF-reacting lignocellulose chip.

Chapter 8. Based on the gravimetric HF adsorption data presented in chapter 5, and the reaction rate/sugar yield data presented in chapter 6, a differential material balance and kinetic model for the vapor-phase HF solvolysis of a single lignocellulose chip is developed in chapter 8. This model will predict glucosyl fluoride production in the HF-reacting lignocellulose chip as a reaction time, temperature, and HF loading. Also in chapter 8, kinetic parameters posed by this model are estimated.

Chapter 9. Based on the gravimetric HF adsorption data, reaction rate/sugar yield data, and particle temperature data presented in chapters 5 to 7, a differential energy balance and heat transport model is developed in chapter 9. This model will predict the particle temperature distribution in the HF-reacting prehydrolyzed wood chip as a function of reaction time, chip thickness, and 100% HF vapor conditions.

Chapter 10. Finally, in chapter 10, the differential material balance and kinetic model is combined with the differential energy balance and heat transport model and solved. The combined model is called the detailed kinetic and heat transport model. This combined model describes the HF adsorption, cellulose solvolysis, energy release, and heat transport processes in the HF-reacting lignocellulose chip under conditions where gas-phase mass transfer resistances are minimized.

The differential material and energy balance model equations are reduced to finite-difference equations and integrated numerically on computer. The resulting computer simulation predicts the gravimetric HF adsorption, sugar yield, particle temeprature distribution, and energy release in a single HF-reacting lignocellulose chip as a function of reaction time, chip thickness, 100% vapor conditions, under conditions where gas-phase mass-transfer resistances are minimized. These model predictions are compared directly to glucose yield vs. time data, and centerline particle temperature vs. data for the vapor-phase HF solvolysis of single prehydrolyzed (hemicellulose-free) wood chips at 100% HF vapor stream temperatures ranging from 52 °C to 68 °C.

Chapter 11. The major results and conclusions from chapters 4 to 10 are summarized in chapter 11. The significance of these results and conclusions is then overviewed. Finally, suggested avenues for future research are outlined.

Chapter 4. Experimental Design

The solvolysis of a single lignocellulose chip by anhydrous Hydrogen Fluoride (HF) vapor vapor is studied with the aid of two carefully-controlled, milligram-scale laboratory experiments. The first experiment measures the gravimetric uptake of HF vapor onto a single lignocellulose chip as a function of time and HF vapor conditions (gravimetric HF adsorption experiment). The second experiment measures the sugar yield and cellulose conversion within the HF-reacting lignocellulose chip as a function of reaction time and HF vapor conditions (vapor-phase HF solvolysis experiment).

This chapter is organized into four sections, labeled I to IV. In section I, the physical properties of HF liquid and vapor are overviewed. Also in section I, lignocellulose substrate preparation, composition, and properties are detailed. In section II, the vapor-phase HF solvolysis experiment is described. In section III, the gravimetric HF adsorption experiment is described. Finally, the miscellaneous experimental techniques used in this dissertation which were not covered in sections I to III are described in section IV.

I. HF Properties and Lignocellulose Substrate Preparation

A. Anhydrous Hydrogen Fluoride: Selected Liquid and Vapor Properties

Liquid Anhydrous Hydrogen Fluoride (HF) of 99.9% purity was obtained from Matheson Gas Products. The HF liquid (n.b.p. 19.54 ^{o}C) was contained in a steel

cylinder of 1600 mL capacity equipped with a Monel (alloy 400) manual control valve (Matheson model 55-A). The closed cylinder was stored under its own vapor pressure at room temperature (0.6 psig at 21 °C) within a fume hood.

The physical properties, safety factors, manufacture, and industrial significance of HF are reviewed by Gall (1980).

Selected volumetric, thermodynamic, and transport property data for liquid HF are presented in Table 4.1. Liquid HF properties are summarized by Simons (1950). The formula weight of HF is 20.01 g/mole. The normal boiling point of HF liquid is 19.54 °C. The melting point of HF is -83.36 °C, and the heat of fusion at the melting point is 46.93 cal/g HF (Hu et al., 1953). The vapor pressure of HF (P_{HF}^{*}) is estimated by the correlation

$$\log_{10} P_{HF}^{*} \text{ (mm Hg)} = 7.37 - 1315/T_g \qquad [4\text{-}1]$$

where T is temperature (K), and P_{HF}^{*} has units of mm Hg (see also a similar correlation by Jarry and Davis, 1953). The HF liquid density, $\rho_{HF,l}$ (g/cm^3) is estimated by the correlation (Simons, 1950)

$$\rho_{HF,l} = 1.0020 - 2.2625\ 10^{-3}T + 3.125\ 10^{-5}T^2 \text{ (T in °C)} \qquad [4\text{-}2]$$

where T has units of °C. The surface tension, $\gamma_{HF,l}$ (dyne/cm) is estimated by the correlation (Simons, 1950)

$$\gamma_{HF,l} = 40.7\ [1 - T/503.2]^{1.78} \text{ (T in K)} \qquad [4\text{-}3]$$

Table 4.1. Selected anhydrous HF liquid properties.

T	$\rho_{HF,l}$	$C_{p,HF,l}$	$k_{HF,l}$	$k_{w,l}$	$\gamma_{HF,l}$	P_{HF}°	ΔH_v°
°C	g/cm³ [a]	cal/g°C [b]	cal/cm-sec°C 10^5 [c]	cal/cm-sec°C 10^5 [d]	dyne/cm [e]	atm [f]	cal/g HF [g]
0	1.002	0.584	-	-	10.09	0.470	62.9
10	0.980	0.603	-	144	9.32	0.696	72.3
20	0.958	0.622	-	146	8.58	1.003	80.8
30	0.937	0.642	101.0	148	7.87	1.410	88.9
40	0.917	0.661	98.5	151	7.18	1.940	96.3
50	0.897	0.680	96.0	153	6.53	2.618	103.2
60	0.878	0.700	93.5	155	5.90	3.469	109.7
70	0.858	0.719	91.0	157	5.29	4.522	115.6

Notes:

[a] Estimated via equation [4-2].

[b] Extrapolated from data of Hu et al. (1953).

[c] Estimated from nomograph of Schaefer and Thodos (1959) at saturation line.

[d] Data for liquid water given by Perry and Chilton, p. 3-210 (1973).

[e] Estimated via equation [4-3].

[f] Estimated via equation [4-1].

[g] Heat of vaporization; data of Jarry and Davis (1953).

The heat of solution data for liquid HF in water is provided by Johnson et al. (1973).

Selected volumetric, thermodynamic, and transport property data for anhydrous, 100% HF vapor at 1.0 atm and temperatures from 20 °C to 80 °C are presented in Table 4.2. HF vapor at 1.0 atm and 20 °C to 80 °C is very nonideal, because HF molecules in the vapor state associate by hydrogen bonding to form oligomers from 2 to 6 units in size. The ratio of H-bonded HF oligomer to HF monomer increases with increasing HF partial pressure and decreasing temperature (Long et al., 1943, Smith, 1958). The heat of depolymerization of the hydrogen-bonded HF oligomer is endothermic (+40.8 kcal/mol $(HF)_6$; Long et al., 1943). The association of HF vapor is well-documented in several German papers (Strohmeier and Briegleb, 1953; Briegleb and Strohmeier, 1953; Franck and Spalthoff, 1957; Spalthoff and Franck, 1957; Franck and Meyer, 1959). At 1.0 atm and 100 °C, all gas-phase HF molecules exist as monomers, and HF behaves like an ideal gas.

Detailed thermodymamic properties of nonideal HF vapor are provided by Vanderzee and Rodenburg (1970). The "equation of state" for nonideal HF vapor is given by

$$P'_{HF}\,\hat{V}_g = RT_g/f \qquad [4\text{-}4a]$$

and the density of HF vapor ($\rho_{HF,g}$) is calculated by

$$\rho_{HF,g} = P'_{HF}\,f\,M_{w,HF}/RT_g \qquad [4\text{-}4b]$$

Table 4.2. Selected anhydrous, 100% HF vapor properties at 1.0 atm.

T_g	$\mu_g \times 10^2$	$C_{p,g}$	$k_g \times 10^5$	Pr	f	ρ_g
°C	g/cm-sec [a]	cal/g°C [b]	cal/cm-sec°C [c]	[d]	[e]	g/L [f]
20	0.0113	2.99	140	0.24	3.21	2.67
30	0.0120	9.62	140	0.82	2.26	1.82
40	0.0126	9.84	140	0.89	1.46	1.14
50	0.0133	4.18	54	1.03	1.10	0.83
60	0.0140	1.43	40	0.50	1.02	0.74
70	0.0148	0.60	30	0.30	1.00	0.71
80	0.0153	0.48	24	0.30	1.00	0.69

Notes:

[a] Interpolated from data of Posey (1953).

[b] Interpolated from data of Frank and Meyer (1959): $C_{p,g}$ = 0.36 cal/g°C at T_g = 100 °C, 1.0 atm (near ideal gas state).

[c] Extrapolated from data of Franck (1953); see Figure 4.1.

[d] Calculated by equation [9-19].

[e] Calculated using data and correlation of Long et al. (1943); see equations [5-9] and [5-10].

[f] Calculated from equation [4-4b].

where "f" is the association factor for HF vapor (f = apparent ave. mol wt./mol. wt. HF monomer), P'_{HF} is the partial pressure of the nonideal HF vapor (atm), R is the gas constant (0.08206 L-atm/mol K), T is temperature (K), and $\hat{V}_g$ is the molar volume of the HF vapor (L/mole HF). The association factor "f" is a function of P'_{HF}, the nonideal HF vapor partial pressure, and T (see chapter 5, section III for detailed discussion).

Values for nonideal HF vapor viscosity, μ_g (Posey, 1953), heat capacity $C_{p,g}$ (Franck and Meyer, 1959), and thermal conductivity k_g (Franck and Spalthoff, 1953) at 1.0 atm and temperatures from 20 °C to 80 °C are presented in Table 4.2. Thermal conductivity (k_g) values for "low" temperature, nonideal HF vapor given in Table 4.2 were extrapolated from a very limited set of k_g data, as shown in Figure 4.1. The thermal conductivity of ideal HF gas at "high" temperature (100 °C to 149 °C) is given by Baker (1971). The diffusivity of nonideal HF vapor in an inert diluent (e.g. N_2 or He) was not found in the HF properties literature.

Saftey Precautions. Anhydrous HF vapor is potentially fatal if inhaled or ingested. HF also burns skin tissue, with the extent of damage dependent on the HF concentration, amount, and time of contact. HF toxicity levels, first-aid procedures, and safe HF handling procedures are well-documented (Braker and Mossman, 1971; Finkel, 1973; Gall, 1980; Allied Chemical Corporation, 1978, 1984), and are summarized in Appendix C.

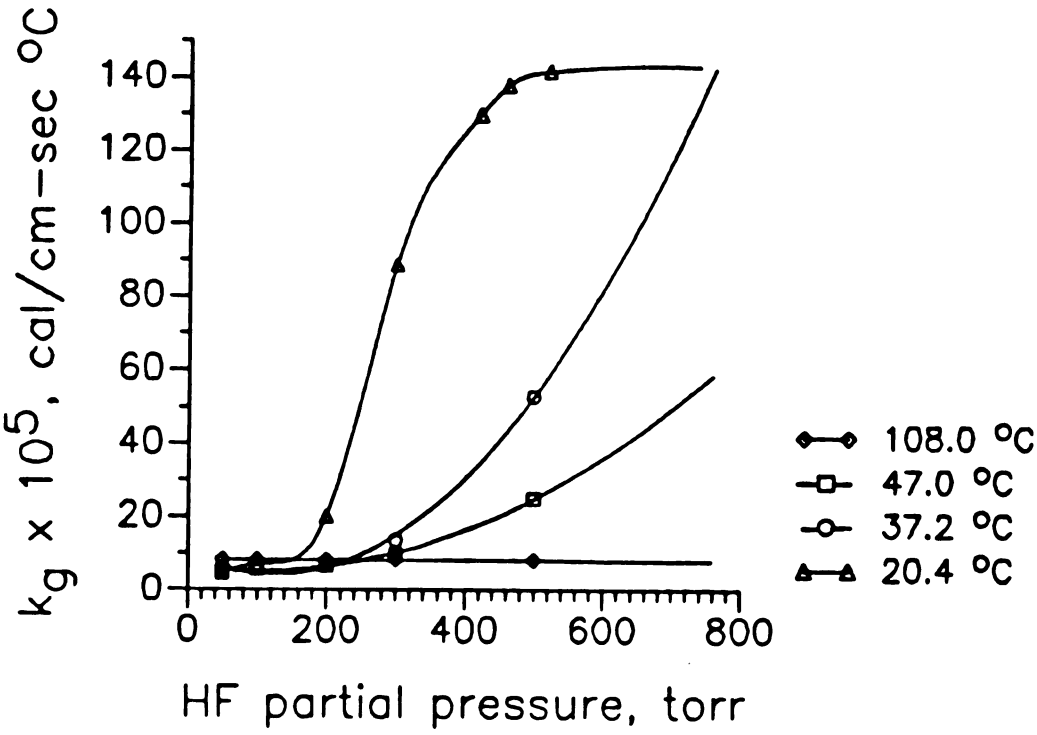


Figure 4.1. Thermal conductivity (k_g) of nonideal HF vapor as a function of temperature (T_g) and HF partial pressure (P'_{HF}; no diluent). Each solid line is a cubic fit of k_g vs. P'_{HF} data; each line is extrapolated to P'_{HF} = 760 torr (1.0 atm).

B. Lignocellulose Preparation, Composition, and Properties

In this dissertation, the vapor-phase HF solvolysis of four lignocellulosic substrates were studied: Bigtooth Aspen wood, prehydrolyzed (hemicellulose-free) Bigtooth Aspen wood, pure cellulose (filter paper), and filter paper/"milled-wood" lignin composite wafers (see Figure 4.2). The preparation, composition, and properties of these four lignocellulosic substrates are provided next.

Bigtooth Aspen Wood. The estimated composition of Bigtooth Aspen wood as stated by Selke (1983) is given in Table 4.3. The detailed composition of Trembling Aspen wood as determined by Timell (1957) is given in Table 4.4. Wood consists mainly of the biopolymers crystalline cellulose (linear glucan polymer, D. P. around 5000 to 10,000), amorphous hemicellulose (xylan polymer with glucoglucuronic acid side chains, average D. P. 200) and the encrustant lignin (branched phenylpropanoid polymer, average D.P. 60). The cellulose and hemicellulose polymer chains are schematically illustrated in Figures 4.3a and 4.3b respectively. The wood sugars are schematically illustrated in Figure 4.4. The architecture and composite microstructure of these three components in the lignocellulosic matrix are detailed in chapter 8, section I (see Figures 8.1 to 8.4). The chemical composition of hardwoods is reviewed by Pettersen (1984b).

Roughly-chipped Bigtooth Aspen wood (2.5 cm mesh, 6% moisture) was microtomed with the grain of the wood into shavings of 0.2 mm or 0.4 mm thickness. The thickness of each wafer was measured to precision of 0.025 mm with a micro-caliper. These shavings are then cut into square wafers of ca. 1.0

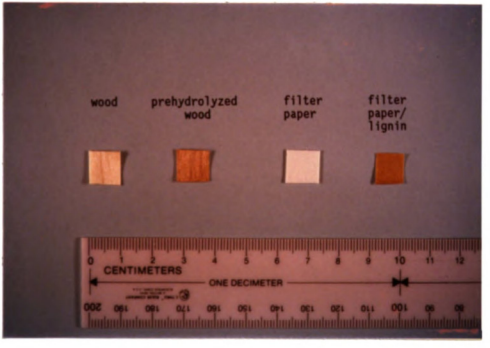


Figure 4.2. Photograph of the four types of lignocellulosic wafers used in this study: Bigtooth Aspen wood, prehydrolyzed Bigtooth Aspen wood, pure cellulose (filter paper), and the filter paper/"milled-wood" lignin composite.

Table 4.3. Detailed composition of Trembling Aspen wood.

Component	Wt.% wood	Wt. % wood (extractive-free) [a]
total glucan [b]	55.0	57.3
glucan as cellulose	51.2	53.3
hemicellulose	29.0	30.2
glucan	3.8	4.0
xylan [c]	15.3	16.0
mannan	2.2	2.3
galactan	0.8	0.8
arabinan	0.4	0.4
uronic acids	3.2	3.3
acetyl groups	3.3	3.4
lignin	15.6	16.3
extractives	4.0	0.0
ash	0.2	0.2

Notes:

[a] Data given by Timell (1957). Composition recalculated assuming 4.0% wt. extractives.

[b] Maximum theoretical glucose yield:
3.395 mmol glucose/g-dry wood, 0.611 g glucose/g-dry wood.

[c] Maximum theoretical xylose yield:
1.159 mmol xylose/g-dry wood, 0.174 g xylose/g-dry wood;
52.7% of hemicellulose estimated as xylan.

Table 4.4. Estimated composition of Bigtooth Aspen wood.

Component	Wt. % wood [a]
total glucan [b]	55.7
glucan as cellulose [c]	50.0
hemicellulose [d]	29.0
extractives	4.1
lignin	16.6
ash	0.3

Notes:

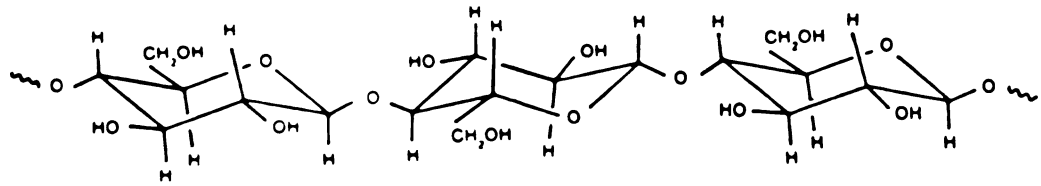
[a] Composition given by Selke (1983).

[b] Maximum theoretical glucose yield: 3.441 mmol/g-dry wood, 0.616 g/g-dry wood; based on material balance experiments of Selke (1983) for liquid-phase HF solvolysis of Bigtooth Aspen wood.

[c] Maximum theoretical glucose yield from cellulose fraction: 0.556 g/g-dry wood (89.7% of total glucan).

[d] Maximum theoretical xylose yield: 1.4 mmol/g-dry wood, 0.210 g/g-dry wood; based on material balance experiments of Selke (1983) for liquid-phase HF solvolysis of Bigtooth Aspen wood. Assuming this value is correct, about 63.8 % of hemicellulose is xylan, 19.5% of hemicellulose is glucan (or 10.3% total glucan is in hemicellulose).

(a) Cellulose Chain (linear $\beta-1,4$ linked glucan)



(b) Hemicellulose Chain (linear $\beta-1,4$ linked xylan with glucan/glucuronic acid side chains)

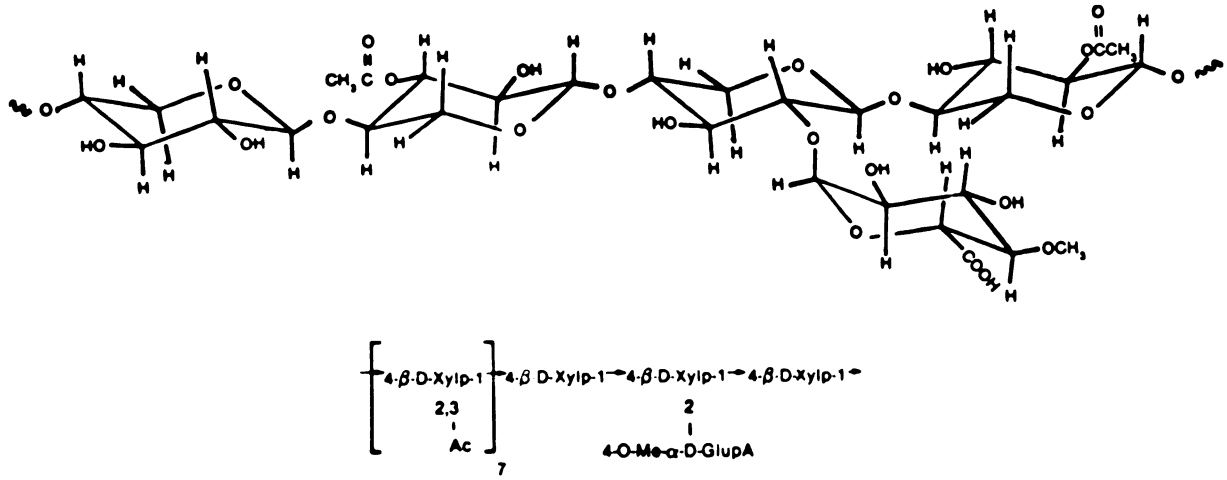
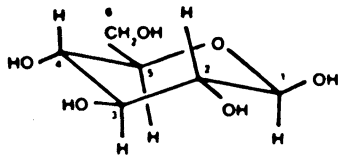
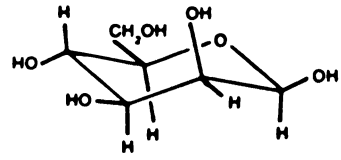


Figure 4.3. Schematics of the cellulose and hemicellulose polymer chains.

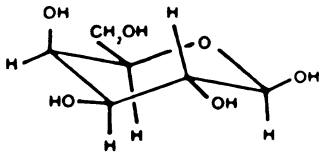
Sugars from Hardwood Hemicellulose



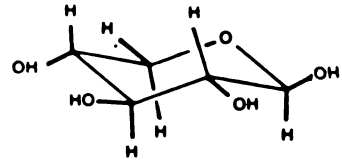
β-D-Glucose
β-D-Glucopyranose
β-D-Glup



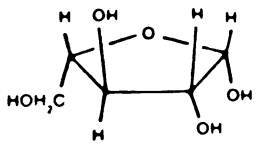
β-D-Mannose
β-D-Mannopyranose
β-D-Manp



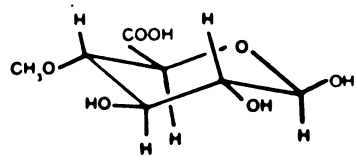
β-D-Galactose
β-D-Galactopyranose
β-D-Galp



β-D-Xylose
β-D-Xylopyranose
β-D-Xylp



α-L-Arabinose
α-L-Arabinofuranose
α-L-Araf



4-O-Methylglucuronic acid
4-O-Methylglucopyranosyluronic acid
4-O-Me-α-D-GlupA

Figure 4.4. Sugars from hardwood hemicellulose. Note: α configurations will exist when hemicellulose is hydrolyzed.

cm/side. The wood wafers were oven-dried at 80 °C and 1.0 atm to less than 2% moisture content. Typical weight of a single 0.4 mm thick wood chip (after drying) was 15 mg.

Prehydrolyzed Bigtooth Aspen Wood. The composition of Bigtooth Aspen wood is simplified considerably if the hemicellulose and extractive components are selectively removed. Dilute acid at mild temperature (e.g. 100 °C) hydrolyzes the hemicellulose component to soluble sugars (xylose mainly) and removes extractives. However, theses conditions are not sufficient to hydrolyze the crystalline cellulose. The lignocellulosic solid residue, called "prehydrolyzed wood", retains the native architecture of wood, but contains mainly two chemical components, crystalline cellulose (about 75%), and lignin (about 25%).

Typically, "prehydrolyzed" Bigtooth Aspen wood wafers were prepared by refluxing a batch of Bigtooth Aspen wood wafers (0.4 mm x 1.0 cm/side) in 2 N Trifluoroacetic Acid (TFA) at 100 °C for 4 h. The typical batch was 0.6 g Bigtooth Aspen wood (about 40 wafers) in 60 mL 2 N TFA (2 N TFA preparation: 16.8 mL TFA diluted to 100 mL with H_2O). A time course of the sugars released to the hydrolysate during a typical prehydrolysis is shown in Figure 4.5. During prehydrolysis, a thin waxy film floated to the surface of the hydrolyzate, indicating extractives removal from wood. The hydrolysate was yellow in color. Xylose dehydration to furfural occurred during TFA prehydrolysis (Fanta et al. 1984). The xylose yield (uncorrected for dehydration) shown in Figure 4.5 was determined by High-Performance Liquid Chromatography (see section II), using myo-inositol in the

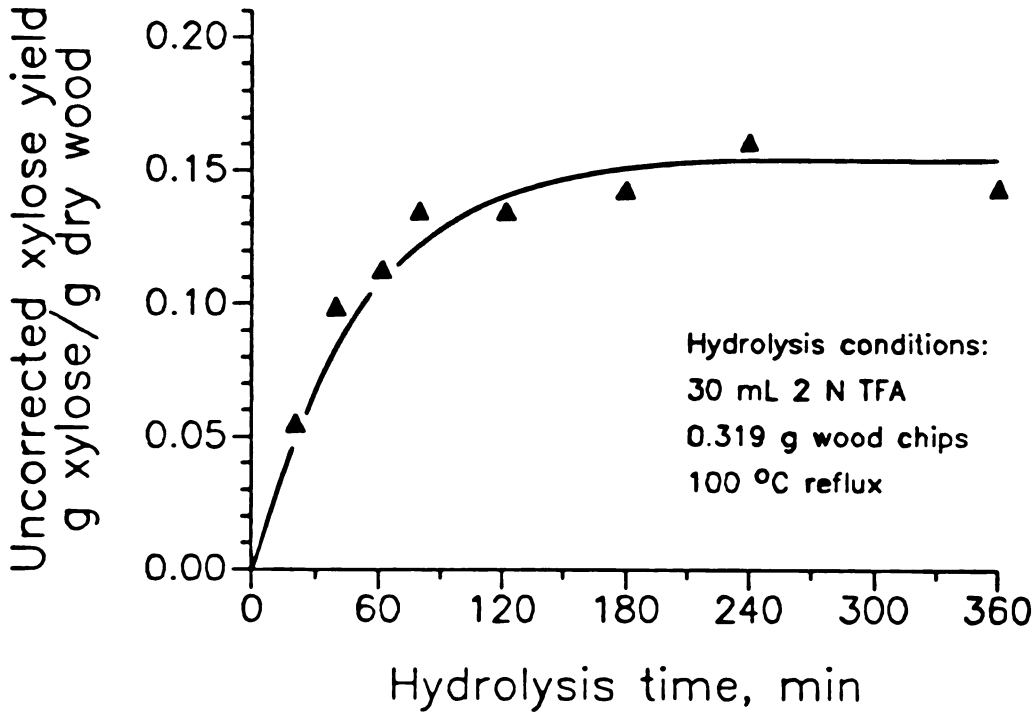


Figure 4.5. Xylose yield vs. time profile for Bigtooth Aspen wood prehydrolysis in 2 N trifluoroacetic acid (TFA) at 100 °C.

hydrolysate (1 mg/mL) as the internal standard.

The solid residue after prehydrolysis was filtered from the hydrolysate and washed several times with tepid distilled water, until the washings were pH neutral. The wet "prehydrolyzed" wood wafers were handled carefully to prevent fragmentation. The wet prehydrolyzed wood wafers were then oven dried at 80 °C and 1.0 atm. The dried wafers were light brown or beige in color. Dry solid recovery, R_{LC}, averaged 0.679 +/- 0.002 g "prehydrolyzed" wood per 1 g of original Bigtooth Aspen wood. Based on this data, and previous material balance studies on 1 N TFA prehydrolysis of lignocellulosic materials at 100 °C (Fanta et al., 1984), the composition of prehydrolyzed Bigtooth Aspen wood was estimated, as shown in Table 4.5. The typical weight of a dried prehydrolyzed wood chip ranged from 10 to 12 mg (wood 15 mg to 17 mg).

Pure Cellulose (Filter Paper). Whatman filter paper No. 3 (99.9% crystalline cellulose of ca. 0.5 mm thickness) was cut into squares of ca. 1.0 cm/side. The filter paper wafers were oven-dried at 80 C and 1.0 atm. Typical weight of filter paper wafers (after drying) was 20 mg.

Filter Paper/"Milled-Wood" Lignin Composite Wafers. A pure cellulose/lignin composite substrate of precisely known glucan and lignin composition was prepared by solvent-impregnating "milled-wood" lignin onto filter paper.

"Milled-wood" lignin (MWL) is a near chemically-intact lignin isolated from wood by ball-milling and mild solvent extraction (Bjorkman, 1956, 1957a, 1957b, 1957c, 1957d; Glasser et al., 1983). The preparation of "milled-wood" lignin from

Table 4.5. Estimated composition of prehydrolyzed Bigtooth Aspen wood.

Component	Wt. % prehydrol. wood [a-c]
total glucan [d]	74.6
residual xylan	2.7
other residual components	0.7
lignin	22.0

Notes:

[a] Prehydrolysis conditions: reflux in 2 N TFA at 100 °C for 4 h.

[b] Assumptions for composition estimation:
1) composition of Bigtooth Aspen wood given in Table 4.4 is correct
2) 90% removal of hemicellulose (Fanta et al., 1984); all hemicellulose component removed equally
3) 10% of original lignin solubilized in hydrolyzate (Fanta et al., 1984) 0.0166 g lignin/g-original wood
4) 100% removal of extractives
5) 100% removal of ash.

[c] Theoretical solid recovery after prehydrolysis is 0.678 g/g-original wood; average measured solid recovery after prehydrolysis is 0.679 +/- 0.002 g/g-original wood.

[d] Maximum theoretical glucose yield: 4.61 mmol/g prehydrol. wood, 0.83 g/g-prehydrol. wood.

Bigtooth Aspen wood, and the subsequent preparation of the filter paper/ "milled-wood" lignin composite substrate is overviewed here.

Step 1: preparation of extractive-free wood grindings. About 100 g Bigtooth Aspen wood was ground in a Wiley mill and then sifted to size 0.25 mm and smaller. The sifted wood grindings were Soxhlet-extracted in 2:1 v/v benzene/ethanol per ASTM Standard Method D1105-84 (1984) to remove the "extractives" fraction, and then dried in vacuo at room temperature for 1 week.

Step 2: dry ball-milling of extractive-free wood grindings. In general, the ball-milling procedure disintegrates the structure of the secondary cell wall of wood and reduces the particle size to less than 1 μm (Bjorkman, 1956, 1957d). A dry ball-milling procedure described by Glasser et al. (1983) was used. A 1.3 gallon ceramic milling jar was filled about two-thirds full with ceramic 3/4 inch milling stones. About 25 g of extractive-free wood grindings were charged into the milling jar, along with about 20 g of dry ice (the dry ice will sublime and flush out the air to provide an inert CO_2 blanket over wood grindings). The sealed milling jar and contents were dry ball-milled on a roller (120 rpm) at room temperature for 2 weeks. This method of dry ball-milling described by Glasser et al. (1983) was preferred over Bjorkman's vibro-rotary ball-milling method (1957), which used toluene as a non-swelling dispersant for milling.

Step 3: extraction and purification of milled-wood lignin (MWL). After ball-milling, 3 L of 9:1 v/v acetone/water was added directly to the milling jar, in order to extract the crude MWL (Glasser et al., 1983). The acetone/water was

allowed to soak in the jar (under occasional agitation of the jar) for 2 days at room temperature. After extraction, the light brown solvent fraction was decanted, the milling stones were washed with 9:1 v/v acetone/water, and the washings were added to the solvent fraction.

The solvent fraction, which contained the dissolved crude MWL, was filtered and then rotary-evaporated at room temperature to dryness. The dried residue, or crude MWL, was purified by successive solvent extraction with acetic acid and 1,2-dichloroethane/ethanol (2:1 v/v), as detailed by Bjorkman (1956), without modification.

The purified MWL from Bigtooth Aspen wood was a cream or tan colored fluffy solid. The yield was not calculated, but Bjorkman (1956) reports that about 50% of the wood's original lignin can be isolated as MWL, which on a Bigtooth Aspen wood basis, corresponds to 1 g MWL per 25 g original wood. A UV spectum of the purifed MWL in 2-ethoxyethanol solvent (see Figure 4.6) shows a maximum at about 280 nm, which is characteristic of purified MWL (Bjorkman, 1957a). The residual carbohydrate content of purified MWL is about 0.019 g/g MWL (Bjorkman, 1956).

Step 4: solvent impregnation of MWL onto filter paper. A single disk of Whatman filter paper No. 1 (55 mm x 0.1-0.2 mm thick, ca. 200 mg) was oven-dried at 80 °C and 1.0 atm and weighed to precision of +/- 0.1 mg. For a given mass of the dry filter paper disk (m_{FP}), the mass of MWL (m_{MWL}) needed to set the desired concentration of MWL on the filter paper/ "milled-wood" lignin

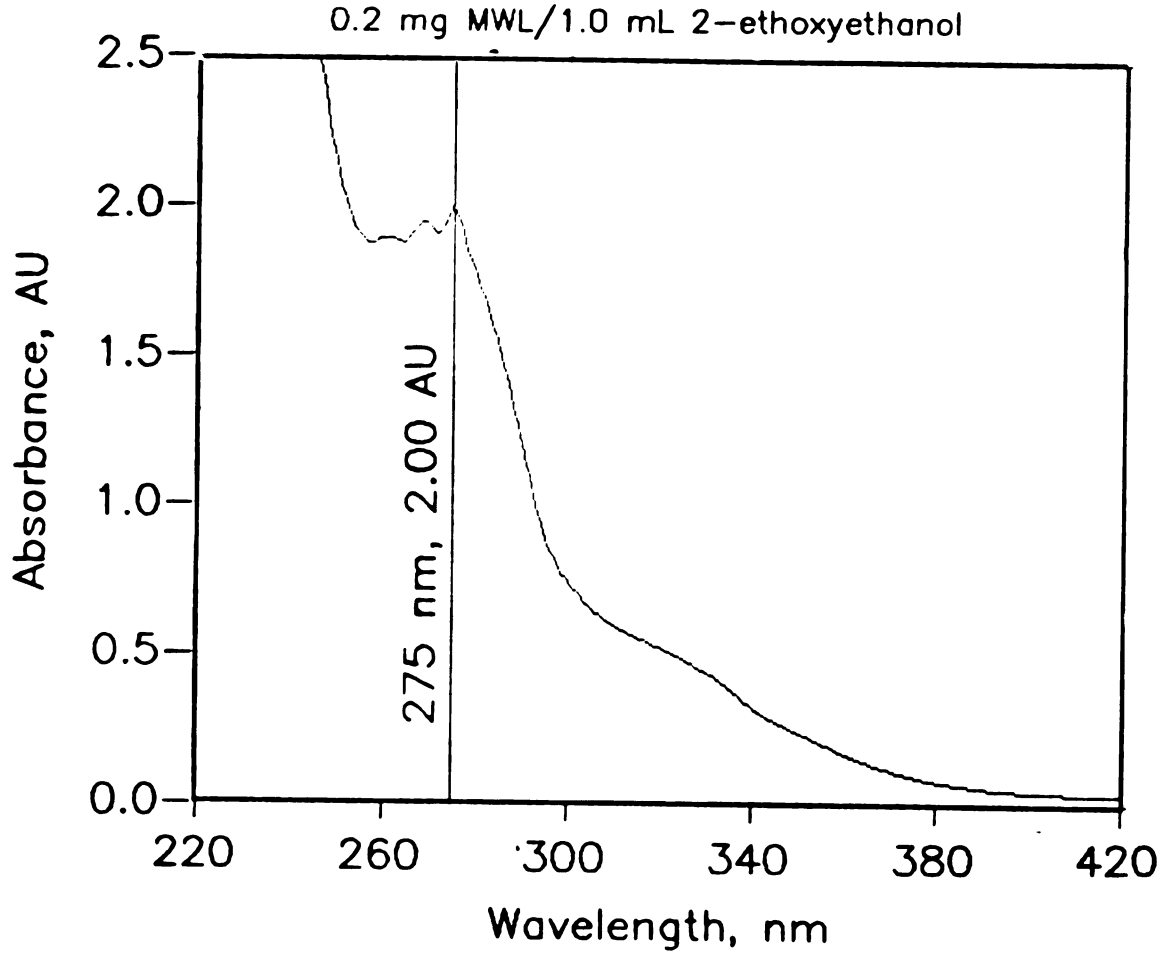


Figure 4.6. UV spectrum of "milled-wood" lignin (MWL) isolated from Bigtooth Aspen wood.

composite was calculated by

$$m_{MWL} = m_{FP} [MWL]/(1 - [MWL]) \quad [4\text{-}5a]$$

where [MWL] is weight fraction of MWL, i.e. g MWL/g-composite.

The required amount of MWL was weighed out and dissolved in 2:1 v/v 1,2-dichloroethane/ethanol (5 mg MWL per 1.0 mL solvent). The filter paper disk was then placed in a 60 mm petri dish, and 200 μL increments of the MWL solution were carefully and evenly pipetted onto the porous filter paper disk. Between each 200 μL MWL solution addition, the filter paper disk was basted in the solution until the excess solvent evaporated.

Eventually, all the MWL in solution was solvent-impregnated onto the filter paper disk. The MWL-impregnated filter paper disk was dried in vacuo at room temperature for 2 days in order to evaporate any excess solvent and/or water. The dried MWL-impregnated filter paper disk (filter paper/"milled-wood" lignin composite) was weighed to precision of 0.1 mg (m_{LC}). The actual [MWL] in the filter paper/"milled-wood" lignin composite was then calculated by

$$[MWL] = 1 - m_{FP}/m_{LC} \quad [4\text{-}5b]$$

The MWL-impregnated filter paper disk was then cut into wafers of ca. 1.0 cm/side, just like wood and pure filter paper. The wafers were light yellow in color.

Wood Sugar and Klason Lignin Determination. Sulfuric acid (H_2SO_4) hydrolysis is a common method for wood sugar and Klason lignin determination (Petersen, 1984b). This method hydrolyzes cellulose and hemicellulose in wood to their consituent monomer sugars in two steps: concentrated H_2SO_4 main

hydrolysis at 30 °C, followed by dilute H_2SO_4 posthydrolysis at 121 °C.

The two-step sulfuric acid hydrolysis procedure is described here. Bigtooth Aspen wood chips were ground in a Wiley mill to 60 mesh (< 0.2 mm). A 200 mg portion of the wood grindings were weighed in a 25 mL conical flask. The wood grindings were dried at 80 °C and 1.0 atm and reweighed to precision of 0.1 mg. After drying and weighing, 5.0 mL of 72% wt. sulfuric acid solution (preparation: 10.0 mL 96.4% wt. conc. H_2SO_4 in 7.0 mL H_2O) was added to the wood grindings in the 25 mL flask, and the mixture was agitated gently for 1 h in a shaking water bath maintained at 30 °C (main hydrolysis). The entire reaction mixture (hydrolysate plus residue; a black gooey liquor) was diluted to 130 mL total volume (2.8 wt.% H_2SO_4) in a 250 mL conical flask, and then autoclaved at 121 °C under 15 psig steam pressure for 1 h (posthydrolysis).

After posthydrolysis, vacuum-dried myo-inositol (100 mg) was added to the flask and thoroughly mixed. The myo-inositol served as an internal standard for later quantitative analysis by High Performance Liquid Chromatography (HPLC). The mixture was then filtered. The hydrolysate was light yellow, and the water-insoluble residue was medium brown. The solid residue was washed several times with tepid distilled water, dried, and weighed. The dried solid residue is the Klason lignin. A 10 mL aliquot of the filtered hydrolyzate was neutralized with a boiling-hot, saturated barium (II) hydroxide solution under stirring. The neutralized hydrolysate was centrifuged to remove the barium sulfate precipitate, and then syringe-filtered through a 0.45 μm filter. The yield of each sugar was

then determined by High-Performance Liquid Chromatography, as detailed in section II. This two-step sulfuric acid hydrolysis for wood sugar determination was repeated in triplicate, and the results were averaged.

Volumetric and Thermal Properties of Wood and Prehydrolyzed Wood. Selected volumetric and thermal properties of Bigtooth Aspen wood and prehydrolyzed Bigtooth Aspen wood are presented in Tables 4.6 and 4.7 respectively.

Wood is both microporous and macroporous, as detailed in chapter 5 (section III) and chapter 8 (section I). The density of dry lignocellulosic solid, ρ'_{LC} (no void) is approximately 1.5 g/cm^3 (Wegner et al., 1984). The void fraction of wood (ϵ) is estimated by

$$\epsilon = 1 - \rho_{LC}/\rho'_{LC} \qquad [4\text{-}6]$$

where ρ_{LC} (g/cm^3) is the bulk density of wood (oven dry weight/volume at 12% moisture). The total void (pore) volume (V_p, cm^3/g) in the wood chip is estimated by

$$V_p = \epsilon/\rho_{LC} \qquad [4\text{-}7]$$

The density of prehydrolyzed wood (assuming no shrinkage) is estimated by multiplying the bulk density of wood by the dry solid residue recovery, R_{LC}.

The heat capacity of dry lignocellulose, $C_{p,LC}$ (cal/g^{o}C) is estimated by

$$C_{p,LC} = 0.266 + 0.00116\ T \quad (T \text{ in } ^oC) \qquad [4\text{-}8]$$

Table 4.6. Volumetric properties of dry Bigtooth Aspen wood and dry prehydrolyzed Bigtooth Aspen wood (literature and estimated).

lignocellulosic substrate	ρ_{LC} g/cm³ [a]	ϵ [b]	V_p cm³/g [c]	Reference for ρ_{LC}
Aspen [d]	0.40	0.73	1.83	Wegner et al. (1984) p. 583
Aspen [d]	0.35	0.77	2.20	Browning (1971) p. 10
Trembling Aspen	0.38	0.75	1.97	Browning (1971) p. 16
Prehydrol. Aspen [e]	0.26	0.83	3.21	

Notes:

[a] Bulk density, ρ_{LC}, defined as mass oven-dry wood/volume at 12% moisture (Wegner, 1984; Skaar, 1984).

[b] Total void fraction, ϵ, estimated by equation [4-6].

[c] Total pore volume, V_p, estimated by equation [4-7].

[d] Species not specified.

[e] Bulk density estimated using trembling aspen wood density and 0.678 g/g-original wood recovery (no shrinkage upon prehydrolysis assumed).

Table 4.7. Selected thermal properties of dry Aspen wood and dry prehydrolyzed aspen wood.

lignocellulosic substrate	T_g °C	$C_{p,LC}$ cal/g-wood°C [a]	k_{LC} cal/cm-sec°C [b]
Trembling Aspen	30	0.30	0.00024
	60	0.34	
prehydrol. Aspen	30	0.30	0.00018
	60	0.34	

Notes:

[a] Heat capacity, $C_{p,LC}$, for dry Aspen wood and dry prehydrolyzed Aspen wood at Tg estimated by equation [4-8].

[b] Thermal conductivity, k_{LC}, for dry Aspen wood and dry prehydrolyzed Aspen wood at 30 °C estimated by equation [4-9] at 0% moisture; k_{LC} for heat flow against wood grain (e.g. perpendicular to macropores); k_{LC} weakly dependent on temperature but assumed constant.

where T has units of (^{o}C). Equation [4-8] is valid from 0 ^{o}C to 100 ^{o}C (Browning, 1971; Skaar, 1984). The across-grain effective thermal conductivity of lignocellulose, k_{LC} (cal/cm-sec^{o}C) at ambient temperature is estimated by

$$k_{LC} = [0.60 + \rho_{LC}(4.1 + 5.1\ m)]\ 10^{-4} \qquad [4\text{-}9]$$

where m is the moisture content (g water/g-dry wood), and ρ_{LC} is measured in g/cm^3 (Skaar, 1984). The effect of moisture content on the volumetric and thermal properties of wood is exhaustively reviewed by Skaar (1984).

II. Vapor-Phase HF Solvolysis Experiment

The solvolysis of a single lignocellulose chip by an anhydrous HF vapor is dependent on several process variables, including 1) reaction time, 2) HF-N_2 gas stream flowrate, 3) HF-N_2 gas-stream temperature, 4) gas-stream HF partial pressure, and 5) lignocellulose wafer thickness.

The reaction of a single lignocellulose chip with an anhydrous HF vapor stream is carried out within the reactor in the vapor-phase HF solvolysis apparatus. For a given experimental run, constant HF-N_2 gas-stream conditions are maintained, and a series of single lignocellulose chips are reacted with the HF-N_2 gas stream. Each chip is reacted for a given reaction time.

The glucose yield in the water-soluble reaction products (after posthydrolysis) gauges the extent of glucosyl fluoride production and cellulose conversion in each

HF-reacted lignocellulose chip. Thus, the vapor-phase HF solvolysis experiment generates glucose (and xylose) yield data as a function of reaction time, chip size, and HF vapor conditions (reaction rate and sugar yield data).

The reaction rate and sugar yield data obtained from the vapor-phase HF solvolysis experiment are presented and discussed in chapter 6.

A. Vapor-Phase HF Sovolysis Apparatus and Reaction Procedure

The flow diagram of the vapor-phase HF solvolysis apparatus is schematically illustrated in Figure 4.7. The HF vapor mass flowmeter calibration is given in Figure 4.8. The reactor detail is schematically illustrated in Figures 4.9 and 4.10. Photographs describing the operation of the sampling mechanism in operation are provided in Figures 4.11a to 4.11d. A flowsheet summarizing the vapor-phase HF solvolysis and product recovery protocol is presented in Figure 4.12. The range of reactor conditions are provided in Table 4.8.

As mentioned in section I, anhydrous HF vapor is extremely toxic and corrosive. Therefore, the entire apparatus is contained within a fume hood. The apparatus is designed to completely contain the HF vapor within the apparatus even when rapid access to the HF-reacting lignocellulose sample is desired.

Materials of Construction. All HF vapor wetted tubing (1/4 inch O.D.), fittings (Swagelok, Inc.), valves (Whitney, Inc.), and pressure gauges (Matheson Gas Products) are of HF-resistant Monel metal (alloy 400, about 2/3 nickel, 1/3 copper). All valves have KEL-F valve stems. The reactor is constructed of plain-carbon steel, which is suitable for HF vapor service provided water vapor is

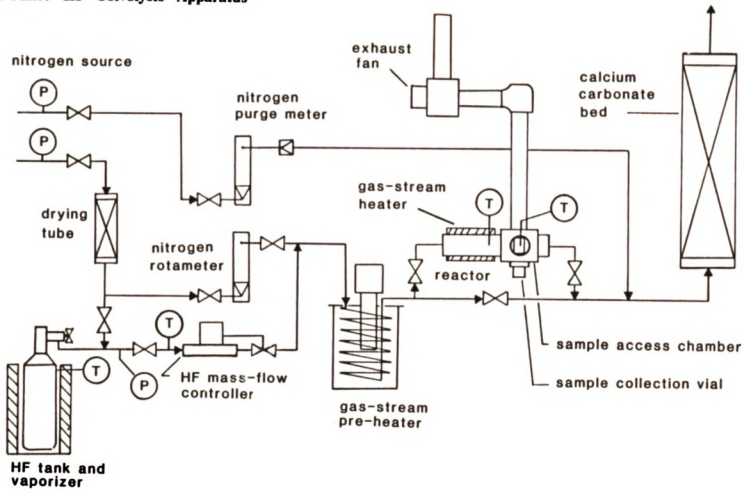


Figure 4.7. Vapor-phase HF solvolysis apparatus: flow diagram.

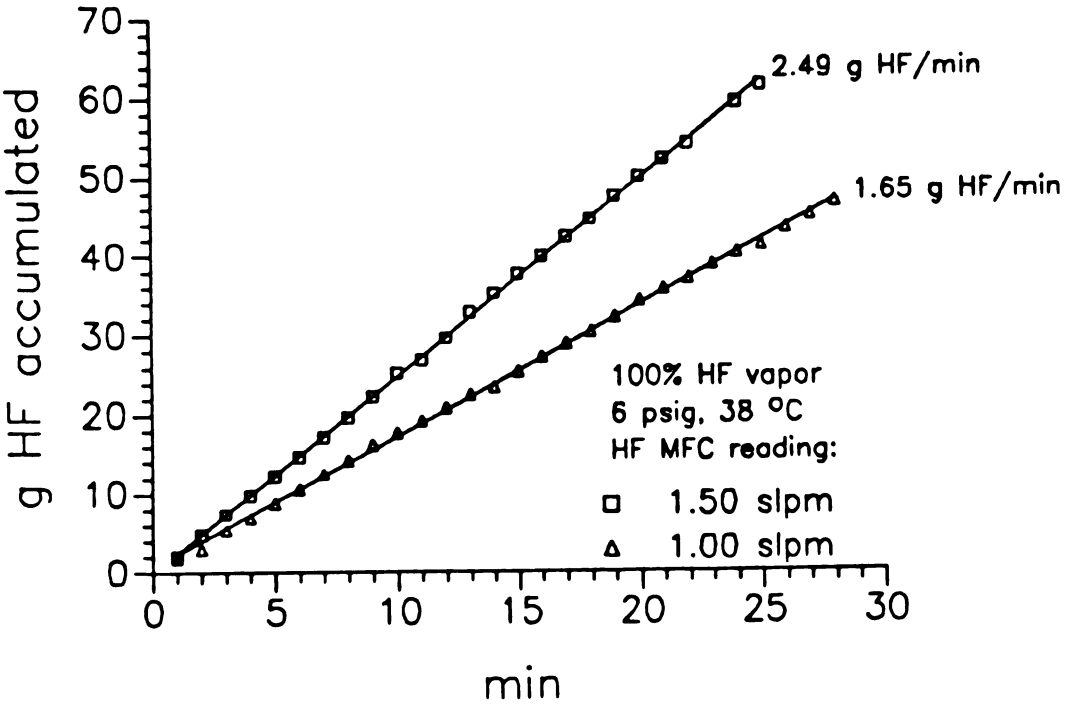
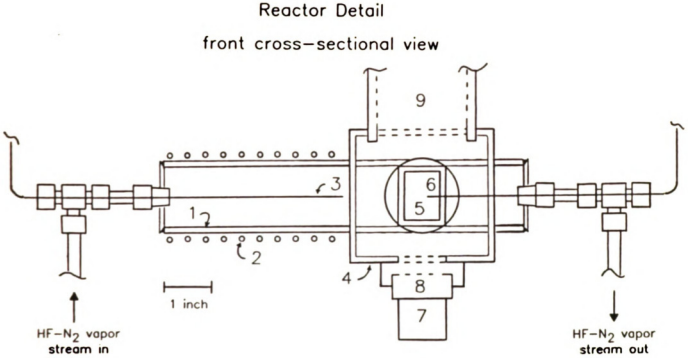


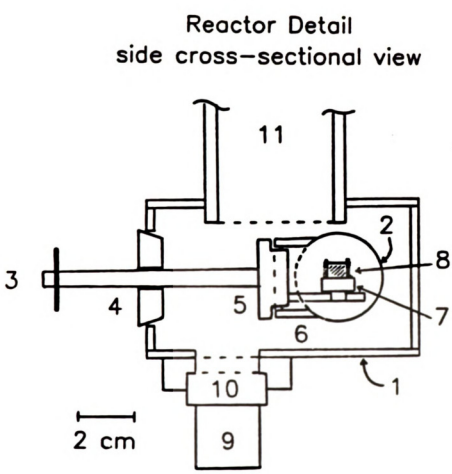
Figure 4.8. Calibration of the Monel mass-flow transducer/controller (Matheson model 8205, HF-MFC) for HF vapor flow. Note: mass-flow transducer/controller setting (F_{MFC}) reads uncalibrated slpm.



Legend:

1 -- Tubular section of reactor running through sample access port
2 -- Heating element (connected to PID temperature controller)
3 -- Thermocouple T1 (connected to PID temperature controller)
4 -- Sample access chamber; Teflon sampling mechanism not shown (see Figure 4.10)
5 -- Sample access port
6 -- Thermocouple T2 (to digital thermometer)
7 -- 15 mL Teflon "Tuf-Tainer" sample collection vial containing 5 mL water (for quenching the reaction products)
8 -- Sample collection vial mount
9 -- Conduit to exhaust fan (schedule-40 2 inch PVC pipe); sucks up HF vapors released during sampling

Figure 4.9. Vapor-phase HF solvolysis apparatus: reactor detail (front cross-sectional view).



Legend:

1 -- Sample access chamber
2 -- Tubular section of reactor running through sample access chamber (conduit for HF vapor at controlled conditions)
3 -- Teflon sampling probe and mechanism
4 -- Re-sealable Teflon plug for sample access chamber
5 -- Re-sealable Teflon plug for sample access port
6 -- Sample access port
7 -- Teflon sample cartridge
8 -- Single wood chip sample propped upright on Teflon sample cartridge
9 -- 15 mL Teflon "Tuf-Tainer" sample collection vial containing 5 mL water
10 -- Sample collection vial mount
11 -- Conduit to exhaust fan (sucks up HF vapors released during sampling)

Figure 4.10. Vapor-phase HF solvolysis apparatus: reactor and sampling mechanism detail (side cross-sectional view).

(a)

(b)

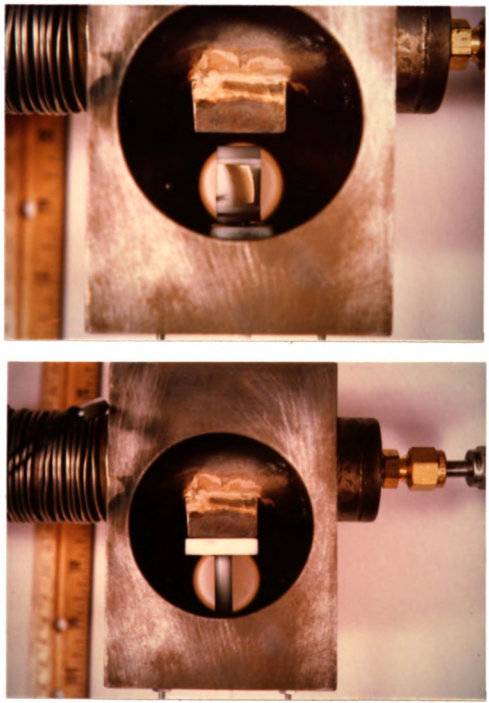
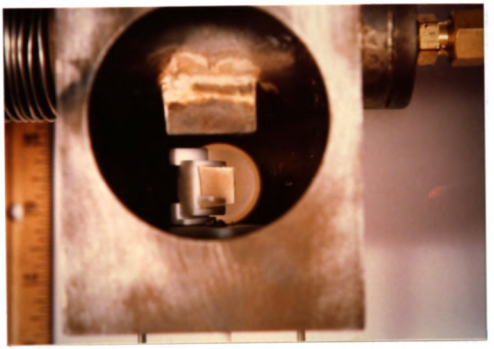


Figure 4.11. Vapor-phase HF solvolysis apparatus: photographs of sampling mechanism operation (top view). (a) Placement of Teflon sampling mechanism in the sample access chamber; (b) insertion of the Teflon sample sample cartridge and lignocellulose wafer into the tubular section of reactor (the tubular section of the reactor is now sealed; polyethylene gasket not shown).

(c)



(d)

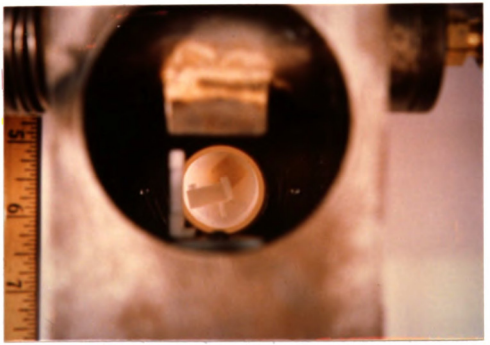
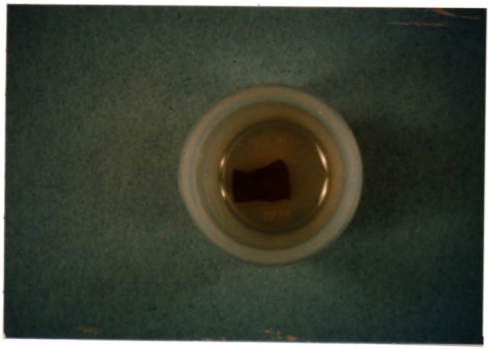


Figure 4.11 (cont'd.). (c) removal of Teflon sample cartridge lignocellulose wafer from the tubular section of the reactor; (d) rotation of the Teflon sampling probe 90^0 drops the Teflon sampling cartridge and lignocellulose wafer into the water-filled sample collection vial.

(e)



(f)

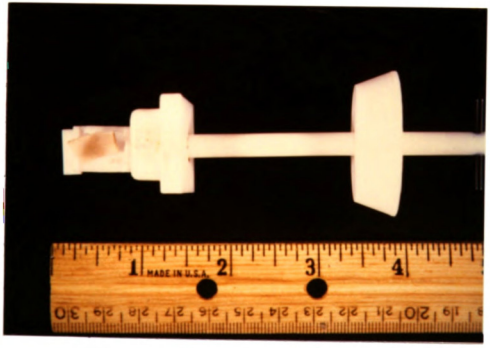


Figure 4.11 (cont'd.). (e) water-quenched reaction products and residual lignin shell; (f) top view of Teflon sampling mechanism and Teflon sample cartridge.

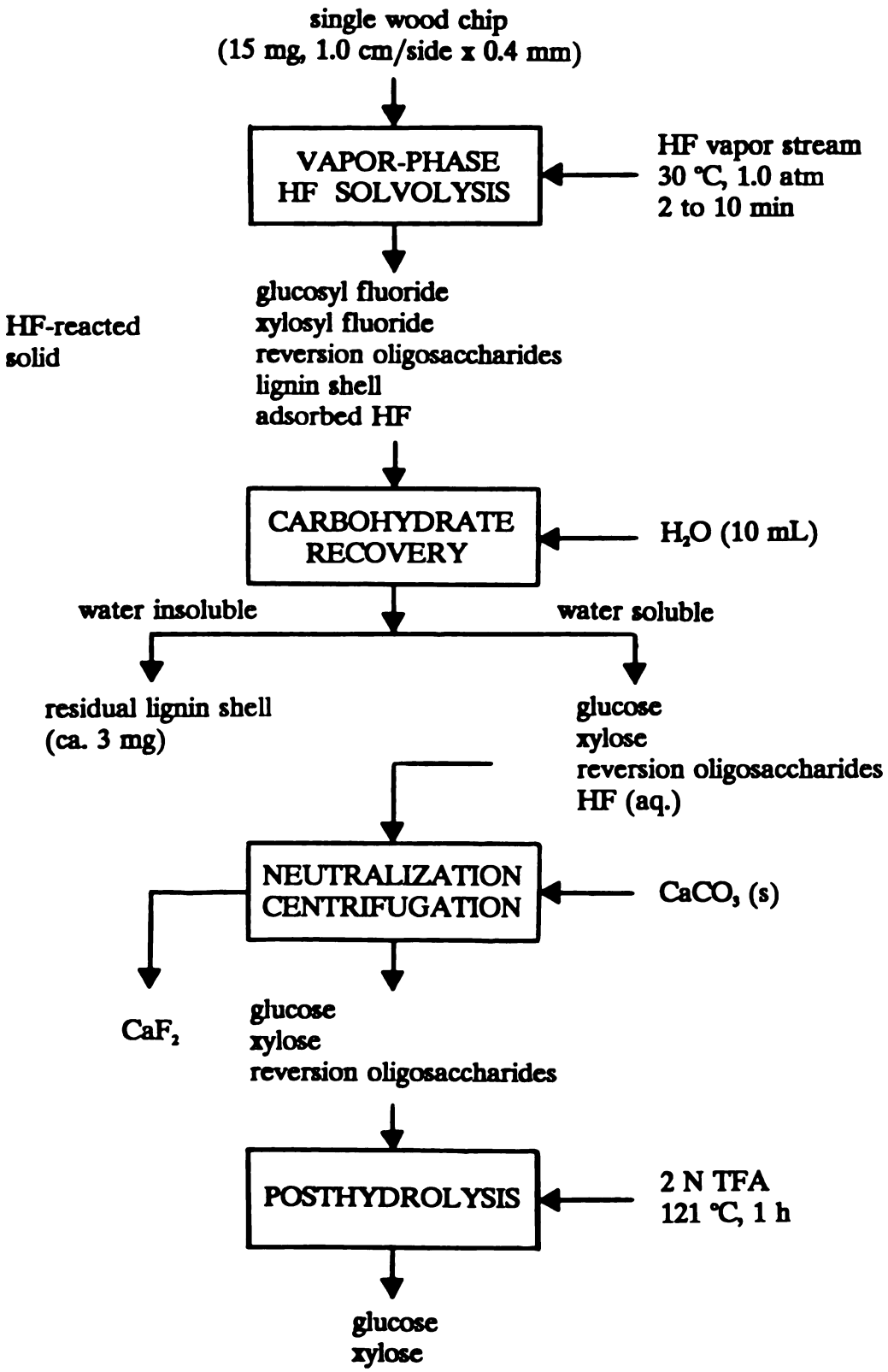


Figure 4.12. Flowsheet: vapor-phase HF solvolysis and product recovery protocol.

Table 4.8. Range of reactor conditions for the vapor-phase HF solvolysis apparatus.

Process Parameter	Variable	Range and Units
HF + N_2 gas-stream temperature in reactor	T_g	30 to 90 °C
HF vapor flowrate through reactor [a]	m_{HF} F_{HF} G_{HF}	0 to 5 g/min 0 to 0.25 mol/min 0 to 0.63 g/cm²-min
N2 diluent flowrate through reactor	m_{N2} F_{N2}	0 to 6.35 g/min 0 - 0.22 mol/min
HF partial pressure in reactor [b]	P_{HF}	0 to 1.0 atm
Total reactor pressure	P_T	1.0 atm
Typical sample size	 2L z m_{LC}	1 wood wafer 0.4 mm thick 1.0 cm/side 15 mg
Maximum sample size		1 wood chip 0.5 cm thick 1.0 cm/side 200 mg

Notes:

[a] Reactor cross-sectional area, A_x = 7.9 cm². Typically, m_{HF} = 1.5 to 3.0 g min.

[b] HF partial pressure, P_{HF}, calculated by equation [6-3]

not present. The tubular portion of the reactor is a 7.5 inch section of 1.25 inch I.D./1.5 inch O.D. ASTM schedule-40 cold-rolled carbon steel pipe. The calcium carbonate bed shell is fabricated from polyvinylchloride (PVC) 6-inch schedule-80 pipe and socket bushings. All socket connections are sealed with PVC cement.

Although the design of the vapor-phase HF solvolysis apparatus is apparent from Figures 4.7 to 4.11, several features merit special description.

HF Vapor Delivery and Flow Control. Anhydrous HF liquid (normal boiling point 19.54 °C) is vaporized directly from the HF cylinder (1600 mL capacity, Matheson Gas Products) by insulated heating tape (2 inch x 6 ft, 900 W) wrapped around the outside of the cylinder. Power input to the heating tape is set by a Variac voltage controller, and is usually set at 5 to 10% of full scale. At this setting, the cylinder skin temperature is maintained at 35 °C, and is monitored by a surface thermocouple. An HF cylinder temperature of 50 °C is the recommended safety limit (Braker and Mossman, 1971). The 30-35 °C HF cylinder temperature provides 1) slow and even HF vapor evolution, and 2) an HF vapor pressure (3 to 10 psig) sufficient for driving HF vapor across the mass flowmeter control valve at a constant rate.

All lines in contact with HF vapor, including the HF vapor mass-flow transducer and control valve, are wrapped with heating cord and heated to about 40 °C, in order to prevent HF vapor condensation.

The HF vapor flowrate is monitored and controlled by a Matheson Instruments model 8205 (0-5 slpm reading) Monel mass-flow transducer, Monel-plated magnetic

control valve, and electronic control box. The HF vapor back-pressure on the control valve is maintained between 3 and 6 psig (throttled by the HF cylinder manual control valve), and the HF vapor inlet temperature is maintained at about 40 °C. The outlet HF vapor stream pressure after the control valve is 1.0 atm. All HF-wetted parts within the mass-flow transducer and control valve are plated with HF-resistant Monel metal.

The transducer is calibrated for HF vapor mass flow by measuring the net weight loss of the HF cylinder as a function of time at a given mass-flow controller setpoint (HF-MFC reading, in uncalibrated slpm). Specifically, during a calibration run, the HF cylinder is mounted an electronic balance (Sartorius model 3808, 30 kg, 0.1 g resolution) and weighed continuously. From these measurements, the grams of HF vapor through the reactor are determined as a function of time (Figure 4.8), and from the least-squares slope of this data, the HF vapor mass flowrate (g HF/min) is calculated. As shown in Figure 4.8, the response of the HF mass-flow transducer is linear. The mass flowrate of HF vapor ($m_{HF,g}$) is calculated at a given mass-flow controller setting by

$$m_{HF,g} = 1.65 \text{ g HF/min} \times F_{MFC} \text{ [slpm]} \qquad [4\text{-}10a]$$

where F_{MFC} is the mass-flow controller reading (in uncalibrated [slpm]; 1.00 slpm = 1.65 g HF/min). The molar flowrate of HF vapor (F_{HF}, mol HF/min, based on monomeric HF) is calculated by

$$F_{HF} = m_{HF,g}/M_{w,HF} \qquad [4\text{-}10b]$$

where $M_{w,HF}$ is the molecular weight of the HF monomer (20 g/mol). If no N_2 diluent gas is used, the 100% HF vapor superficial mass velocity (G_{HF}) in the reactor is calculated by

$$G_{HF} = m_{HF,g}/A_x \qquad [4\text{-}11]$$

where A_x is the cross-sectional area of the tubular section of reactor (for 1.25 inch I.D., A_x = 7.9 cm^2). At a 100% HF vapor mass flowrate of 1.65 g/min, the Reynold's number in the tubular section of the reactor is 728 at T_g = 30 °C.

If a N_2 diluent gas is used, the N_2 gas is mixed with the HF vapor stream before being fed into the reactor. The N_2 diluent gas flowrate (F_{N2}, slpm or mol/min) is easily determined from the calibration chart provided with the N_2 gas flowmeter (Matheson variable-area flowmeter, model 603 flowtube (150 mm), glass float, 0 to 2550 cc/min air at 1.0 atm, 21 °C).

The water bath (40 °C) preheats the mixed HF-N_2 gas-stream. The mixed HF-N_2 gas stream enters the reactor at about 30 °C. The preheating is needed because the heat of dilution of HF vapor in inert N_2 gas is endothermic (see HF properties, section I).

<u>HF-N_2 Gas-Stream Temperature Control</u>. The HF-N_2 gas-stream temperature within the tubular portion of the reactor is heated to the desired reaction temperature by a 300 W heating coil (316 stainless-steel sheath of 1/16 inch diameter by 6 ft. straight length). The heating coil is wrapped around the outside of the tubular section of the reactor, so that corrosion of the heating coil by HF

vapor is prevented. Power input to the heating coil is provided by a Barber-Coleman model 580A PID temperature controller.

The HF-N_2 gas-stream temperature in the reactor is measured two by Omega Engineering type-J Inconel-sheathed thermocouples (1/16 inch diameter x 12 inch length). The thermocouple on the left-hand side of the reactor (T1, see Figure 4.9) is aligned along the axial centerline of the reactor tube, with the tip positioned at the end of the heated zone, which is about 4 cm from the sample access port. Thermocouple T1 is interfaced to the Barber-Coleman PID (proportional-integral-derivative) temperature controller. The thermocouple on the right-hand side of the reactor (T2) is also aligned along the axial centerline of the reactor tube, with the tip positioned about 0.5 to 1.0 cm behind the HF-reacting lignocellulose chip. Thermocouple T2 is separately interfaced to a Omega model 660 digital thermometer. This thermocouple measures the HF-N_2 gas-stream temperature experienced by the single HF-reacting lignocellulose chip.

The two-thermocouple arrangement is needed for steady HF-N_2 gas-stream temperature control. Since T1 is positioned upstream of the sample access port, HF-N_2 gas-stream temperature transients during sampling are not measured by T1, and hence the temperature controller does not have to respond to these temperature transients induced by sampling. The HF-N_2 gas-stream temperature at T1 is usually constant to within +/- 1 ^{o}C of setpoint. Since a small HF-N_2 gas-stream temperature drop occurs from thermocouple T1 position to the thermocouple T2 position, T2 is calibrated as a function of T1 at a given HF vapor

(or HF-N_2 gas-stream) flowrate. The T1 setpoint temperature is set to provide the desired HF-N_2 gas-stream temperature measured at T2.

Reactor Detail and Sampling Mechanism. The solvolysis of a single lignocellulose sample to solid sugar fluorides, reversion oligomers, and residual lignin by an anhydrous HF vapor stream is carried out within the reactor of the vapor-phase HF solvolysis apparatus (Figures 4.9 to 4.11). Specifically, within the tubular portion of the reactor, a single lignocellulose sample is exposed to an HF-N2 gas stream of precisely controlled HF vapor flowrate, N_2 diluent flowrate, and HF-N_2 gas stream temperature for a given reaction time. The relative HF and N2 flowrates set the gas-phase HF concentration in the reactor. Total pressure in the reactor is always 1.0 atm. The complete range of reactor operating conditions are summarized in Table 4.8.

The Teflon sampling mechanism, inserted in the reactor, is schematically illustrated in Figure 4.10. The Teflon sampling mechanism inserts a single lignocellulose wafer into the tubular section of the reactor, rapidly retrieves the HF-reacted wafer from the tubular section of the reactor, and then quenches the HF-reacted wafer in water in order to stop the reaction. As shown in Figure 4.10, the sample access chamber contains the Teflon sampling mechanism and sample access port. The lignocellulose wafer (typically 15 mg) rests on the Teflon sample cartridge. The Teflon sample cartridge rests on the tip of the sampling probe. If the sample dissolves or loses its shape during reaction (as is the case with filter paper experiments), then the reaction products are collected in the trough of the

Teflon sample cartridge.

When the Teflon sampling mechanism is inserted into the tubular portion of the reactor (see Figures 4.11a, 4.11b), a Teflon plug (with polyethylene gasket not shown) mounted at the base of the sampling probe seals the reactor at the sample access port. The sample cartridge and lignocellulose wafer are now inserted within the tubular portion of the reactor. After a given reaction time, the sampling probe is unplugged and rotated one-half turn (see Figures 4.11c, 4.11d). The HF-reacted wafer and Teflon sample cartridge are deposited into a 15 mL Teflon "Tuf-Tainer" vial (Pierce Chemical) screwed into the base of the sample access chamber. Total time for sample removal and quenching is about 1 second. This vial contains 5.00 mL deionized/distilled water and a known inclusion of vacuum-dried myo-inositol (typically 6.00 mg), an internal standard.

The water immediately quenches the reaction by dissolving the adsorbed HF and sugar products away from the HF-reacted wafer. The known amount of myo-inositol in the product solution internally references the amount of sugar product in the product solution, i.e. the glucose/myo-inositol ratio is fixed. Thus, the myo-inositol internal standard can compensate for product solution dilution, losses, or aliquots. The "internal standard" method is then used for later quantification of the sugar products by High-Performance Liquid Chromatography.

HF disposal. During sampling, the seal between the tubular portion of the reactor and the sampling mechanism at the sample access port is momentarily broken. An exhaust blower (Dayton model 4C005, 1/25 hp) plumbed into the

sample access chamber sucks up the fugative HF-vapors and vents them to the fume-hood exhaust (see Figures 4.7 and 4.10).

In normal operation, the reactor effluent HF vapor stream is passed through a 8 kg bed of dry calcium carbonate chips (Frank's Trims marble chips, crushed to 1 to 2 cm mesh). The calcium carbonate ($CaCO_3$) neutralizes the HF vapor to calcium fluoride (CaF_2, solid), water, and carbon dioxide gas (CO_2). By reaction stoichiometry, 4 kg calcium carbonate chips are sufficient to neutralize 1600 mL liquid HF. Usually, the calcium carbonate bed is recharged with fresh calcium carbonate chips whenever the HF cylinder (1600 mL capacity) is changed. The gas stream exiting the bed is vented to the fume hood exhaust. Extreme caution must be exercised when recharging the $CaCO_3$ bed. Adsorbed HF trapped in the $CaCO_3$ chips or adsorbed in the water released during neutralization can flash off the bed when the sealed bed vessel is opened.

This laboratory experiment does not attempt to recycle or reuse HF.

Summary Reaction Procedure. Dried lignocellulose wafers (1.0 cm/side, 0.4 mm thick, 15 mg) were weighed to precision of 0.1 mg. The HF cylinder was slowly heated to constant skin temperature of 35 °C. A preheating time of 2 h was sufficient. The HF vapor flowrate, N_2 flowrate, and HF-N_2 gas-stream temperature in the reactor were set and allowed to stabilize.

A single lignocellulose sample was then loaded into the reactor via the Teflon sampling mechanism described previously. After a specified reaction time (typically 30 sec to 10 min), the HF-reacted solid was removed from the reactor by

the Teflon sampling mechanism and quenched in water in order to stop the reaction. The Teflon sample cartridge was washed with an additional 5.00 mL deionized/distilled water (washings added to reaction products) and then carefully dried with a cotton swab before reloading.

The reaction procedure was repeated with a new lignocellulose chip for the desired reaction time and HF vapor conditions until a series of single HF-reacted lignocellulose chips were obtained.

Shut Down. At the end of a series of reactions, the HF vapor flow was turned off and the apparatus flow system, including the HF mass-flow controller, was flushed thoroughly with N_2 gas at 2.00 L/min for at least 30 min. The HF tank heater, HF line heaters, and reactor heater were also shut off. Finally, the $CaCO_3$ bed was purged with N_2 gas at 20 L/min for 2 h.

Safety Precautions. Anhydrous HF is both toxic and corrosive. The vapor-phase HF solvolysis apparatus must be located within a fume hood. The HF vapors must be contained within the apparatus. Protective garments, including full face shield, elbow-length impermeable gloves (Viton, Neoprene, or PVC), and labcoat must be worn during all experimental work with HF. All personnel working with HF must be acquainted with HF toxicity levels, safe HF handling procedures, and first-aid in the event of direct exposure to HF via inhalation or skin contact. The "HF Safety" information is detailed in Appendix C.

B. Reaction Product Recovery and Sugar Analysis

Water-Soluble Carbohydrate and Residual Lignin Recovery. When the HF-reacted sample was quenched in water, sugar fluorides and oligomers dissolved from the HF-reacted sample and left behind a water-insoluble lignin residue. Any HF physically adsorbed on the HF-reacted sample also dissolved. The dissolved HF made the product solution weakly acidic (pH 2 to 3).

Although glucosyl fluoride is stable in water at pH 7, it rapidly hydrolyzes to free glucose and generates HF in mildly-acidic aqueous solution at ambient temperature (Barnett, 1969). Therefore, glucosyl fluoride in the (acidic) product solution hydrolyzes to glucose. Thus, free glucosyl fluoride in the HF-reacted lignocellulose chip is quantified as glucose in the water-soluble reaction products. Total glucosyl fluoride production in the HF-reacted lignocellulose chip (glucosyl fluoride plus "reversion" oligosaccharides) is quantified as glucose in the water-soluble reaction products after posthydrolysis.

The residual lignin shell (brown in color) was removed from the water-soluble products, rinsed thoroughly and gently with deionized/distilled water, and then oven-dried at 80 °C and weighed. This residual lignin shell was flaccid and easily fragmented, and so was handled carefully with tweezers.

Aqueous HF Neutralization. Calcium carbonate powder ($CaCO_3$) was added incrementally (10 to 20 mg) to the water-soluble product solution. Upon addition of the $CaCO_3$ powder, the solution fizzed. The calcium carbonate reacted with the dissolved HF to form a calcium fluoride precipitate, CaF_2 (s), CO_2 gas, and

water. The neutralized sugar product solution (pH 5 to 7) was then centrifuged (4000 rpm x 5 min), decanted from the insoluble calcium carbonate and calcium fluoride, syringe-filtered through a 0.45 μm filter, and frozen for storage.

Posthydrolysis. During the liquid-phase HF solvolysis of lignocellulose, glucosyl fluoride and other sugar fluorides products repolymerize to short-chain, water-soluble reversion oligosaccharides in temperature and concentration dependent equilibrium. (Rogovin and Pogosov, 1959; Defaye et al., 1982, 1983; Franz et al., 1987; Hardt and Lamport, 1982b).

Glucosyl fluoride repolymerization also occurs during vapor-phase HF solvolysis of lignocellulose. In order to recover the parent glucose (and other monomer sugars) from these reversion oligosaccharides, the water-soluble products were hydrolyzed in dilute acid under mild conditions. Specifically, a 100 μL aliquot of the water-soluble product solution (typically containing 0 to 100 μg each sugar) was blown down to dryness over flowing N_2 gas at 50 °C, and then hydrolyzed in 200 μL of 2 N trifluoroacetic acid (TFA) for 1 h at 121 °C within a septum-sealed 1.0 mL conical glass "reacti vial" (Pierce Chemical), which was heated in a dry heating block (half-depth holes, 13 mm diameter). These hydrolysis conditions were sufficient to hydrolyze sugar fluorides and reversion oligomers to monomer sugars with negligible sugar dehydration (Fengel et al., 1977). The hydrolyzed sample was then blown down to dryness over a N_2 gas stream at 50 °C in order to evaporate the volatile TFA (boiling point 72.4 °C). The dry sample was then redissolved in 20 μL to 50 μL of degassed HPLC-grade water and vortexed prior to sugar analysis

by High-Performance Liquid Chromatography (HPLC).

A minor amount of sugar degradation occurred during 2 N TFA posthydrolysis at 121 °C for 1 h. The post-hydrolysis correction factor $K_{f,s}$ is defined as

$K_{f,s}$ = g sugar before posthydrolysis/g sugar after posthydrolysis [4-13]

The K_f's for glucose and xylose were determined by control experiments wherein 160 μg glucose, 140 μg xylose, and 160 μg myo-inositol (internal standard) were reacted in 200 μL of 2 N TFA at 121 °C for 1 h. Results: $K_{f,s}$ = 1.03 for glucose, $K_{f,x}$ = 1.14 for xylose (average of five assays). Minor sugar degradation during 2 N TFA hydrolysis at 121 °C is quantified in detail by De Ruiter and Burns (1986).

Sugar Yield Assay by HPLC. Glucose and xylose yields in the water-soluble reaction products (after posthydrolysis) were assayed by High-Performance Liquid Chromatography (HPLC). A Spectra-Physics isocratic HPLC system, consisting of a SP8810 precision isocratic pump, Rheodyne 7125 injector (20 μL sample loop), SP8790 column heater/controller, and SP6040 differential refractive index (RI) detector was used for carbohydrate analysis by HPLC. Refer to Figure 4.13 for a schematic of the carbohydrate HPLC system.

Glucose, xylose, mannose and myo-inositol (the internal standard) were separated on a BIO-RAD Laboratories HPX-87P monosaccharide analysis HPLC column. The 20 μL assay sample (see posthydrolysis) was injected directly onto the column (via the injector) without derivatization. A BIO-RAD Laboratories "Microguard" deashing column (1 anion, 1 cation exchange cartridge) is plumbed

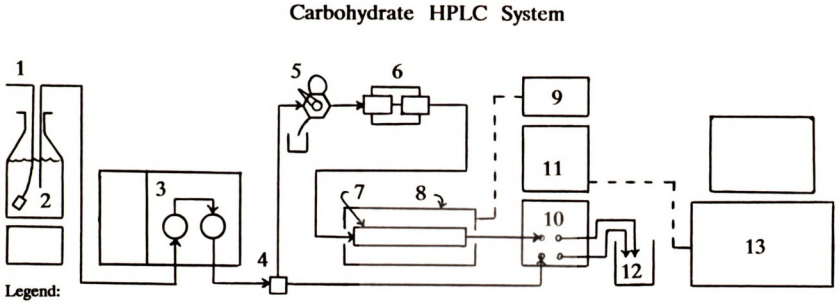


Figure 4.13. Schematic of the High-Performance Liquid Chromatograph (HPLC) for carbohydrate analysis.

in front of the analysis column to remove and particulates or residual acid (TFA) present in the 20 μL injection sample. The column mobile phase was degassed HPLC-grade water at 0.6 mL/min, and the column temperature was isothermally maintained at 85 °C by the column oven. Column effluent sugars were detected by differential refractive index (RI) with respect to water.

The yield (Y_s) of each sugar in the water-soluble reaction products after posthydrolysis (e.g. μmol glucose recovered/mg-dry wood) was determined by the "internal standard" method:

$$Y_s = \frac{A_s \, R_{F,I} \, w_I}{A_I \, R_{F,s} \, w_o} \, C \, K_{f,s} \qquad [4\text{-}14]$$

where A_s is the peak area of a given sugar (μV-sec per 20 μL sample injected), A_I is the peak area of the myo-inositol internal standard (μV-sec per 20 μL sample injected), C is a units conversion factor (e.g. for μmol glucose/mg-wood, C = 5.556 μmol myo-inositol/mg myo-insoitol), $K_{f,s}$ is the posthydrolysis correction factor (see equation [4-13]), $R_{F,s}$ is the detector response factor for a given sugar (μV-sec/μmol), $R_{F,I}$ is the detector response factor for the myo-inositol internal standard (μV-sec/μmol), w_I is the amount of the myo-inositol internal standard (mg) in the Teflon reaction vial and w_o is the dry weight of the lignocellulose chip before reaction (mg).

It is important to recognize that equation [4-14] calculates the water-soluble sugar yield obtained from the whole HF-reacted lignocellulose chip. The sugar yield, Y_s (or Y_g for glucose), is usually rescaled to more convenient units, for

example, g glucose/g-dry wood or mmol glucose/g-dry wood.

Sample HPLC chromatograms of the water-soluble sugar reaction products (after posthydrolysis) obtained from the vapor-phase HF solvolysis of Bigtooth Aspen wood, prehydrolyzed Bigtooth Aspen wood, and pure cellulose (filter paper) are presented in Figures 4.14, 4.15, and 4.16 respectively. Typical sugar retention times and detector response factors are given in Table 4.9. Analysis of wood sugars by carbohydrate HPLC is also described by Pettersen (1984a).

III. Gravimetric HF Adsorption Experiment

The flow diagram for the milligram-scale gravimetric HF adsorption apparatus is schematically illustrated in Figure 4.17a, and the reactor detail is schematically illustrated in Figure 4.17b. This apparatus measures the in situ gravimetric uptake of HF vapor onto a single wood chip as a function of time and HF-N_2 gas-stream conditions of flowrate, HF partial pressure, and temperature. HF adsorption/ desorption data from this experiment are presented and discussed in chapter 5.

A description of the gravimetric HF adsorption apparatus is provided in the following paragraphs. A more comprehensive description is provided by Mohring (1987).

As with the vapor-phase HF solvolysis apparatus, the gravimetric HF desorption apparatus is contained within a fume hood. The apparatus contains the HF vapors within a closed system. All HF vapor-wetted tubing (1.4 inch O.D.), fittings (Swagelok, Inc.), and valves (Whitney, Inc.) are constructed of HF-resistant

Table 4.9. Typical retention times and response factors for monosaccharide analysis via HPLC (see notes [a] to [d]).

Sugar	M_w	Retention Time (min)	Response Factor, $R_{F,s}$ (μV-sec/μmol injected) +/- 1s (n=11)
α-D-glucose	180	13.00 +/- 0.10	1.546 x 10^6 +/- 7.281 x 10^4
α-D-xylose	150	14.20 +/ 0.10	1.218 x 10^6 +/- 6.165 x 10^4
α-D-mannose	180	17.10	1.52 x 10^6
myo-inositol [e]	180	22.30 +/- 0.10	1.721 x 10^6 +/- 8.236 x 10^4

Notes:

[a] Column: BIO-RAD HPX-87P monosaccharide analysis HPLC column, 30 x 7.8 mm, 8% cross-linked resin in lead form. BIO-RAD "Microguard" column, with one cation-exchange and one anion-exchange cartridge (in series).

[b] Column operating conditions:
mobile phase of 0.6 mL/min HPLC-grade degassed H_2O (isocratic),
85 °C column temperature (isothermal),
400 psi pressure drop (including gaurd column).

[c] Detection: differential refractive index (RI) with respect to respect to H_2O reference, thermostated 10 μL flow cell at 40 °C. Range = 16x (16 x 10^{-6} RIU/10 mV).

[d] Sample: aqueous monosaccharides, 50-100 μg loading in 20 μL injection volume, pH-neutral, particulate-free.

[e] Myo-inositol is the internal standard.
Ratio response factors (+/- 1s):
$R_{F,I}/R_{F,g}$ = 1.113 +/- 0.014, $R_{F,I}/R_{F,x}$ = 1.413 +/- 0.017.

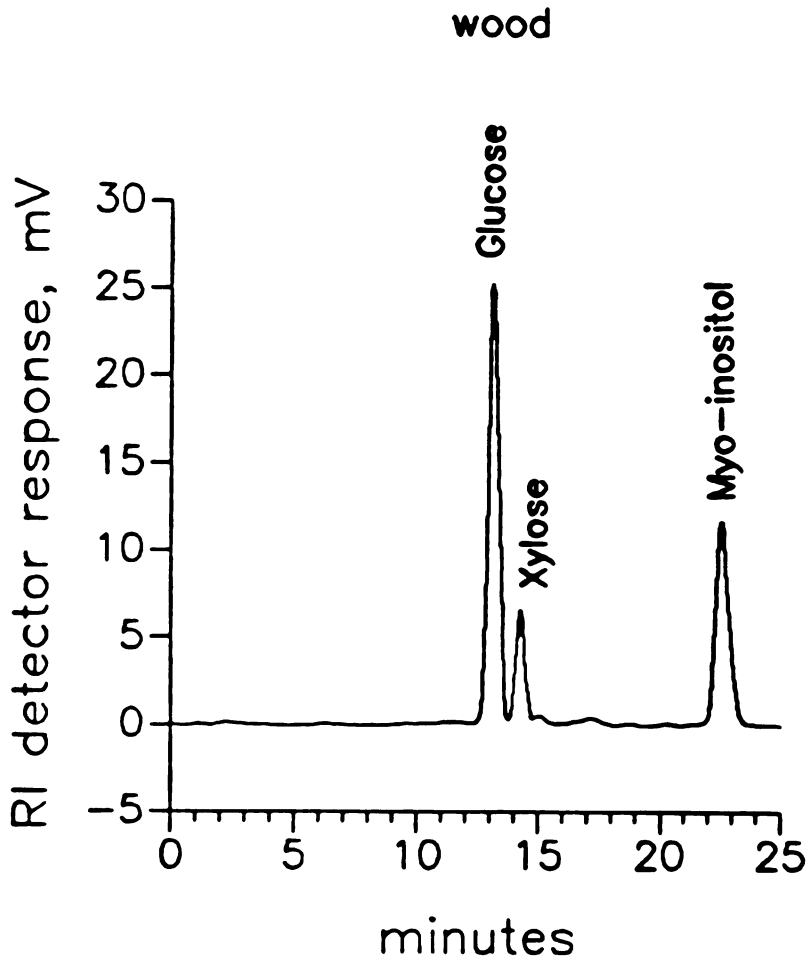


Figure 4.14. HPLC chromatogram of the water-soluble sugar products (after posthydrolysis) obtained from the vapor-phase HF solvolysis of Bigtooth Aspen wood. Column loading: 100 μg glucose; see Table 4.9 for column and operating conditions.

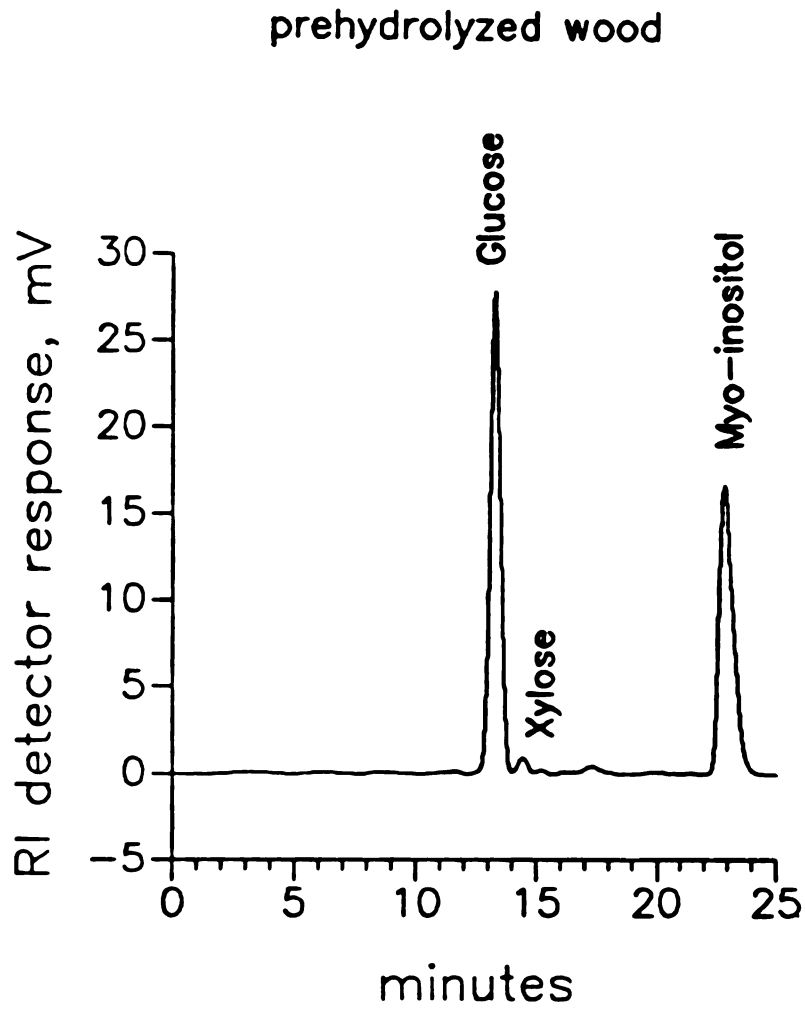


Figure 4.15. HPLC chromatogram of the water-soluble sugar products (after posthydrolysis) obtained from the vapor-phase HF solvolysis of prehydrolyzed Bigtooth Aspen wood. Column loading: 100 μg glucose; see Table 4.9 for column and operating conditions.

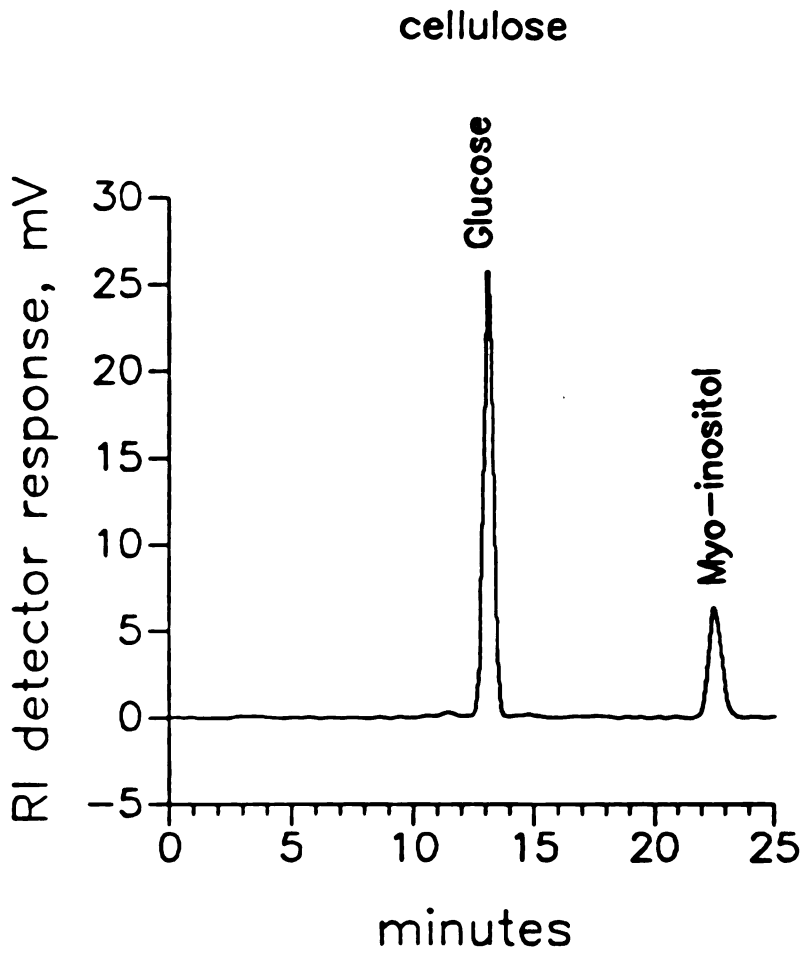
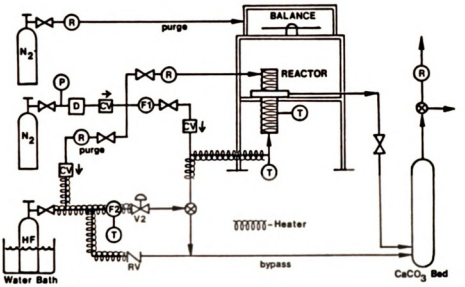


Figure 4.16. HPLC chromatogram of the water-soluble sugar products (after posthydrolysis) obtained from the vapor-phase HF solvolysis of pure cellulose (filter paper). Column loading: 100 μg glucose; see Table 4.9 for column and operating conditions.

Gravimetric HF adsorption Apparatus

(a) Flow Diagram



(b) Reactor Detail

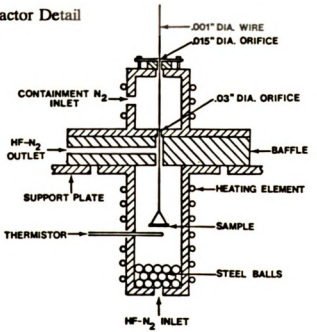


Figure 4.17. Gravimetric HF adsorption apparatus: (a) flow diagram; (b) reactor detail.

Monel (alloy 400) metal. The reactor is fabricated from 304 stainless steel, and the calcium carbonate bed shell is fabricated from 6 inch schedule-80 PVC pipe and flanges.

HF Vapor Delivery and Control. HF is vaporized from a steel cylinder of anhydrous HF liquid (1600 mL capacity of liquid HF, 99.9% purity, Matheson Gas Products). The tank is held in a water bath maintained at 24 °C (slightly above 19.54 °C, the normal boiling point of HF), to provide 2 psig of HF vapor pressure for driving and maintaining HF flow across the HF mass flow control valve.

The HF vapor flow is metered and controlled by a Monel mass-flow transducer, Monel-plated magnetic control valve, and electronic control box (Matheson model 8210, 0-3 slpm reading). The mass flow transducer is calibrated for HF vapor mass flow by measuring the change in weight of the HF tank for a given time at a given flow setting, as described earlier for the vapor-phase HF solvolysis apparatus. The N_2 diluent gas is dried by passage through a molecular-seive bed. The N_2 gas flowrate is metered by a stainless-steel mass-flow transducer (Matheson model 8141, 0-3 slpm range), and controlled by a manual metering valve. All HF vapor lines are heated with heating cord in order to prevent HF condensation. The gas-stream HF concentration in the reactor is determined from the HF and N_2 inlet molar flowrates.

The mixed HF-N_2 gas stream is preheated to the reactor temperature before being fed into the reactor. Temperature control for preheating is provided by a PID temperature controller and stainless-steel sheathed 1/8 inch diameter

thermocouple (type T) inserted in the HF-N_2 reactor feed line.

Reactor Detail. The reactor shown in Figure 4.17b is a novel design adapted from Costa and Smith (1971). The reactor shell is constructed of 1.5 inch I.D. section of schedule-40 304 stainless-steel pipe. The top and bottom ends are flanged to permit sample replacement.

A sample holder containing a single wood chip is suspended within the lower chamber of the reactor by a 0.001 in. diameter Chromel wire connected to a Cahn 2000 electrobalance positioned above the reactor. Within the sample holder, the wood chip is sandwiched between a folded-over, Teflon-coated Monel screen which contains the reaction products and keeps the wood chip aligned perpendicular to the HF-N_2 gas stream. The hang wire is threaded through two orifices which tapped through top and bottom ends of the upper chamber of the reactor. The electrobalance/reactor stand aligns the electrobalance and reactor so that the hang-wire does not contact the walls of the orifices.

The upper chamber of the reactor contains the HF vapors within the lower chamber and prevents HF from leaking out of the hang-wire orifices. A low flowrate (100 mL/min) of N_2 gas is fed into the upper chamber of the reactor. This N_2 gas flow slightly pressurizes the the upper chamber, due to the pressure drop through the upper and lower orifices. This pressurization prevents HF vapors in the lower chamber of the reactor from escaping the apparatus through the hang-wire orifice. Pressure in the lower chamber of the reactor is 1.0 atm.

The temperature in the lower chamber of the reactor is maintained within 1 °C of setpoint by an electrical resistance heater wrapped around the outside of the reactor. Power input to the heater is controlled by a proportional temperature controller (OMEGA model 49) and Teflon-coated thermistor probe positioned 1.0 cm below the sample. The gas-stream temperature measured by the thermistor is assumed to be the gas-stream temperature contacting the wood chip.

The electrobalance housing is purged continuously with N_2 gas. This prevents any fugative HF vapors from damaging the electromechanical mechanism of the balance.

HF Disposal. The reactor effluent HF-N_2 gas stream is passed through a bed containing calcium carbonate chips (about 8 kg, 1-2 cm mesh). The calcium carbonate neutralizes HF in the reactor effluent gas stream to calcium fluoride, carbon dioxide, and water. The gas-stream exiting the bed is vented to the fume hood exhaust. This experiment does not attempt to recover or reuse HF.

Safety Precautions. The safety precautions for HF handling with the gravimetric HF adsorption apparatus are identical to those described for the vapor-phase HF solvolysis apparatus. The "HF Safety" information is detailed in Appendix C.

Measurement of Equilibrium HF Adsorption Isotherms. A single wood chip (1.0 cm/side, 0.5 mm thick, 20 mg, or 1.0 cm/side, 0.2 cm thick, 80 mg) was placed onto the tared sample holder and weighed to precision of 0.1 mg. The reactor was then heated to 100 °C with dry N_2 at 1.00 L/min for 30 min in order to dry

the wood chip. After the wood chip was dried to constant weight (<1% moisture content), the reactor setpoint temperature was set, and the reactor temperature (under 1.00 L/min N_2 flow) was allowed to stabilize around the setpoint. At this time the HF cylinder bath heater, HF line heater, and reactor pre-heater temperatures were set, and the entire apparatus was allowed to warm up for 30 min. The N_2 diluent gas flowrate was then reset to the desired value for the experiment, and the HF vapor flow setpoint was set to the desired value for the experiment. The HF tank was then opened to introduce HF vapor into the apparatus. HF vapor was metered and controlled by the HF mass-flow transducer/controller, mixed with N_2 gas, and fed into the reactor.

At constant HF-N_2 gas stream temperature, the HF:N_2 flowrate ratio was incrementally increased. Usually, the calibrated HF vapor mass flowrate was kept fixed at 0.20 or 0.81 g HF/min. The increased HF:N_2 flowrate ratio increased the HF partial pressure in the reactor. After each gas-stream HF partial pressure increase, the HF-adsorbed/reacted sample weight (wood chip plus adsorbed HF) increased and was allowed to stabilize to a constant (equilibrium) weight. This constant weight was maintained for at least 5 min. Sample weight measurements (mg), HF-N_2 gas-stream temperature measurements (^{o}C), HF mass-flow transducer readings (uncalibrated slpm), and N_2 gas mass-flow transducer readings (calibrated slpm) were captured online as a function of time by an IBM PC/XT computer equipped with Data Translation PC-THERM analog data acquisition board and software (for a listing of the data acquisition program, see Mohring, 1987).

The HF loading (θ, mg HF adsorbed/mg-dry wood, or g HF adsorbed/g-dry wood) on the single wood chip was calculated by

$$\theta = [w_s - w_{c1} - w_{c2}]/w_o \qquad [4\text{-}15]$$

where w_s is the weight of the wood chip plus adsorbed HF (mg), w_o is the dry weight of the wood chip before reaction, w_{c1} is the correction for the electrobalance control unit and/or computer data acquisition offset (mg), and w_{c2} is the weight correction for physical adsorption of HF on the sample holder and gas-stream drag on the sample holder (mg).

Shut Down. The HF-adsorbed wood chip is desorbed under flowing N2 gas at 1.00 L/min for at least 1 h at 80 °C to desorb HF from the HF-reacted solid and purge the apparatus.

IV. Miscellaneous Experimental Design

Specimen Preparation for Light Microphotography. The vapor-phase HF solvolysis experiment generates an anatomically-intact residual lignin framework free of polysaccharides. A technique for preparation of the residual lignin framework for visualization by light microscopy is briefly described here.

In general, the framework of the whole HF-reacted lignocellulose wafer is best preserved if the equilibrium HF loading on the sample is between 0.4 and 1.0 g HF/g dry wood. Higher equilibrium HF loadings tend to disintegrate or break apart the lignocellulose chip. For example, after solvolysis of wood by 100% HF

vapor at 30 °C and 1.0 atm (HF loading 1.5 g HF/g wood), the HF-reacted lignocellulose particle is easily broken into several fragments. In general, for preparation of an intact residual lignin framework of the whole HF-reacted wafer, HF-N_2 gas-stream reaction conditions of P_{HF} = 0.6 atm (1.5:1 HF/N_2 molar flow ratio) at 30 °C, or 100% HF vapor at 50 °C and 1.0 atm are most suitable.

The water-soluble reaction products are washed from the HF-reacted lignocellulose wafer. A 2 mm x 2 mm specimen is cut from the residual lignin shell. The specimen is solvent-dried in 1.0 mL acetone/1% 2,2-DMP for 24 h. The acetone is decanted, and the specimen is impregnated with 1.0 mL 1:1 v/v dry acetone/"spurrs" resin (22.5% wt.% or vol.% vinyl cyclohexane dioxide, 18.0% diglycidyl ether of propylene glycol, 56.6% nonenyl succinic anhydride, and 0.9% dimethylaminoethanol) for 24 h at room temperature under slow wrist-action shaking. The impregnation procedure is repeated with 1.0 mL 2:1 v/v dry acetone/ "spurrs" resin, 1.0 mL 3:1 v/v dry acetone/ "spurrs" resin, and finally, 1.0 mL "spurrs" resin. The specimen and resin are then poured into a casting mold, and the "spurrs" resin is cured in the casting mold within a vacuum oven at 60 °C for 24 h. Several 2 μm thick cross-sections are sliced from the imbedded specimen using a glass-blade mechanical ultramicrotome. The sections are stained successively with methylene blue and basic fuchsin (lignin - blue/purple, cellulose - red/pink) and visualized directly via light microscopy.

Sample light micrographs (200x) of the native lignocellulosic matrix, partially HF-reacted lignocellulosic matrix, and HF-reacted residual lignin shell are presented

in Figures 8.5a to 8.5d.

In related previous work, Sachs et al. (1963) used aqueous Hydrogen Fluoride (5 to 80% wt.) to dissolve polysaccharides away from the lignocellulosic matrix of pine wood. Sachs then observed the lignin distribution in the residual lignin framework by electron microscopy.

Solid Residue Analysis. Refer to chapter 6, section III.

HPLC-Oligosaccharide Profiling. Refer to chapter 6, section IV.

Particle Temperature Measurement. Refer to chapter 7, section I.

Chapter 5. Gravimetric HF Adsorption Experiments

Introduction

The solvolysis of a single lignocellulose chip by anhydrous Hydrogen Fluoride (HF) vapor is an unsteady-state, noncatalytic, gas-solid reaction system governed by heat/mass transport, HF-adsorption, and reaction processes. Anhydrous HF vapor at ambient conditions readily diffuses into the porous lignocellulose chip and physically adsorbs onto the lignocellulosic matrix. The adsorbed HF disrupts the hydrogen bonding network of the paracrystalline cellulose microfibril and "solvates" individual cellulose chains by displacing OH...OH hydrogen bonds with stronger HO...HF hydrogen bonds. Adsorbed HF then solvolytically cleaves the HF-solvated cellulose chains to glucosyl fluoride, which sticks to the lignin framework of the HF-reacting lignocellulosic matrix. The glucosyl fluoride can repolymerize to "reversion" oligosaccharides and regenerate HF, or hydrolyze with water in the solid to yield fermentable glucose and regenerate HF. The HF adsorbed on the lignocellulosic matrix is desorbed by decreasing the HF partial pressure and increasing the temperature of the gas over the HF-adsorbed/reacted solid.

In summary, HF vapor adsorbs onto lignocellulose chip, and then the adsorbed HF cleaves cellulose to glucosyl fluoride. In this chapter, the HF adsorption process is investigated on a laboratory scale under carefully-controlled conditions. Specifically, HF loading data (e.g. g HF adsorbed/g-wood) are obtained using the milligram-scale gravimetric HF adsorption apparatus (Figures 4.17a and 4.17b) described in chapter 4. This apparatus measures the in situ gravimetric uptake of

HF vapor onto a single wood chip as a function of time, gas-stream HF partial pressure and temperature (HF adsorption data). Since no gas-phase reaction products are generated, the gravimetric data is specific to HF adsorption/desorption. Details of the apparatus design and procedure are provided in chapter 4.

This chapter is organized into three sections, labeled I to III. In section I, equilibrium HF adsorption isotherm data for the vapor-phase HF solvolysis of a single, dry Bigtooth Aspen wood chip are presented. Also in section I, the heat of adsorption is calculated as a function of HF loading by application of the Clausius-Clapeyron equation to the HF adsorption isotherm data. In section II, HF loading vs. temperature data for the vapor-phase solvolysis of a single, dry "prehydrolyzed" (hemicellulose-free) wood chip are presented. Also in section II, HF desorption data as a function of desorption time and 100% HF vapor temperature are presented. Finally, in section III, capillary condensation of nonideal HF vapor into the microporous volume of wood is discussed, and the critical micropore radius for nonideal HF vapor capillary condensation (r_k) is calculated as a function of HF partial pressure and temperature.

The adsorption of HF onto lignocellulose is the important first step in the overall process for the vapor-phase HF solvolysis of lignocellulose. The HF adsorption data is necessary for chemical reactor analysis and process development. For example, consider a semi-batch reactor for the vapor-phase HF solvolysis of a packed-bed of wood chips. HF adsorption data is needed to calculate the equilibrium HF loading at a given HF vapor partial pressure and temperature, the HF requirements for reaction, the HF-adsorption time, and the HF vapor flow into the reactor. Heat of

adsorption data are also needed to calculate the heat load on the reactor during exothermic adsorption of HF, and the energy input to the reactor during endothermic desorption of HF. The desorption of adsorbed HF from the HF-reacted wood is also a very important step to the overall process because the recovery and recycle of expensive HF is crucial to overall process economics (Hawley et al., 1986).

The HF adsorption/desorption data presented in this chapter will be used repeatedly in chapters to follow. In chapter 6, HF adsorption data for wood and prehydrolyzed wood will be used to clarify the dependence of reaction rate and sugar yield data on HF vapor conditions and HF loading. In chapter 8, the HF adsorption data from prehydrolyzed wood will be used to develop and evaluate a differential material balance and kinetic model for the reaction of a single lignocellulose chip with a 100% HF vapor stream. In chapters 9 and 10, HF adsorption data from prehydrolyzed wood and heat of adsorption vs. HF loading calculations will be used to develop and evaluate an energy balance and heat transport model for the reaction of a single lignocellulose chip with an anhydrous HF vapor stream.

I. HF Adsorption Data and Heat of Adsorption Data for the Vapor-Phase HF Solvolysis of Bigtooth Aspen Wood

A. Equilibrium HF Adsorption Isotherms

The equilibrium HF adsorption isotherms for the vapor-phase HF solvolysis of Bigtooth Aspen wood are presented in Figure 5.1a (30 °C to 50 °C) and Figure 5.1b

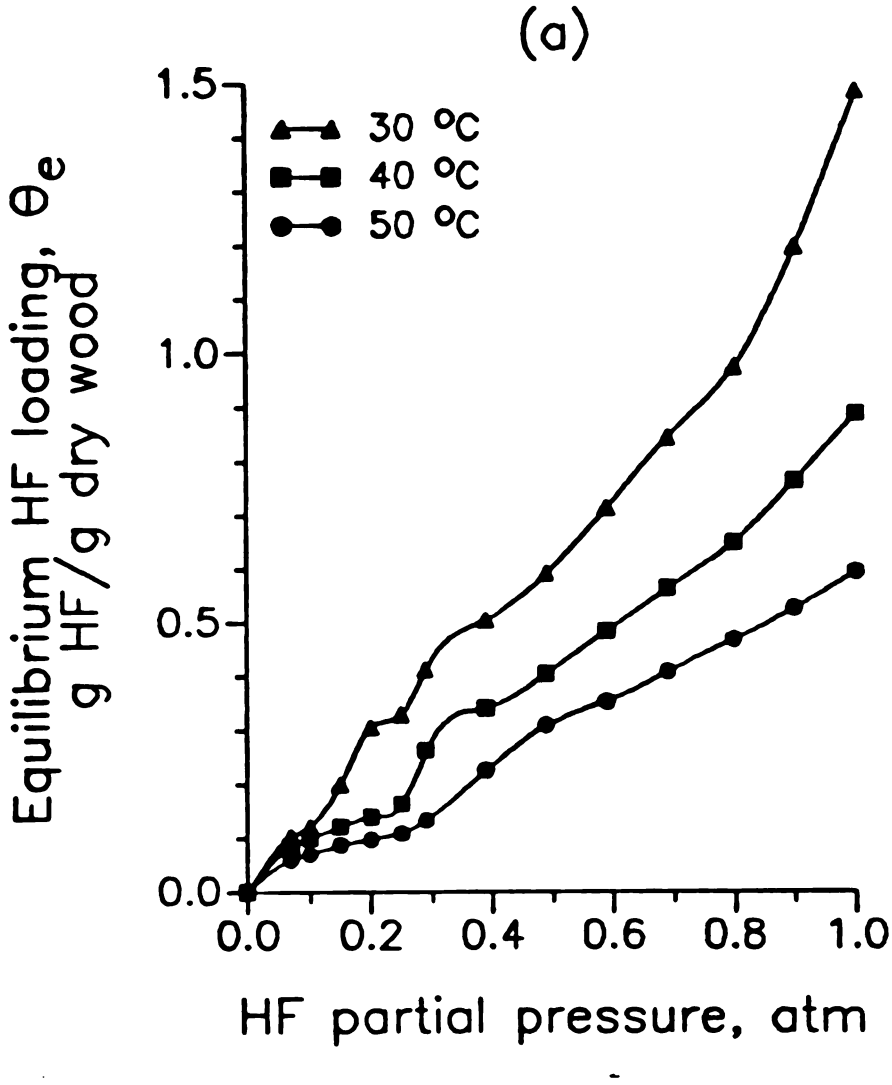


Figure 5.1a. Equilibrium HF adsorption isotherms on dry Bigtooth Aspen wood: (a) T_g = 30 °C, 40 °C, 50 °C.

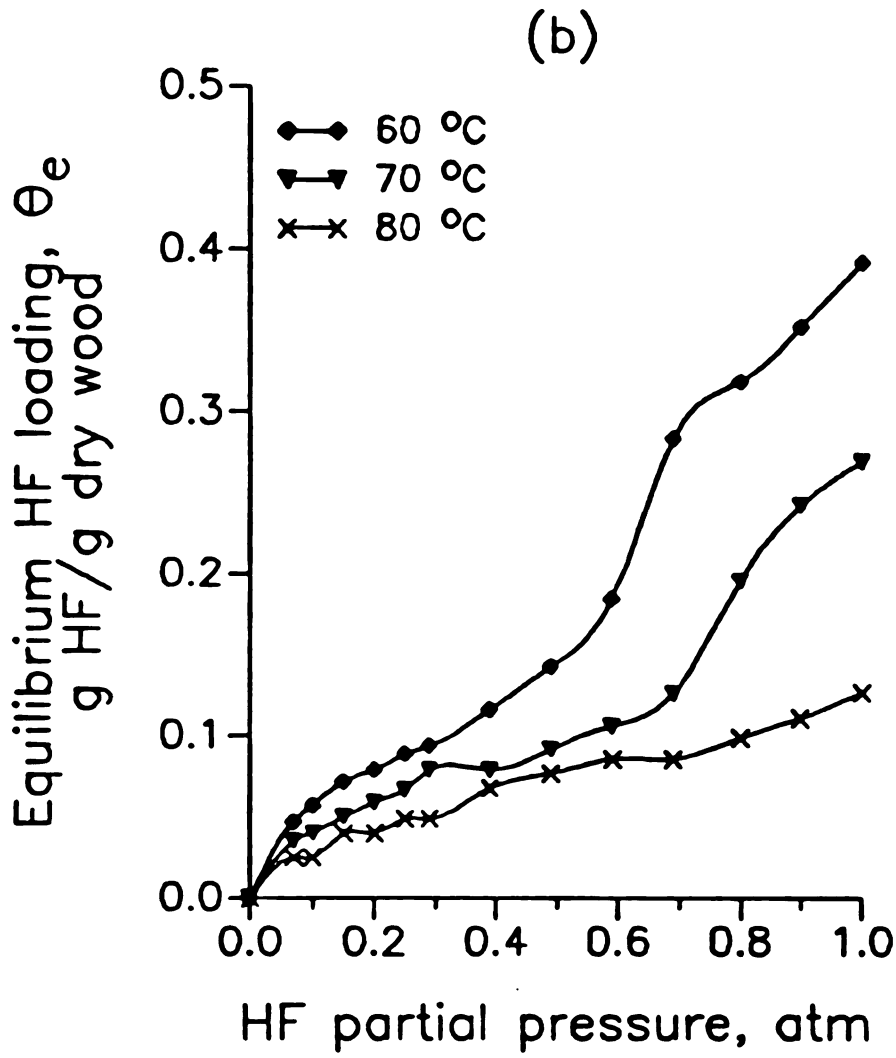


Figure 5.1b. Equilibrium HF adsorption isotherms on dry Bigtooth Aspen wood: (b) T_g = 60 °C, 70 °C, 80 °C.

(60 °C to 80 °C). The equilibrium HF loading (θ_e) at a given gas-stream HF partial pressure (P_{HF}) and temperature (T_g) is defined as

$$\theta_e(P_{HF},T_g) = \frac{\text{equil. wt. HF adsorbed on the wood chip}}{\text{wt. of wood chip before reaction}} \qquad [5\text{-}1]$$

The units of θ_e are g HF/g-wood.

The HF partial pressure (P_{HF}) is defined as

$$P_{HF} = y_{HF}\, P_T \qquad [5\text{-}2]$$

where y_{HF} is the mole fraction of HF in the HF-N_2 gas stream (see equation [6-2]), and P_T is the total system pressure (1.0 atm). Although HF in the vapor phase can form hydrogen-bonded HF-oligomers, y_{HF} and P_{HF} are based on monomeric HF (mol. wt. 20 g/mol), i.e. all HF molecules (oligomers and monomers) are considered as HF monomers. If 100% HF vapor at 1.0 atm (no N_2 diluent) is used, then y_{HF} = 1.0, and P_{HF} is taken at 1.0 atm, even though gas-phase HF-oligomers may be present.

The HF adsorption isotherm data for Bigtooth Aspen wood given in Figures 5.1a and 5.1b were obtained by Mohring (1987). The data relevant to this present investigation is reinterpreted here.

The equilibrium HF adsorption isotherms were characteristic of physical adsorption of a condensible gas onto a porous, reacting solid. The equilibrium loading of HF vapor onto the lignocellulosic matrix increased with increasing HF partial pressure and decreased with increasing gas-stream temperature away from

the normal boiling point of HF (19.54 °C), i.e. $\theta_s \uparrow P_{HF} \uparrow T_s \downarrow$.

The HF loading on wood is the sum of five processes:

1. Physical adsorption of HF on the hydroxyl (-OH) groups and glycosidic linkages (-O-) of cellulose and hemicellulose
2. HF consumed by solvolysis of cellulose and hemicellulose to glucosyl and xylosyl fluoride
3. Physical adsorption of HF on hydroxyl groups and ether linkages on lignin
4. Multilayer adsorption of HF onto existing HF-adsorbed sites
5. Pore-condensation of HF vapor into the micropores within secondary cell walls of the lignocellulosic matrix.

The HF-adsorption processes superimpose by order of 1 to 5. For example, when HF vapor at 30 °C and 1.0 atm is contacted with wood, the equilibrium HF loading on wood is 1.5 g HF/g-wood, the highest HF loading observed over the range of HF vapor conditions studied. The individual contributions to the total HF loading are summarized in Table 5.1. An HF loading of about 0.4 g HF/ g-wood by processes 1 and 2 is required for complete solvation and solvolytic cleavage of cellulose and hemicellulose to sugar fluorides. Therefore, the remaining HF adsorbed (1.1 g HF/g-wood) by processes 3 to 5 is in excess to that required for complete cellulose and hemicellulose solvolysis. If the HF loading is below 0.4 g HF/g-wood, then adsorbed HF is the limiting reagent. Therefore, maximum cellulose and hemicellulose conversion is limited by adsorbed HF. The dependence of cellulose conversion and glucose yield on HF loading is detailed in chapter 6.

Table 5.1. Summary of the estimated contributions to the total HF loading on Bigtooth Aspen wood by 100% HF vapor at 30 °C and 1.0 atm.

Process	HF loading contribution g HF/g-wood	Site-specific	Adsorption mechanism	Adsorption energy (relative)
1 [a]	0.097	yes	HF consumed to sugar fluorides	high
2 [a]	0.290	yes	HO...HF complex	high
3 [b]	0.033	yes	OH groups on lignin	med.
4 & 5 [c]	1.070	no	multilayer adsorption & pore-filling	low
total [d]	1.490			

Notes:

[a] Calculated assuming glucan composition of Bigtooth Aspen wood is 3.441 mmol/g, and xylan composition is 1.4 mmol/g; 1 mole HF per 1 mole glucan or xylan for process 1, 3 moles HF per 1 mole glucan or xylan for process 2 (1 HF molecule for each of the 3 -OH groups on glucan or xylan).

[b] Roughly estimated assuming
1) formula for hardwood lignin phenylpropanoid unit is approximately $C_9H_8O_{3.5}OCH_3$ (mol. wt. 203) (Pettersen, 1984b)
2) two -OH group HF-adsorption sites per phenylpropanoid unit
3) 0.166 g lignin/g-wood.

[c] By difference; HF consumption by ash not estimated.

[d] Measured by the gravimetric HF-adsorption experiment.

In general, the magnitude of the adsorption energy decreases from processes 1 & 2 (highest) to process 5 (lowest). Correspondingly, the ease of HF desorption increases from processes 1 & 2 to process 5. The adsorption of HF vapor onto the lignocellulosic matrix is an exothermic process, whereas the desorption of adsorbed HF from the HF-reacted solid is an endothermic process. In processes 1, 2, and 3, HF molecules are tightly bound to specific sites on the lignocellulosic matrix. Processes 1 and 2 are modeled in chapter 8 (see Figures 8.4 to 8.8). In process 2, the HF is consumed to form sugar fluorides and so is chemically bound. In processes 2 and 3, the HF is tightly complexed to -OH groups by hydrogen bonding. However, HF can still be desorbed from the HO...HF complex. In processes 4 and 5, the HF adsorption is not site specific. Therefore, HF adsorbed onto the lignocellulosic matrix by processes 4 and 5 is easily desorbed. In process 5, the adsorbed HF is actually condensed into the cell-wall micropores, and so adsorption is similar to condensation, and desorption is similar to vaporization. Process 5 will only occur at low temperature and high HF partial pressure (e.g. 30 °C and 1.0 atm). Process 5 is discussed further in section III of this chapter.

Note that most HF adsorption isotherms show a large increase in HF loading after HF loadings (θ_s) of 0.1-0.2 g HF/g-wood. At HF loadings of 0.1 g HF/g-wood and below, HF molecules adsorb onto O-glycosidic linkages and exposed -OH groups created by imperfections in the hydrogen-bonding network of cellulose chains within the crystalline cellulose microfibril. This low HF loading is not sufficient to solvate the crystalline cellulose microfibril and solvolytically cleave HF-adsorbed cellulose to glucosyl fluoride (see chapter 6). However, at slightly higher HF

loadings, the hydrogen-bonding network of the crystalline cellulose microfibril disrupts as adsorbed HF displaces OH...OH hydrogen bonds with HO...HF hydrogen bonds. This unravels cellulose chains away from the crystalline microfibril and exposes more -OH groups for adsorption by HF.

The sharp increase in HF loading is only observed when the gas-stream HF partial pressure is increased to increase the HF loading on the lignocellulosic matrix. When the HF loading is decreased (desorbed) by decreasing the HF partial pressure, no sharp decrease is observed, because the disruption of the hydrogen-bonding network of cellulose chains within the cellulose microfibril had already occurred during HF adsorption. This HF desorption data is described in detail by Mohring (1987).

B. Comments on HF Desorption

The HF physically adsorbed on the wood chip can be desorbed by decreasing the gas-stream HF partial pressure and/or increasing the temperature. For complete desorption of HF, an inert diluent stream (e.g. N_2 gas) at elevated temperature must be passed over the HF-adsorbed/reacted solid. For example, adsorbed HF can be desorbed down to within 0.2% of the original weight of the wood chip by passing a 100% N_2 gas stream at 80 °C for 1 h over the HF-adsorbed/reacted solid (Mohring, 1987). Alternatively, adsorbed HF can be completely desorbed (+99% recovery) by evacuation (Luers, 1938). Detailed experimental and theoretical characterization of the thermodynamics and mass transport of the HF desorption process is beyond the scope of this dissertation and is reserved for future study.

HF desorption is complicated by sugar fluoride repolymerization and hydrolysis. During vapor-phase HF solvolysis of wood and subsequent HF desorption, sugar fluorides repolymerize to "reversion" oligosaccharides and regenerate HF (see Figure 6.19). The in situ hydrolysis of sugar fluorides to free sugars by water in the wood chip also regenerates HF (see Figure 6.19). Both reactions compete for available sugar fluorides. Since both processes regenerate HF from sugar fluorides, this "regenerated" HF can also be desorbed from the HF-reacted wood chip.

C. Heat of Adsorption

The heat of adsorption, ($\Delta H_A(\theta_e)$, cal/mol HF or cal/g-HF adsorbed) of HF vapor onto the lignocellulosic matrix at a given HF loading (θ_e) is calculated from the equilibrium HF adsorption isotherm data using the Clausius-Clapeyron equation. The Clausius-Clapeyron equation is normally derived in terms of the heat of vaporization, which is an endothermic process. The Clausius-Clapeyron equation is modified for exothermic adsorption by changing the sign of the enthalpy term. Specifically, the Clausius-Clapeyron equation for HF adsorption is given by

$$\log_{10} P_{HF} = 2.303 \frac{\Delta H_A(\theta_e)}{R} \cdot \frac{1}{T_g} + C \qquad [5\text{-}3a]$$

where C is an integration constant (intercept), P_{HF} is the gas-stream partial pressure (atm, based on monomeric HF), R is the thermodynamic gas constant (1.987 cal/mol), and T_g is the gas-stream temperature (K). In order to calculate $\Delta H_A(\theta_e)$, values for P_{HF} and T_g at a given constant equilibrium HF loading (θ_e) were first determined. At constant θ_e, $\log_{10} P_{HF}$ was then plotted against $1/T_g$ (Figure 5.2).

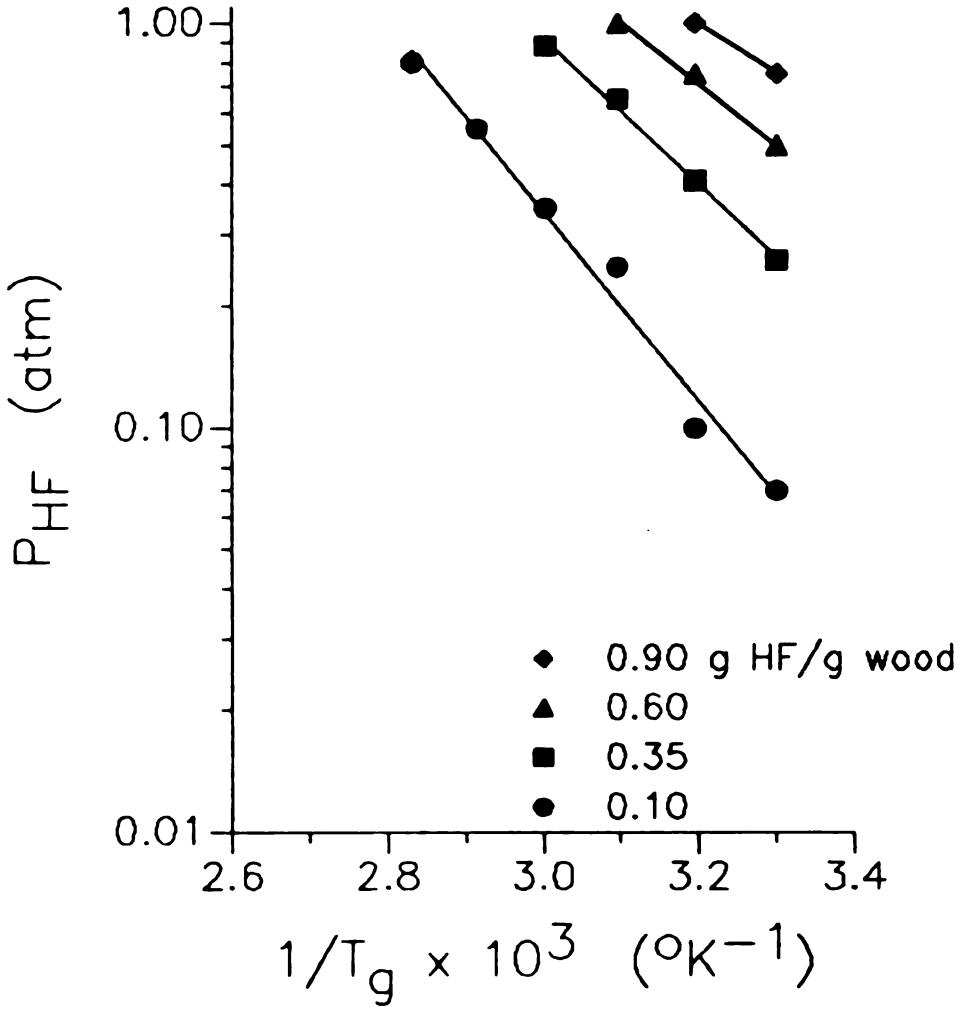


Figure 5.2. Clausius-Clapeyron plots ($\log_{10}P_{HF}$ vs. $1/T_g$) at fixed HF loading (θ_e).

The heat of adsorption at each HF loading was calculated from the least-squares slope of the $\log_{10} P_{HF}$ vs. $1/T_g$ data (Table 5.2).

Recall from chapter 4 that HF vapor at 1.0 atm from 20 °C to 80 °C is a nonideal gas, because HF molecules associate by hydrogen bonding to form HF-oligomers of dimer to hexamer in size. Therefore, the heat of adsorption should be determined by a Clausius-Clapeyron plot modified for a nonideal gas, e.g. ln f_{HF} vs. $1/T_g$ where f_{HF} is the fugacity of the nonideal HF vapor. A simpler but less accurate correction for the nonideality of HF vapor was derived by Mohring, (1987). Specifically, Mohring incorporated "f", the nonideal HF vapor association factor (see equation [5-8a]) into the Clausius-Clapeyron equation, so that

$$\log_{10} P_{HF} = 2.303 \frac{\Delta H_A(\theta_e)\, f}{R} \cdot \frac{1}{T_g} + C \qquad [5\text{-}3b]$$

The adsorption of HF vapor onto a single wood chip is an exothermic process. The absolute value of the heat of adsorption decreased with increasing HF loading, as shown in Table 5.2 and Figure 5.3. The solid line in Figure 5.3 is a least-squares fit of the $\Delta H_A(\theta_e)$ vs. θ_e values to the empirical equation

$$\Delta H_A(\theta_e) = H_o \theta_e^{-a} \qquad [5\text{-}4]$$

with H_o = -205 cal/g-HF adsorbed, and a = 0.457. Equation [5-4] is assumed valid from θ_e = 0.05 to 1.5 g HF/g-wood.

The decrease in the absolute value of $\Delta H_A(\theta_e)$ with increasing θ_e reflects the adsorption energy of the particular process(s) of HF adsorption, as discussed earlier

Table 5.2. Calculated heat of adsorption, $\Delta H_A\theta_e$), vs. equilibrium HF loading (θ_e) for the adsorption of HF vapor onto dry Bigtooth Aspen wood.

θ_e (g HF/g wood)	$-\Delta H_A(\theta_e)$ (cal/g HF ads)		
	from Fig. 5.2 [a]	corrected for non-ideal HF vapor [b]	from Eqn. [5-6] [c]
0.10	535	535	587
0.35	415	395	331
0.60	342	285	259
0.90	270	180	215

Notes:

[a] Calculated by application of Clausius-Clapeyron equation [5-3a] to HF adsorption isotherm data (see Figure 5.2).

[b] Corrected for nonideal HF vapor by Mohring (1987).

[c] Corrected $\Delta H_A(\theta_e)$ values fitted to equation [5-6].

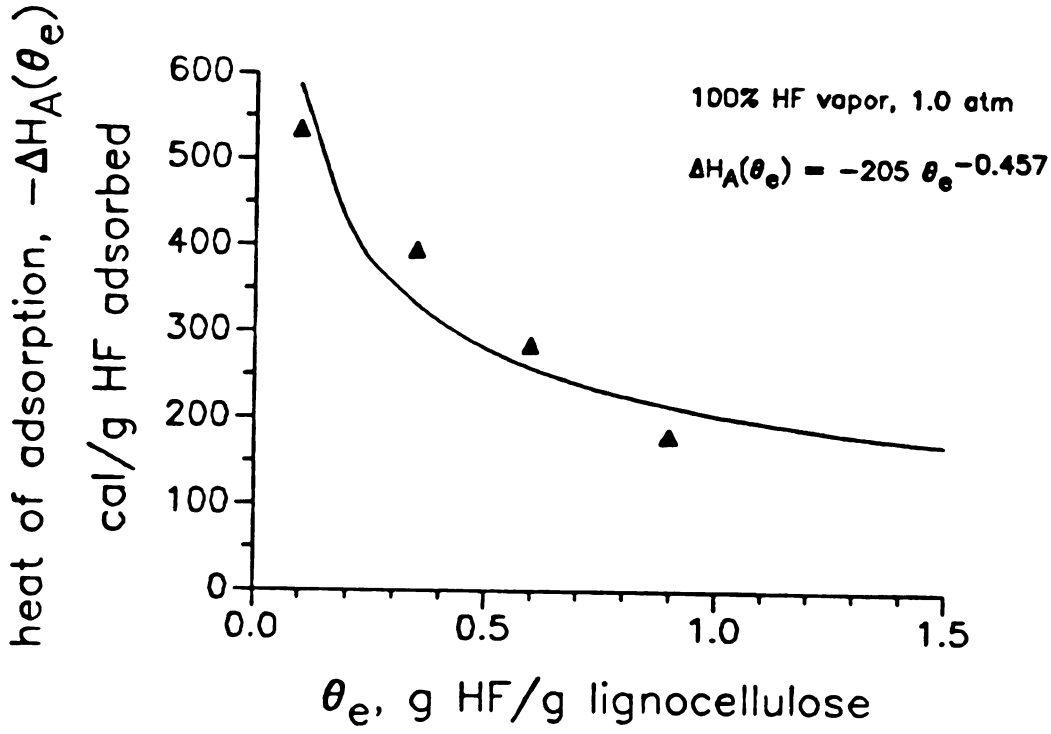


Figure 5.3. Heat of adsorption,-$\Delta H_A(\theta_e)$, vs. HF loading (θ_e) (see Table 5.2).

in this section. At low HF loadings, e.g. 0.1 to 0.4 g HF/g-wood, adsorbed HF is tightly bound to OH groups or consumed to glucosyl fluoride. This HF adsorption is site-specific, and the binding energy is high. At high HF loadings, e.g. 1.0 to 1.5 g HF/g-wood, part of the adsorbed HF is condensed into the secondary cell wall micropores of the lignocellulosic matrix. This portion of the total HF loading is nonspecific, and the binding energy is low and close to the energy of vaporization.

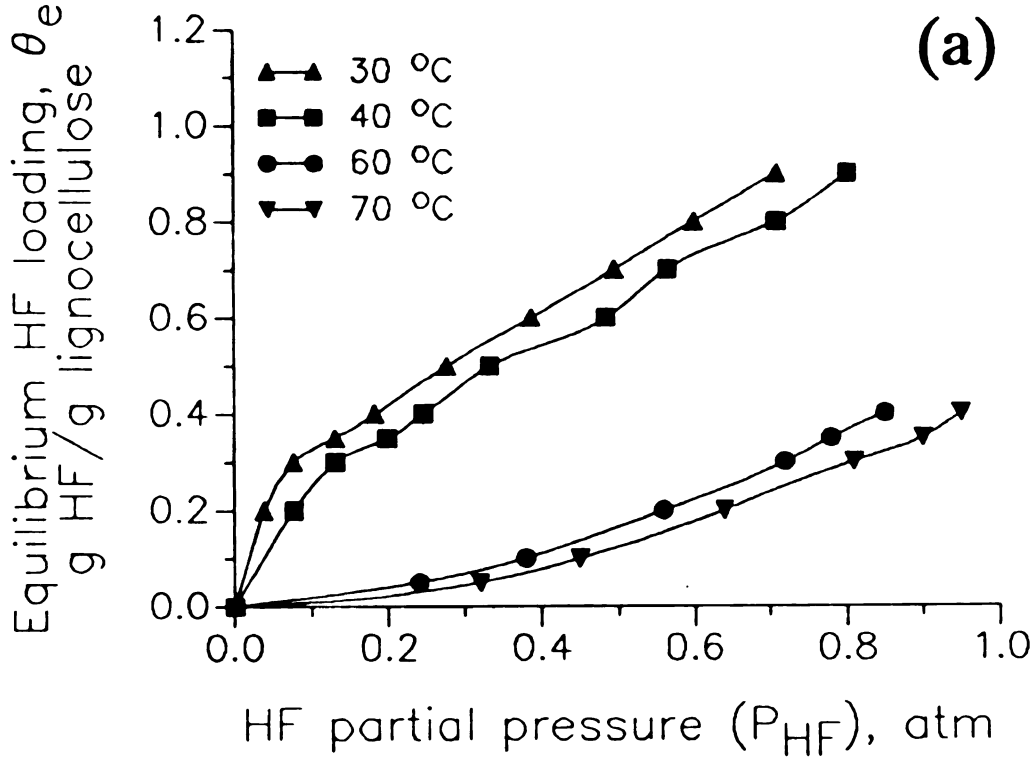
D. Comparsion to Literature Data

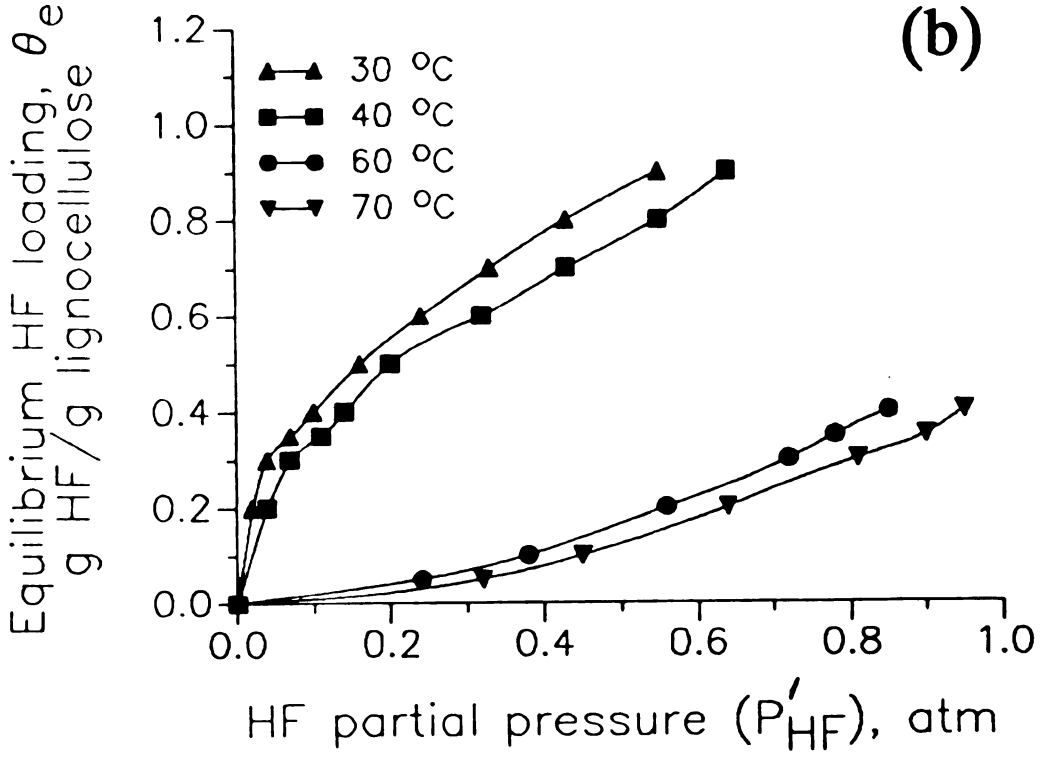
Equilibrium HF adsorption isotherm data and heat of desorption data were obtained by Franz et al. (1982, 1987) for the vapor-phase HF solvolysis of prehydrolyzed (hemicellulose-free) sprucewood. Franz et al.'s data is compared to the data presented earlier in this section.

In Franz et al.'s experiment, the sorption of HF vapor (in N_2 diluent) onto 10 g lignocellulose (1 mm particles, ca. 10% moisture) was measured within a temperature-controlled, 5 cm x 3 cm stainless-steel mantle reactor mounted on a balance. The relative flowrates of HF vapor and N_2 diluent into the reactor set the gas-stream HF partial pressure.

The sorption isotherms of Franz et al. (1987) are presented in Figure 5.4. In general, at a given HF partial pressure and temperature, the HF loading on prehydrolyzed sprucewood (10% moisture) reported by Franz is higher than the HF loading on dry Bigtooth Aspen wood given in Figures 5.1a and 5.1b. Since different lignocellulosic substrates were used for each study, direct comparison is difficult. However, the moisture in the prehydrolyzed sprucewood might have enhanced the amount of HF hydroscopically adsorbed.

Figure 5.4. Literature comparison: equilibrium HF sorption isotherms on prehydrolyzed spruce wood at 30 °C, 40 °C, 60 °C, and 70 °C. Data of Franz et al. (1987). (a) Scaled for P_{HF} (all HF molecules in monomeric form); (b) rescaled for P_{HF} (hydrogen-bonded, nonideal HF vapor).


(a)
30 °C
40 °C
60 °C
70 °C
Equilibrium HF loading, θ_e
g HF/g lignocellulose
1.2
1.0
0.8
0.6
0.4
0.2
0.0
0.0
0.2
0.4
0.6
0.8
1.0
HF partial pressure (P_{HF}), atm


(b)
30 °C
40 °C
60 °C
70 °C
Equilibrium HF loading, θ_e
g HF/g lignocellulose
1.2
1.0
0.8
0.6
0.4
0.2
0.0
0.0
0.2
0.4
0.6
0.8
1.0
HF partial pressure (P'_{HF}), atm

From the sorption data given in Figure 5.4, Franz et al. calculated the heat of desorption by the Clausius-Clapeyron equation. The heat of desorption as a function of HF loading and temperature is given in Figure 5.5. The discrepancy between Franz et al.'s values and the values reported in this dissertation are due to the differences in the HF sorption data just described. With independent calorimetric measurements, Franz et al. determined by direct calorimetric measurement that the isothermic heat of sorption was 340 cal/g HF adsorbed, and the heat of desorption from HF-adsorbed lignocellulose (0.6 g HF/g-lignocellulose) was 207 cal/g HF desorbed.

II. HF Adsorption/Desorption Data for the Vapor-Phase HF Solvolysis of Prehydrolyzed Wood

In this section, HF adsorption/desorption data for the solvolysis of a single prehydrolyzed (hemicellulose-free) Bigtooth Aspen wood chip by a 100% HF vapor stream at 1.0 atm are presented.

Prehydrolyzed wood, or "lignocellulose", is a model lignocellulosic substrate which possesses the native architecture and composite microstructure of wood but contains only two chemical components, crystalline cellulose and lignin. As described in chapter 4, prehydrolyzed wood is prepared by selective, mild-acid hydrolysis of the hemicellulose fraction from Bigtooth Aspen wood (e.g. reflux of wood chips in 2 N TFA at 100 °C for 4 h). This prehydrolysis also removes the "extractives" fraction from the wood. The solid residue from prehydrolysis (about 68% of the original weight of the wood) is primarily cystalline cellulose (75%) and

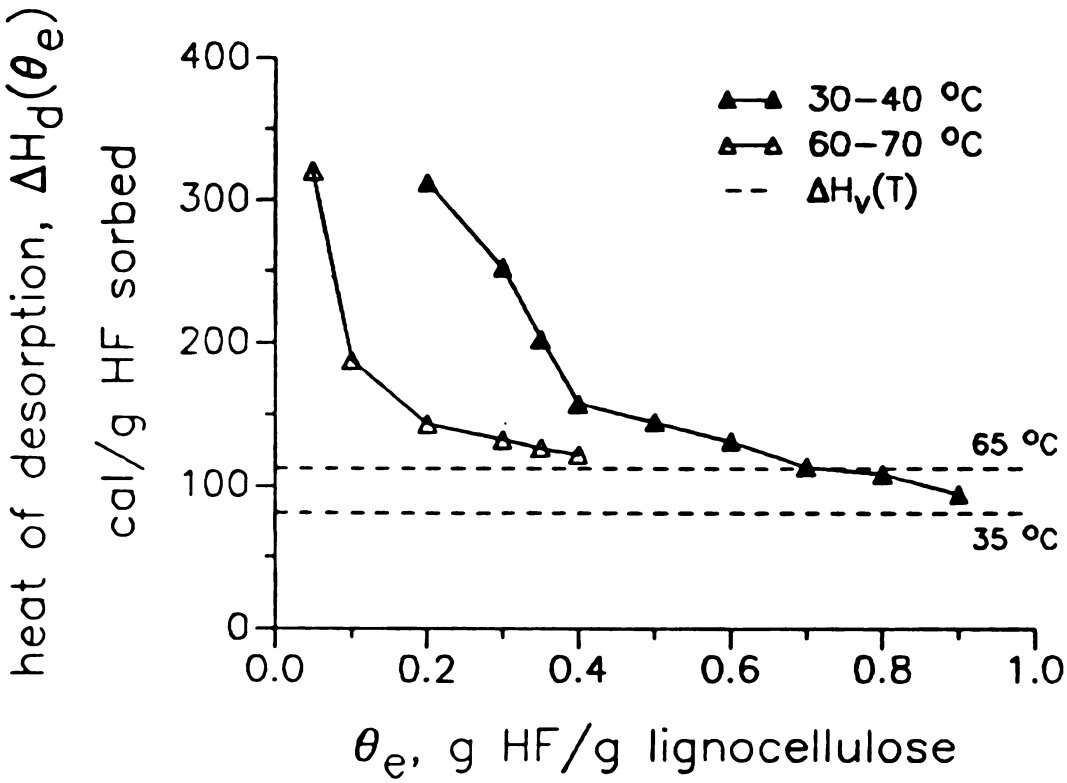


Figure 5.5. Literature comparison: heat of desorption from HF-adsorbed, prehydrolyzed spruce wood. Data of Franz et al. (1987).

lignin (22%) and retains the overall features of the original wood. Since gravimetric HF adsorption/desorption data from prehydrolyzed wood are not complicated by the presence of hemicellulose and extractives, the adsorption/desorption processes of the vapor-phase HF solvolysis of crystalline cellulose on an intact lignin framework can be focused upon and studied.

A. The HF Adsorption/Desorption Experiment

A single HF adsorption/desorption experiment was performed in two steps. In step 1, a 100% HF vapor stream at 0.81 g HF/min, 31 °C, and 1.0 atm was contacted with a single, dry prehydrolyzed wood chip. The in situ gravimetric HF adsorption of 100% HF vapor onto the prehydrolyzed wood chip was measured as a function of reaction time until the equilibrium HF loading was achieved. During the HF-adsorption process, any air initially within the porous volume of the wood chip diffused out of the HF-reacting solid and into the surrounding HF vapor stream. In step 2, the 100% HF vapor stream temperature was increased to 40 °C. At this higher temperature, the HF adsorbed on the HF-reacted lignocellulose was desorbed until a lowered equilibrium HF loading was achieved. The 100% HF vapor temperature was then successively increased in 10 °C increments (to 80 °C), and the equilibrium HF loading was measured after each temperature increase. The HF-adsorbed sample weight, HF vapor temperature, and HF vapor flowrate measurements were captured as a function of time using the computer data acquisition system described by Mohring (1987). Program DATA1.BAS, listed in Appendix D, was used to process and manipulate the raw data file.

HF loading vs. time data from the complete, two-step adsorption/desorption

experiment are presented in Figure 5.6a. The 100% HF vapor stream temperature vs. time curve used to set the HF loading vs. time curve is given in Figure 5.6b. The HF adsorption vs. time profile ($\theta_{HF}(t)$ vs. t) for the solvolysis of a single prehydrolyzed wood chip by a 100% HF vapor stream at 1.0 atm and 31 °C is presented in Figure 5.7.

B. Equilibrium HF loading vs. 100% HF vapor temperature

The equilibrium HF loading vs. 100% HF vapor temperature data (θ_e vs. T_g) are presented in Table 5.3 and Figure 5.8. The equilibrium HF loading (θ_e) is defined as

$$\theta_e = \frac{\text{equil. wt. HF adsorbed on prehydrolyzed wood chip}}{\text{wt. of prehydrolyzed wood chip before reaction}} \qquad [5\text{-}5]$$

Typical units for θ_e are g HF/g-lignocellulose. The θ_e vs. T_g data were fitted to the cubic polynomial

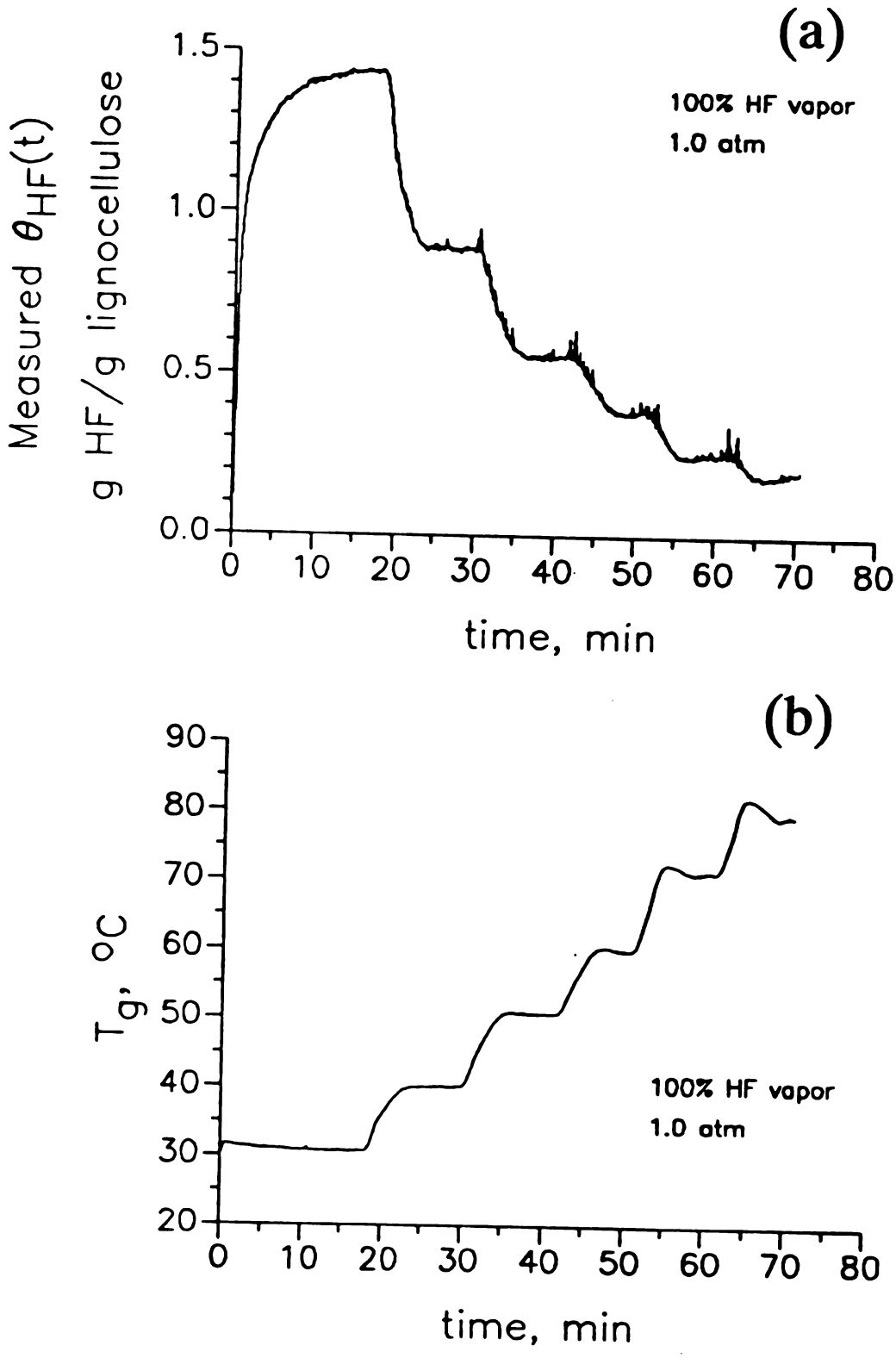
$$\theta_e(T) = a_0 + a_1 T + a_2 T^2 + a_3 T^3 \qquad [5\text{-}6]$$

where a_0, a_1, a_2, and a_3 are fitted constants. The numerical values of a_0 to a_3 are given in Tables 5.3 and 10.3. The solid line in Figure 5.8 is the least-squares fit of the θ_e vs. T_g data. Equation [5-6] is assumed valid from T = 30 °C to 90 °C.

C. HF Desorption

Recall that the adsorbed HF was incrementally desorbed by incrementally increasing the 100% HF vapor stream temperature over the HF-adsorbed/reacted

Figure 5.6. HF adsorption/desorption data for the solvolysis of a single prehydrolyzed wood chip by a 100% HF vapor stream at 1.0 atm. (a) HF adsorption/desorption profile, $\theta_{HF}(t)$; (b) 100% HF vapor stream temperature vs. time profile, $T_g(t)$, used to set the HF adsorption/desorption profile. Note: $\dot{m}_{HF}$ = 0.81 g HF/min.


(a)
100% HF vapor
1.0 atm
Measured $\theta_{HF}(t)$
g HF/g lignocellulose
1.5
1.0
0.5
0.0
0
10
20
30
40
50
60
70
80
time, min
(b)
T_g, °C
90
80
70
60
50
40
30
20
100% HF vapor
1.0 atm
0
10
20
30
40
50
60
70
80
time, min

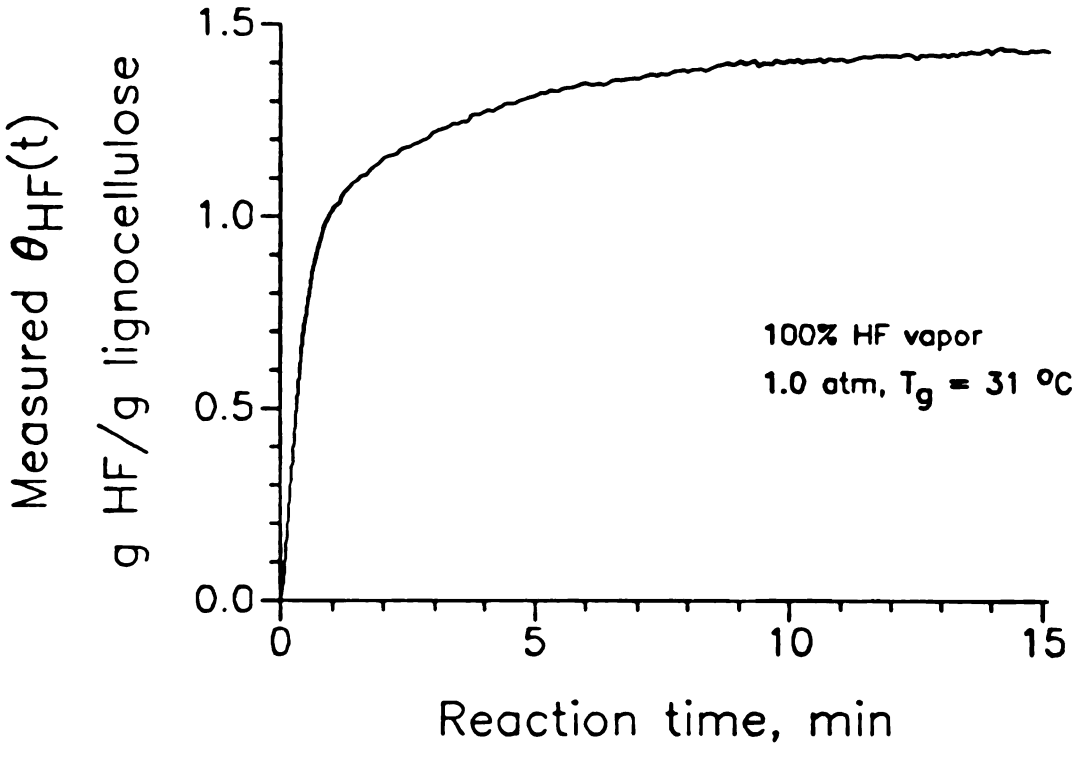


Figure 5.7. HF adsorption vs. reaction time profile, $\theta_{HF}(t)$, for the solvolysis of a single prehydrolyzed wood chip by an anhydrous, 100% HF vapor stream at T_g = 31 °C and 1.0 atm.

Table 5.3. Equilibrium HF loading (θ_e) vs. 100% HF vapor stream temperature (T_g) at 1.0 atm for the vapor-phase HF solvolysis of prehydrolyzed wood (see Figure 5.8).

Time Window in Figure 5.6a						
begin min	end min	duration min	n	$T_{g,ave}$ C	$\theta_{e,ave}$ g HF/g [a,b]	$\theta_{e,calc}$ g HF/g [a,c]
13.53	18.73	5.30	63	30.9	1.433	1.427
23.67	30.27	6.60	80	40.1	0.890	0.905
35.02	41.87	6.85	83	50.8	0.561	0.546
47.58	51.13	3.55	43	60.1	0.387	0.381
55.30	61.62	6.32	76	71.5	0.255	0.266
67.50	69.68	2.18	27	79.5	0.195	0.187

Notes:

[a] g HF/g = g HF adsorbed/g lignocellulose.

[b] HF loading calculated by equation [4-15] (w_o = 25.9 mg; two prehydrolyzed wood chips, ca. 0.4 mm x 1.0 cm/side, pressed together to increase sample weight).
Correction factors:
w_{c1} = +1.9 mg computer data acquisition offset
w_{c2} = weight correction for drag of HF vapor stream on sample holder and HF vapor condensation on sample holder
w_{c2} = +1.0 mg at 31 °C, +0.4 mg at 40 °C, 0.0 mg at 50 °C.

[c] Equilibrium HF loading (θ_e, g HF/g) vs. 100% HF vapor temperature (T_g, °C) at 1.0 atm calculated by least-squares cubic polynomial of the form

$$\theta_e = a_o + a_1 T + a_2 T^2 + a_3 T^3$$

with fitted constants a_o = 5.440502, a_1 = -0.2024107, a_2 = 2.748926 10^{-3}, a_3 = -1.300829 10^{-5}.

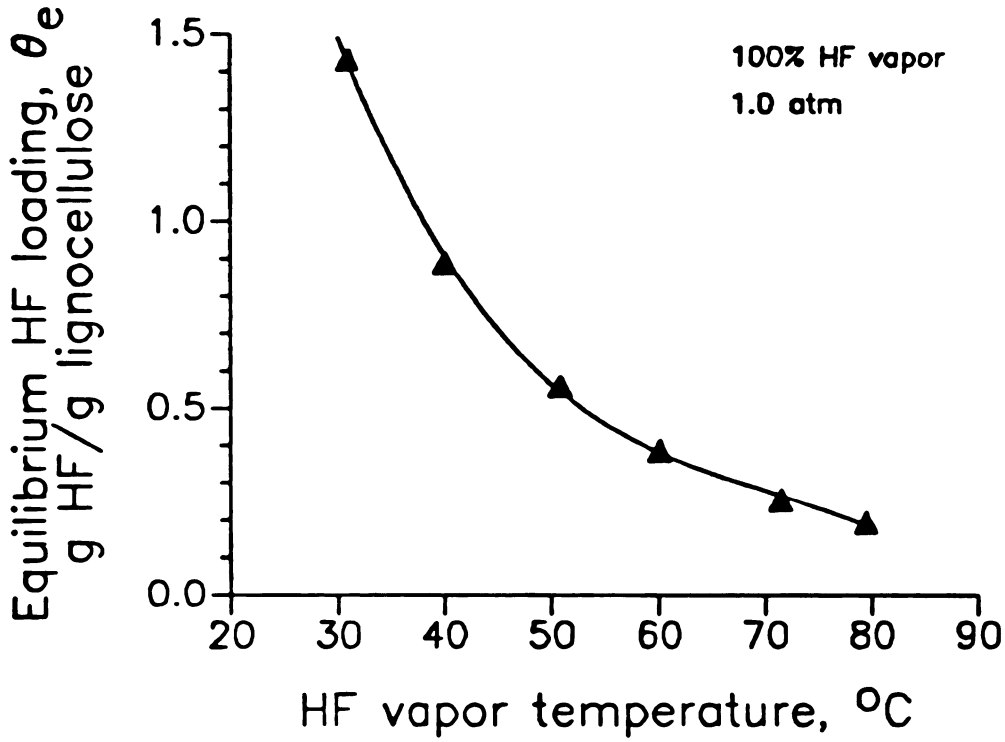


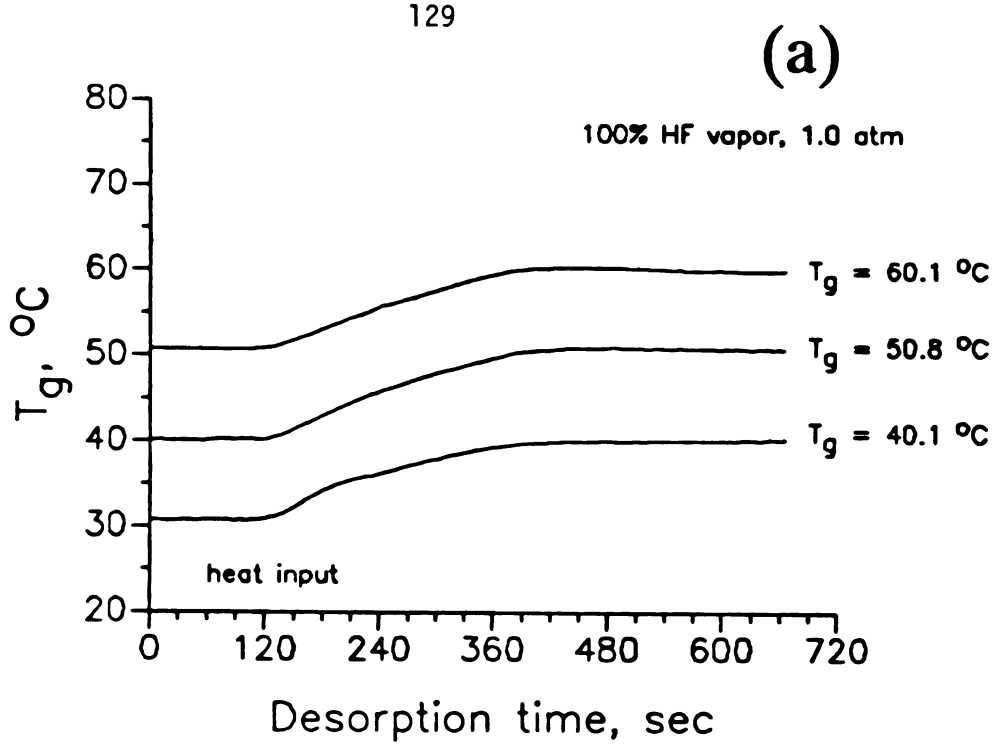
Figure 5.8. Equilibrium HF loading on prehydrolyzed wood (θ_e) vs. 100% HF vapor stream temperature (T_g) (see Table 5.3).

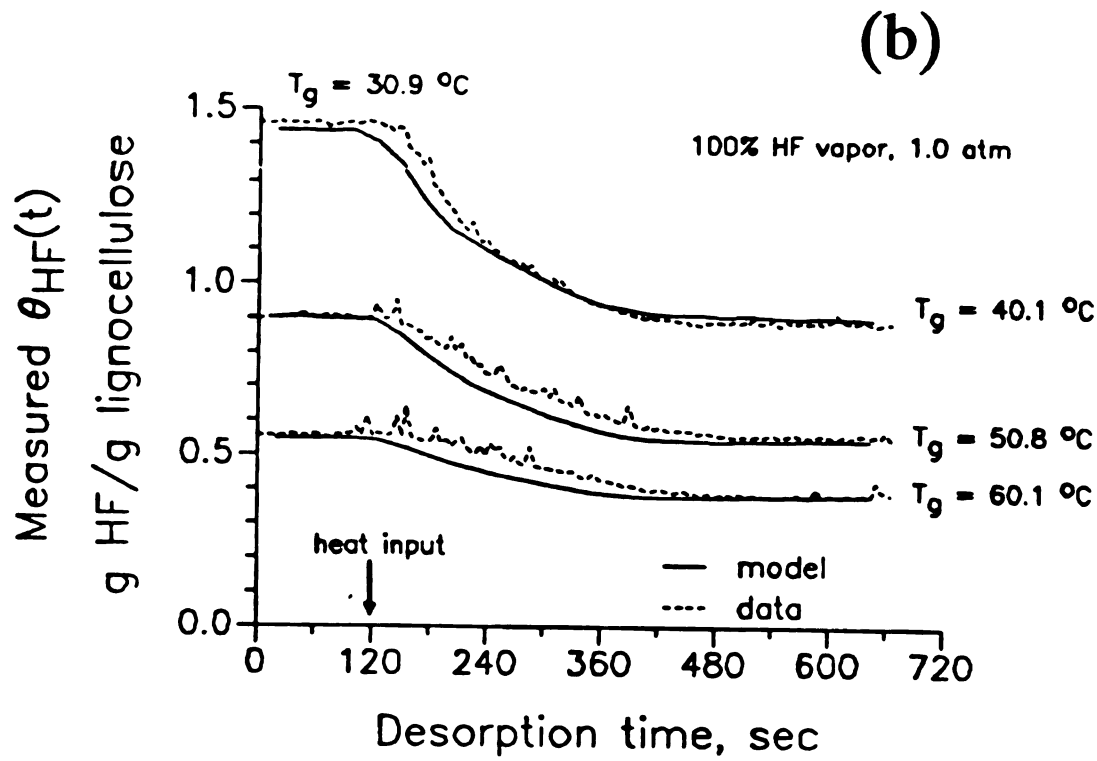
prehydrolyzed wood chip. Selected 100% HF vapor stream temperature (T_s) vs. desorption time profiles are presented in Figure 5.9a. The complimentary HF loading vs. desorption time profiles are presented in Figure 5.9b. The desorption time was rescaled by program DATA1.BAS so that several desorption profiles could be compared onto one plot. In this special type of desorption experiment, no gas-phase mass-transfer resistances are present, because no gas-phase reaction products are generated, and 100% HF vapor always is present over the HF-desorbing chip.

The "model" line for the HF loading vs. desorption time profiles shown in Figure 5.9b was calculated by inserting the T_s vs. t data from Figure 5.9a into equation [5-6]. Thus, the model line is the equilibrium HF loading evaluated at the current HF vapor stream temperature at time t, i.e. $\theta_e[T_s(t)]$.

Note from Figure 5.9b the equilibrium HF loading at $T_s(t)$ was slightly lower than the HF loading vs. time data. Since gas-phase mass transfer resistances are not present in this desorption experiment, heat transfer resistances must be the source of the deviation. Because the heat of desorption is endothermic, energy must be transferred from the 100% HF vapor stream to the HF-desorbing chip. Therefore, the chip will be cooler than the surrounding 100% HF vapor stream if heat transfer resistances are present. If the temperature of chip is cooler than the surrounding HF vapor stream, then the HF loading on the chip will be higher than $\theta_e(T_s)$, because the HF loading increases with decreasing temperature. Thus the deviation between the equilibrium line and the data can be explained by a heat transfer resistance during HF desorption.

Figure 5.9. Selected HF desorption profiles: (a) 100% HF vapor stream temperature vs. time profile, $T_g(t)$, used to set the HF desorption profile; (b) HF loading vs. desorption time profile, $\theta_{HF}(t)$, set by $T_g(t)$. Solid line is equilibrium HF loading (θ_e) evaluated at $T_g(t)$. Note: desorption time rescaled to compare HF desorption profiles on a single plot.


(a)
100% HF vapor, 1.0 atm
T_g = 60.1 °C
T_g = 50.8 °C
T_g = 40.1 °C
heat input
T_g, °C
80
70
60
50
40
30
20
0
120
240
360
480
600
720
Desorption time, sec


(b)
T_g = 30.9 °C
100% HF vapor, 1.0 atm
T_g = 40.1 °C
T_g = 50.8 °C
T_g = 60.1 °C
heat input
model
data
Measured $\theta_{HF}(t)$
g HF/g lignocellulose
1.5
1.0
0.5
0.0
0
120
240
360
480
600
720
Desorption time, sec

III. Pore-Condenstation of Nonideal HF Vapor into the Microporous Volume of Wood

In this section, pore-condensation of HF vapor into the microporous volume of wood is investigated. The main objective is to quantify the contribution of pore-condensation to the total HF loading on wood. More specifically, the critical pore radius (r_k) for pore condensation is calculated as a function of HF vapor partial pressure (P_{HF}) and temperature (T_g). The fraction of the total micropore volume with micropore radii less than or equal to r_k is then calculated, and from this, the total amount of HF loaded into the micropores by pore condensation is calculated.

The lignocellulosic matrix of hardwood is both microporous and macroporous. However, pore condensation of HF vapor into the porous volume of wood or prehydrolyzed wood is localized in the microporous volume within the secondary cell wall. The micropore volume ($V_{p,u}$), macropore volume ($V_{p,m}$), and bulk density can vary widely between lignocellulosic substrates. For "prehydrolyzed mixed hardwood" (prehydrolysis of 90% birch and 10% maple in 1% H_2SO_4 at 100 °C for 5 h), the total micropore volume is 0.7 mL/g, and the micropores range from 0 to 11 nm in diameter with a mean of about 2 nm (Grethlein, 1985). The macropores, or secondary cell wall lumen, range from about 5 to 30 μm in diameter, about 3 orders of magnitude larger than the micropores.

The Kelvin Equation. The capillary condensation of a vapor into a microporous solid is a well-studied surface thermodynamic phenomena (Adamson, 1982). At thermodynamic equilibrium, the Kelvin Equation predicts the maximum pore radius at which capillary condensation will occur at a given vapor partial pressure and

temperature. In other words, all micropores with diameter r_k and below fill with condensed vapor by the mechanism of capillary condensation. This critical pore radius (r_k) increases with increasing partial pressure and decreases with increasing temperature ($r_k \uparrow$ $P_{HF} \uparrow$ $T_g \downarrow$).

The Kelvin Equation for capillary condensation of nonideal HF vapor is given by

$$r_K = \frac{-2\ \gamma_{HF,l}\ v_{HF,l}}{R\ T_g\ \ln\ (x_{HF}\ P'_{HF}/x_{HF}^{*}\ P_{HF}^{*})} \qquad [5\text{-}7]$$

where P_{HF}' is the real partial pressure of the HF vapor based on the apparent molecular weight of the HF vapor (see equation [5-11]), P_{HF}^{*} is the vapor pressure of HF at T_g (atm), r_k is the critical pore radius for pore condensation (cm or A), R is the gas constant (82.05 cm^3 atm/mol K), x_{HF} is the fugacity coefficient for the HF vapor at P_{HF}' and T_g, x_{HF}^{*} is the fugacity coefficient for P_{HF}^{*} at T_g, $v_{HF,l}$ is the molar volume of liquid HF (cm^3/mol HF liquid), $\gamma_{HF,l}$ is the surface tension of the liquid HF (g/cm-sec^2). The HF vapor pressure, P_{HF}^{*}, is estimated by equation [4-1]], $\gamma_{HF,l}$ is estimated by equation [4-3], and $v_{HF,l}$ is estimated from the HF liquid density via equation [4-2].

Characterization of the nonideality of the HF vapor is necessary for calculation of the fugacity coeficients, x_{HF}, and x_{HF}^{*}. Recall that 100% HF vapor at 1.0 atm and 20 °C to 80 °C -- the range of HF vapor conditions of interest for HF-adsorption on lignocellulose -- forms hydrogen-bonded HF oligomers in the gas phase. The

average molecular weight of these hydrogen bonded HF-oligomers increases with increasing HF vapor partial pressure and decreases with increasing temperature. Therefore, HF vapor at these conditions behaves as a nonideal gas. The association (nonideality) factor, f, is defined as

$$f = \frac{\text{ave. mol. wt. of H-bonded HF oligomers in gas phase}}{\text{mol. wt. of HF monomer (20 g/mol)}} \qquad [5\text{-}8]$$

The association factor "f" is a function of P_{HF}', the nonideal HF vapor partial pressure, and T_g. Specifically, by assuming a gas-phase HF monomer/hexamer equilibrium for the HF-oligomers, i.e. 6 HF = $(HF)_6$ (a simple model which adequately fits the nonideal HF vapor data), Long et al. (1943) report that "f", the HF vapor association factor, is related to P_{HF}' by

$$P'_{HF} = \left[\frac{5^5 (f - 1)}{K\,(6 - f)^6} \right]^{0.2} \qquad [5\text{-}9]$$

where K is the equilibrium constant for the HF monomer/hexamer equilibrium. Please note that P_{HF}' is not the same as P_{HF}, which by equation [5-2] is the HF partial pressure if all the HF in the gas phase exists as monomer. The dependence of equilibrium constant K on T_g (or T) is given by

$$-\log_{10} K = 2.303 \frac{\Delta H_{HF,1-6}}{R} \frac{1}{T_g} + \log_{10} K_o \qquad [5\text{-}10a]$$

$$\log_{10} K = 8910/T_g - 43.65 \qquad [5\text{-}10b]$$

where $\Delta H_{HF,1\text{-}6}$ is the enthalpy of formation of the H-bonded HF hexamer (-40.8 kcal/mol $(HF)_6$, or -8.1 kcal/H-bond formed,; the enthalpy of endothermic depolymerization has the same value but is positive).

As an aside note, recall that P_{HF} is defined as the HF partial pressure that would exist if all HF molecules in the vapor state were monomeric (equation [5-2]). However, P_{HF}', the HF partial pressure of the nonideal HF vapor, is the sum of the HF monomer ($P_{HF,1}$) and HF hexamer ($P_{HF,6}$) partial pressures actually existing in the nonideal HF vapor state:

$$P'_{HF} = P_{HF,1} + P_{HF,6} \qquad [5\text{-}11]$$

By equation [5-11], the equilibrium constant, K, is defined as $K = P_{HF,1}/P_{HF,6}^{6}$. P_{HF} is related to $P_{HF,1}$ and $P_{HF,6}$ by

$$P_{HF} = P_{HF,1} + 6P_{HF,6} \qquad [5\text{-}12]$$

and f is related to P_{HF}', $P_{HF,1}$, and $P_{HF,6}$ by

$$f = (P_{HF,1} + 6P_{HF,6})/P'_{HF} \qquad [5\text{-}13]$$

Consequently, P_{HF} is related to P_{HF}' and f by

$$P_{HF} = f\, P'_{HF} \qquad [5\text{-}14]$$

For reference, the equation of state for nonideal HF vapor is given by equation [4-4a].

The fugacity coefficients χ_{HF} and $\chi_{HF}^{\cdot}$ in equation [5-7] correct for the nonideality of the HF vapor. The HF vapor fugasity coefficent χ_{HF} at P_{HF}' and T_g is calculated by the integral

$$\ln \chi_{HF} = \int_0^{P'_{HF}} \frac{(1/f - 1)}{P'_{HF}} \, dP'_{HF} \qquad [5\text{-}15]$$

Equation [5-15] is adapted from a similar but more generic equation given by Denbigh (1981).

Given the nonlinear dependence of "f" on P_{HF}' and T_g, it is obvious that equation [5-15] cannot be integrated analytically. Therefore, equation [5-15] was integrated numerically. Specifically, at a given T_g, K was calculated by equation [5-10b], and then f was calculated as a function of P_{HF}' by equation [5-9]. With f vs. P_{HF}' known, $(1/f - 1)/P_{HF}'$ vs. P_{HF}' was integrated numerically from $P_{HF}' = 0$ to $P_{HF}' = P_{HF}'$. From this integral, χ_{HF} was determined. The same procedure was used to calculate $\chi_{HF}^{\cdot}$ at $P_{HF}^{\cdot}$.

Once χ_{HF} and $\chi_{HF}^{\cdot}$ at P_{HF}' and T_g were determined, r_k at P_{HF}' and T_g was calculated by equation [5-7]. Calculated values for r_k as a function of T_g and P_{HF}' are given in Figure 5.10. All calculations were carried out by program **RK.BAS**, which is listed in Appendix D.

If the cumulative micropore volume, $V_{p,u}(r)$ (cm^3/g-wood) in the HF-reacted wood chip is known, then the total HF loading to to pore condensation ($\theta_{e,p-c}$) is estimated by

$$\theta_{e,p-c} = \rho_{HF,l} \, V_{p,\mu}(r_k) \qquad [5\text{-}16]$$

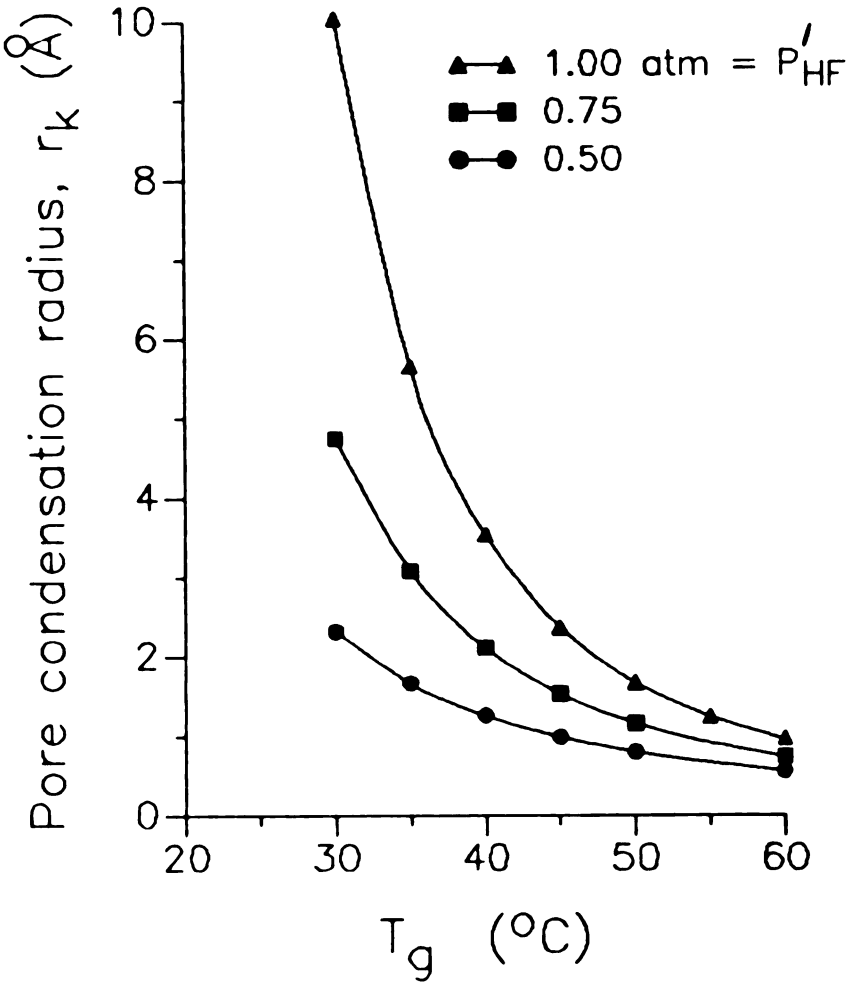


Figure 5.10. Maximum micropore radius (r_k) for capillary condensation of nonideal HF vapor: effect of nonideal HF vapor partial pressure (P'_{HF}) and temperature (T_g).

Alternatively, $\theta_{e,p-c}$ can be estimated from the micropore size distribution by

$$\theta_{e,p-c} = \rho_{HF,l} \int_{o}^{r_k} \frac{dV_{p,\mu}(r)}{dr} dr \qquad [5\text{-}17]$$

The cumulative micropore volume $V_{p,\mu}(r)$ for the HF-reacted wood chip after HF-desorption must be determined experimentally. A common, nonevasive method is N_2 physisorption and pore filling. Specifically, $V_p(r)$ is measured as a function of P_{N2}/P_{N2}° by the N_2 vapor physical sorption isotherm at high P_{N2}/P_{N2}° and T_s = -195.8 °C (n.b.p. N_2). The pore-condensation radius (r_k) for N_2 vapor at T_s = -195.8 °C is then determined as a function of P_{N2}/P_{N2}° by the Kelvin Equation for ideal N_2 vapor. Since V_p and r are known as a function of P_{N2}/P_{N2}°, $V_p(r)$ is easily determined.

Unfortunately, $V_p(r)$ for the HF-reacted wood chip was not determined here. Therefore, $V_p(r_k)$ as a function of r_k for nonideal HF vapor was not determined, and hence $\theta_{e,p-c}$ was not determined. These determinations are highly recommended for future study. As a final note, the total micropore volume and micropore size distribution of the HF-reacted wood chip is most likely different than that for a native wood chip. Therefore, $V_p(r)$ for the HF-reacted wood chip is a function of reaction conditions.

Chapter 6. Reaction Rate and Sugar Yield Experiments

Introduction

The solvolysis of lignocellulose by anhydrous Hydrogen Fluoride (HF) vapor is an unsteady-state, noncatalytic, gas/solid reaction that generates solid sugar fluoride products, reversion oligosaccharides, and residual lignin. This chapter presents reaction rate and sugar yield data for the solvolysis of a single lignocellulose chip by an anhydrous HF vapor stream as a function of reaction time, chip thickness, and HF vapor conditions.

The reaction rate and sugar yield data presented in this chapter were obtained using the vapor-phase HF solvolysis apparatus and reaction procedure described in chapter 4. Specifically, a single lignocellulose chip was contacted with an anhydrous HF vapor stream of fixed flowrate, temperature, and HF partial pressure for a given reaction time within a carefully-controlled, milligram scale laboratory reactor. After a given reaction time, the HF-reacted lignocellulose chip was removed from the reactor and quenched with water by a novel Teflon sampling mechanism built into the reactor. The glucose and xylose yields in the water-soluble reaction products after "posthydrolysis" were then assayed by High-Performance Liquid Chromatography (HPLC). By these experimental techniques, sugar yield vs. time data for the solvolysis of a single lignocellulose chip by anhydrous HF vapor were generated as a function of HF vapor stream flowrate, temperature, and HF partial pressure. These data are collectively referred to as "reaction rate and sugar yield"

data.

Please note that the glucose yield in the water-soluble reaction products after posthydrolysis quantifies glucosyl flouride production and cellulose conversion in the HF-reacted wood chip. Likewise, the xylose yield in the water-soluble reaction products after posthydrolysis quantifies xylosyl fluoride production and hemicellulose conversion in the HF-reacted wood chip. The presence of glucose polymers in hemicellulose complicates the correlation of glucose yield to cellulose conversion, because about 10% of the maximum theoretical glucose yield from Bigtooth Aspen wood comes from hemicellulose (see Tables 4.3 and 4.4).

The specific lignocellulosic materials studied in this dissertation included Bigtooth Aspen wood, prehydrolyzed (hemicellulose-free) Bigtooth Aspen wood, pure cellulose (filter paper), and filter paper/"milled-wood" lignin composite wafers. The typical lignocellulose chip was about 0.4 mm thick, 1.0 cm/side, and weighed about 12 mg (prehydrolyzed wood) to 15 mg (wood). In most of the experiments, the lignocellulose samples were dried to less than 2% moisture before reaction. However, a limited series of experiments were conducted with methanol-absorbed wood and pure cellulose. The specific process parameters studied included reaction time (t), lignocellulose chip thickness (2L, half-thickness L), 100% HF vapor mass velocity (G_{HF}), gas-stream HF partial pressure or mole fraction (P_{HF} or y_{HF}), and gas-stream temperature (T_g). In all experiments, the total system pressure (P_T) was fixed at 1.0 atm.

This chapter is organized into five sections, labeled I to V. In section I, the physical observations of wood and pure cellulose before and after reaction with HF vapor are summarized. In section II, reaction rate and sugar yield data from the vapor-phase HF solvolysis of Bigtooth Aspen wood and pure cellulose (filter paper) are presented and discussed. In section III, reaction rate and sugar yield data from "prehydrolyzed" (hemicellulose-free) Bigtooth Aspen wood are presented and discussed. In section IV, maximum sugar yield and total product recovery data from Bigtooth Aspen wood, prehydrolyzed Bigtooth Aspen wood, pure cellulose (filter paper), and filter paper/"milled-wood" lignin composite substrates are compared. Finally, in section V, the "reversion" oligosaccharide distribution in the water-soluble reaction products before posthydrolysis is profiled by HPLC. Specifically, in section V, reversion oligosaccharide profiles from the vapor-phase HF solvolysis of pure cellulose and prehydolyzed wood are shown as a function of reaction time, 100% HF vapor temperature, and substrate methanol content.

The reaction rate and sugar yield data presented in this chapter constitute the benchmark experiments for the vapor-phase HF solvolysis of lignocellulose. In chapters 8 to 10, these data will be used to develop and evaluate a mathematical model for the reaction of a single wood chip with an anhydrous HF vapor stream. The data and model for the single chip system can then be extended to develop chemical reactor concepts for the production of fermentable sugars from wood via vapor-phase HF solvolysis. These reactor concepts might include packed-bed or fluidized bed configurations for HF vapor/wood contacting and reaction.

I. Physical Observations of Wood and Filter Paper Wafers Before and After Exposure to HF Vapor

Before I present the reaction rate and sugar yield data for the vapor-phase solvolysis of Bigtooth Aspen wood and pure cellulose, I will describe the appearance of a single wood chip and filter paper wafer before and after exposure to HF vapor.

Photographs of Bigtooth Aspen wood, prehydrolyzed Bigtooth Aspen wood, and filter-paper/"milled-wood" lignin composite wafers before and after exposure to HF vapor are shown in Figures 6.1a to 6.1c.

The overall wood chip structure remained intact upon exposure to HF vapor whereas the filter paper wafer gradually "melted" to a clear, glutinous drop. At a reaction time sufficient for complete cellulose conversion (2 to 15 min, depending on reaction conditions), the HF-adsorbed and reacted wood chip was dark-brown to black in color. Typically, the longer the reaction time, the darker the color. At low 100% HF vapor temperatures, e.g. 30 °C to 40 °C (conditions for high HF loading on the solid), the HF-reacted wood chip looked wetted, flaccid, sticky and shiny. However, the overall shape of the HF-reacted wood chip did not swell significantly. The HF-reacted "prehydrolyzed" wood chip did not appear as "sticky" as an HF-reacted wood chip obtained under the same reaction conditions. At higher 100% HF vapor temperatures (> 50 °C) and/or low HF partial pressures (e.g. 0.4 atm at 30 °C), the HF-reacted wood chip was rigid and brittle. The HF-reacted solid could be easily crumbled to a fine brown-black powder. These

(a)

(b)

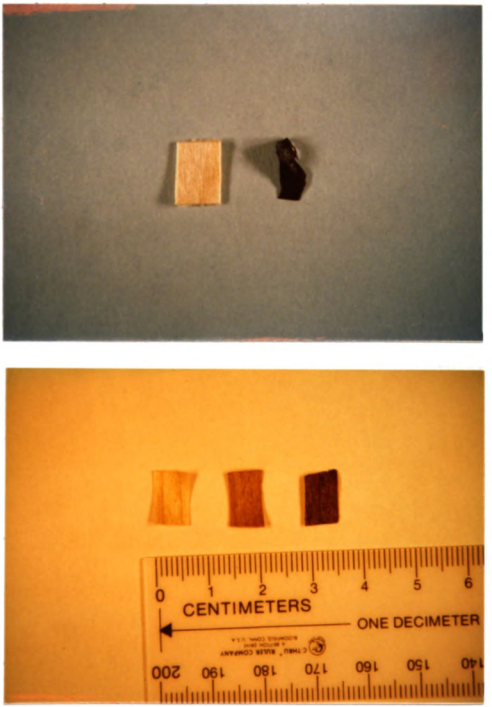
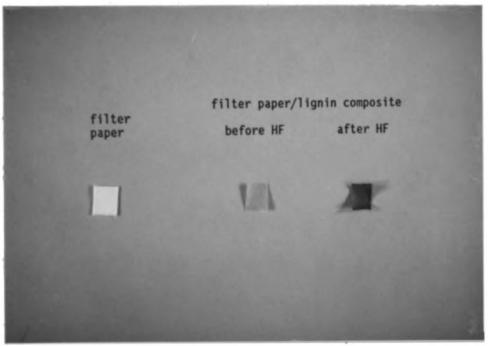


Figure 6.1. Photographs of single lignocellulose wafers before and after reaction with HF vapor: (a) Bigtooth Aspen wood; (b) pre-hydrolyzed Bigtooth Aspen wood (middle). Notes: for photographs (a) and (b), the HF-reacted solid (after HF desorption) is shown.

(c)



(d)

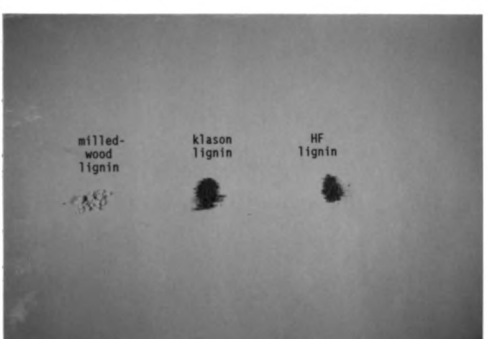


Figure 6.1 (cont'd.). (c) filter paper/"milled-wood" lignin composite substrate; (d) residual lignins. Note: for photograph (c), the water-insoluble, residual lignin shell is shown.

solid properties were also observed when the HF adsorbed on the HF-reacted wood chip was desorbed under flowing N_2 gas.

At complete conversion, all the reaction products of the vapor-phase HF solvolysis of filter paper were soluble in water, whereas for wood, a cinnamon-brown lignin shell remained insoluble. This residual lignin shell remained essentially intact and retained the overall shape of the original wood chip. However, at low 100% HF vapor temperatures, the residual lignin shell often disintegrated into large fragments and fine material. The adsorbed HF did not dissolve the lignin shell, because lignin is insoluble in liquid HF (Smith et al, 1983).

The water-soluble product solution (typically 5 - 10 mg sugar-oligomer in 10 mL H_2O) from the vapor-phase HF solvolysis of Bigtooth Aspen wood chips was either clear or pale yellow in color, depending on reaction conditions. Usually, at long reaction times and low HF vapor temperatures (e.g. 100% HF vapor at 30 ^oC), the product solution was pale yellow. The product solution from the vapor-phase HF solvolysis of filter paper was always clear.

The effect of vapor-phase HF solvolysis on the composite microstructure of the lignocellulosic matrix was also observed directly via light microscopy. See chapter 8, Figures 8.5a to 8.5d for microphotographs of the native and HF-reacted lignocellulosic matrix.

II. Reaction Rate and Sugar Yield Data from the Vapor-Phase HF Solvolysis of Bigtooth Aspen Wood and Pure Cellulose

In this section, reaction rate and sugar yield data obtained from the vapor-phase HF solvolysis of single Bigtooth Aspen wood or pure cellulose (filter paper) wafers are presented. First, gas-phase external mass-transfer resistances are minimized by determining the 100% HF vapor flowrate at which the glucose production rate is independent of flowrate. Similarly, intraparticle mass-transfer resistances are minimized by establishing a particle size (i.e. chip thickness) at which the glucose yield vs. time profile is independent of lignocellulose chip thickness. Under conditions where mass-transfer resistances are experimentally minimized, the effects of HF-N_2 gas-stream HF partial pressure and temperature on the glucose yield vs. time profile are then investigated.

A comparison of the maximum sugar yields and total product recovery data from Bigtooth Aspen wood, prehydrolyzed wood, pure cellulose (filter paper), and pure cellulose/"milled-wood" lignin composite wafers is reserved for section IV.

A. Minimization of Mass-Transfer Resistances: Effect of HF Vapor Flowrate and Wood Chip Thickness

External Mass Transfer Resistances. The solvolysis of a single wood chip by anhydrous HF vapor is a noncatalytic gas-solid reaction subject to external and internal mass-transfer resistances. Since the reaction of 100% (undiluted) HF vapor with a dry wood chip generates only solid sugar fluoride products which stick to the intact and porous lignin framework, in principle no external gas-phase mass-transfer resistances can exist because no HF vapor gradient can exist between the bulk HF

vapor and the wood chip surface. However the void volume of the very porous (about 2 mL/g) Bigtooth Aspen wood chip is initially filled with air. When the wood chip contacts the 100% HF vapor, air diffuses out of the porous volume of the wood chip and temporarily creates a HF-air film around the wood chip through which incoming HF vapor molecules must diffuse. When all of the air diffuses out of the porous volume of the HF-reacting wood chip, any HF vapor concentration gradients are eliminated, and the HF vapor concentration near and within the porous volume of the HF-reacting wood chip is equal to the 100% bulk HF vapor stream concentration.

The 100% HF vapor stream mass velocity (G_{HF}) sufficient for minimizing external mass-transfer resistances for wood chips of 0.4 mm thick x 1.0 cm/side was determined by increasing the HF mass velocity until the glucose production rate was independent of HF mass velocity, as shown in Figure 6.2 (see also Figures 6.11 and 6.12). Based on the data given in Figure 6.2, a mass velocity of $G_{HF} > 0.3$ g HF/cm^2-min was assumed sufficient for minimizing external mass-transfer resistances. The Reynolds number (Re_z) given in Figure 6.2 for 100% HF vapor flowing over the wood chip is defined as

$$Re_z = G_{HF}\, z/2\, \mu_g \qquad [6\text{-}1]$$

where G_{HF} is the 100% HF vapor stream superficial mass velocity (g HF/cm^2-min or g HF/cm^2-sec), z is the face length of the wood chip (z = 1.0 cm), and μ_g is the visocity of HF vapor (μ_g = 0.013 cp or 1.3 10^{-4} g/cm-sec at 30 ^{o}C; see Table

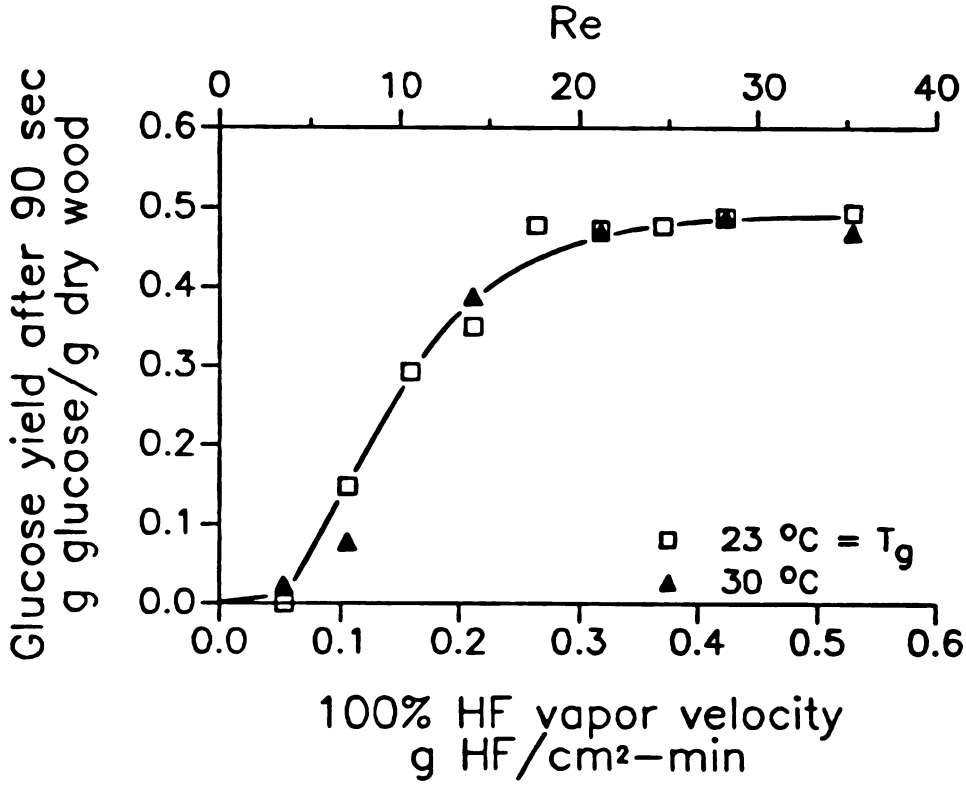


Figure 6.2. Vapor-phase HF solvolysis of a single Bigtooth Aspen wood chip (2L = 0.4 mm): effect of 100% HF vapor velocity (G_{HF}, g HF/ cm^2-min) on the glucose production rate.

4.2 and Posey, 1953).

Internal Mass Transfer Resistances. In order to determine if wood chips of 0.4 mm thickness were sufficient to minimize internal mass-transfer resistances, glucose yield vs. time data from wood chips of 0.4 mm thickness was compared to glucose yield vs. time data from wood chips of 0.2 mm thickness, as shown in Figure 6.3. Based on the data in Figure 6.3, wood chips of 0.4 mm thickness were sufficient for minimizing internal mass-transfer resistances. The data presented in Figure 6.3 were obtained under an overall HF-N_2 gas-stream mass velocity of 0.3 g/cm^2-min, so that external mass-transfer resistances were experimentally minimized. The HF vapor stream was diluted with an N_2 gas stream so that binary diffusion of HF vapor in N_2 could always occur within the porous volume of the wood chip. Furthermore, since binary diffusion of HF vapor in N_2 would always occur within the porous volume of the wood chip, a permanent gas-phase HF concentration gradient could exist during HF adsorption/reaction as well. However, these gas-phase diffusional limitations were assumed to be experimentally minimized.

A detailed investigation of the effect of wood chip thickness (2L) on the global glucose production rate was beyond the scope of this dissertation. However, a detailed experimental and mathematical analysis of the effect of external and intraparticle gas-phase mass transport resistances on glucose production rate is highly recommended for future study.

In summary, it was assumed that if the gas-stream mass-velocity was at least 0.3 g/cm^2-min, and the wood chip thickness was 0.4 mm, then gas-phase

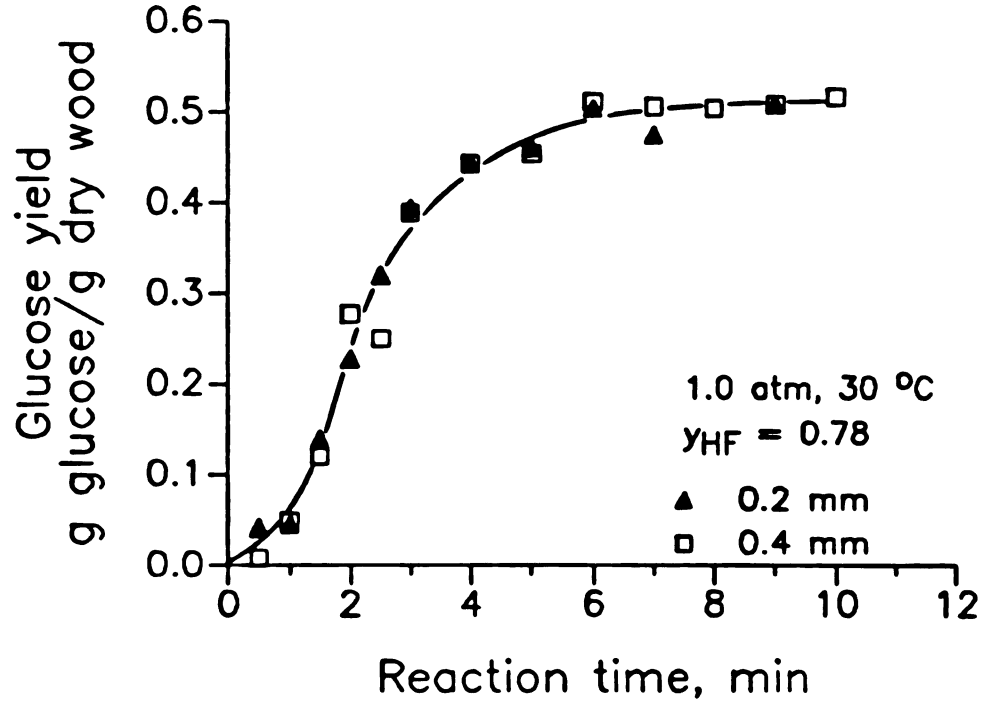


Figure 6.3. Vapor-phase HF solvolysis of a single Bigtooth Aspen wood chip: effect of chip thickness (2L = 0.4 mm vs. 0.2 mm) on the glucose yield vs. time profile. Note: G = 0.3 g/cm^2-min.

mass-transfer resistances were experimentally minimized.

Although mass-transfer resistances were minimized, external and internal heat-transfer resistances may still exist. Recall from chapter 5 that the heat of adsorption of HF vapor onto the lignocellulosic matrix is exothermic. If heat-transfer resistances are present, then the temperature of the HF-reacting lignocellulose chip will increase as HF adsorbs onto the solid. Particle temperature measurements for a single prehydolyzed wood chip in a 100% HF vapor stream are described in chapter 7. A differential energy balance and heat transport model for the solvolysis of a single lignocellulose chip by a 100% HF vapor stream is developed and solved in chapters 9 and 10.

B. Effect of Gas-Stream HF Partial Pressure (or Mole Fraction) on the Glucose Yield vs. Time Profile

Glucose yield vs. time profiles obtained from the solvolysis of single, dry Bigtooth Aspen wood chips by a HF-N_2 gas-stream at 30 °C, 1.0 atm total pressure and HF mole fraction (y_{HF}) ranging from 0.4 to 1.0 are presented in Figure 6.4. The gas-stream HF concentration was decreased by increasing the N_2 gas flowrate at a fixed HF vapor flowrate of 1.65 g HF/min (0.21 g HF/cm^2-min). The total HF-N_2 gas-stream mass velocity (G) was always maintained at at least 0.3 g/cm^2-min, so that gas-phase external mass transfer resistances were experimentally minimized. The wood chip thickness was fixed at 0.4 mm, so that intermal mass transfer resistances were also experimentally minimized.

The mole fraction of HF in the gas stream (y_{HF}) is calculated from the molar

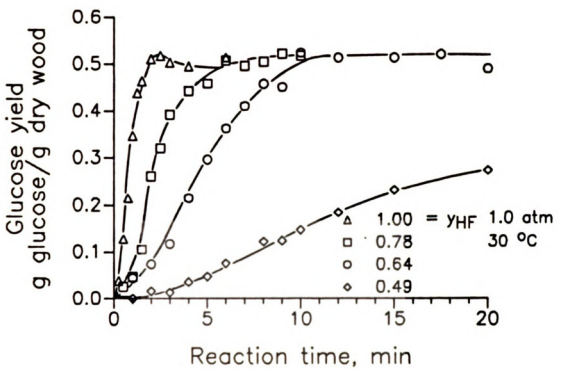


Figure 6.4. Vapor-phase HF solvolysis of a single Bigtooth Aspen wood chip (2L = 0.4 mm): effect of gas-phase HF mole fraction, y_{HF} on the glucose yield vs. time profile at 1.0 atm and T_g = 30 °C. Note: HF vapor mass flowrate fixed at 1.65 g HF/min (0.0825 mol/min), N_2 flowrate increased accordingly.

flowrates of HF (F_{HF}) and N_2 (F_{N2}) by

$$y_{HF} = F_{HF}/(F_{HF} + F_{N_2}) \qquad [6\text{-}2]$$

The HF-N_2 gas-stream HF partial pressure (P_{HF}) is calculated by

$$P_{HF} = y_{HF}\, P_T \qquad [6\text{-}3]$$

where P_T is the total system pressure, which is always fixed at 1.0 atm. Although HF in the vapor-phase can form hydrogen-bonded HF-oligomers, the HF molar flowrate (F_{HF}), HF mole fraction (y_{HF}), and HF partial pressure (P_{HF}) are calculated under the basis that all HF molecules are in the monomeric state (20 g HF vapor = mole HF vapor). If 100% HF vapor at 1.0 atm system pressure is used, the HF partial pressure P_{HF} is taken as 1.0 atm, even though gas-phase HF-oligomers may be present.

In general, the glucose yield vs. time profile decreased with decreasing gas stream HF partial pressure. Since HF must first physically adsorb onto the lignocellulosic matrix before cellulose solvolysis can occur, the dependence of glucose production rate on HF concentration is more accurately described by the HF loading on the wood chip (θ_e) as opposed to the gas stream HF partial pressure (P_{HF}).

The glucose yield vs. time profile was also sigmoidal in shape. Again, if it is assumed that HF must first physically adsorb onto the lignocellulosic matrix before reaction with cellulose, then the adsorption and reaction steps are sequential. In

general, for a sequential reaction scheme, the final product concentration vs. time curve is sigmoidal, or S-shaped. Therefore, the sigmoidal shape of the glucose yield vs. time profile is the result of the sequential processes of 1) physical adsorption of HF vapor onto the lignocellulosic matrix, 2) solvation of the cellulose microfibril by adsorbed HF via displacement of OH...OH hydrogen bonds with stronger HO...HF hydrogen bonds, and 3) solvolytic cleavage of HF-solvated cellulose chains to glucosyl fluoride. Recall that the glucosyl fluoride generated within the HF-reacted wood chip is quantified experimentally as the glucose yield in the water-soluble reaction products after posthydrolysis. The sequential adsorption and reaction processes are mathematically modeled in chapter 8.

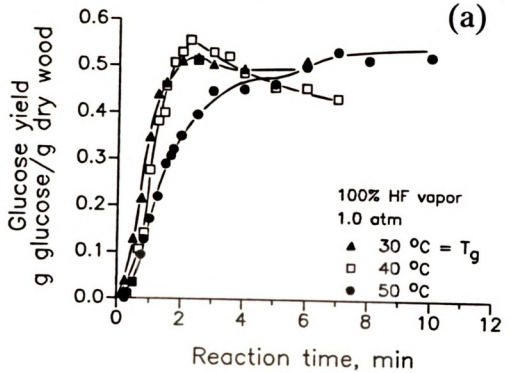
External mass transfer resistances may exist when the HF vapor stream is diluted in N_2 gas, because the physical properties of the HF-N_2 mixture are different than the physical properties of 100% HF vapor, and so therefore the mass transfer coefficient is affected by HF partial pressure. In this study, I simply assumed that if the total HF-N_2 gas-stream flowrate was at least 0.3 g/cm^2-min (the mass velocity sufficient for minimizing external mass-transfer resistances for the reaction of 100% HF vapor with wood), then external mass-transfer resistances were minimized regardless of gas-phase HF partial pressure. The possibility of external mass-transfer resistances for HF vapor diluted in N_2 gas can be tested by increasing the total mass flowrate at fixed HF:N_2 ratio and observing if the glucose production rate increases. This experiment was not attempted in this study, however.

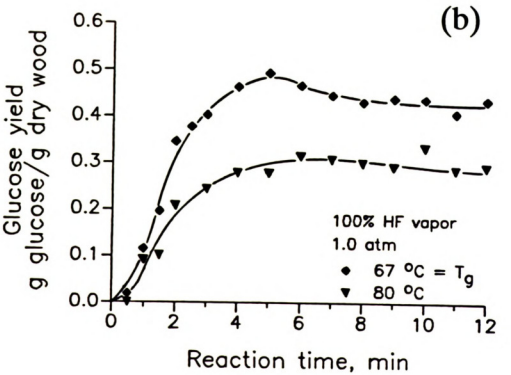
C. Effect of 100% HF Vapor Stream Temperature on the Glucose Yield vs. Time Profile

Glucose yield vs. time profiles obtained from the solvolysis of single, dry Bigtooth Aspen wood chips (0.4 mm thick x 1.0 cm/side) by a 100% HF vapor stream at 1.0 atm and temperatures (T_g) from 30 °C to 80 °C are given in Figures 6.5a and 6.5b. Glucose yield vs. time profiles obtained from the solvolysis of pure cellulose wafer (Whatman filter paper No. 3, ca. 0.5 mm thick x 1.0 cm/side) by a 100% HF vapor stream at 1.0 atm and temperatures (T_g) of 27 °C, 50 °C, and 77 °C are given in Figure 6.6.

When the 100% HF vapor stream temperature increased, the observed, or global rate of glucose production decreased. Consider here that the rate of glucose production is dependent on the 1) glucan concentration in the unreacted cellulose, 2) HF loading on the lignocellulosic matrix, and 3) the reaction temperature. As the HF vapor stream temperature increases, the HF loading on the lignocellulosic matrix that the cellulose perceives for solvolysis decreases, but the intrinsic rate constant(s) for cellulose solvolysis increases, i.e. $T \uparrow k_i \uparrow \theta_e \downarrow$. Thus, the thermodynamics of HF physical adsorption and the Arrhenius kinetics of cellulose solvolysis work in opposing directions with increasing temperature, and this coupling determines the overall dependence of global glucose production rate on 100% HF vapor stream temperature. This behavior is modeled is chapter 8, and model predictions are compared to data in chapter 10.

Figure 6.5. Vapor-phase HF solvolysis of a single Bigtooth Aspen wood chip (2L = 0.4 mm): effect of 100% HF vapor stream temperature (T_g) on the glucose yield vs. time profile. (a) 30 °C, 40 °C, 50 °C; (b) 67 °C, 80 °C. Note: G_{HF} = 0.31 g HF/cm^2-min.


(a)
Glucose yield
g glucose/g dry wood
0.6
0.5
0.4
0.3
0.2
0.1
0.0
0
2
4
6
8
10
12
Reaction time, min
100% HF vapor
1.0 atm
30 °C = T_g
40 °C
50 °C


(b)
Glucose yield
g glucose/g dry wood
0.6
0.5
0.4
0.3
0.2
0.1
0.0
0
2
4
6
8
10
12
Reaction time, min
100% HF vapor
1.0 atm
67 °C = T_g
80 °C

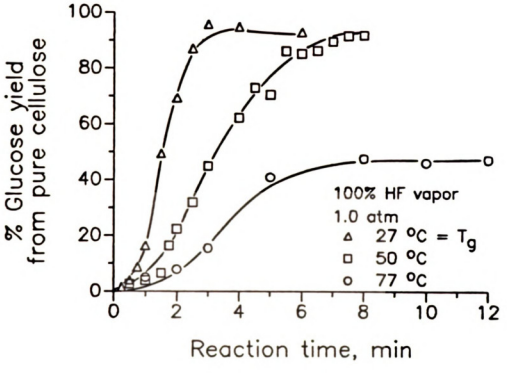


Figure 6.6. Vapor-phase HF solvolysis of a single, pure cellulose wafer (Whatman filter paper No. 3): effect of 100% HF vapor stream temperature on the glucose yield vs. time profile (T_g = 27 °C, 50 °C, 77 °C). Note: G_{HF} = 0.31 g HF/cm^2-min.

D. Effect of 100% HF Vapor Stream Temperature and Equilibrium HF Loading on Maximum Glucose Yield

At 100% HF vapor-stream temperatures (T_g) greater than 60 °C, the maximum experimentally-attainable glucose yield from Bigtooth Aspen wood decreased with increasing temperature, as shown in Figure 6.7 and Table 6.1. At 100% HF vapor temperatures greater than 60 °C, the equilibrium loading of HF on the wood chip (θ_e) was not sufficient to insure a stoichiometric reaction with glucan in cellulose and xylan in hemicellulose. Similarly, the effect of 100% HF vapor stream temperature (27 °C to 90 °C) on the maximum attainable glucose yield from filter paper is shown in Table 6.2.

What is the minimum HF loading on wood necessary for stoichiometric reaction with cellulose and hemicellulose? First, adsorbed HF is required to "solvate" cellulose chains away from the paracrystalline cellulose microfibril by displacing OH...OH hydrogen bonds with stronger HO..HF hydrogen bonds. Each glucan (or xylan) unit has 3 OH groups, so 3 HF molecules per glucan (or xylan) unit are required. Second, one HF molecule is required per HF-solvated glucan (or xylan) unit to solvolytically cleave the ß-1,4-O-glycosidic linkage and yield glucosyl fluoride (or xylosyl fluoride). Therefore 4 HF molecules per glucan unit are required for complete cellulose solvolysis (the same is true for xylan). Thus, theoretical minimum HF loading (θ_{min}) for stoichiometric reaction of cellulose and hemicellulose in Bigtooth Aspen wood is estimated by

$$\theta_{min} = 4\, M_{w,HF}\, ([G_o] + [X_o]) = 0.387 \text{ g HF/g-wood} \qquad [6\text{-}4]$$

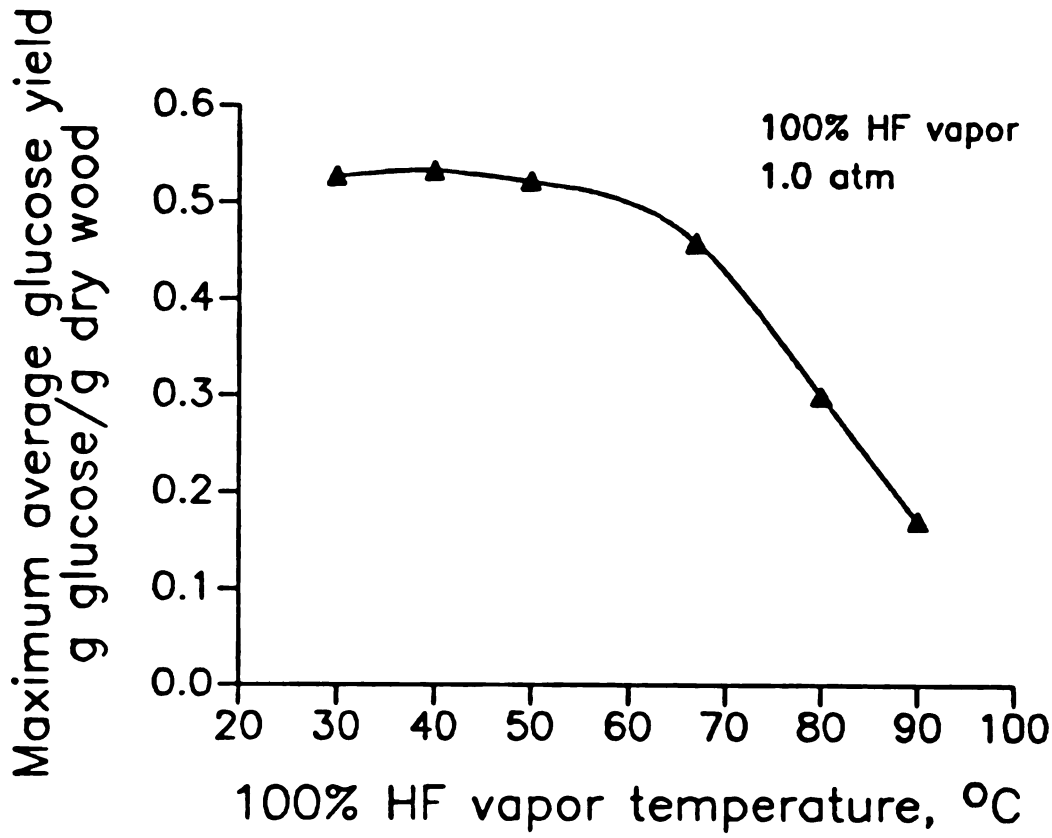


Figure 6.7. Vapor-phase HF solvolysis of Bigtooth Aspen wood: effect of 100% HF vapor temperature (T_g) on the maximum average glucose yield obtained from the water-soluble products (after posthydrolysis).

Table 6.1. Summary of maximum average glucose and xylose yields obtained from the vapor-phase HF solvolysis of Bigtooth Aspen wood as a function of 100% HF vapor temperature (T_g)at 1.0 atm and equilibrium HF loading (θ_e) (water-soluble products after posthydrolysis); see Figure 6.7.

T_g	θ_e	Maximum Glucose Yield		Maximum Xylose Yield	
		Experiment	Eqn. [6-5a]	Experiment	Eqn. [6-5b]
°C	g HF/g [a]	g/g +/- 1s [b]	g/g	g/g +/-1s [c]	g/g
29-30	1.493	0.527 +/-0.028 (n=5)	0.618	0.151 +/-0.024 (n=5)	0.210
40	0.909	0.535 +/-0.016 (n=5)	0.618	0.132 +/-0.013 (n=5)	0.210
50	0.574	0.525 +/-0.017 (n=7)	0.618	0.143 +/-0.027 (n=7)	0.210
67	0.308	0.457 +/-0.027 (n=13)	0.492	0.137 +/-0.010 (n=13)	0.167
80	0.122	0.301 +/-0.062 (n=12)	0.194	0.098 +/-0.013 (n=12)	0.066
90	-	0.171 +/-0.019 (n=5)	-	0.064 +/-0.004 (n=5)	-

Notes:

[a] g HF/g = g HF adsorbed/g-wood

[b] g/g = g glucose/g-wood

[c] g/g = g xylose/g-wood

Table 6.2. Summary of maximum average glucose yields obtained from the vapor-phase HF solvolysis of filter paper as a function of 100% HF vapor temperature (T_s) at 1.0 atm (after posthydrolysis of water-soluble products).

T_s	Maximum Glucose Yield				
°C	mmol/g	+/- 1s [a]	% theoretical [b]		n
27	5.799	+/-0.157	94.0	+/-2.5	4
50	5.658	+/-0.157	91.7	+/-2.5	3
77	2.920	+/-0.054	47.3	+/-0.9	3
90	1.269	+/-0.221	20.6	+/-3.6	5

Notes:

[a] mmol/g = mmol glucose/g filter paper

[b] maximum theoretical glucose yield from Whatman filter paper No. 3 = 6.17 mmol/g

where $[G_o]$ is the estimated glucan concentration in Bigtooth Aspen wood (3.441 mmol/g-wood), $[X_o]$ is the estimated xylan concentration in Bigtooth Aspen wood (1.4 mmol/g-wood), and $M_{w,HF}$ is the molecular weight of HF (20 g/mol).

The theoretical dependence of maximum-attainable glucose yield $[G'_o]$ on equilibrium HF loading (θ_e) is estimated by

$$[G'_o] = \begin{cases} [G_o] & \text{if } \theta_e \geq \theta_{min} \\ [G_o] \cdot \theta_e / \theta_{min} & \text{if } \theta_e < \theta_{min} \end{cases} \quad [6\text{-}5a]$$

Likewise, the theoretical dependence of maximum-attainable xylose yield $[X'_o]$ on equilibrium HF loading (θ_e) is estimated by

$$[X'_o] = \begin{cases} [X_o] & \text{if } \theta_e \geq \theta_{min} \\ [X_o] \cdot \theta_e / \theta_{min} & \text{if } \theta_e < \theta_{min} \end{cases} \quad [6\text{-}5b]$$

Given equation [6-4], equation [6-5a] and equilibrium HF loading vs. 100% HF vapor temperature data (θ_e vs. T_g), the dependence of maximum theoretical glucose xylose yield on θ_e and T_g was calculated. Given θ_e vs. T_g, the dependence of the maximum average experimentally-obtained glucose and xylose yield on θ_e was also determined. The experimental and calculated maximum attainable glucose yield at equilibrium loadings corresponding to 100% HF vapor stream temperatures of 30 °C to 80 °C are compared in Table 6.1. In general, equation [6-5a] predicts the observed data trend, although the calculated vs. experimental yields differ significantly.

The presence of hemicellulose in the wood most likely complicated the effect of HF loading on glucose yield. When parallel experiments were conducted with prehydrolyzed (hemicellulose-free) wood, the agreement between model calculations and data was much improved, as detailed in section III.

Precedent for minimum HF loading requirements is provided by several previous studies of the vapor-phase HF saccharification of wood. In early work, Luers (1938) claimed that for HF loadings of 0.28 to 0.85 kg 95% HF per 1 kg pine wood, 0.40 kg HF/kg-wood was optimal because higher HF loadings did not increase sugar yield although lower HF loadings did decrease sugar yield. Fredenhagen and Cadenbach (1933), and later Sharkov et al. (1972) reported that 1.0 g HF per 1.0 g dry pine wood was needed for complete conversion of cellulosic materials to water-soluble products at 100% HF vapor temperatures of 10 ^{o}C to room temperature. Recently, Franz et al. (1982, 1987) reported that 0.6 g HF per 1 g of "prehydrolyzed" (hemicellulose free) spruce wood was sufficient for complete cellulose conversion. Also, Ostrovski et al. (1985) reported the 0.5 kg HF per 1 kg poplar wood was needed for complete cellulose and hemicellulose conversion. Finally, Reffstrup and Kau (1985) reported that 0.4 g HF per 1 g of barley straw was needed for complete cellulose and hemicellulose conversion. All of these minimum HF loading requirements agree well with the calculated minimum HF loading of 0.387 HF/g-dry wood.

The following experimental data also supports the conclusion that the decrease in maximum attainable glucose yield at 100% HF vapor temperatures greater than

60 °C is due to stoichiometric limitations on adsorbed HF and is not the result of sugar loss.

The decrease in maximum average glucose yield with increasing 100% HF vapor temperatures greater than 60 °C was not due to significant sugar entrapment within lignin. Note from Figure 6.5 and Table 6.2 that the maximum glucose yield from pure cellulose (filter paper) also decreased with increasing temperature at 100% HF vapor stream temperatures greater than 60 °C.

In order to further demonstrate that the decrease in maximum average glucose yield from Bigtooth Aspen wood was due to the limiting stoichiometry of adsorbed HF and was not due to HF-catalyzed glucose degradation at higher temperatures, the dependence of glucose yield vs. time on HF-N_2 gas-stream temperature at a reduced HF concentration (y_{HF} = 0.64) was investigated, as shown in Figure 6.8. Note from Figure 5.1a that at 50 °C and P_{HF} = 0.64 atm, the equilibrium HF loading is about 0.3 g HF/g-wood, which is below θ_{min}. When Figure 6.8 is compared with Figure 6.5a, we see that at a temperature of 50 °C, the lowered glucose yield at an HF partial pressure of 0.64 atm is not due to HF-catalyzed sugar degradation, because, at 50 °C and 1.0 atm, the maximum attainable glucose yield is achieved. In section III, control experiments for the vapor-phase HF solvolysis of prehydrolyzed wood further support these arguments.

Finally, there is a slight possibility that the decrease in glucose yield with increasing 100% HF vapor temperature is due to formation of water-insoluble reversion oligosaccharides. The formation of reversion oligosaccharides by

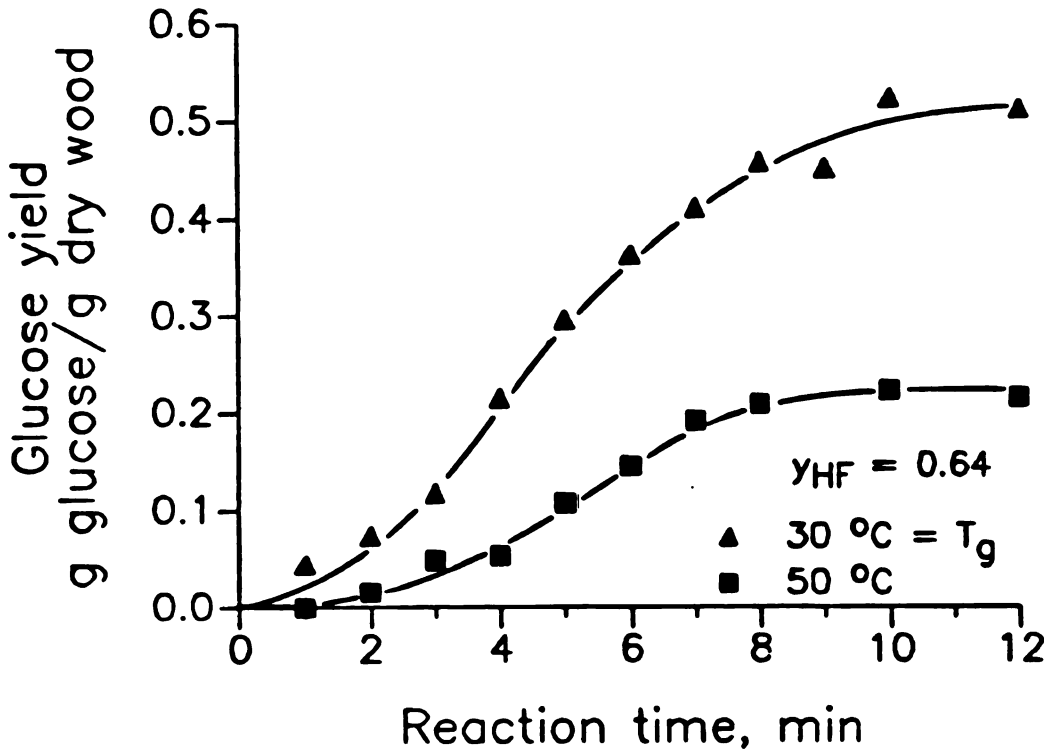


Figure 6.8. Vapor-phase HF solvolysis of a single Bigtooth Aspen wood chip (2L = 0.4 mm): effect of HF-N_2 gas-stream temperature (T_g) on the glucose yield vs. time profile at a reduced mole fraction of HF in the gas phase (y_{HF} = 0.64, P_{HF} = 0.64 atm). Note: G = 0.40 g/cm^2-min.

HF-catalyzed glucosyl fluoride repolymerization during vapor-phase HF solvolysis of lignocellulose is detailed in section V. In general, increasing the temperature increases the average molecular weight of the reversion oligosaccharides. However, the "reversion" oligosaccharides are branched structures with randomized glucosidic linkages, with the α-1,6 linkage predominating (Defaye et al., 1983). These reversion oligosaccharides are thus similar to branched dextrans and pectins, which are very soluble in water at even very high molecular weight due to their branched and amorphous structure. Unfortunately, I did not design the proper control experiment to distinguish unreacted cellulose from water-insoluble reversion oligosaccharides, and so I cannot exclude the possible existence of water-insoluble reversion oligosaccharides.

E. Effects of Gas-Stream HF Partial Pressure (Mole Fraction) and Temperature on the Xylose vs. Time Profile

The xylose yield in the water soluble reaction products after posthydrolysis quantifies the xylosyl fluoride and hemicellulose conversion in the HF-reacted Bigtooth Aspen chip. Therefore, for every glucose yield vs. time curve obtained from the vapor-phase HF solvolysis of Bigtooth Aspen wood, a complimentary xylose yield vs. time profile is also obtained.

The effect of gas-stream HF mole fraction (y_{HF} = 0.4 to 1.0) on the xylose yield vs. time profile at a fixed gas-stream temperature of 30 ^{o}C and 1.0 atm total pressure is shown in Figure 6.9 (compare this figure with the complimentary glucose yield vs. time data given in Figure 6.4). The xylose yield vs. time profile decreased with decreasing gas-stream HF mole fraction, consistent with glucose

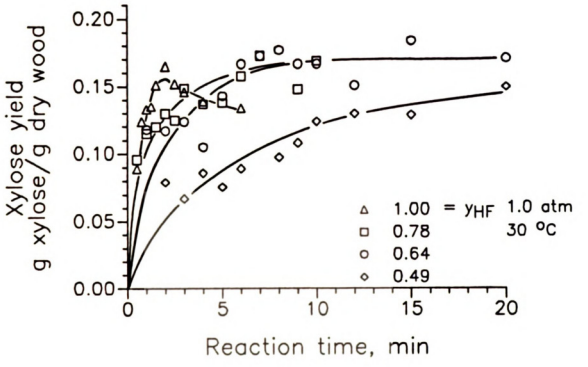


Figure 6.9. Vapor-phase HF solvolysis of a single Bigtooth Aspen wood chip (2L = 0.4 mm): effect of gas-stream HF mole fraction, y_{HF} (or HF partial pressure, P_{HF}) on the xylose yield vs. time profile at T_g = 30 °C (compare with Figure 6.4).

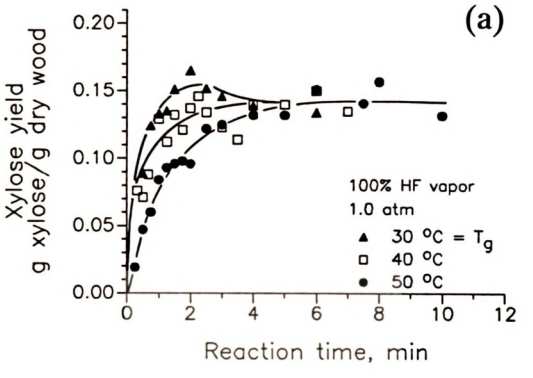
yield vs. time data from Bigtooth Aspen wood obtained under the same conditions.

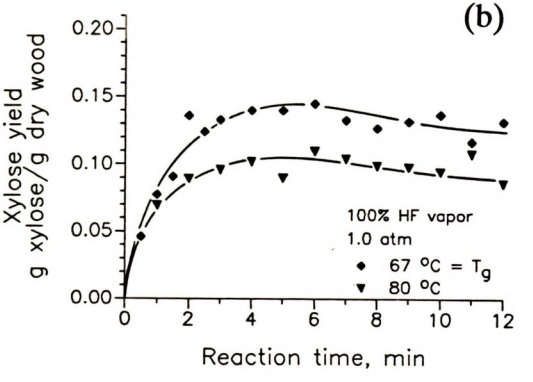
The effect of 100% HF vapor stream temperature (30 °C to 80 °C) on the xylose yield vs. time profile at 1.0 atm is shown in Figures 6.10a and 6.10b (compare these figures with the complimentary glucose yield vs. time data in Figures 6.5a and 6.5b). The xylose yield vs. time profile decreased with increasing 100% HF vapor stream temperature, consistent with glucose yield vs. time data from Bigtooth Aspen wood obtained under the same reaction conditions. The effect of 100% HF vapor temperature on the maximum attainable xylose yield is shown in Table 6.1.

The xylose yield vs. time profile was not S-shaped like the glucose yield vs. time profile. Instead, the xylose yield vs. time profile rapidly approached the maximum-attainable xylose yield. Also, the rate of xylose production was much faster than the rate of glucose production (compare the reaction time frame of Figure 6.5a with Figure 6.10a).

The features of the xylose yield vs. time profile result from the amorphous structure of hemicellulose and its distribution in the lignocellulosic matrix. Recall that hemicellulose is a short-chain, amorphous ß-1,4-linked polymer of anhydroxylose units with gluco-glucuronic acid side chains. This amorphorous hemicellulose is hydrogen bonded to the outer surface of the cellulose microfibril (see Figure 8.3). Therefore, HF vapor preferentially adsorbs and solvates hemicellulose over crystalline cellulose, and thus the rate of xylosyl fluoride production from hemicellulose is faster than the rate of glucosyl fluoride production

Figure 6.10. Vapor-phase HF solvolysis of a single Bigtooth Aspen wood chip (2L = 0.4 mm): effect of 100% HF vapor stream temperature (T_g) on the xylose yield vs. time profile. (a) 30 °C, 40 °C, 50 °C; (b) 67 °C, 80 °C (compare with Figure 6.5).


(a)
Xylose yield
g xylose/g dry wood
0.20
0.15
0.10
0.05
0.00
0
2
4
6
8
10
12
Reaction time, min
100% HF vapor
1.0 atm
30 °C = Tg
40 °C
50 °C


(b)
Xylose yield
g xylose/g dry wood
0.20
0.15
0.10
0.05
0.00
0
2
4
6
8
10
12
Reaction time, min
100% HF vapor
1.0 atm
67 °C = Tg
80 °C

from crystalline cellulose. Furthermore, since the hemicellulose is amorphous and not tightly bound within a paracrystalline hydrogen-bonding network (as is the case with cellulose), the adsorbed HF does not have to work as hard to solvate the hemicellulose.

The maximum xylose recovery in the water-soluble reaction products after posthydrolysis was about 0.153 g xylose/g wood. Since Bigtooth Aspen wood is about 18.5% xylan (Selke, 1983), the maximum theoretical xylose yield is 0.21 g xylose/g wood, and so the typical xylose recovery was about 73% of maximum theoretical. A detailed analysis and comparison of sugar yield recoveries and possible sugar yield losses is reserved for section IV.

III. Reaction Rate and Glucose Yield Data from the Vapor-Phase HF Solvolysis of "Prehydrolyzed" Wood

Prehydrolyzed wood, or "lignocellulose", is a model lignocellulosic substrate which possesses the native architecture and composite microstructure of wood but contains only two chemical components, crystalline cellulose and lignin. As described in chapter 4, prehydrolyzed wood is prepared by selective, mild-acid hydrolysis of the hemicellulose fraction from Bigtooth Aspen wood (e.g. reflux of wood chips in 2 N TFA at 100 °C for 4 h). This prehydrolysis also removes the "extractives" fraction from the wood. The solid residue from prehydrolysis (about 68% of the original weight of the wood) is primarily cystalline cellulose (75%) and lignin (22%) and retains the overall features of the original wood.

Therefore, the reaction of a single prehydrolyzed wood chip with 100% vapor

is a model system for the more complicated HF vapor/wood reaction. Consequently, modeling studies in chapters 8 to 10 will focus on the 100% HF vapor/single prehydrolyzed wood chip reaction system.

Gravimetric HF adsorption, reaction rate, and sugar yield data from the vapor-phase HF solvolysis of prehydrolyzed wood are not complicated by the presence of hemicellulose and extractives. Therefore, from these data, the adsorption and reaction processes of the vapor-phase HF solvolysis of crystalline cellulose within an intact lignin framework can be focused upon and studied. Furthermore, these data can be readily compared to model predictions.

In this section, reaction rate and sugar yield data obtained from the solvolysis of dry, single "prehydrolyzed" (hemicellulose-free) chips by a 100% HF vapor stream fixed at 1.0 atm are presented. First, gas-phase external mass-transfer resistances are minimized by determining the 100% HF vapor flowrate at which the glucose yield vs. time profile is independent of 100% HF vapor flowrate. Under conditions where mass-transfer resistances are experimentally minimized, the effects of 100% HF vapor stream temperature on the glucose yield vs. time profile are then investigated. Also, the effect of 100% HF vapor temperature and equilibrium HF loading on the maximum attainable glucose yield is shown. From this analysis, a simple model for predicting maximum glucose yield from prehydrolyzed wood as a function of 100% HF vapor temperature (T_g) and equilibrium HF loading (θ_e) is developed. Finally, the rate processes of the liquid-phase and vapor-phase HF solvolysis of lignocellulose are compared.

A. Effect of 100% HF Vapor Stream Flowrate and Temperature on the Glucose Yield vs. Time Profile

The reaction of HF vapor with a single, prehydrolyzed wood, or "lignocellulose" chip, is also subject to external mass-transfer resistances. Since this reaction generates only solid glucosyl fluoride products which stick on an intact and porous lignin framework, in principle, no gas-phase external mass-transfer resistances can exist for the reaction of 100% HF vapor (no N_2 diluent) with lignocellulose because no HF vapor concentration gradient can exist between the bulk phase and the lignocellulose chip surface. However, the void volume of the very porous (ca. 3 mL/g) prehydrolyzed chip is initially filled with air. When the chip contacts the 100% HF vapor, air diffuses out of the chip and creates a temporary HF-air film around the chip through which incoming HF vapor must diffuse. The effect of HF vapor flowrate on the glucose production rate is shown in Figures 6.11 and 6.12.

Glucose yield versus time profiles obtained from the reaction of single, dry prehydrolyzed wood chips with HF 100% vapor at 1.0 atm and temperatures (T_g) of 31 °C to 68 °C are given in Figures 6.13a and 6.13b. These data were obtained under conditions of 100% HF vapor mass velocity (0.4 g HF/cm^2-min) and chip thickness (0.4 mm) sufficient to minimize external and internal mass-transfer resistances.

The glucose yield vs. time profile decreased with increasing HF vapor stream temperature. This behavior is explained qualitatively here and quantitatively in chapters 8 and 10. Consider that the glucose production rate is dependent on 1)

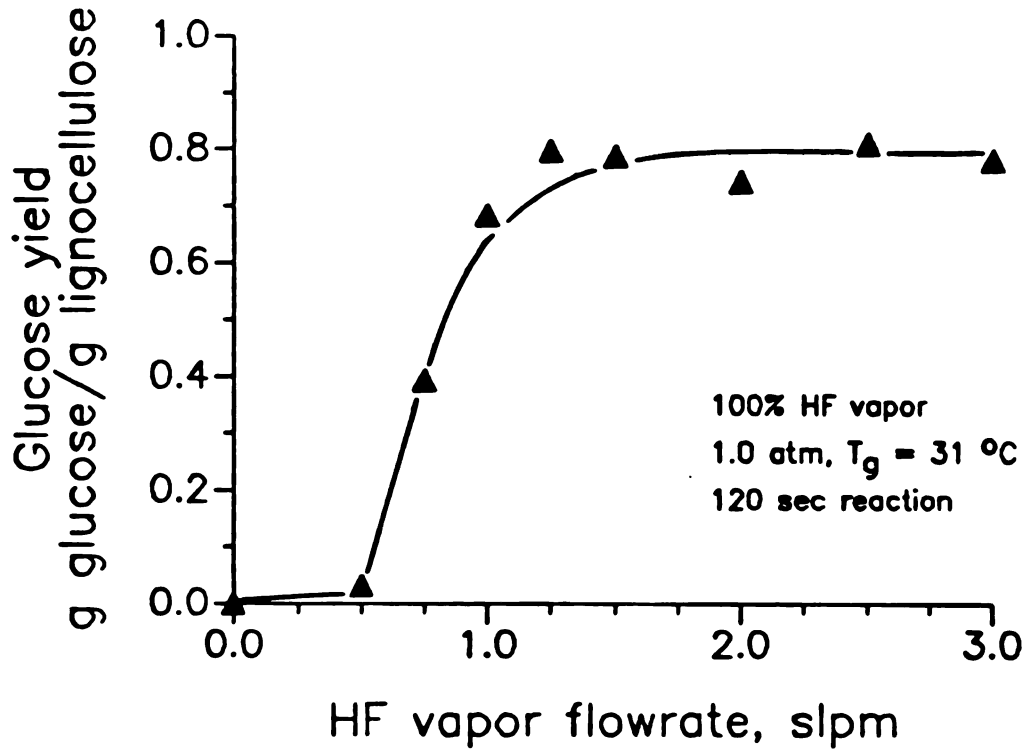


Figure 6.11. Vapor-phase HF solvolysis of a single prehydrolyzed wood chip (2L = 0.4 mm): effect of 100% HF vapor stream flowrate on the glucose production rate at T_g = 31 °C.
Note: $G_{HF} = F_{MFC}$ x 0.21 g-HF/cm^2-min/[1.00 slpm] reading.

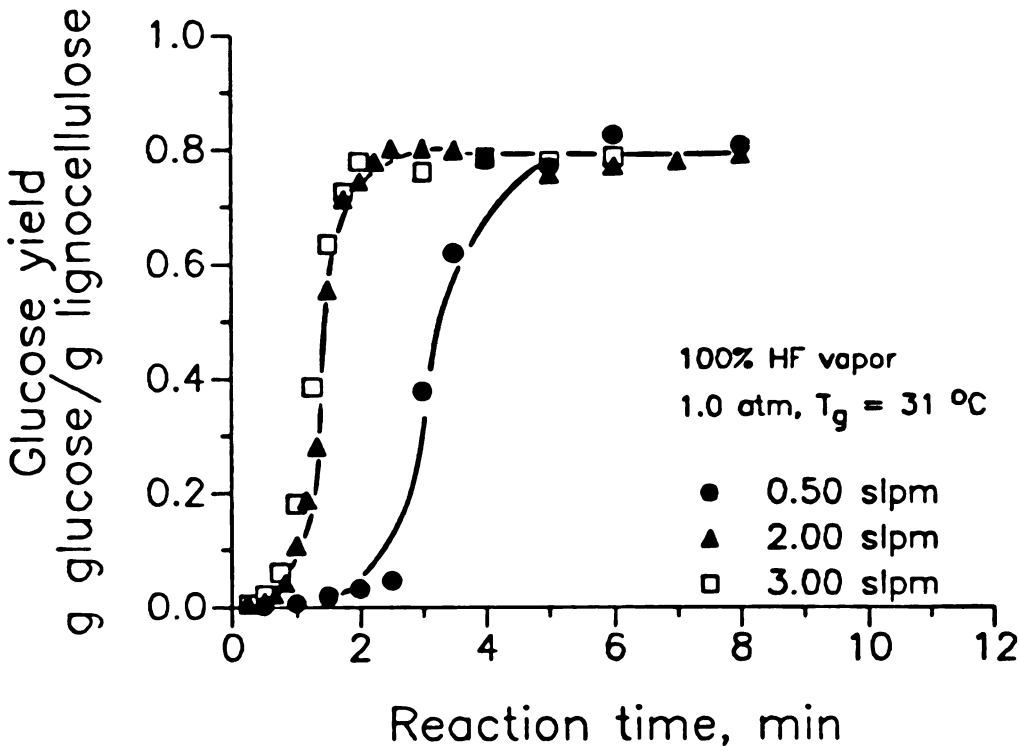


Figure 6.12. Vapor-phase HF solvolysis of a single prehydrolyzed wood chip (2L = 0.4 mm): effect of 100% HF vapor stream flowrate on the glucose yield vs. time profile at T_g = 31 °C.
Note: $G_{HF} = F_{MFC}$ x 0.21 g-HF/cm^2-min/[1.00 slpm] reading.

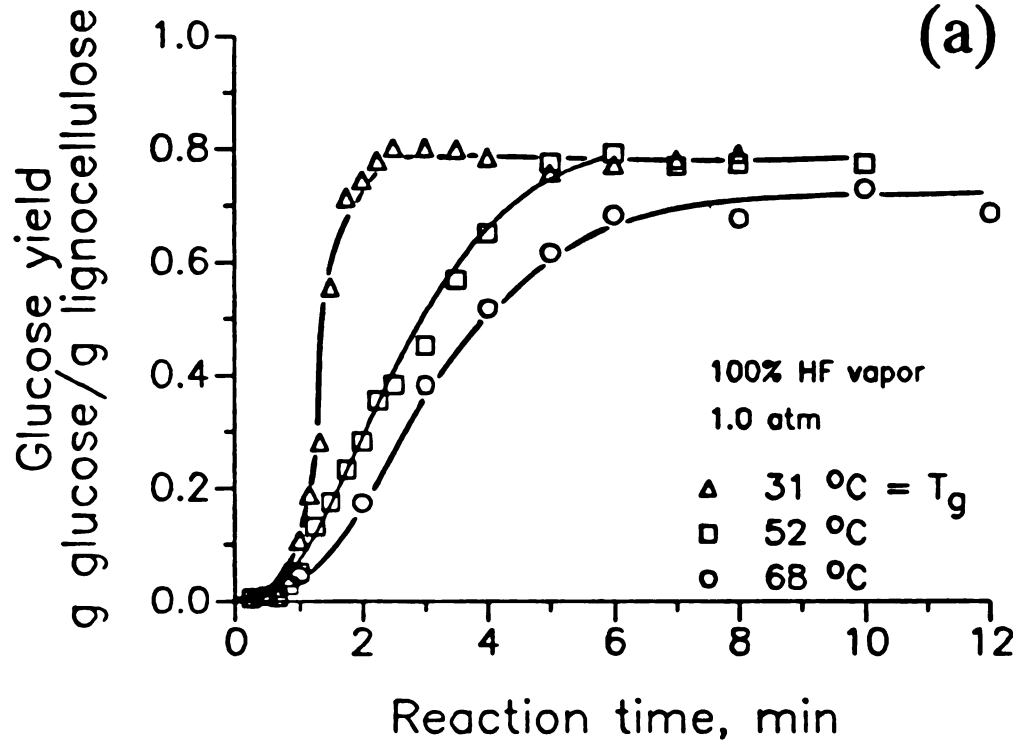


Figure 6.13a. Vapor-phase HF solvolysis of a single prehydrolyzed wood chip (2L = 0.4 mm): effect of 100% HF vapor stream temperature (T_g) on the glucose yield vs. time profile. (a) T_g = 31 °C, 52 °C, 68 °C. Note: G_{HF} = 0.42 g HF/cm^2-min.

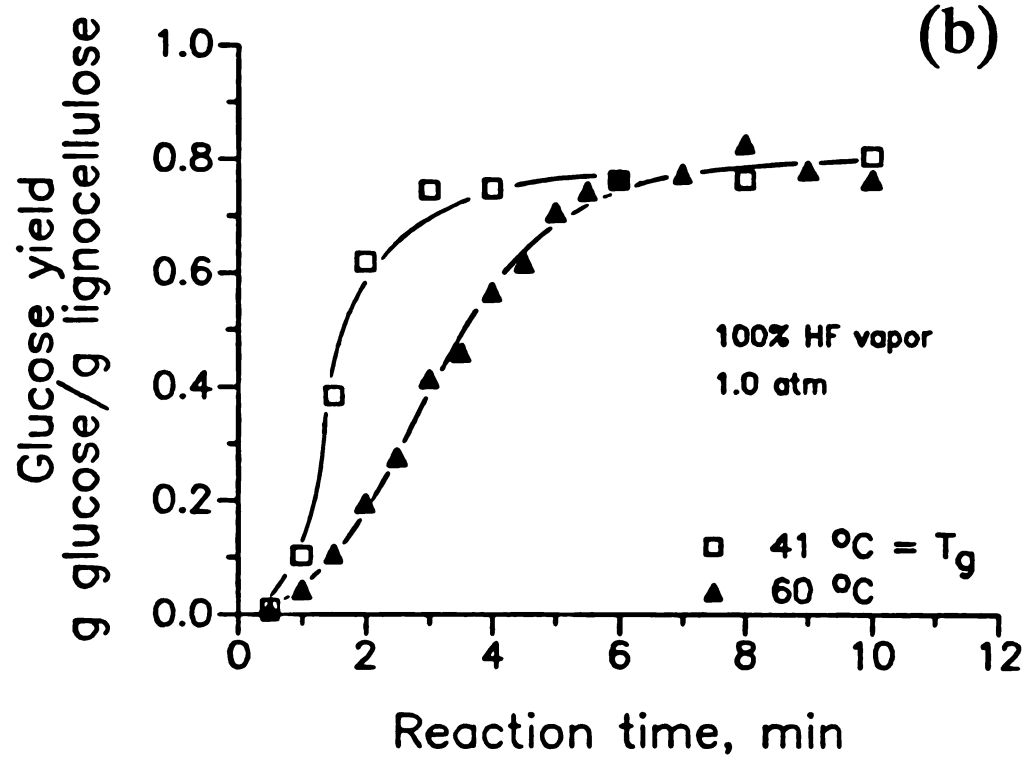


Figure 6.13b. Vapor-phase HF solvolysis of a single prehydrolyzed wood chip (2L = 0.4 mm): effect of 100% HF vapor stream temperature (T_g) on the glucose yield vs. time profile. (b) T_g = 41 °C, 60 °C. Note: G_{HF} = 0.42 g HF/cm^2-min.

glucan concentration in unreacted cellulose, 2) HF loading on the lignocellulosic matrix, and 3) reaction temperature. As the reaction temperature increases, the intrinsic rate constant(s) for cellulose solvolysis increases, but the HF loading (θ_e) on the lignocellulosic matrix that the cellulose perceives for solvolysis decreases ($T \uparrow k_i \uparrow \theta_e \downarrow$). Thus the thermodynamics of HF physical adsorption and Arrhenius kinetics of cellulose solvolysis work in opposing directions with increasing temperature, and this coupling determines the global dependence of glucose production rate on reaction temperature.

B. Effect of 100% HF Vapor Stream Temperature and Equilibrium HF Loading on Maximum Glucose Yield

At 100% HF vapor temperatures greater than 60 °C, the maximum attainable glucose yield was also dependent on the 100% HF vapor stream temperature, as shown in Figure 6.14 and Table 6.3. Since the dependence of equilibrium HF loading (θ_e) on 100% HF vapor temperature (T_g) is known from Figure 5.8 and equation [5-6], the dependence of maximum attainable glucose yield on equilibrium HF loading was determined, as shown in Figure 6.15 and Table 6.3. The theoretical dependence of maximum glucose yield on equilibrium HF loading can be estimated by the equation

$$[G'_o] = \begin{cases} [G_o] & \text{if } \theta_e \geq \theta_{min} \\ [G_o] \cdot \theta_e / \theta_{min} & \text{if } \theta_e < \theta_{min} \end{cases} \qquad [6\text{-}6]$$

where $[G'_o]$ is the maximum glucose yield at a given equilibrium HF loading (θ_e), and θ_e is the theoretical minimum HF loading for stoichiometric reaction with

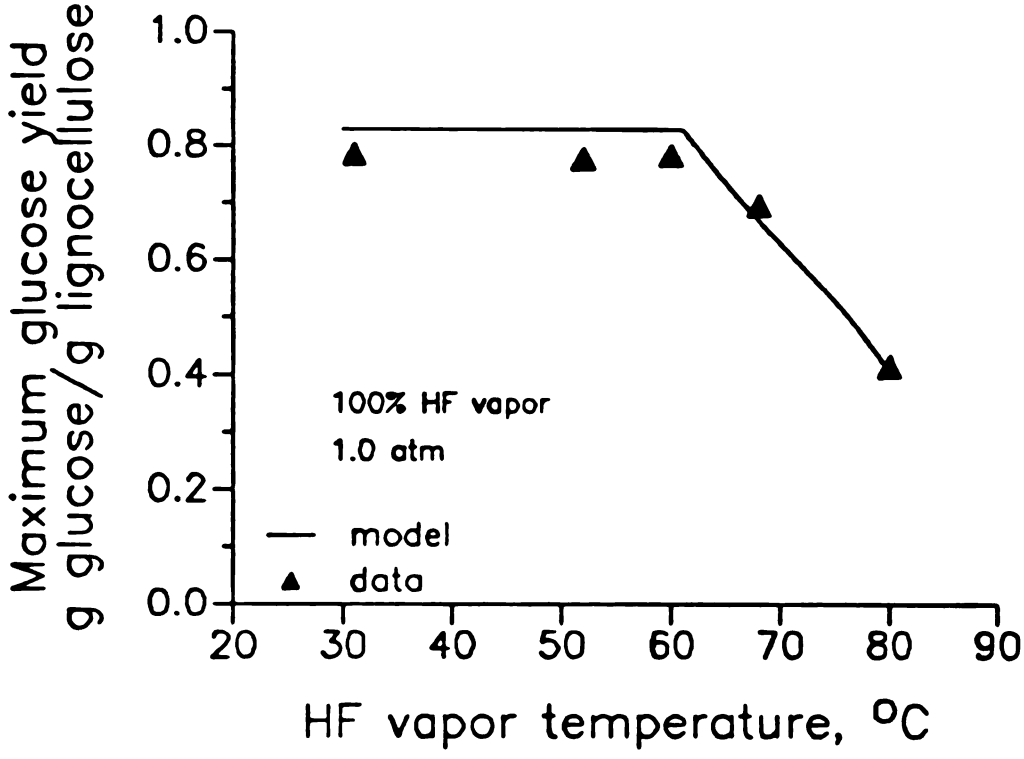


Figure 6.14. Vapor-phase HF solvolysis of prehydrolyzed wood: effect of 100% HF vapor temperature (T_g) on the maximum average glucose yield attainable from the water-soluble products (after posthydrolysis). The solid (model) line was calculated using equations [6-6], [6-7], and [5-6].

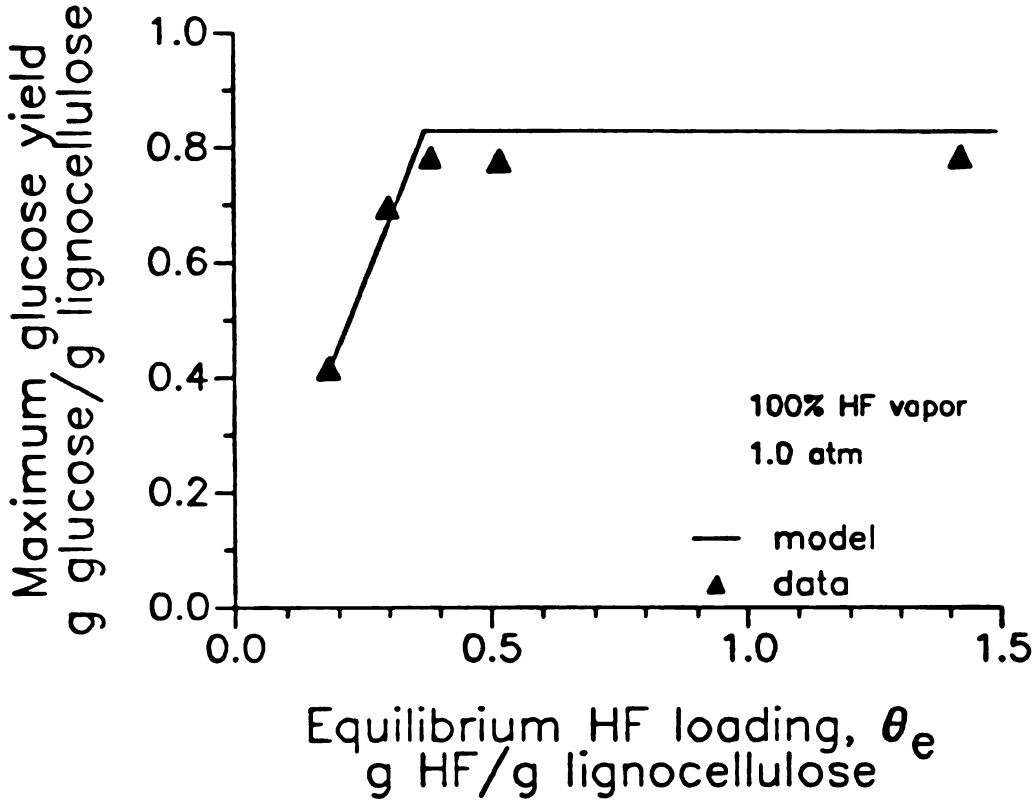


Figure 6.15. Vapor-phase HF solvolysis of prehydrolyzed wood: effect of equilibrium HF loading (θ_e) on the maximum average glucose yield obtained from the water-soluble reaction products (after posthydrolysis). The solid (model) line was calculated using equations [6-6], [6-7], and [5-6].

Table 6.3. Summary of maximum average glucose yields obtained from the vapor-phase HF solvolysis of prehydrolyzed wood as a function of 100% HF vapor temperature (T_g) at 1.0 atm and equilibrium HF loading (θ_e) at 1.0 atm (after posthydrolysis of water-soluble products); see Figure 6.14.

T_g	θ_e	Maximum Glucose Yield				
		Experiment				Eqn. [6-7]
°C	g HF/g [a]	g/g	+/- 1s [b]	% theoretical [c]		g/g [b]
31	1.420	0.786	+/-0.015 (n=9)	94.7	+/-1.8	0.830
41	0.866	0.774	+/-0.025 (n=4)	93.3	+/-3.0	0.830
52	0.519	0.778	+/-0.008 (n=5)	93.7	+/-1.0	0.830
60	0.382	0.784	+/-0.026 (n=5)	94.5	+/-3.1	0.830
68	0.297	0.696	+/-0.024 (n=4)	83.9	+/-2.9	0.669
80	0.181	0.416	+/-0.069 (n=4)	50.1	+/-8.3	0.406

Notes:

[a] θ_e calculated from cubic fit of data (see Figure 5.8). g HF/g = g HF adsorbed/g prehydrolyzed wood (lignocellulose)

[b] g/g = g glucose/prehydrolyzed wood (lignocellulose)

[c] Maximum theoretical glucose yield from prehydrolyzed Bigtooth Aspen wood (lignocellulose) = 0.83 g glucose/g lignocellulose.

lignocellulose. The equilibrium HF loading (θ_e) at a given 100% HF vapor stream temperature (T_g) is calculated by equation [5-6]. The theoretical minimum HF loading, θ_{min}, is calculated by

$$\theta_{min} = 4\ M_{w,HF}\ [G_o] = 0.369\ \text{g HF/g-lignocellulose} \qquad [6\text{-}7]$$

where $[G_o]$ is the total glucan concentration in prehydrolyzed wood (4.61 mmol glucan/g-lignocellulose, or 0.83 g glucose/g lignocellulose). The factor 4 is the number of HF molecules per glucan unit required to convert glucan in crystalline cellulose to glucosyl fluoride: 3 HF molecules for hydrogen bonding with OH groups on glucan (3 OH groups per glucan unit in cellulose), and 1 HF molecule for solvolytic cleavage of the ß-1,4-O-glycosidic linkage joining two glucan units. The chemistry justifying equations [6-6] and [6-7] is detailed in chapter 8.

Equation [6-6] predicts the maximum attainable glucose yield when the HF adsorbed on the lignocellulosic matrix is not sufficient to insure a stoichiometric reaction with cellulose. As demonstrated in Figures 6.14 and 6.15, this simple model agrees accurately with the data. Note also that the model works better for prehydrolyzed wood then for wood (compare Table 6.1 with Table 6.3).

The maximum experimentally attainable glucose yield from prehydrolyzed wood is 0.78 g glucose/g-lignocellulose for equilibrium HF loadings of 0.4 g HF/g-lignocellulose and greater. Since the maximum theoretical glucose yield from prehydrolyzed wood is 0.83 g glucose/g-lignocellulose, the maximum glucose yield averages 94% of maximum theoretical (see Tables 6.3 and 6.4). This explains why

the theoretical line in Figures 6.14 and 6.15 is slightly higher than the data points.

The following experiment further supports the validity of equations [6-6] and [6-7]. Prehydrolyzed wood chips reacted with HF vapor at 80 °C and 1.0 atm did not result in complete cellulose conversion, because θ_e = 0.18 g HF/g-lignocellulose, which is less than θ_{min} (0.369 g HF/g-lignocellulose). However, when the water-insoluble residue of this reaction was re-reacted with HF vapor at 31 °C (where θ_e = 1.42 g HF/g-wood), additional glucose yield was obtained. The sum of the glucose yields after both reactions was the maximum experimentally attainable glucose yield (0.78 g glucose/g-lignocellulose).

C. Comparison of the Rate Processes of Liquid-Phase and Vapor-Phase HF Solvolysis of Lignocellulose

The liquid-phase HF solvolysis and vapor-phase HF solvolysis of lignocellulose are governed by different rate processes. For the liquid-phase process, the cellulose dissolves in the liquid HF and is solvolytically cleaved to glucosyl fluoride in HF solution, where the rate of glucose production increases with increasing temperature by the Law of Arrhenius. However, for the vapor-phase process, HF vapor must first physically adsorb onto the cellulose before reacting. Since the heat of physical adsorption is negative, the equilibrium loading of HF on the lignocellulosic matrix that the cellulose perceives for solvolysis will decrease with increasing temperature by Le Chatelier's Principle. Thus the glucose production rate will be determined by both the Law of Arrhenius and the thermodynamics of HF physical adsorption.

IV. Sugar Yield Comparisons and Total Product Recovery Data from the Vapor-Phase HF Solvolysis of Four Lignocellulosic Substrates

In this section, maximum sugar yield and total product recovery data from the vapor-phase HF solvolysis of single Bigtooth Aspen wood chips, "prehydrolyzed" (hemicellulose- free) Bigtooth Aspen wood chips, pure cellulose (filter paper) wafers, and filter paper/"milled-wood lignin" composite wafers are compared. Also in this section, the possible sources of sugar yield loss, including acid-catalyzed sugar dehydration, HF-catalyzed glucosyl fluoride/lignin condensation, and sugar retention in the water-insoluble residue (solid fraction) are investigated.

A. Sugar Yield Comparisons: Water-Soluble Products

The maximum glucose yields attainable from the water-soluble products of the vapor-phase HF solvolysis of Bigtooth Aspen wood chips, prehydrolyzed Bigtooth Aspen wood chips, pure cellulose (filter paper) wafers, and filter paper/ "milled-wood" lignin composite wafers are compared in Table 6.4. Each dry (< 2% moisture) lignocellulosic substrate was reacted with a 100% HF vapor stream at 1.0 atm and 30 ^{o}C for at least 3 min, so that maximum cellulose conversion was attained. The water-soluble reaction products were then "posthydrolyzed" in 2 N TFA at 121 ^{o} C for 1 h in order to convert any reversion oligosaccharides back to monomer sugars. The water-insoluble residue was washed thoroughly in water, dried, and weighed.

Maximum theoretical glucose yields for the four lignocellulosic substrates are summarized at the bottom of Table 6.4. In general, the wood sugar determinations for aspen wood reported in the literature vary, as shown in chapter

Table 6.4. Comparison of maximum average glucose yields obtained from solvolysis of Bigtooth Aspen wood, prehydrolyzed Bigtooth Aspen wood, filter paper, and filter paper/"milled-wood" lignin (MWL) composite wafers by an anhydrous HF vapor stream at 30-31 °C and 1.0 atm (after posthydrolysis of water-soluble products).

Substrate [d]	Maximum Glucose Yield		
	mmol/g +/-1s [a]	g/g +/- 1s [b]	% theoretical [d]
Bigtooth Aspen wood	2.868 +/-0.059	0.516 +/-0.011	83.5 +/-1.7 (n=10)
prehydrol. Bigtooth Aspen wood	4.369 +/-0.084	0.786 +/-0.015	94.7 +/-1.8 (n=9)
Whatman Filter paper No. 3	5.710 +/-0.172	1.028 +/-0.031	92.5 +/-2.8 (n=5)
filter paper/ MWL composite (23.3% wt. MWL) [c]	4.426 +/-0.156	0.797 +/-0.028	93.5 +/-3.3 (n=15)

Notes:

[a] mmol/g = mmol glucose/g-substrate

[b] g/g = g glucose/g substrate

[c] MWL = "milled-wood" lignin from Bigtooth Aspen wood

[d] Maximum theoretical glucose yield:

Bigtooth Aspen wood (assumed)	Prehydrolyzed Bigtooth Aspen wood (lignocellulose)	Whatman filter paper No. 3	filter paper/ MWL composite (23.3% wt. MWL) Eqn. [4-5b]
3.441 mmol/g	4.61 mmol/g	6.17 mmol/g	4.732 mmol/g
0.618 g/g	0.830 g/g	1.111 g/g	0.852 g/g

4. Therefore, the wood sugar composition of Bigtooth Aspen wood is only an estimate. The maximum theoretical glucose yield from Bigtooth Aspen wood is estimated at 3.441 mmol/g-wood (0.618 g glucose/g-wood), which is based on previous material balance studies for the liquid-phase HF solvolysis of Bigtooth Aspen wood at 0 °C (Selke et al., 1983). The maximum theoretical xylose yield from Bigtooth Aspen wood is estimated at 1.4 mmol/g-wood (0.21 g xylose/g-wood), and is also based on previous material balance studies for the liquid-phase HF solvolysis of Bigtooth Aspen wood at 0 °C (Selke, 1983; Selke et al., 1983). The estimated composition of Aspen wood is given in Tables 4.3 and 4.4. The maximum theoretical glucose yield from prehydrolyzed Bigtooth Aspen wood, or lignocellulose, is estimated at 4.61 mmol/g-wood (0.83 g glucose/g-lignocellulose), based on material balance data given in chapter 4 (see Table 4.5). The maximum theoretical glucose yield from pure cellulose (Whatman filter paper no. 3) is 6.17 mmol/g-filter paper, assuming that Whatman filter paper no. 3 is 99.9% glucan. The maximum theoretical glucose yield from filter paper/"milled-wood" lignin composite wafers is calculated from equations [4-5a] and [4-5b].

On a percent (%) of theoretical recovery basis, the maximum averaged glucose yield obtained from the vapor-phase HF solvolysis of Bigtooth Aspen wood was about 10% lower than the maximum average glucose yield obtained from the vapor-phase HF solvolysis of prehydrolyzed Bigtooth Aspen wood, filter paper, and filter paper/"milled-wood" lignin composite wafers. Maximum glucose yields from Bigtooth Aspen wood averaged 0.516 g glucose/g-wood, or about 84% of

theoretical. Maximum glucose yields from prehydrolyzed wood averaged 0.78 g glucose/g lignocellulose, or about 94% of theoretical. Maximum glucose yields from filter paper and filter paper/"milled-wood" lignin composite wafers (23.3% wt. lignin) also averaged about 94% of maximum theoretical.

Maximum xylose yields from the vapor-phase HF solvolysis of Bigtooth Aspen wood averaged 0.153 g xylose/g wood, or about 73% of maximum theoretical.

Glucose and xylose yields from both the liquid- and vapor-phase HF solvolysis of Bigtooth Aspen wood are compared in Table 6.5. In general, sugar yields from liquid-phase HF solvolysis are equal to or slightly higher than those from vapor-phase HF solvolysis. However, since the reported sugar yields from liquid-phase HF solvolysis vary considerably, it is hard to say positively that the liquid-phase process provides higher sugar yields than the vapor-phase process.

B. Total Product Recovery Comparisons

Total Measured Product Recovery Data. The measured total product recovery from each of the four lignocellulosic substrates after vapor-phase HF solvolysis never quite reached 100%, as shown in Table 6.6. This was particularly true for Bigtooth Aspen wood, where the total measured product recovery after vapor-phase HF solvolysis was about 85%. The total measured product recovery from prehydrolyzed wood, filter paper, and filter paper/"milled-wood" lignin composite wafers was about 94%. The measured water-soluble sugar and water-insoluble residue from the vapor-phase HF solvolysis of prehydrolyzed wood is plotted as a function of reaction time in Figure 6.16. Note from Figure 6.16 and Table 6.6 that

Table 6.5. Comparison of the maximum average glucose and xylose yields obtained from the liquid-phase and vapor-phase HF solvolysis of Bigtooth Aspen wood (after posthydrolysis of water-soluble products).

Treatment	Maximum Glucose Yield		Maximum Xylose Yield	
	g/g [a] (+/- 1s)	% theoretical [b] (+/- 1s)	g/g [a] (+/- 1s)	% theoretical (+/- 1s)
anhyd. liq. HF 4 °C, > 15 min (n=6 points) [c]	0.560 +/- 0.032	90.4 +/-5.2	0.170 +/-0.022	81.2 +/-10.4
anhyd. liq. HF -4 °C, > 35 min (n=3 points) [c]	0.578 +/- 0.011	93.3 +/-1.8	0.176 +/-0.008	83.9 +/- 3.8
anhyd. liq. HF 0 °C, 1 h [d]	0.47	76.5	0.15	71.4
anhyd. liquid HF 23 °C, 1 h [d]	0.46	74.4	0.16	76.2
4% H_2O in liq. HF 23 °C, 1 h [d]	0.54	87.3	0.17	81.0
100% HF vapor 30-31 °C, 1.0 atm 3 to 8 min (n=10 points)	0.516 +/- 0.011	83.5 +/-1.7	0.153 +/-0.009	72.9 +/- 4.1

Notes:

[a] g/g = g glucose/g-wood, or g xylose/g-wood

[b] maximum theoretical glucose yield = 0.618 g glucose/g-wood
maximum theoretical xylose yield = 0.210 g xylose/g-wood
(see Table 4.4)

[c] reference: Selke (1983)

[d] reference: Selke et al. (1982)

Table 6.6. Comparison of total average measured product recoveries obtained from solvolysis of Bigtooth Aspen wood, prehydrolyzed Bigtooth Aspen wood, filter paper, and filter paper/ "milled-wood" lignin (MWL) composite wafers by an anhydrous HF vapor stream at 30-31 °C and 1.0 atm (after posthydrolysis of water-soluble products).

Substrate	Glucose as Glucan [a] g/g (+/- 1s)	Xylose as Xylan [a] g/g (+/- 1s)	Other Sugars [b] g/g (+/- 1s)	Solid Residue g/g (+/- 1s)	Total Measured Recovery g/g [c] (+/- 1s)
Bigtooth Aspen wood	0.464 (0.010)	0.135 (0.009)	0.028	0.220 (0.016)	0.847
prehydrol. Bigtooth Aspen wood	0.707 (0.014)	0.029 [d] (0.003)	-	0.199 (0.004)	0.935
Whatman filter paper no. 3	0.925	-	-	0.000	0.925
filter paper/ MWL composite (23.3% wt MWL)	0.717 (0.025)	-	-	0.223 (0.009)	0.940

Notes:

[a] All sugar yields are reported as their anhydrosugars, e.g. glucan from glucose, xylan from xylose.
M_w glucose = 180, M_w glucan = 162
M_w xylose = 150, M_w xylan = 132

[b] Galactose and mannose, (as galactan and mannan); see Table 6.7.

[c] Sum of glucan, xylan, galactan, mannan and solid residue.

[d] Residual xylan in prehydrolyzed wood is also released by vapor-phase HF solvolysis; about 10% of the xylan in untreated wood is retained in the prehydrolyzed wood.

[e] See also Figure 6.16; compare with the prehydrolyzed wood composition given in Table 4.5.

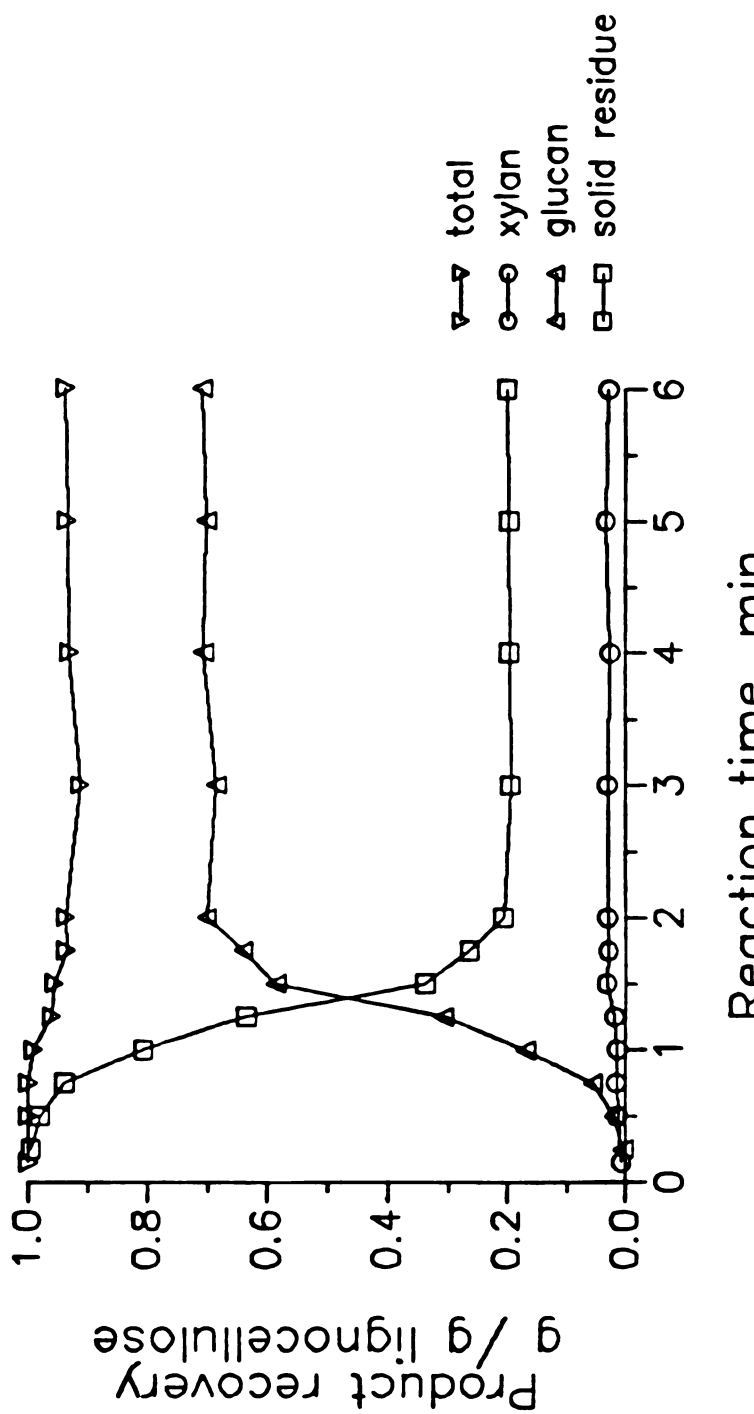


Figure 6.16. Vapor-phase HF solvolysis of a single prehydrolyzed wood chip (2L = 0.4 mm): glucan, xylan, solid residue, and total product recovery as a function of reaction time. Reaction conditions: 100% HF vapor at 1.0 atm, T_g = 31°C, G_{HF} = 0.42 gHF/cm^2-min.

the vapor-phase HF solvolysis of prehydrolyzed wood released minor amounts of xylose. This is because the prehydrolysis step hydrolyzed about 90% of the total hemicellulose, and so residual xylan was present in the prehydrolyzed wood.

Comparsion with Two-Step Sulfuric Acid Hydrolysis. In Table 6.7, the sugar yields and total measured product recovery from Bigtooth Aspen wood chips after vapor-phase HF solvolysis are compared to the total measured product recovery from Willey-milled (60 mesh) Bigtooth Aspen wood after two-step surfuric acid (H_2SO_4) hydrolysis. This two-step sulfuric acid hydrolysis is a common method for wood sugar and Klason lignin determination (Timell, 1957; Pettersen, 1984a, 1984b). The maximum glucose yield after two-step sulfuric hydrolysis averaged 0.556 g glucose/g-wood, and the maximum xylose yield averaged 0.191 g xylose/g-wood.

The total measured recovery after two-step sulfuric acid hydrolysis was 87.3%. The organic "extractives" fraction (3-4% wt. of wood; Pettersen, 1984b), acetyl groups (3.3% wt. of wood; Timell, 1957), and uronic acids (3.2% wt. of wood; Timell, 1957) in Bigtooth Aspen wood were not quantified. However, if these (unmeasured) components are factored in, the total recovery is 97-98%. The balance is ash, acid-soluble lignin, and arabinose.

In Table 6.7, note that the glucose and xylose yields from two-step sulfuric acid hydrolysis were higher than the glucose and xylose yields from vapor-phase HF solvolysis. The wood sugars in Bigtooth Aspen wood as determined by two-step sulfuric acid hydrolysis may also serve as a basis for normalizing the glucose and

Table 6.7. Total product recovery from Bigtooth Aspen wood: vapor phase HF solvolysis (dry and methanol-absorbed wood) vs. two-step sulfuric acid hydrolysis.

Component	Two-step sulfuric acid hydrolysis [a]	Vapor-phase HF solvolysis [b]	
		dry	+ methanol
	mg/100 mg wood +/- 1s, n=3 (% theoretical)	mg/100 mg wood +/- 1s, n=10 (% theoretical)	mg/100 mg wood +/- 1s, n=3 (% theoretical)
Glucose	55.6 +/- 0.4 (89.7 +/- 0.6)	51.6 +/- 1.1 (83.5 +/-1.7)	55.8 +/- 1.1 (90.1 +/- 1.7)
Xylose	19.1 +/- 0.6 (91.1 +/- 2.8)	15.3 +/- 0.9 (72.9 +/- 4.1)	15.7 +/- 0.7 (74.6 +/- 3.5)
Mannose	2.1 +/- 0.2	2.0 +/- 0.4	1.6 +/- 0.2
Galactose	1.1 +/- 0.1	1.1 +/- 0.2	1.1 +/- 0.1
Total sugar recovery	77.9	70.0	74.2
Solid residue [c]	17.7 +/- 0.1 [d]	22.0 +/- 1.6	-
Total measured recovery [e]	87.4	84.7	-

Notes:

[a] The wood sugar determination is carried out by two-step sulfuric acid hydrolysis described by Timell (1957) and Pettersen (1984a, 1984b). 200 mg dried wiley-milled wood grindings are hydrolyzed in 5.0 mL 72% (wt.) sulfuric acid at 30 °C for 1 h; products are diluted with water to 3% (wt.) sulfuric acid solution and post-hydrolyzed in autoclave at 121 °C for 1 h. Solid residue is filtered, washed, dried, and weighed. Posthydrolysis loss factors for glucose (1.045), xylose (1.116), galactose (1.077), and mannose (1.071) given by Pettersen (1984b).

[b] Single, dry Bigtooth Aspen wood chips (0.4 mm x 1.0 cm/side, 15 mg) are reacted with 100% HF vapor at 30 °C and 1.0 atm for 3 to 8 min. Methanol-absorbed wood chips (15 μL/10 mg, or ca. 1:1 wt.) are reacted with HF vapor at the same conditions for 6 min. The water-insoluble residue is washed, dried, and weighed. The water-soluble products (1% wt) are posthydrolyzed in 2 N TFA at 121 °C for 1 h.

[c] The estimated lignin composition of Bigtooth Aspen wood is 0.166 g lignin/g-wood (see Tables 4.3 and 4.4).

[d] Klason lignin content; acid-soluble lignin was not quantified.

[e] Sum of sugar recovery (expressed as their anhydrosugars) and solid residue. Arabinose, uronic acids, acetyl, ash, wood "extractives" were not quantified. Compare with composition of Bigtooth Aspen wood (Tables 4.3 and 4.4).

xylose yields from the vapor-phase HF solvolysis of Bigtooth Aspen wood. Note also that the solid residue from vapor-phase HF solvolysis weighed more than the solid residue from two-step sulfuric acid hydrolysis. This increased weight is due to "extractives" and sugar retention in the solid residue, and is discussed later in this section.

C. Possible Sources of Sugar Yield Loss

On a glucan basis, the maximum percent glucose yields in the water-soluble reaction products obtained from the vapor-phase HF solvolysis of the four lignocellulosic substrates ranged from 84% of theoretical (Bigtooth Aspen wood) to 94% of theoretical (prehydrolyzed Bigtooth Aspen wood, filter paper, and filter paper/"milled-wood" lignin composite wafers), and never achieved 100% of maximum theoretical. Possible sources of glucose yield loss include water-soluble sugar degradation products, HF-catalyzed condensation of sugar fluorides onto lignin, and sugar retention in the water-insoluble residue.

Water-Soluble Sugar Degradation Products. The solvolysis of pure cellulose (filter paper) by 100% HF vapor and the subsequent dilute-acid posthydrolysis of the water-soluble reaction products did not provide the maximum theoretical yield of glucose, although maximum glucose yields approaching 94% of theoretical were consistently obtained. To account for the 6% loss, I searched for the usual products of acid-catalyzed glucose dehydration, 1,6-anhydroglucose (levoglucosan) and 5-hydroxymethylfurfural (HMF) in the water-soluble reaction products both before and after dilute-acid posthydrolysis (2 N TFA at 121 ^{o}C for 1 h).

Although the analytical procedure for levoglucosan and HMF detection worked nicely, only traces of levoglucosan and HMF were found. A standard mixture of levoglucosan and HMF in aqueous solution was successfully separated and detected via carbohydrate HPLC on a BIO-RAD HPX-87P column at the operating conditions given in chapter 4 (differential refractive index (RI) detection, 0.6 mL/min H_2O as column mobile phase, 85 °C column temperature). The retention times for levoglucosan and HMF were 28.5 minutes and 33.0 minutes, respectively. HMF was not detected in the water-soluble reaction products obtained from the vapor-phase HF solvolysis of filter paper, either before or after posthydrolysis. However, levoglucosan was detected in small amounts (0.5 to 1.0 wt.% of original cellulose) in the water-soluble reaction products, both before and after posthydrolysis. Posthydrolysis did not appear to hydrolyze levoglucosan back to glucose significantly, but quantification was difficult because the amount of levoglucosan in the water-soluble reaction products was near the lower quantitative detection limit of the carbohydrate HPLC system. Trace amounts of levoglucosan were also detected in the reaction products of the liquid-phase HF solvolysis of cellulose after reaction at 0 °C for 1 h (Hardt and Lamport, 1982a, 1982b).

It is possible that the glucose degradation that occurred during posthydrolysis was not the result of acid-catalyzed glucose dehydration. When 160 μg glucose and 160 μg myo-inositol (internal standard) were reacted in 200 μL of 2 N TFA at 121 °C for 1 h, a net loss of 3% glucose occurred (average after 5 assays), with the dried reaction products possessing a faint yellow-red color. This result confers

with the work of De Ruiter and Burns (1986) who reported a net 3% glucose loss at the same hydrolysis conditions. De Ruiter and Burns attributed the glucose loss to the formation of a glucosyl trifluoroacetic ester.

Due to glucose and xylose yield losses during posthydrolysis, in all glucose yield and xylose yield determinations, posthydrolysis yield loss factors for each sugar (see chapter 4, equation [4-13]) were used to correct for sugar loss during posthydrolysis.

Although the average xylose yield from the water-soluble reaction products of the vapor-phase HF solvolysis of Bigtooth Aspen wood was much lower than the average glucose yield (73% of theoretical vs. 84% of theoretical), possible xylose dehydration products were not characterized and quantified. The first glucose dehydration product to look for in the water-soluble products is furfural. However, I did not attempt to analyze furfural in the water-soluble reaction products, either before or after posthydrolysis.

As a final note, glucose yield loss was not due to vaporization or sublimation of glucosyl fluoride, because glucosyl fluoride melts at 118 °C and decomposes at 125 °C (Micheel and Klemer, 1961).

HF-Catalyzed Condensation of Sugar Fluorides onto Lignin I: Hypothesis and Literature Review. Recall that the percent glucose recovery from the water-soluble reaction products of the vapor-phase HF solvolysis of Bigtooth Aspen wood (84% of maximum theoretical) was about 10% less than that from filter paper (94% of maximum theoretical). A 10% difference in water-soluble, normalized glucose recovery pure cellulose and wood is significant, despite the

uncertainty of the estimated glucan composition of Bigtooth Aspen wood. It is possible that the lowered glucose recovery from wood results from condensation of glucosyl fluoride onto lignin, catalyzed by HF adsorbed on the wood. The specific mechanism might involve an HF-catalyzed, Friedel-Crafts alklyation of glucosyl fluoride with phenylpropanoid units constituting lignin, resulting in formation of a stable carbon-carbon bond between the C-1 carbon of the sugar and the phenolic ring structures in lignin (see Figure 6.17). This glucosyl fluoride/lignin condensation would produce a water-insoluble adduct, and would thus decrease the glucose yield obtainable from the water-soluble product fraction.

The possibility of HF-catalyzed condensation glucosyl fluoride onto lignin may explain one unusual trend of the glucose yield vs. time data from the vapor-phase HF solvolysis of Bigtooth Aspen wood. Note from Figures 6.5a and 6.5b that the glucose yield vs. time profile often passed through a maximum before settling down to a slightly lowered maximum glucose yield, indicating that some of the glucose may be forming water-insoluble products.

Experimental evidence already exists for condensation of sugars onto aromatic compounds and lignin (which contains phenolic structures) in liquid HF. Homogeneous, Friedel-Crafts alkylation of sugars and polyhydroxyalcohols with aromatic compounds in liquid HF is described by Lenard (1969). Fredenhagen and Cadenbach (1933) reported that when sugars were mixed with lignin in the presence of HF liquid, the residual solid gained weight in an amount corresponding to 15% of the initial sugar weight, indicating sugar condensation onto lignin. Heerema et

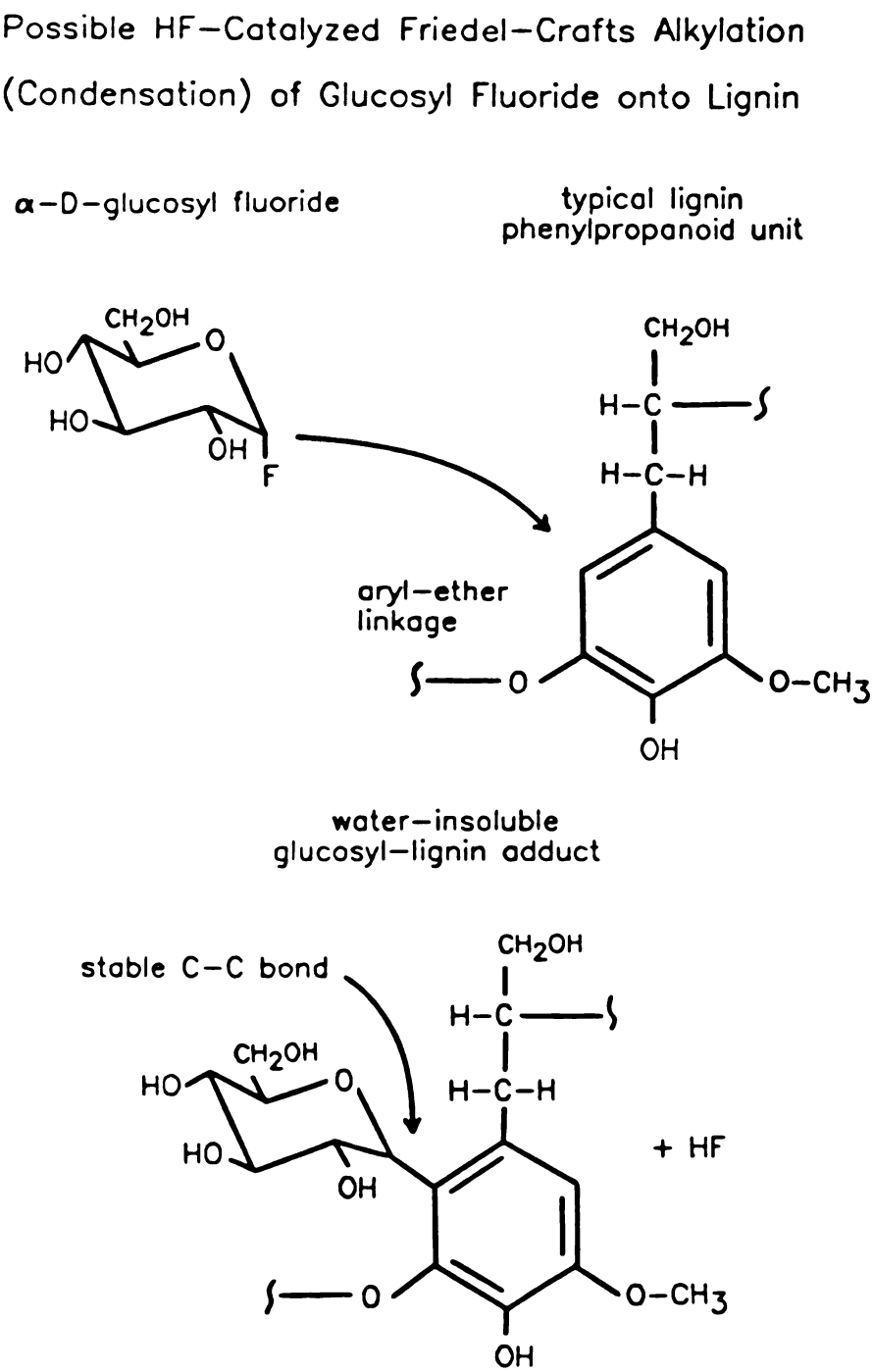


Figure 6.17. Hypothetical mechanism for HF-catalyzed, Friedel-Crafts alkylation of glucosyl fluoride onto lignin.

al. (1958) reported that the C1 carbon of glucose alkylated with o-xylene in liquid HF to form 1-deoxy-1,1-bis(3,4-dimethylphenyl)-D-glucitol in 85% yield. Defaye et al. (1983) reported that during the liquid-phase HF solvolysis of birchwood at 28 °C, the glucose yield vs. time curve passed through a maximum of 95% after 30 min, and then slowly decreased to a limiting value of 80% with increasing reaction time over a period of 3 h. However, at 0 °C, a maximum glucose yield of 95% was attained and remained steady with increasing reaction time. Defaye hypothesized that HF liquid was catalyzing the condensation of glucosyl fluoride onto lignin at the higher reaction temperature. Smith et al. (1983) and Defaye et al. (1983) also reported that significant auto-condensation of lignin occurred during liquid-phase HF solvolysis of wood.

HF-Catalyzed Condensation of Sugar Fluorides onto Lignin II: A Control Experiment with the Filter Paper/"Milled-Wood" Lignin Composite Wafer. A control experiment was designed to test the hypothesis of glucosyl fluoride/lignin condensation during the vapor-phase HF solvolysis of lignocellulose. The experiment was designed to emulate the HF vapor/wood chip reaction system with a pure cellulose/lignin composite wafer of precisely known glucan and lignin composition. Specifically, filter paper/"milled-wood" lignin (MWL) composite wafers were reacted with an HF vapor stream for a given reaction time. The reaction time and HF vapor conditions for the filter paper/"milled-wood" lignin composite wafer experiments were matched to those for the wood chip and filter paper experiments. The water-soluble reaction products (after posthydrolysis) were

assayed for glucose yield by HPLC, and the water-insoluble residue was thoroughly washed, dried, and weighed.

Recall from chapter 4 that pure cellulose/"milled-wood" lignin composite wafers of precisely known glucan and lignin composition were prepared by 1) extraction of "milled-wood" lignin (MWL) from Bigtooth Aspen wood, 2) solvent-impregnation of "milled-wood" lignin onto filter paper, 3) solvent removal, 4) cutting of the "milled-wood" lignin-impregnated filter paper into square wafers the same size as the wood chips, and 5) calculation of glucan and lignin composition by equations [4-5a] and [4-5b].

Glucose yield vs. time data (after posthydrolysis) obtained from the solvolysis of filter paper/"milled-wood" lignin composite wafers (23.3% wt. MWL) and pure cellulose (filter paper) wafers by a 100% HF vapor stream at 1.0 atm and 31 ^{o}C are compared in Figure 6.18. Each data point shown in Figure 6.18 is the average of three trials. Total product recovery data (water-soluble sugars plus solid residue) are given in Table 6.5.

The maximum average glucose yields (expressed as % of maximum theoretical) from the water soluble reaction products of vapor-phase HF solvolysis of filter paper/ "milled-wood" lignin composite wafers were identical to those from filter paper. Also, the water-insoluble residue recovery from the composite wafer (0.223 g/g-wood) did not show any weight increase over the original weight of lignin in the wafer (0.233 g MWL/g-composite wafer). These results indicate that glucosyl fluoride did not condense onto lignin to form a water-insoluble product. Evidently,

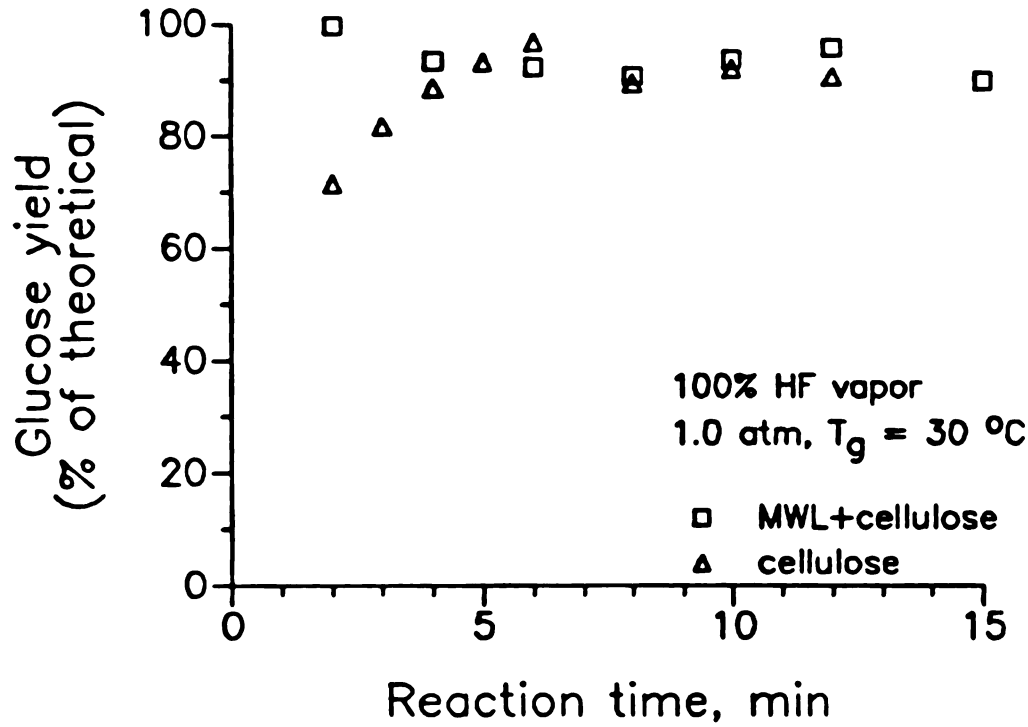


Figure 6.18. Comparison of glucose yield vs. time profiles obtained from the solvolysis of a single pure cellulose (filter paper) wafer and a single pure cellulose/"milled-wood" lignin (MWL) composite wafer by a 100% HF vapor stream at T_g = 30-31 °C. Notes: G_{HF} = 0.42 g HF/cm^2-min, [MWL] = 0.233 g MWL/g-composite substrate.

the glucosyl fluoride released from the vapor-phase HF solvolysis of the cellulose fraction did not condense onto lignin to form a water-insoluble adduct. However, autocondensation of the lignin fraction most likely occurred during vapor-phase HF solvolysis, because the composite wafer changed from a light yellow color to a dark brown color, and the water-insoluble residue remained intact as a single honeycombed structure. Since the mixing of cellulose with lignin in the composite wafer was not as intimate as that which exists within the native lignocellulosic matrix of wood, lignin probably condensed onto itself faster than glucosyl fluoride condensed onto the lignin.

Based on the results of the control experiment described above, glucosyl fluoride from the vapor-phase HF solvolysis of cellulose in wood does not condense with lignin in the presence of adsorbed HF over the range of reaction conditions studied. However, it is still likely that glucosyl flouride and xylosyl fluoride from the hemicellulose fraction condenses onto lignin. Xylosyl fluoride condensation onto lignin may explain the low percent xylose yields (about 73% of theoretical). Since hemicellulose is more intimately interweaved into lignin than crystalline cellulose (see Figure 8.3), attack of glucosyl fluoride and xylosyl fluoride from hemicellulose onto lignin might predominate. Furthermore, since about 10% of the total glucan in Bigtooth Aspen wood comes from the hemicellulose fraction, glucosyl fluoride from hemicellulose could condense onto lignin and still lower the water-soluble glucose yield, even though glucosyl fluoride from cellulose does not condense onto lignin.

Although the vapor-phase HF solvolysis experiments with the filter paper/"milled-wood" lignin composite wafers did not show any evidence of HF-catalyzed condensation of glucosyl fluoride onto lignin, I still believe that this reaction is possible. In future work, it would be informative to conduct a parallel set of control experiments with hemicellulose/"milled-wood" lignin composite substrates. Also, in order to understand chemistry of sugar fluoride condensation onto lignin, the reaction and products of sugars and model lignin compounds in liquid HF should be investigated.

Finally, note that for the vapor-phase HF solvolysis of prehydrolyzed wood, glucose yields of 94% of theoretical were obtained from the water-soluble reaction products. Evidently, HF-catalyzed glucosyl fluoride/lignin condensation does not occur during the vapor-phase HF solvolysis of prehydrolyzed wood. This may be due in part to the dilute-acid prehydrolysis step used for prehydrolyzed wood preparation, which may chemically alter the lignin and leave it less susceptible to HF-catalyzed condensation with glucosyl fluoride.

Improvement of Sugar Yield Recovery by In situ Methanolysis. In situ methanolysis of glucosyl fluoride to 1-O-methyl glucose is known to inhibit glucosyl fluoride reversion during liquid-phase HF solvolysis of cellulose (Franz et al., 1987). In situ methanolysis of sugar fluorides to 1-O-methyl sugars may likewise inhibit possible sugar fluoride/lignin condensation by consuming reactive glucosyl fluoride, which otherwise might repolymerize to higher oligosaccharides or condense onto lignin (see Figure 6.17).

In fact, when methanol-absorbed Bigtooth Aspen wood chips (15 μL methanol/10 mg wood or about 1:1 by weight) were reacted with 100% HF vapor at 1.0 atm and T_g = 30 °C, the sugar yields were increased relative to dry wood, as shown in Table 6.7.

Solid Residue Analysis. Note from Tables 6.6 and 6.7 that the water-insoluble, solid residue recovery from the vapor-phase HF solvolysis of Bigtooth Aspen wood was greater than the estimated lignin composition of lignin Bigtooth Aspen wood (0.220 g solid residue/g-wood vs. 0.169 g lignin/g-wood). This implies that the solid residue contains material other than lignin. The following experiments will attempt to characterize the composition of some of the extraneous materials in the water-insoluble solid residue.

The solid residue was analyzed for "organic extractives" and residual carbohydrates. The results of these analyses are given in Table 6.8. First, the solid residue (typically 3 to 3.5 mg per 15 mg of the original wood) was extracted with 2.0 mL 9:1 v/v acetone:water at room temperature for 24 h -- a typical wood "extractives" removal procedure (Pettersen, 1984b). After acetone-washing, drying in vacuo, and weighing, about 14.1% of the original weight of the solid residue was removed, which corresponds to about 3% of the original weight of the wood. This material is most likely the organic "extractives" fraction of the original wood (typically 3 to 4% wt. of the wood). Thus, a good portion of the orignal wood's extractives are retained in the solid residue after vapor-phase HF solvolysis.

Table 6.8. Composition of the water-insoluble solid residue obtained from the solvolysis of Bigtooth Aspen wood by 100% HF vapor at 1.0 atm, 30-31 °C.

Component	Wt. % of Solid Residue	Wt. % of Dry Wood
total solid residue	100.0	22.0 +/- 1.6
acetone-extractable [a] material in solid residue	14.1 +/- 2.3	3.1 +/- 0.5
glucan in residue [b]	7.5 +/- 0.8	1.7 +/- 0.2
xylan in residue [b]	4.3 +/- 0.6	1.0 +/- 0.1
glucan + xylan in residue	11.8	2.7
total acetone-extractable and carbohydrate residual	25.9	5.7
Remaining solid	74.1	16.3 [c]

Notes:

[a] Solid residue extracted with 9:1 v/v acetone/water at room temperature for 24 h (average of 3 assays).

[b] Solid residue hydrolyzed in 2 N TFA (100 μL per 1 mg) at 121 °C for 1 h. Water-soluble products assayed for glucose and xylose by HPLC (average of 4 assays). On a glucan basis, 3.0% additional glucose was recovered from the solid residue. On a xylan basis, 5.3% additional xylose was recovered from the solid residue.

[c] For comparison, the estimated lignin composition of Bigtooth Aspen wood is 0.166 g lignin/g-dry wood (see Tables 4.3 and 4.4).

Second, the solid residue (typically 3 to 3.5 mg) was hydrolyzed with 300 μL 2 N TFA at 121 °C within a septum-sealed Kontes 1.0 mL "reacti vial" under dry-block heating for 1 h. This hydrolysis converted any oligomers trapped in the solid residue to free sugars, which were in turn released to the hydrolysate. After hydrolysis, myo-inositol internal standard (100 μg in 100 μL H_2O) was added to the vial. The water-soluble fraction was then blown down to dryness three times over flowing N_2 gas at 50 °C to remove the volatile TFA, resuspended in 100 μL water, microcentrifuged, and then analyzed by carbohydrate HPLC as described in chapter 4.

By experimental methods just described, about 7.5% of the weight of the original weight of the solid residue was glucan, and about 4.3% was xylan. On a glucan basis, this procedure yielded 3.0% additional glucose yield. On a xylan basis, this procedure yielded 5.3% additional xylose yield. The source of the carbohydrates trapped in the solid residue could be oligomer/lignin adducts. The hydrolysis of an oligomer chain anchored onto lignin would release all sugars from the oligomer except the sugar which is directly alkylated onto the lignin structure.

In summary, the solid residue contains much of the wood's original "extractives" and a small amount of residual carbohydrates removable by hydrolysis. In Table 6.9, the sugar recovery from the water-soluble products of the vapor-phase HF solvolysis of wood are combined with the sugar recovery from the solid residue. The total glucose yield is about 0.54 g glucose/g-wood, or about 87% of theoretical. This glucose yield would also be obtained if the whole HF-reacted wood chip was

Table 6.9. Incremental improvement of maximum average glucose and xylose yield from the vapor-phase HF solvolysis of Bigtooth Aspen wood.

Basis/Correction	Adjusted Glucose Yield			Adjusted Xylose Yield		
	g/g wood	% [a]	% [b]	g/g-wood	% [a]	% [b]
water-soluble reaction products after post-hydrolysis	0.500	80.9	90.0	0.134	63.9	70.2
correction for glucose and xylose yield degrad. during posthydrolysis, K_{Lg} = 1.03, K_{Lx} = 1.14	0.516	83.5	92.8	0.153	72.9	80.1
0.019 g glucose/g wood, 0.009 g xylose/g wood released upon hydrolysis of solid residue [c] (see also Table 6.8)	0.535	86.5	96.2	0.162	77.2	84.8

Notes:

[a] Maximum theoretical glucose yield taken as 0.618 g/g-wood, maximum theoretical xylose yield taken as 0.210 g/g-wood (Selke, 1983).

[b] Percent % sugar recovery normalized with respect to two-step sulfuric acid hydrolysis for wood sugar determination; maximum glucose recovery taken as 0.556 g/g-wood, maximum xylose recovery taken as 0.191 g/g-wood (see Table 6.7).

[c] This would be the expected glucose and xylose yield if the HF-reacted wood chip was posthydrolyzed, i.e., the water-soluble products and water-insoluble solid residue are posthydrolyzed together in one vessel.

posthydrolyzed directly, as opposed to posthydrolysis of its water-soluble product solution separated from the solid residue.

The lignin in the solid residue was not characterized at all. The possibility of water-soluble lignin after vapor-phase HF solvolysis of wood was also not investigated.

V. HF-Catalyzed Glucosyl Fluoride Repolymerizaton and Reversion Oligosaccharide Profiling

A. Reversion Chemistry

The liquid-phase HF solvolysis of cellulose yields glucosyl fluoride in HF solution. The glucosyl fluoride repolymerizes to "reversion" oligosaccharides in HF solution in concentration and temperature dependent equilibrium, as shown in Figure 6.19 (Rogovin and Pogosov, 1959; Hardt and Lamport, 1982a; Defaye et al., 1982, 1983; Mort and Parker 1982; Franz et al., 1987). In general, these "reversion oligosaccharides" are water-soluble, range from 2 to 20 anhydroglucose units in size, and are joined together by two or more types of O-glycosidic linkages. Specifically, glucosyl fluoride repolymerizes when the C-1 fluoride on a given glucosyl fluoride molecule attacks an open OH group on another glucosyl fluoride, free sugar, or oligosaccharide molecule. This condensation reaction creates an ether linkage (an O-glycosidic linkage) and regenerates HF. For example, if the fluoride on C-1 carbon of glucosyl fluoride attacks the O-6 oxygen (-OH group) on another glucosyl fluoride, and the linkage formed at C-1 is oriented below the plane of the glucosyl ring containing this C-1 carbon, then an

α-1,6-O-glycosidic linkage is formed (see Figure 6.19).

The extent of glucosyl fluoride repolymerization, or reversion, is a function of HF solvolysis conditions. In general, for the anhydrous liquid-phase HF solvolysis of cellulose, the extent of reversion increases with increasing reaction time, temperature, and initial cellulose concentration in liquid HF. The oligosaccharide distribution shifts toward the monomer with increasing water content in the liquid HF (1 to 10% wt H_2O). Also, the oligosaccharide product distribution is dramatically affected by HF removal conditions. For example, if the liquid-phase HF solvolysis of cellulose (1 g in 10 mL) at 0 °C for 1 h is "quenched" by rapidly pouring the reaction mixture into a cold calcium carbonate slurry (20 g $CaCO_3$ in 100 mL dichloroethane under cooling by liquid N_2), then the D.P. of the oligosaccharide product distribution ranges from 1 to 6, with an average D.P. of 2. However, if the HF liquid is removed by vacuum evaporation at 100 °C, then extent of reversion increases (although the oligomers still remain water-soluble), with an average oligomer D.P. of 6 (Hardt and Lamport, 1982a). In general, the glycosidic linkage composition of reversion oligosaccharides is randomized, with the α-1,6 linkage predominant (Defaye et al., 1982, 1983; Franz et al., 1987).

B. HPLC Oligosaccharide Profiling

In light of the previous studies of glucosyl fluoride repolymerization during liquid-phase HF solvolysis of lignocellulose, it is desirable to characterize the reversion oligosaccharide product distribution obtained from the vapor-phase HF solvolysis of dry pure cellulose (filter paper) or "prehydrolyzed" wood

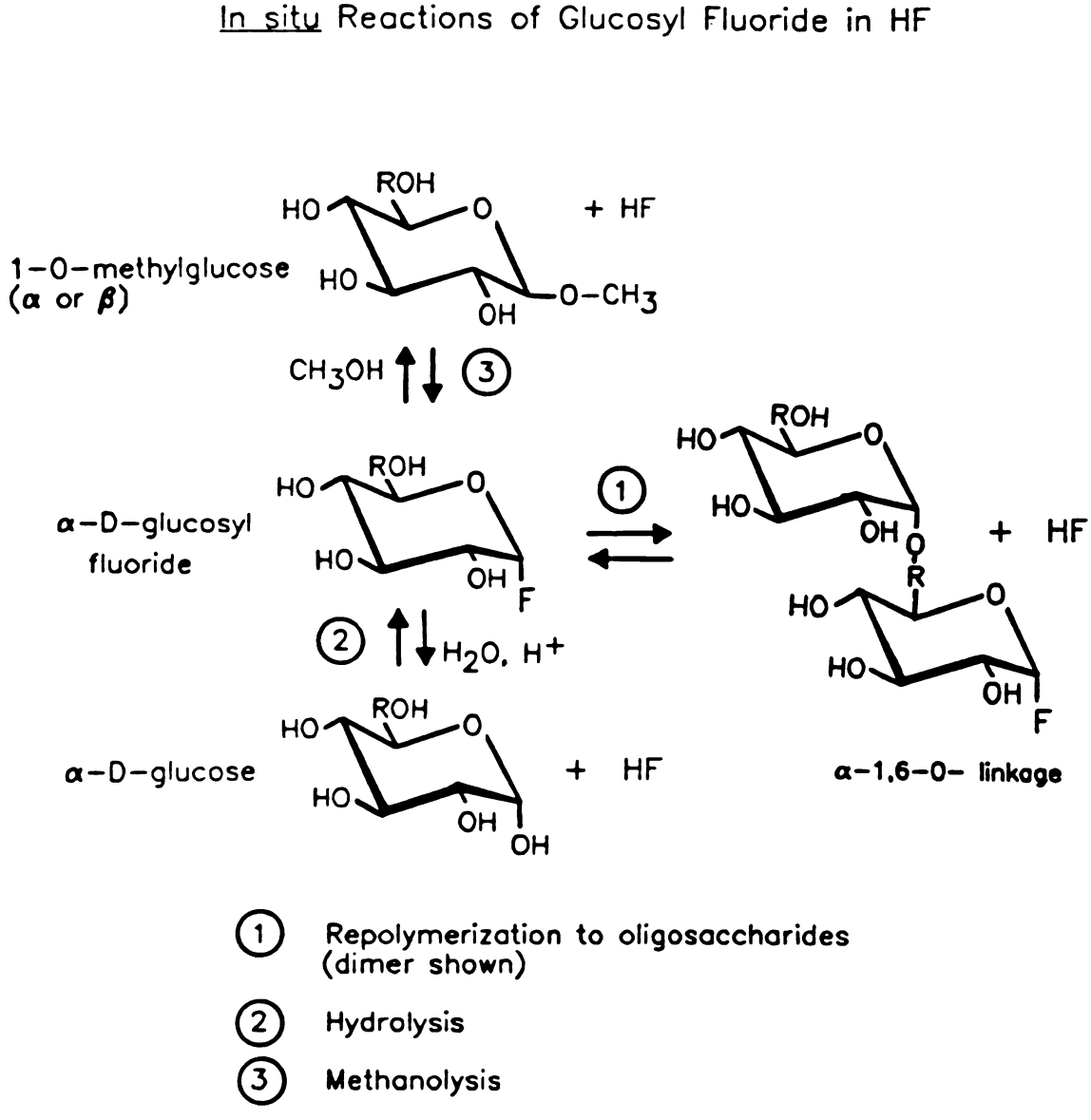


Figure 6.19. In situ reactions of glucosyl fluoride in HF.

(lignocellulose) as a function of reaction time and HF vapor conditions.

As described in chapter 4, the reaction is "quenched" by dropping the HF-reacted lignocellulose chip into a large volume of water in order to dissipate the adsorbed HF. This technique "freezes" the oligosaccharide product distribution at a given reaction time and HF vapor conditions and hydrolyzes the free glucosyl fluoride to glucose. Although the product solution is weakly acidic due to dissolved HF, at room temperature the conditions are not sufficiently severe to hydrolyze the reversion oligosaccharides. Also, the product solution is is neutralized with $CaCO_3$ powder to remove aqueous HF as a CaF_2 precipitate.

The oligosaccharide product distribution in the water-soluble reaction products before dilute-acid posthydrolysis was profiled by High-Performance Liquid Chromatography (HPLC). Specifically, free glucose and oligosaccharides of D.P. 2 to D.P. 6 were separated on a BIO-RAD HPX-42A HPLC-oligosaccharide analysis column at the operating conditions specified in chapter 4 (RI detection, 0.6 mL/min HPLC-grade H_2O as the column mobile phase, 85 ^oC column temperature). Oligosaccharides of D.P. 6 to 10 were not well separated, and oligosaccharides of D.P. greater than 10 voided the column completely.

Effect of Reaction Time. HPLC oligosaccharide profiles obtained from the solvolysis of dry filter paper by an anhydrous, 100% HF vapor stream at 30 ^oC and reaction times from 2 to 12 min are presented in Figure 6.20. Although the filter paper was completely converted to water-soluble products within a 3 minute reaction time, the oligosaccharide product distribution continued to shift toward

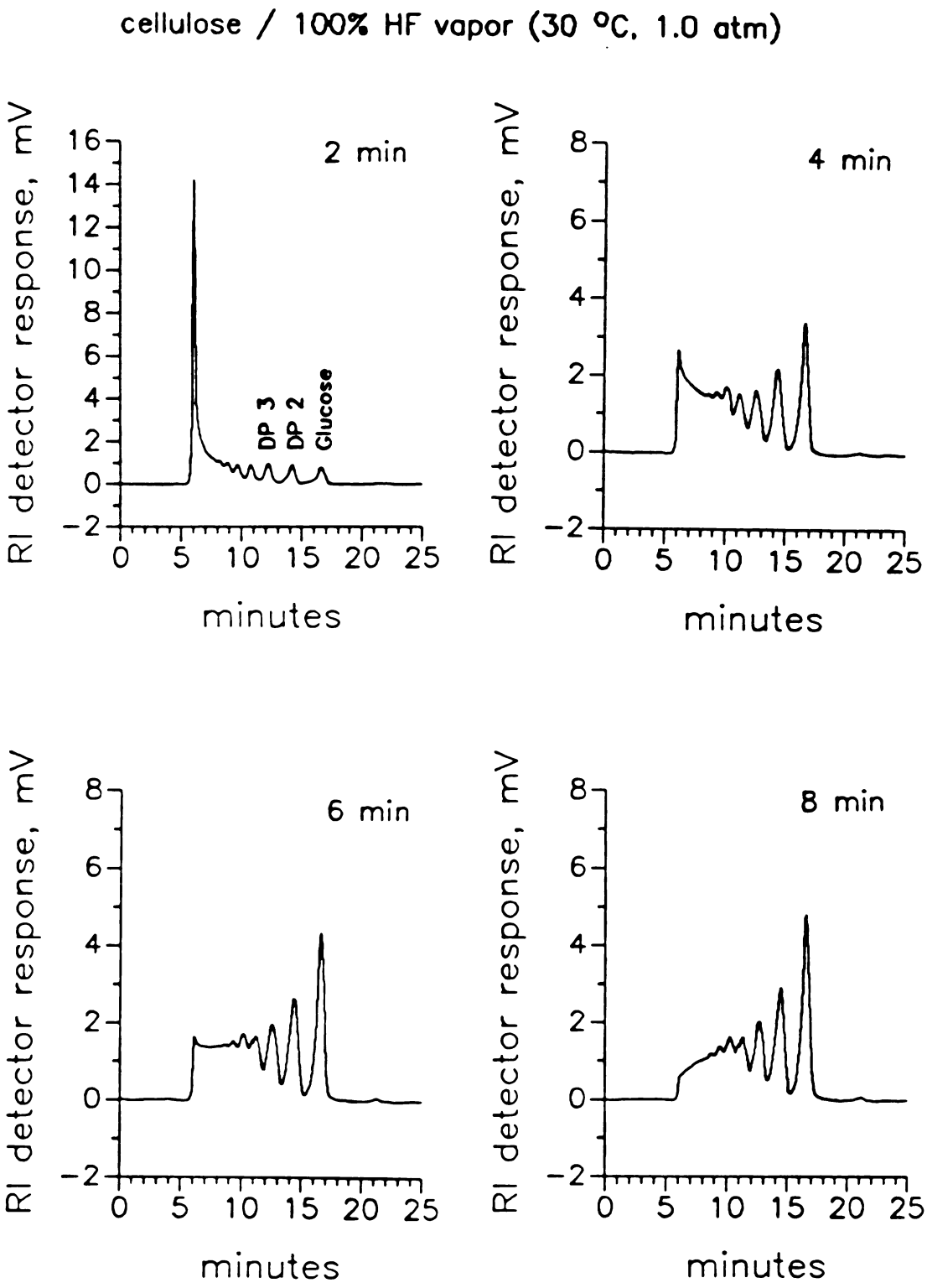


Figure 6.20. Solvolysis of a single, dry, pure cellulose wafer (Whatman filter paper No. 3) by a 100% HF vapor stream at T_g = 30 °C: HPLC-oligosaccharide profiles before posthydrolysis as a function of reaction time. Notes: G_{HF} = 0.42 g HF/cm^2-min, 100 μg total oligomer loaded onto BIO-RAD HPX-42A column.

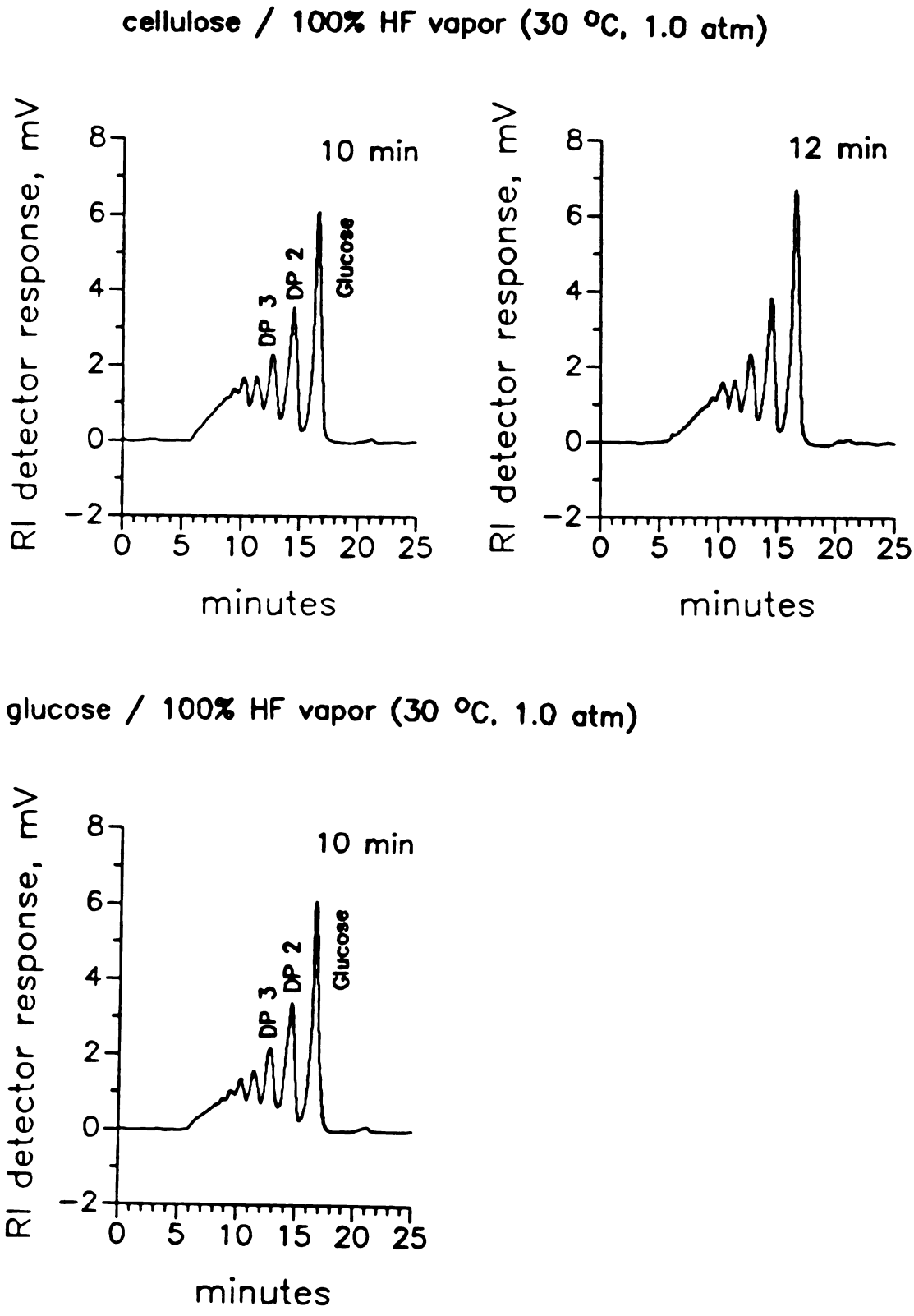


Figure 6.20 (cont'd.). Special note: the last HPLC oligosaccharide profile is from the reaction of solid α-D-glucose with 100% HF vapor at T_g = 30 °C.

glucose as a function of reaction time from 2 min to 12 min. Evidently, even though cellulose solvolysis was complete, the glucosyl fluoride/reversion oligomer distribution was still changing. Eventually, the reversion oligosaccaride product distribution settled down to equilibrium at a reaction time of 10 to 12 min. At a given temperature, the equilibrium oligosaccharide distribution resulted when the rate of formation of reversion oligosaccharides by HF-catalyzed condensation equaled the rate of solvolysis of oligosaccharides by adsorbed HF.

The shift of the oligosaccharide distribution toward monomer as a function of time is due in part to the particle temperature vs. time profile in the HF-reacting solid. As HF adsorbs on the filter paper, heat is generated within the HF-reacting filter paper by the exothermic processes of HF physical adsorption and HF-solvation of cellulose chains. This generated heat increases the particle temperature, and hence increases the extent of reversion. Once HF adsorption is complete, adsorption heat is no longer generated, the solid cools off, and the temperature of the solid decreases back toward the surrounding HF vapor stream temperature. Correspondingly, as the temperature of the HF-reacting solid decreases, the extent of reversion decreases, and so the reversion oligosaccharide product distribution slowly shifts back toward glucose and eventually reaches an equilibrium product distribution with respect to the 100% HF vapor stream temperature.

In all experiments, dry filter paper was reacted with anhydrous HF vapor. Therefore, the reaction medium was essentially anhydrous. If moisture was present

in the filter paper, then in situ hydrolysis of glucosyl fluoride to glucose could occur (see Figure 6.19). This hydrolysis would compete with the glucosyl fluoride available for repolymerization, and thus shift the oligosaccharide product distribution back toward the monomer. In this present study, the effect of moisture content on the oligosaccharide product distribution was not investigated. However, the effect of methanol (saturated in the cellulose) on the oligosaccharide product distribution was investigated. These experiments are described later in this section.

Finally, as a control experiment, solid α-D-glucose was reacted with 100% HF vapor at 30 °C for 10 min. The water-soluble reaction products were then profiled by HPLC, as shown in Figure 6.20. The oligosaccharide profile from glucose was similar to the oligosaccharide profile from pure cellulose at the same reaction conditions. Initially, I expected that the reversion oligosaccharide profile would be shifted more toward glucose, because when glucosyl fluoride is formed from glucose, water is released. The water would shift the equilibrium product distribution toward lower oligosaccharides by hydrolyzing some of the glucosyl fluoride back to glucose. Most likely, however, some of the water evaporated to the surrounding HF vapor stream, and so the effect the water on the oligosaccharide product distribution was correspondingly diminished.

Effect of 100% HF Vapor Temperature. HPLC oligosaccharide profiles obtained from the solvolysis of dry, prehydrolyzed wood by an anhydrous, 100% HF vapor stream at 31 °C, 41 °C, and 52 °C are presented in Figures 6.21, 6.22, and 6.23 respectively. Note from Figures 6.21 to 6.23 that as the 100% HF vapor

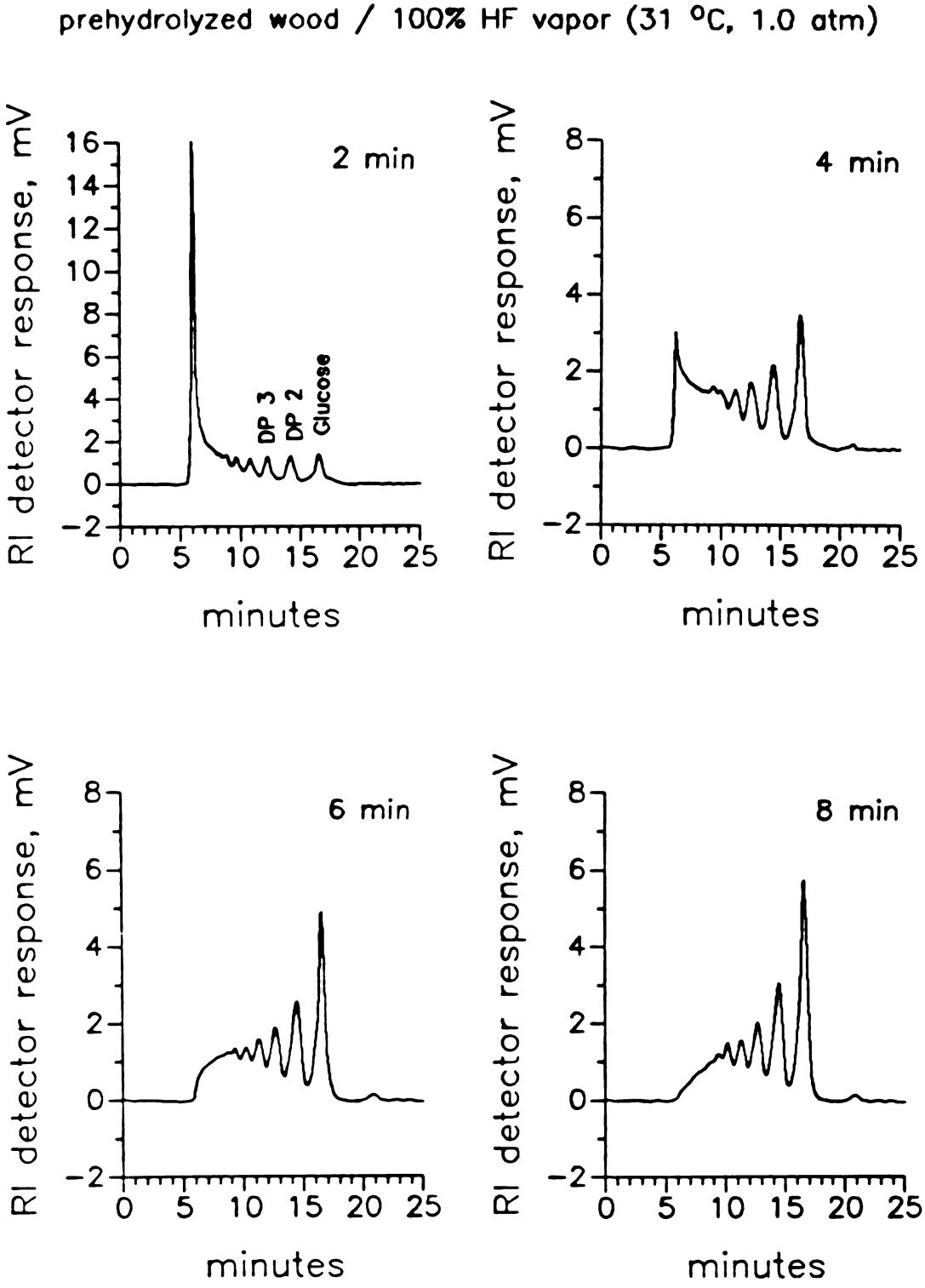


Figure 6.21. Solvolysis of a single, dry, prehydrolyzed wood chip (2L = 0.4 mm) by a 100% HF vapor stream at T_g = 31 °C: HPLC-oligosaccharide profiles before posthydrolysis as a function of reaction time. Notes: G_{HF} = 0.42 g HF/cm^2-min, 100 μg total oligomer loaded onto BIO-RAD HPX-42A column.

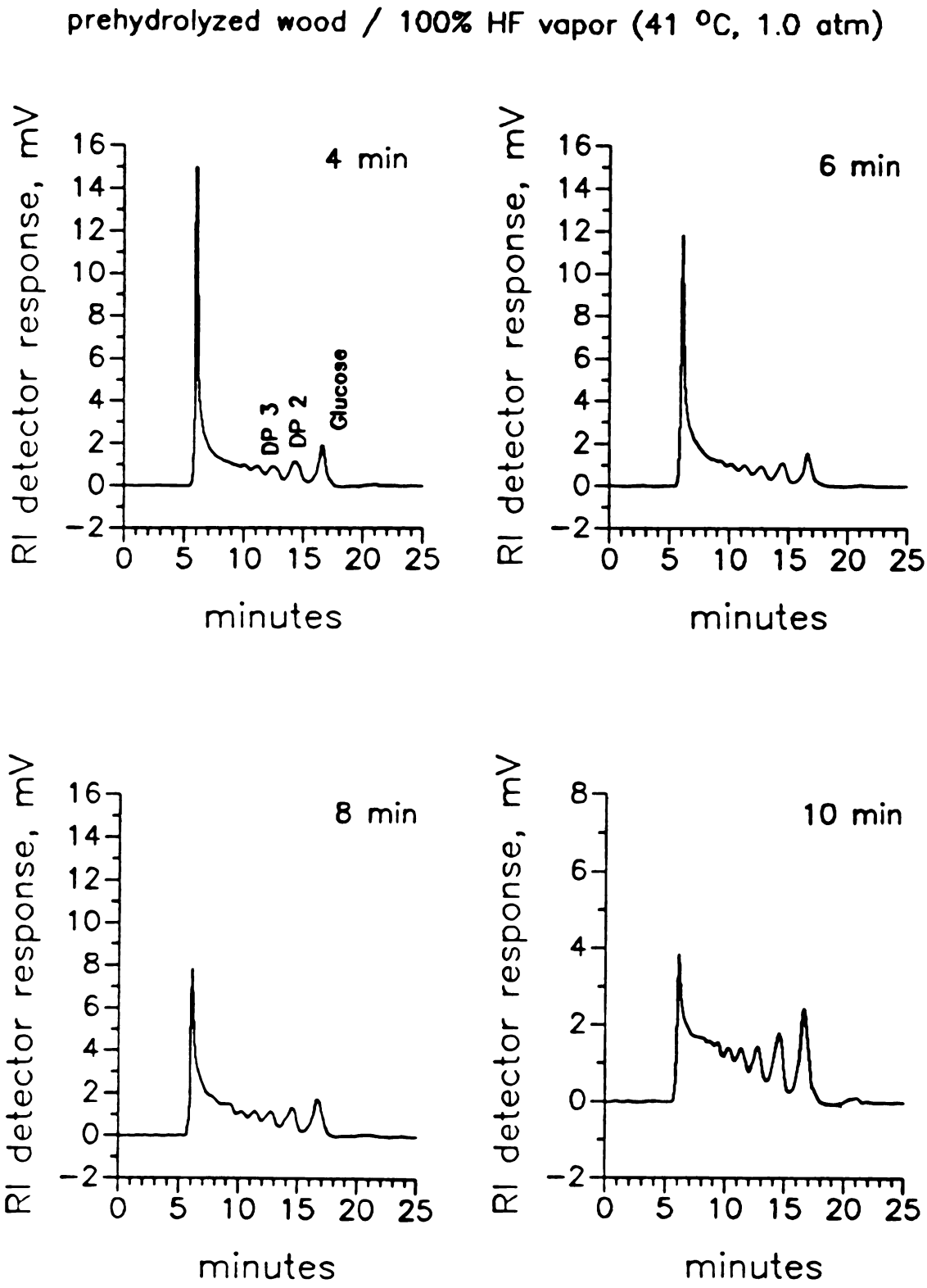


Figure 6.22. Solvolysis of a single, dry, prehydrolyzed wood chip (2L = 0.4 mm) by a 100% HF vapor stream at T_g = 41 °C: HPLC-oligosaccharide profiles before posthydrolysis as a function of reaction time. Notes: G_{HF} = 0.42 g HF/cm^2-min, 100 μg total oligomer loaded onto BIO-RAD HPX-42A column.

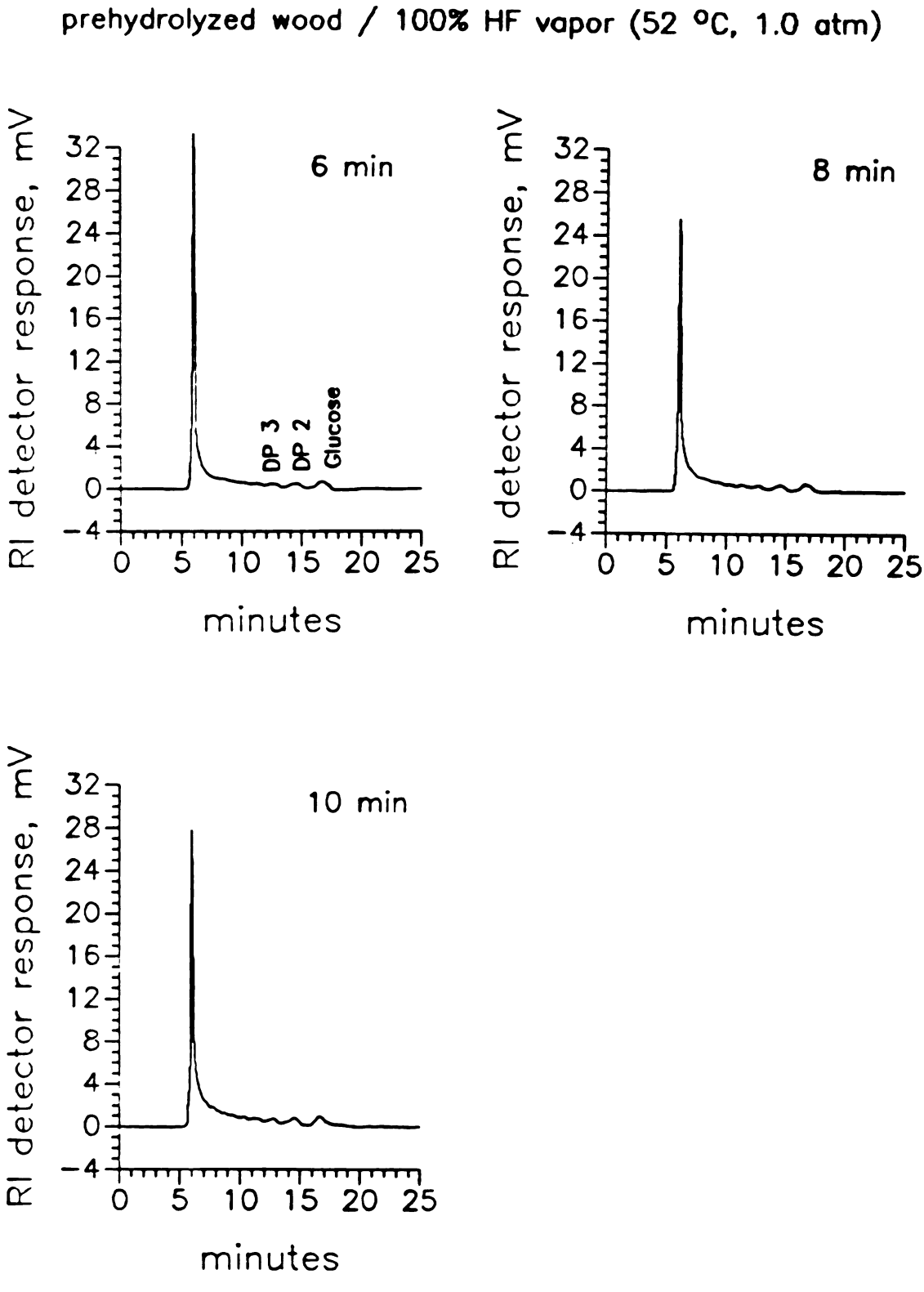


Figure 6.23. Solvolysis of a single, dry, prehydrolyzed wood chip (2L = 0.4 mm) by a 100% HF vapor stream at T_g = 52 °C: HPLC-oligosaccharide profiles before posthydrolysis as a function of reaction time. Notes: G_{HF} = 0.42 g HF/cm^2-min, 100 μg total oligomer loaded onto BIO-RAD HPX-42A column.

stream temperature increased, the extent of reversion (i.e. the average D.P. of the reversion oligomers) increased dramatically. At a 100% HF vapor stream temperature of 52 °C, the D.P. of most of the oligosaccharides was greater than 10, and so these higher oligomers voided the BIO-RAD HPX-42A oligosaccharide-profiling HPLC column. These higher molecular weight oligomers were still soluble in water. Most likely the oligomers are similar to dextrans (α-1,6-linked polymers of glucose), which are soluble in water at high molecular weights (Neely, 1960).

The extent of reversion also increases with decreasing HF loading. This is because as the HF loading on the solid decreases, the sugar concentration in the HF-adsorbed solid increases. Recall that the HF loading decreases with increasing temperature. Therefore, as the 100% HF vapor stream temperature increases, the oligosaccharide profiles given in Figures 6.21 to 6.23 are shifted to higher oligomers by the superimposed effects of increased temperature and decreased HF loading. The effect of HF loading on the extent of reversion at a fixed temperature was not measured directly. However by HPLC-oligosaccharide profiling the water-soluble reaction products from the vapor-phase HF solvolysis of lignocellulose at various HF partial presures and fixed temperature.

In general, the extent of reversion for the vapor-phase HF solvolysis of cellulose was much higher than that for the liquid-phase HF solvolysis of cellulose. During the solvolysis of cellulose by HF vapor, glucosyl fluoride, glucose, and oligomers resided on the HF-adsorbed/reacted substrate. In contrast, for the solvolysis of cellulose by HF liquid, glucosyl fluoride, free glucose, and reversion

oligomers were diluted in HF solution. Since the concentration of glucosyl fluoride and glucose in the HF reaction medium was higher for the vapor-phase process than the liquid-phase process, the extent of reversion was correspondingly greater. The extent of reversion was also increased as the result of reaction temperature, which was always higher for the vapor-phase process than for the liquid-phase process.

Glucose Yields Before and After Posthydrolysis. The water-soluble reaction products from the vapor-phase HF solvolysis of prehydrolyzed wood are a mixture of glucose and reversion oligosaccharides. A dilute-acid posthydrolysis of the water-soluble products at mild conditions (2 N TFA at 121 °C for 1 h) readily converts the reversion oligosaccharides back to glucose. For the oligosaccharide profiles given in Figure 6.21 to 6.23, the glucose yields both before and after post-hydrolysis are compared in Table 6.10. The glucose yield in the water-soluble products before posthydrolysis is a measure of the free glucosyl fluoride in the HF-adsorbed/reacted lignocellulose.

Future Analytical Studies. At higher 100% HF vapor temperatures, the oligosaccharide product distribution was not well resolved by the BIO-RAD HPX-42A oligosaccharide HPLC column, because the oligomers were too large. Since the oligosaccharide product distribution was complex and not fully resolved by our present HPLC-oligosaccharide profiling technique, the oligomer product distribution beyond glucose was not quantified. In future work, the high molecular weight

Table 6.10. Glucose yields before and after posthydrolysis of the water-soluble reaction products obtained from the solvolysis of dry, prehdyrolyzed wood by a 100% HF vapor stream at 1.0 atm and temperatures of 31 °C, 41 °C, and 52 °C. See also Figures 6.21 to 6.23.

Reaction Time	T_s	Glucose Yield Before Posthydrolysis		Glucose Yield After Posthydrolysis	
min	°C	g/g [a]	% [b]	g/g [a]	% [b]
2.0	31	0.066	7.9	0.745	89.8
4.0	31	0.216	26.0	0.786	94.7
6.0	31	0.211	25.4	0.773	93.1
8.0	31	0.253	30.5	0.793	95.5
2.0	41	0.033	4.0	0.620	74.7
4.0	41	0.080	9.6	0.749	90.2
6.0	41	0.073	8.8	0.764	92.0
8.0	41	0.118	14.2	0.766	92.3
10.0	41	0.090	10.8	0.807	97.2
6.0	52	0.040	4.8	0.793	95.5
8.0	52	0.034	4.1	0.776	93.4
10.0	52	0.053	6.4	0.775	93.3

Notes:

[a] g/g = g glucose/g prehydrolyzed wood (lignocellulose)

[b] % = % of maximum theoretical glucose yield, 0.83 g glucose/g-lignocellulose

oligomers should be analyzed by aqueous gel-permeation chromatography (GPC). The Waters Associates Ultrahydrolgel DP/2 GPC column (size exclusion limit of 5000, cat. no. 11550) is suitable for this purpose (in fact, I purchased this column in 1988 but never used it!). It would also be desirable to isolate each oligomer and determine its O-glycosidic linkage composition via Hakomori methylation (Hakomori, 1964) and subsequent gas-liquid chromatography of the alditol-acetate derivatives (Albersheim et al., 1967) of the methylated, hydrolyzed products.

C. Modification of the Oligosaccharide Distribution by In situ Methanolysis

The liquid-phase HF solvolysis of cellulose generates glucosyl fluoride in HF solution. The glucosyl fluoride repolymerizes to "reversion" oligosaccharides, with the equilibrium reversion oligosaccharide product distribution dependent on temperature and glucosyl fluoride concentration. When methanol is added to liquid HF, in situ methanolysis of glucosyl fluoride to 1-O-methyl glucose occurs. This in situ methanolysis competes with glucosyl fluoride repolymerization and thus shifts the oligosaccharide distribution back toward the monomer. A detailed study on the effect of mono- and polyhydroxy alcohols on the reversion oligosaccharide product distribution generated by the liquid-phase HF solvolysis of cellulose is described by Franz et al., (1987).

In principle, if methanol is added to filter paper, and the methanol-absorbed filter paper is reacted with HF vapor, then the reversion oligosaccharide distribution in the water-soluble reaction products should be dramatically shifted back toward the monomer, relative to control experiments with dry filter paper. From a

process standpoint, shifting the oligosaccharide product distribution toward 1-O-methyl glucose or lower oligosaccharides is desirable for two reasons. First, if glucosyl fluoride reversion can be blocked completely, then the need for posthydrolysis is eliminated, and the overall process for production of monomer (fermentable) sugars from vapor-phase HF solvolysis of lignocellulse is simplified and improved. Second, even if glucosyl fluoride reversion cannot be blocked completely, in situ methanolysis can still reduce the extent of reversion and control the oligosaccharide product distribution.

In light of the possible process benefits of in situ methanolysis, I explored the effect of methanol on the reversion oligosaccharide product distribution generated by vapor-phase HF solvolysis of pure cellulose. The methods and results of this preliminary investigation are provided here. Experimentally, methanol (density 0.79 g/mL at room temperature) was pipetted carefully onto a single, dry filter paper wafer (ca. 15 μL/10 mg or about 1:1 by weight), allowed to soak for 30 sec, and then reacted with a 100% HF vapor stream at 30 °C for 2 to 12 min. This methanol loading saturated the filter paper and corresponded to about a five-fold molar excess to that required for stoichiometic reaction of glucosyl fluoride to 1-O-methyl glucose. The oligosaccharides in water-soluble reaction products were then profiled by HPLC as described earlier in this section. The HPLC-oligosaccharide profiles are shown in Figure 6.24.

The addition of methanol to cellulose dramatically shifted the oligosaccharide distribution back toward the monomer (compare Figure 6.20 with Figure 6.24).

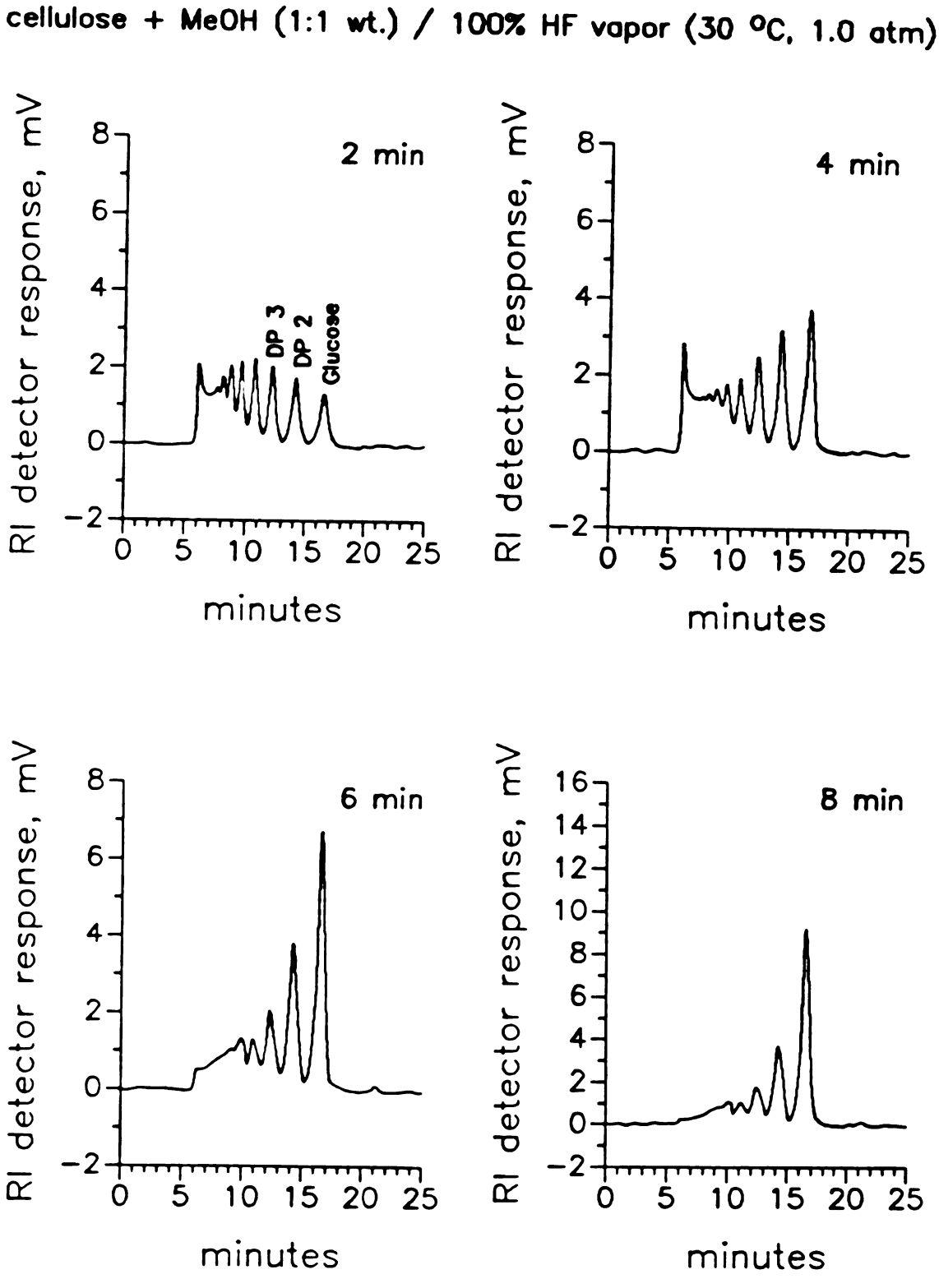


Figure 6.24. Solvolysis of a single, methanol-absorbed pure cellulose wafer by a 100% HF vapor stream at T_g = 30 °C: HPLC-oligosaccharide profiles before posthydrolysis as a function of reaction time. Notes: GHF = 0.41 g HF/cm^2-min, 15 μL methanol per 10 mg dry pure cellulose (ca. 1:1 wt.), 100 μg oligomer loaded on column.

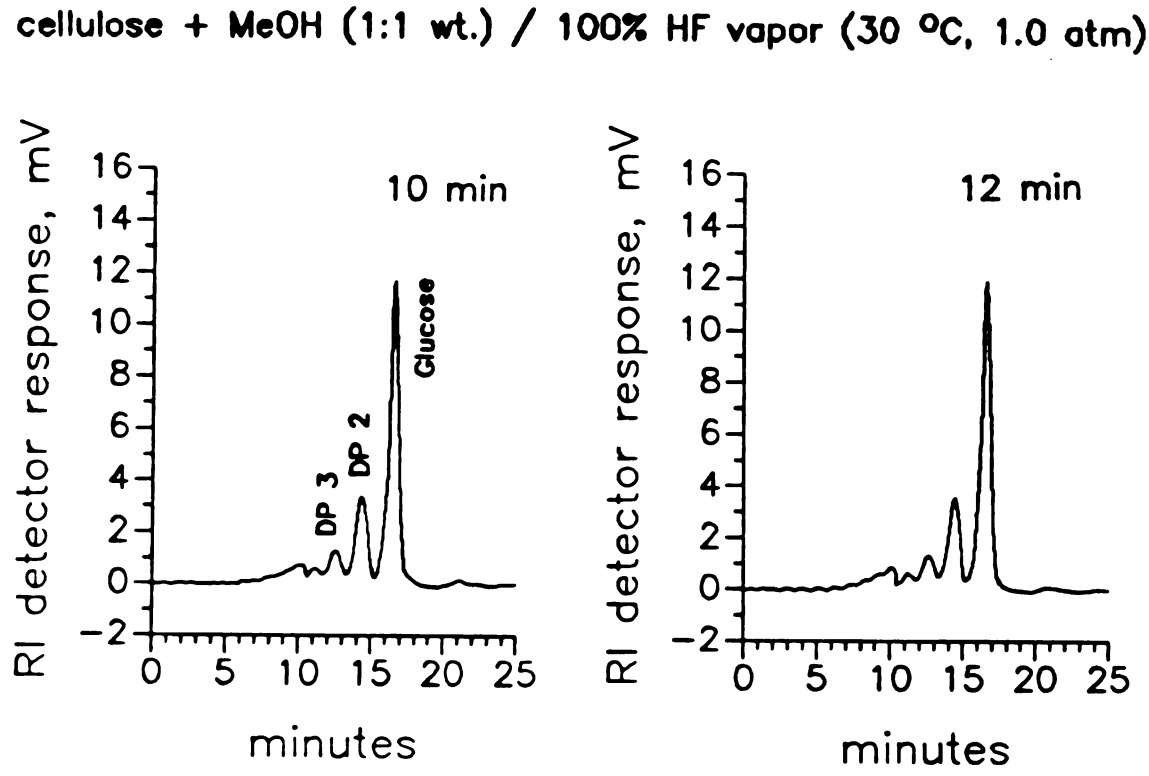


Figure 6.24 (cont'd.).

This is clearly evident from Figure 6.25, where the reversion oligosaccharide profiles from the vapor-phase HF solvolysis of dry and methanol-absorbed cellulose are superimposed onto one chromatogram.

I first attempted to analyze for 1-O-methyl glucose in the water-soluble reaction products before posthydrolysis via HPLC with the BIORAD HPX-87P monosaccharide analysis column (same operating conditions as the standard monosaccharide analysis). To my surprise, more glucose (i. e. glucosyl fluoride in the solid) was formed than 1-O-methyl glucose, although the respective amounts were hard to quantify because 1-O-methyl glucose partially co-chromatographed onto glucose. Also, I noted that methanol evaporates from the methanol-absorbed cellulose. In fact about 8% of the total absorbed methanol evaporated during the 30 sec soaking time. Therefore, the amount of methanol in the HF-reacting cellulose was probably decreasing over time.

Monomer yields (glucose and 1-O-methylglucose) in the water-soluble reaction products of the vapor-phase HF solvolysis of dry filter paper and methanol-absorbed filter paper before posthydrolysis are plotted together as a function of reaction time, as shown in Figure 6.26 compared on the same graph). From Figure 6.25, the glucose yield from dry cellulose was leveling off at about 35% of theoretical, whereas the glucose yield from methanol-absorbed cellulose was leveling off at about 60% of maximum theoretical. Recall that these glucose (or glucose plus 1-O-methyl glucose) yields quantify the glucosyl fluoride concentration (or glucosyl fluoride plus 1-O-methyl glucose concentration) in the HF-reacting solid.

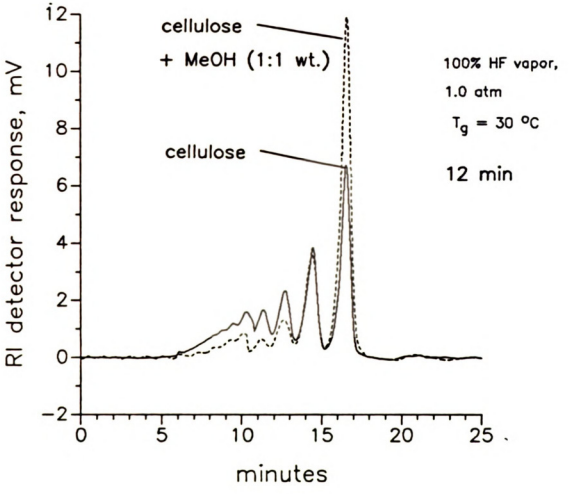


Figure 6.25. Comparison of HPLC-oligosaccharide profiles obtained from the vapor-phase HF solvolysis of pure cellulose and methanol-absorbed pure cellulose (see Figures 6.20 and 6.24).

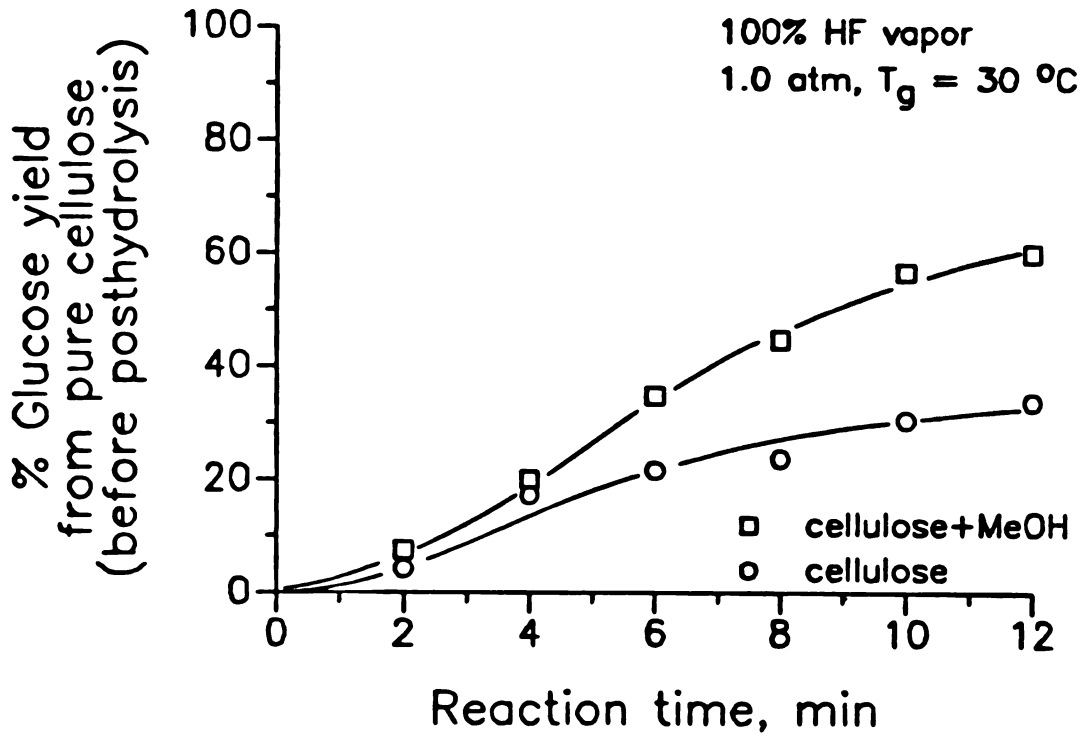


Figure 6.26. Solvolysis of a single, dry cellulose (filter paper) wafer and a single, methanol-absorbed filter paper wafer by a 100% HF vapor stream at T_g = 30 °C: comparison of the glucose (glucose + 1-O-methyl glucose) yields before posthydrolysis as a function of reaction time.

Obviously, these preliminary experiments show that in situ methanolysis and perhaps other in situ reaction chemistries can control the oligosaccharide product distribution, and perhaps generate useful chemical intermediates as well.

Chapter 7. Particle Temperature Measurements

Introduction

The adsorption of HF vapor onto a single lignocellulose chip is an exothermic process. If heat transfer resistances are present near and within the HF-adsorbing lignocellulose chip, then energy accumulates within the solid and increases the particle temperature. This particle temperature increase is offset by convection of heat from the hot particle surface to the cooler surrounding HF vapor stream. Eventually, the rate of heat transported to the surrounding HF vapor stream by convection is larger in magnitude than the rate of exothermic heat generated by HF adsorption. In this regime, the particle temperature decays slowly back to the surrounding HF vapor stream temperature.

In summary, if heat transfer resistances are present, then the HF-reacting lignocellulose particle temperature will rise rapidly to a maximum temperature and then decay slowly back to the HF vapor stream temperature over time.

In this chapter, the temperature within a single HF-reacting lignocellulose chip is measured as a function of reaction time, 100% vapor temperature, and 100% HF vapor flowrate. These particle temperature measurements are valuable for three reasons. First, the particle temperature measurements gauge the significance of heat transfer resistances. Second, since the HF-reacting lignocellulose chip is nonisothermal, particle temperature vs. time data are needed for kinetic parameter estimation (chapter 8, section V). Finally, particle temperature vs. time data are

needed to validate energy balance model predictions (see chapters 9 and 10).

This chapter is organized into three sections, labeled I to III. In section I, the experimental design for measurement of the temperature at the center of a single HF-reacting lignocellulose chip as a function of reaction time and HF vapor conditions is described. In section II, the effect of 100% HF vapor stream temperature on the particle temperature vs. time data is presented and discussed. Finally, in section III, the effect of 100% HF vapor flowrate on the particle temperature vs. time data is presented and discussed.

I. Experimental Design

In this section, I describe the experimental design for in situ measurement of the temperature within a single HF-reacting lignocellulose chip as a function of reaction time and HF vapor conditions. The experimental design includes:

A. Modification of the vapor-phase HF solvolysis apparatus sampling probe to accommodate a Teflon-encased thermocouple microprobe

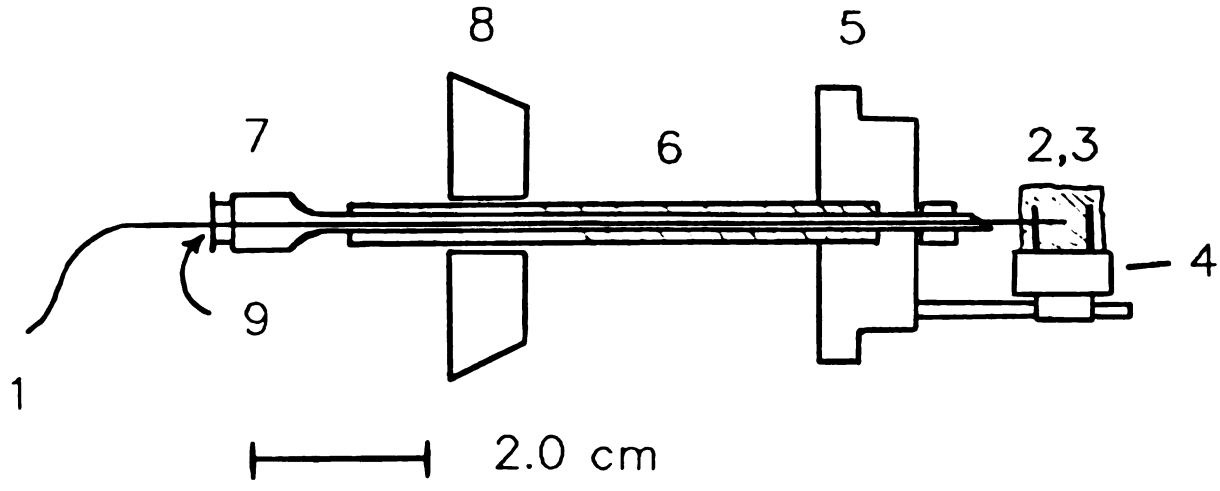
B. Development of a computer data acquisition system for in situ particle temperature measurement

C. Development of computer software for post-run processing of raw particle temperature vs. time data

D. Online measurement of the 100% HF vapor stream temperature, T_g.

A. Sampling Probe Modification

The sampling probe of the vapor-phase HF solvolysis apparatus was easily modified to accommodate a Teflon-encased thermocouple microprobe, as shown in Figures 7.1 (compare with Figure 4.10). First, the existing sampling probe arm was



Legend:

1. Sensortek type-T Teflon encased thermocouple microprobe (0.6 mm diameter)
2. Two prehydrolyzed wood chips of 0.4 mm thickness pressed together (see Figure 7.2)
3. Folded-over Monel screen (see Figure 7.2)
4. Teflon sample cartridge
5. Sample access port plug
6. 6.35 cm x 6.35 mm diameter Teflon dowel (1.5 mm diameter hole drilled down length)
7. 17-gauge hypodermic needle
8. Sample access chamber seal
9. Teflon sealing tape between hypodermic needle and microprobe

Figure 7.1. Modification of the Teflon sampling probe for particle temperature measurement studies.

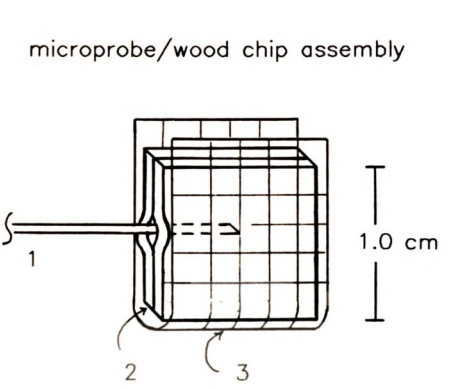
unscrewed from the base of the sample access port plug. In its place, a hollow 6.35 mm diameter Teflon dowel with a 1.5 mm diameter hole bored down its length was inserted through the sample access chamber seal and into the base of the sample access port plug. A 17-gauge hypodermic needle was then inserted through the bore hole and pushed through the sample access port plug. The tip of the needle was extended approximately 1 cm past the inner surface of the sample access port plug. The base of the needle was extended outside of the reactor through the sample access chamber seal. A Teflon-encased thermocouple microprobe (Sensortek IT-18 type T, 0.6 mm outer diameter, 0.1 sec response time) was threaded through the bore of the hypodermic needle. The tip of the thermocouple microprobe was extended approximately 2 cm past the inner seal of the sample access port plug. The base of the hypodermic needle (not the tip) and the Teflon-encased microprobe lead wire were sealed tightly together with Teflon tape. This seal prevented HF vapors from ventilating through the bore of the hypodermic needle.

Given the thermocouple microprobe configuration, the center of the HF-reacting lignocellulose chip was the best position to measure particle temperature. Since the thickness of the lignocellulose chip was only 0.4 mm and the Teflon-encased microprobe is 0.6 mm in diameter, the microprobe was not directly embedded into the center of a single lignocellulose chip. Instead, the tip of the microprobe was sandwiched between two lignocellulose chips, each of 0.4 mm thickness. The two chips were pressed together and molded around the

microprobe by a Monel screen, as shown in Figure 7.2. The entire assembly rested on the Teflon sample cartridge.

The reaction procedure for particle temperature measurement was similar to the vapor-phase HF solvolysis procedure described in chapter 4, section II. For a given particle temperature vs. time measurement, the lignocellulose chip/microprobe sandwich was assembled and positioned on the Teflon sampling probe, as described in the preceding paragraph. The Teflon sampling probe and microprobe-embedded lignocellulose chip assembly were then inserted into the reactor, and the reaction was allowed to proceed for a specified reaction time, typically 8 minutes. The microprobe-embedded lignocellulose chip could not be rapidly disengaged from the sampling mechanism and dropped into the water-filled quenching vial. Therefore, after a given particle temperature vs. time profile was measured, the sampling mechanism and thermocouple microprobe assembly were removed from the reactor. When the HF-reacted lignocellulose chip was retrieved from the tubular section of the reactor, the adsorbed HF was first allowed to flash off the sample within the sample access chamber. When the sampling mechanism was completely disengaged from of the reactor, the Monel screen and HF-reacted lignocellulose chips were pulled off the microprobe. The lignocelluose chip/microprobe sandwich was then reassembled with two fresh lignocellulose chips, and the procedure was repeated.

I did not attempt to measure the surface temperature of the HF-reacting lignocellulose chip because I could not find a commercially available, HF-inert surface microprobe.



Legend:

1. Sensortek type-T Teflon-encased thermocouple microprobe (0.6 mm diameter)
2. Two prehydrolyzed wood chips of 0.4 mm thickness pressed together
3. Folded-over Monel screen

Figure 7.2. The thermocouple microprobe/wood chip assembly.

B. Computer Data Acquisition

Since the particle temperature rise is rapid, particle temperature vs. time data was captured and stored by computer. The computer data acquisition system is schematically illustrated in Figure 7.3.

An IBM-9000 benchtop computer, equipped with sensor board and "CAPS" software (Chromatography Applications Package, IBM Instrument Corporation) was retro-fitted to accept a linearized thermocouple input. The CAPS software could not reference and linearize a direct thermocouple input voltage. However, the CAPS software could accept a normal 0 to 1000 millivolt input. Therefore, the thermocouple microprobe was connected first to a type-T Omega 660 digital thermometer. The digital thermometer referenced and linearized the thermocouple input to 1 mV/ ^{o}C (0 mV = 0 ^{o}C). The digital thermometer analog output port was then interfaced to one of the four channels on the IBM-9000's sensor board. With these modifications, the CAPS sensor board and software could read in and store the thermocouple reading as a referenced 1 mV/ ^{o}C reading and display this reading in real time to the CRT monitor.

The referenced and linearized 1 mV/ ^{o}C readings for 5 consecutive particle temperature vs. time measurements of 8 minutes duration were collected contiguously into one CAPS raw data file over period of 60 minutes. The data acquisition rate was set at 1 point/sec, which in the CAPS software setup menu corresponded to PW=100. At this data acquistion rate, 3600 millivolt readings in 60 minutes were collected sequentially into a single CAPS "raw" data file. During

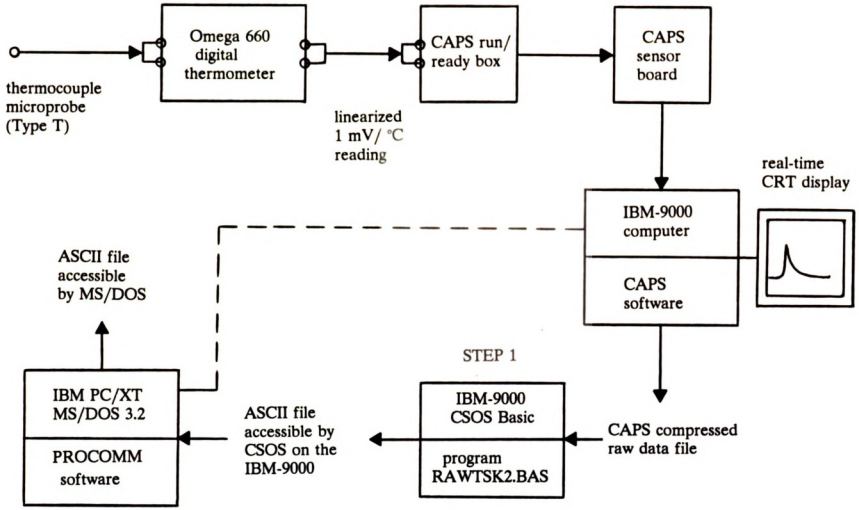


Figure 7.3. Retrofitted computer data acquisition system for particle temperature measurement.

the 60 minute data acquisition period, the initial and final time of each individual particle temperature vs. time measurement were recorded so that the portion of the data file corresponding to that particle temperature vs. time measurement could be retrieved from the contiguous data file. For example, if given particle temperature vs. time measurement is started at a data acquisition time of 10 min and ended at 18 min, then the reaction time can be rescaled to read 0 to 8 min.

C. Post-Run Processing of Data

Once the thermocouple readings were captured and stored on the IBM-9000 via the CAPS sensor board and software, three steps were required to convert the contiguous millivolt data file back to individual particle temperature vs. reaction time data files. These three steps are summarized in Figures 7.3 and 7.4.

Step 1. The CAPS raw data file was converted to an ASCII file and then downloaded to an MS/DOS environment. The CAPS software stored the contiguous stream of millivolt (1 mV/ ^{o}C) readings into a compressed raw data file on the CSOS/IBM-9000 operating system. Within CSOS Basic on the IBM-9000, the CAPS raw data file was converted to a ASCII data file by program RAWTSK2.BAS, listed in Appendix D. Unfortunately, this ASCII file was still loaded on the storage disk of the IBM-9000 benchtop computer and could only be accessed by the CSOS operating system. Therefore, this ASCII file in the CSOS operating system was downloaded from the IBM-9000 benchtop computer to an IBM PC/XT personal computer (MS/DOS operating system) via PROCOMM, a communications protocol software package for IBM compatible PC's. The ASCII

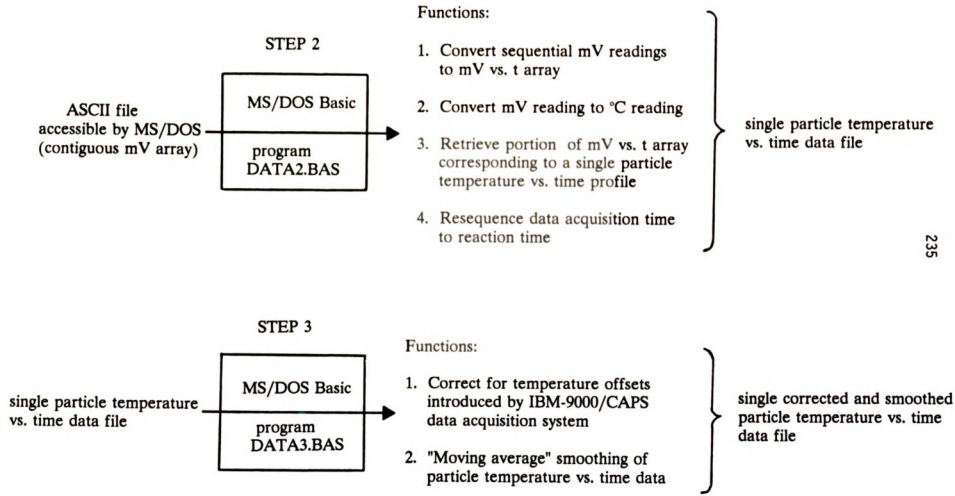


Figure 7.4. Processing of the raw particle temperature vs. time data file.

file was now stored on the hard disk of the PC/XT and could be easily accessed by the MS/DOS operating system.

Step 2. The ASCII file containing the sequential millivolt (1 mV/ ^{o}C) readings was processed to recover the individual particle temperature vs. time measurements. This task was carried out by computer program DATA2.BAS, listed in Appendix D.

The program DATA2.BAS performed three functions. First, the program converted the sequential millivolt readings to a millivolt vs. time array (mV_i,t_i). Second, given the initial and final times for a single particle temperature vs. time measurement within the 60 minute data acquisition period, the program retrieved the portion of (mV_i, t_i) array corresponding to that particle temperature vs. time measurement. Third, the program rescaled the millivolt reading to a ^{o}C reading, and resequenced the data acquistion time to a reaction time. For example, if the initial and final times for a given particle temperature vs. time measurement were at data acquisition times of 10 min and 18 min respectively, then the time array was resequenced to read 0 to 8 min. This resequenced particle temperature vs. reaction time array was then stored into an individual ASCII data file.

Step 3. Each particle temperature vs. reaction time data file was corrected and smoothed. The computer data acquisition system introduced two offsets to the temperature (millivolt) reading. First, the CAPS software and CAPS raw data file conversion program RAWTSK2.BAS introduced a linear offset to the millivolt input readings. This offset was quantified by interfacing a DC millivolt

output/Wheatstone bridge directly to one of the channels of the CAPS sensor board. The "true" input voltage set by the wheatstone bridge was then compared to the input voltage recorded by the CAPS software and CAPS raw data file conversion program RAWTSK2.BAS. In Figure 7.5, the difference between "true" millivolt reading and the millivolt reading ultimately recorded by the IBM-9000/CAPS data acquisition system is shown as a function of the "true" millivolt input reading. Second, the analog millivolt output from the digital thermometer (1 mV/ ^{o}C) only had a resolution of 0.5 mV. Therefore, the unsmoothed particle temperature vs. time profile appeared "staircased", as shown in Figure 7.6.

Computer program DATA3.BAS (see listing Appendix D) rescaled and smoothed the particle temperature vs. reaction time profile to correct for the two afore-mentioned computer data acquisition offsets. First, the program rescaled the temperature (millivolt) readings to correct for the linear offset introduced by the CAPS software and CAPS raw data file conversion program RAWTSK2.BAS. Second, the program performed a "moving average" on all temperature readings in order to smooth the "staircased" particle temperature vs. time profile.

In Figure 7.6, an unprocessed particle temperature vs. time profile is compared to its corrected and smoothed particle temperature vs. time profile.

D. HF Vapor Stream Temperature Measurement

The particle temperature vs. time profile is a function of the temperature of the HF vapor stream surrounding the HF-reacting lignocellulose chip. Therefore,

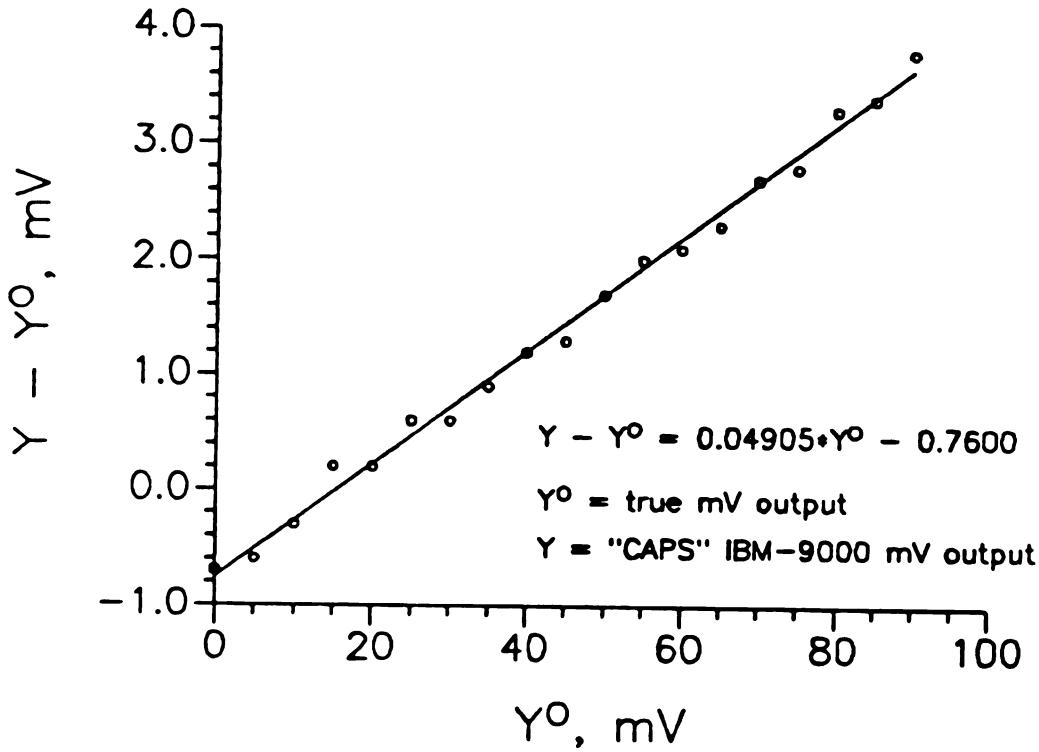


Figure 7.5. Calibration of the computer data acquisition system for linear voltage offset.

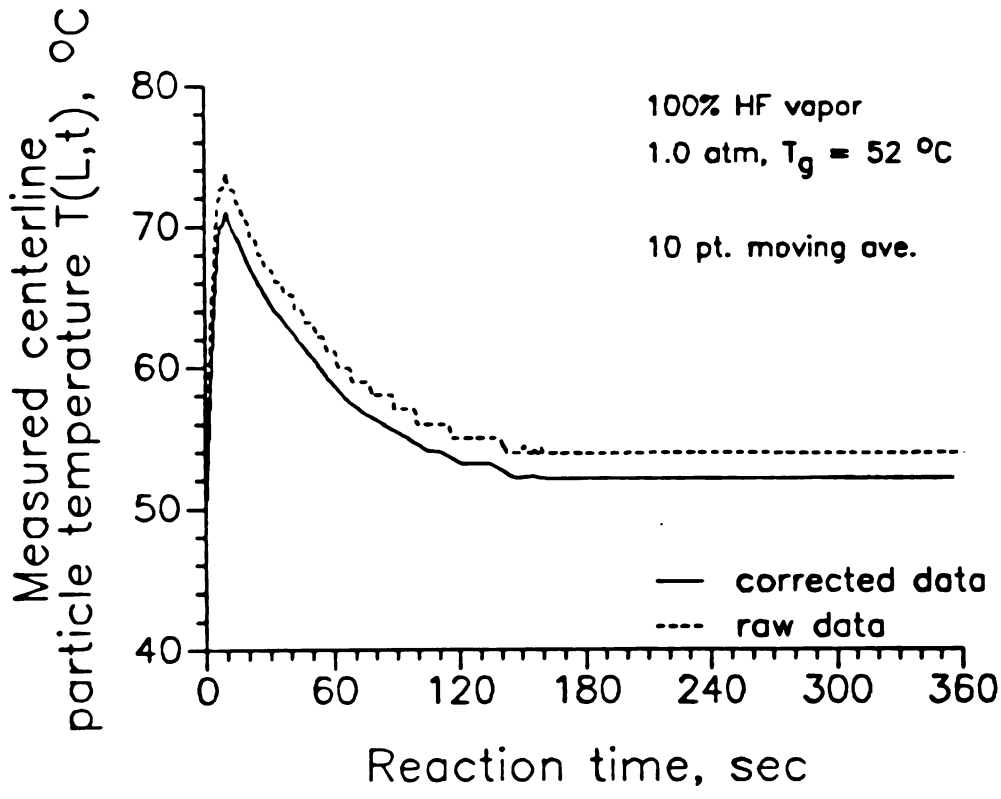


Figure 7.6. Correction and smoothing of the particle temperature vs. reaction time profile.

for each particle temperature vs. time measurement, the HF vapor steam temperature vs. time profile was also captured and stored by computer via the IBM-9000/CAPS data acquisition system described earlier. The HF vapor stream temperature vs. time measurements were processed in the same manner as the particle temperature vs. time measurements.

A sample 100% HF vapor stream temperature vs. time profile is shown in Figure 7.7. Note in Figure 7.7 that the HF vapor stream temperature takes about 15 seconds to reach the setpoint value of 60 °C. When the sample access port is unplugged, the escaping HF vapor mixes with the surrounding air exhaust stream. The endothermic heat of mixing between the HF vapor and the air exhaust stream lowers HF vapor stream temperature near the sample access port. When the sample access port is replugged with the sampling mechanism, a short time is required to flush out this cooler HF vapor.

II. Effect of 100% HF Vapor Stream Temperature on the Particle Temperature vs. Time Profile

In this section, the effect of 100% HF stream temperature on the centerline particle temperature vs. time profile is investigated under conditions where gas-phase external mass-transfer resistances are experimentally minimized. Minimization of external gas-phase mass-transfer resistances for the reaction of a single prehydrolyzed wood chip with a 100% HF vapor stream is described in chapter 6, section III.

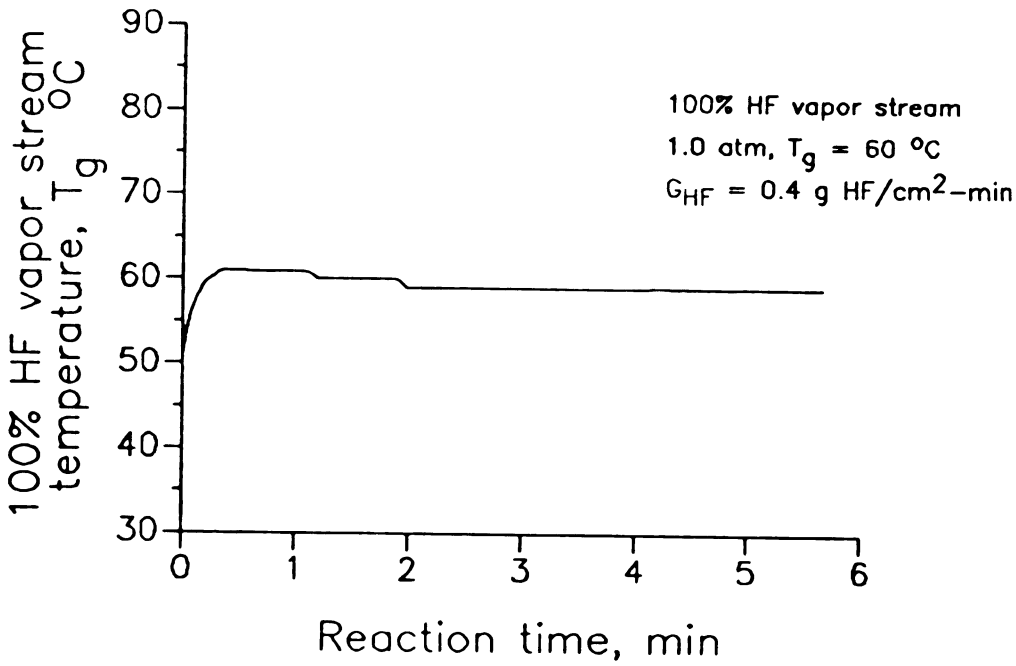


Figure 7.7. 100% HF vapor stream temperature (T_g) vs. reaction time (t).

In all particle temperature measurements, prehydrolyzed wood, or lignocellulose is used. Prehydrolyzed wood is a model lignocellulosic substrate which possesses the native architecture and composite microstructure of wood but contains only two chemical components, crystalline cellulose(75%) and lignin (25%). The reaction of a single pehydrolyzed wood chip with a 100% HF vapor stream is a model system for the HF vapor/wood reaction. Consequently, the 100% HF vapor/prehydrolyzed wood chip system is more accurately modeled. Therefore, particle temperature vs. time data from prehydrolyzed wood are compared to the complimentary model predictions (see chapter 10).

The centerline particle temperature within a HF-reacting, prehydrolyzed wood chip of equivalent half-thickness L = 0.4 mm was measured as a function of reaction time at a fixed 100% HF vapor stream temperature and flowrate. The effect of HF vapor stream temperature on the centerline particle temperature vs. time profile is shown in Figure 7.8. The particle temperature measurements were acquired under a 100% HF vapor flowrate of 0.42 g HF/cm^2-min, which was sufficient to minimize external mass-transfer resistances. As detailed in section I of this chapter, the "centerline" particle temperature was actually measured by molding two prehydrolyzed wood chips, each of 0.4 mm thickness, around a Teflon-encased thermocouple microprobe. The particle temperature vs. time measurements at all HF vapor stream temperatures were generally repeatable to within 0.5 °C to 1.0 °C.

Figur

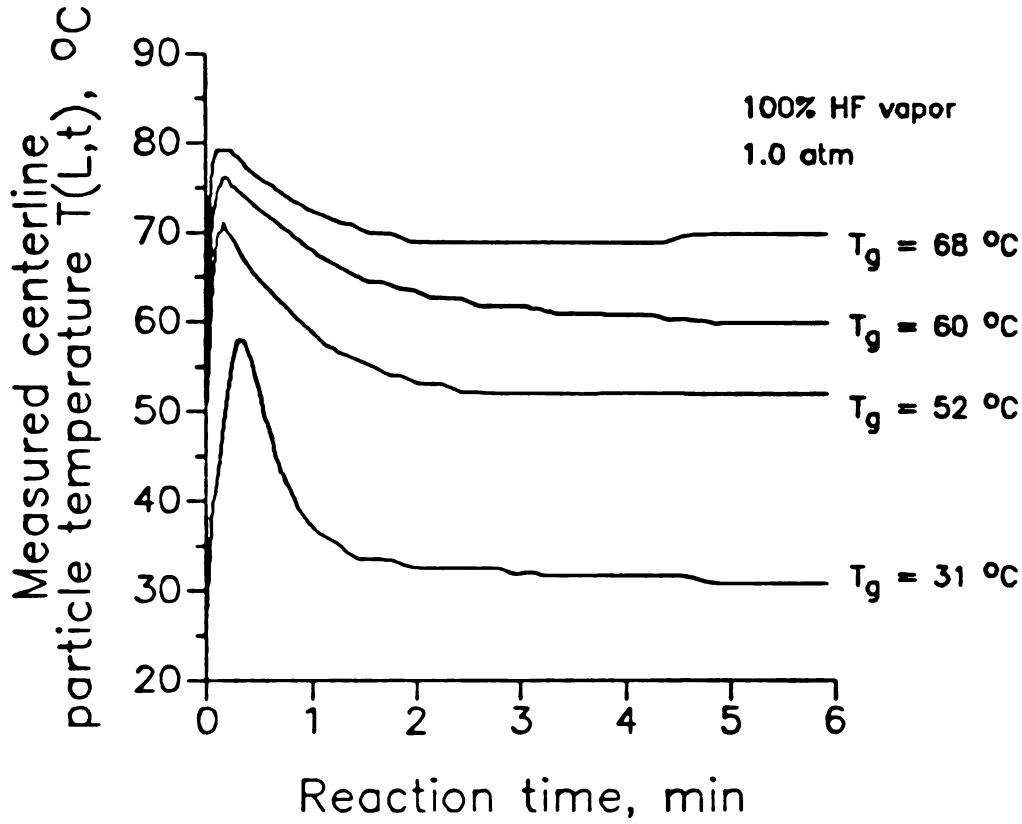


Figure 7.8. Vapor-phase HF solvolysis of a single prehydrolyzed wood chip (L = 0.4 mm): effect of 100% HF vapor stream temperature (T_g) on the centerline particle temperature vs. reaction time profile. Note: G_{HF} = 0.42 g HF/cm^2-min.

In general, the centerline particle temperature vs. time profile increased rapidly to a maximum temperature and then slowly decayed back to the HF vapor stream temperature. The transient particle temperature rise was largely dissipated before significant glucose yield was generated. For example, at T_g = 52 °C the particle temperature increased to a maximum of 71 °C within 15 seconds and then decayed to within 3 °C of the HF vapor stream temperature after about 2 min. However, at a 2 min reaction time, the glucose yield was only about 0.176 g glucose/g prehydrolyzed wood, or about 21% of theoretical. Therefore, the rate of heat generation by the processes of HF adsorption and and HF-solvation of crystalline cellulose was more rapid than the rate of heat generated by the solvolytic cleavage of HF-solvated cellulose chains to glucosyl fluoride.

Since the transient particle temperature rise is significant, heat transfer resistances are as well significant. Further, it is interesting to note that even when gas-phase mass-transfer resistances are minimized, heat transfer resistances are still significant. I believe that this behavior is due to the low thermal conductivity and high porosity of the lignocellulosic matrix.

In general, when the HF vapor stream temperature is increased, the particle temperature vs. time profile is not affected significantly. The only noticeable trend is that as the HF vapor stream temperature is increased, the maximum particle temperature rise (relative to the 100% HF vapor stream temperature) slightly decreases.

The particle temperature vs. time measurements were subject to experimental errors. The possible sources of experimental error are qualitatively overviewed here. First, since two prehydrolyzed wood chips were molded around the thermocouple microprobe, a "contact resistance" probably existed between the wood chip/microprobe interface and wood chip/wood chip interface. This contact resistance would tend to lower the particle temperature measurements. Second, in the first 15 seconds of the particle temperature vs. time measurement, the HF vapor stream temperature was not yet up to the setpoint temperature, as discussed in section II of this chapter. This behavior would also tend to lower the particle temperature measurements, because the temperature gradient for convective heat transfer from the hot particle surface to the cooler surrounding HF vapor stream is increased if the HF vapor stream temperature is initially below the setpoint temperature. Third, the prehydrolyzed wood chips were not preheated to the HF vapor stream temperature, although for model calculations given in chapter 10, it is assumed that the particle temperature is initially at the HF vapor stream temperature. Finally, the accuracy of the Sensortek IT-18 thermocouple microprobe was +/- 0.5 ^{o}C.

III. Effect of 100% HF Vapor Flowrate on the Particle Temperature vs. Time Profile

In this section, the effect of 100% HF vapor flowrate on the centerline particle temperature vs. time profile is briefly explored.

The centerline particle temperature within a HF-reacting, prehydrolyzed wood

chip of equivalent half-thickness L = 0.4 mm was measured as a function of reaction time at a fixed 100% HF vapor stream temperature and flowrate. The effect of 100% HF vapor flowrate on the particle temperature vs. time profile at a fixed HF vapor stream temperature of 31 °C is shown in Figure 7.9. In Figure 7.9, at an HF vapor stream flowrate of 0.1 g HF/cm^2-min and temperature of 31 °C, both external heat and gas-phase mass-transfer resistances are distorting the particle temperature vs. time profile (compare with Figure 6.12). At these conditions, the particle temperature vs. time profile has two maxima. I do not have a clear explanation for this behavior. However, at a 100% HF vapor temperature of 31°C, pore-condensation of HF vapor occurs and subsequently complicates mass and heat transfer within the system. Since a detailed analysis of coupled gas-phase mass and heat transfer resistances was beyond the scope of this dissertation, I will not attempt any further analysis here.

Recommended Future Studies

The particle temperature measurements were originally intended as control experiments to determine if the HF-reacting lignocellulose particle was isothermal under conditions where the glucose yield vs. time data were obtained. Since I originally did not gauge the significance of the particle temperature measurements, I merely retro-fitted my present vapor-phase HF solvolysis apparatus. The results of the experiments showed that the HF-reacting lignocellulose particle was nonisothermal under conditions where gas-phase mass-transfer resistances to the glucose yield vs. time profile were minimized. Therefore, the particle temperature

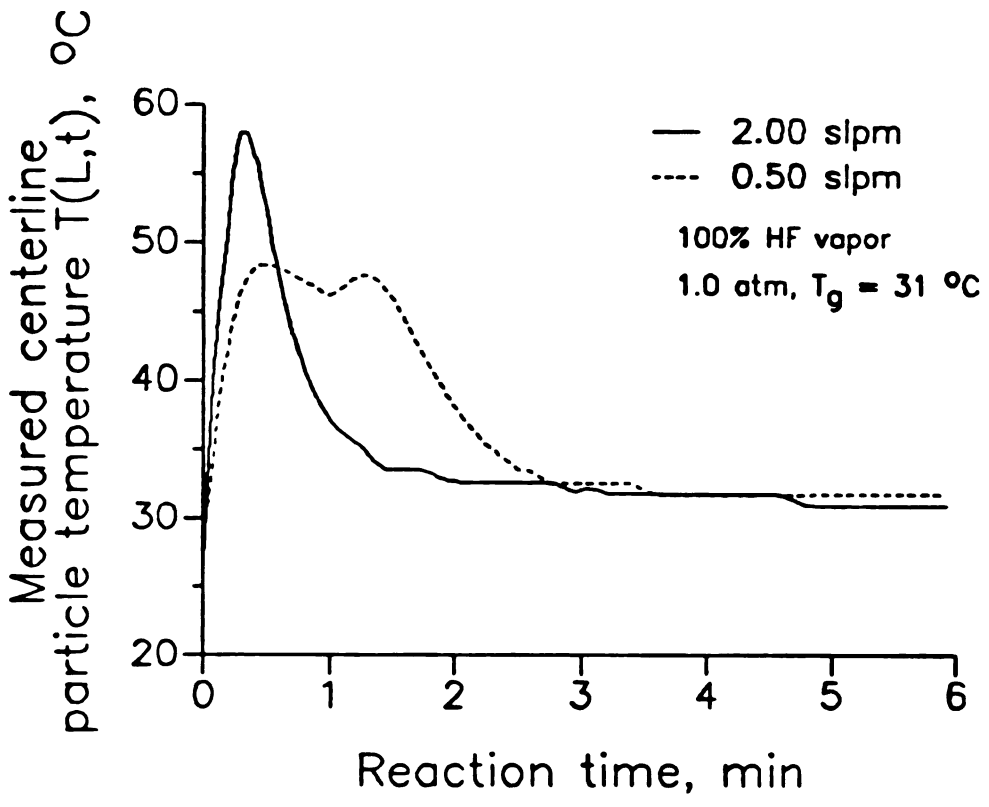


Figure 7.9. Vapor-phase HF solvolysis of a single prehydrolyzed wood chip (L = 0.4 mm): effect of 100% HF vapor stream flowrate on the centerline particle temperature vs. time profile at T_g = 31 °C. Note: $G_{HF} = F_{MFC}$ x 0.21 g HF/cm^2-min/[1.00 slpm] reading.

vs. time measurements proved to be more important, at least from a theoretical standpoint, than I had originally anticipated.

The particle temperature measurements presented in this dissertation are only preliminary in scope. In future studies, I recommend a detailed analysis of heat transfer resistances and heat release from a single HF-reacting lignocellulose chip under carefully-controlled HF vapor conditions. This analysis would require 1) an improved reaction apparatus, implant microprobe, and procedure to measure both the interior and surface temperature of a single HF-reacting lignocellulose chip, 2) direct measurement of the heat transfer coefficient for 100% HF vapor flowing over a single wafer, and 3) direct calorimetric measurement of the heat release from a single HF-reacting lignocellulose chip.

Chapter 8. Model Development I: Material Balance and Kinetic Model

Introduction

The solvolysis of a single lignocellulose chip by anhydrous Hydrogen Fluoride (HF) vapor is an unsteady-state, noncatalytic, gas-solid reaction that generates solid glucosyl fluoride reaction products (see Figure 3.3). In this chapter, I will develop an unsteady-state material balance and intrinsic kinetic model for the solvolysis of a single, prehydrolyzed wood (lignocellulose) chip by a 100% anhydrous HF vapor stream. This model will predict glucosyl fluoride yield within a single HF-reacting lignocellulose chip as a function of reaction time, particle temperature, HF vapor conditions, and HF loading.

The intrinsic form of this model assumes that gas-phase external (film) and internal (intraparticle) mass transfer resistances are minimized. This assumption implies that the HF vapor concentration gradients near and within the HF-reacting lignocellulose chip are negligible, so that the HF vapor concentration near and within the HF-reacting lignocellulose chip is equal to the bulk HF vapor stream concentration.

The differential material balance and kinetic model is valid for prehydrolyzed (hemicellulose-free) wood. Prehydrolyzed wood, or lignocellulose, is a model lignocellulosic substrate which possesses the native architecture and composite microstructure of wood but contains only two chemical components, crystalline cellulose (75%) and lignin (25%).

This chapter is organized into five major sections, labeled I to V. In section I, the structure of the lignocellulosic matrix is described. In section II, the effect of vapor-phase HF solvolysis on the structure of the lignocellulosic matrix is shown via light microscopy of HF-reacted wood chip cross-sections. In section III, an intrinsic adsorption/reaction scheme for the solvolysis of crystalline cellulose to glucosyl fluoride by anhydrous HF vapor is proposed. In section IV, a differential material balance and kinetic model is formulated from the intrinsic adsorption/reaction scheme. Finally, in section V, the kinetic parameters posed by the differential material balance and kinetic model are estimated. Development of the differential energy balance and heat transport model is reserved for chapters 9 and 10.

I. The Lignocellulosic Matrix

The modeling begins with a description of the structure of the lignocellulosic matrix of prehydrolyzed (hemicellulose-free) wood. The lignocellulosic matrix of prehydrolyzed wood is an anistropic, highly porous composite of the biopolymers cellulose (75%) and lignin (25%). The single lignocellulose chip (in contact with HF vapor) and lignocellulosic matrix cross-section are schematically illustrated in Figures 8.1a and 8.1b respectively. The detailed composition and physical properties of wood and prehydrolyzed wood are given in chapter 4.

The gross architecture of the lignocellulosic matrix is defined by vascular tubules bundled together in parallel array. The vascular macropores range from

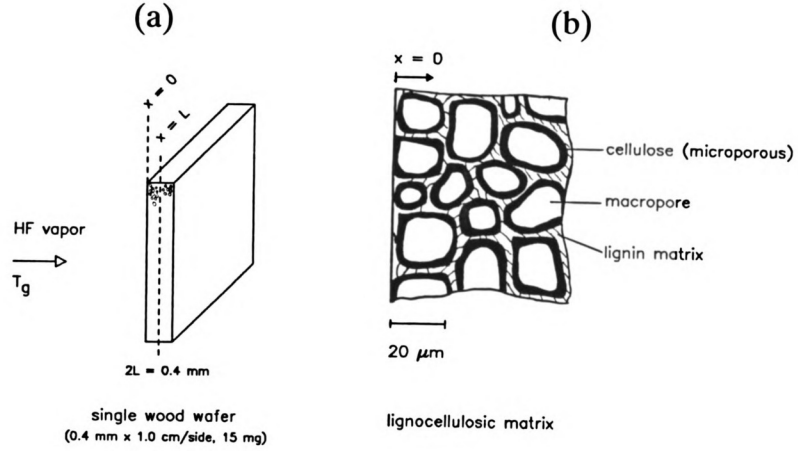


Figure 8.1. Schematics of: (a) a single wood wafer aligned perpendicular to the HF vapor stream; (b) the lignocellulosic matrix cross-section.

5 to 30 μm in diameter. The tubule wall, or secondary cell wall, is a composite of cellulose fibers and lignin (Figure 8.2). All of the cellulose is contained within the secondary cell wall. Lignin, a complex, three-dimensional, hydrophobic polymer based on the phenylpropane unit (see Figure 6.17) serves as the matrix that binds the cellulose fibers together within the secondary cell wall. The middle lamella is a lignin framework that binds the secondary cell walls together in parallel array. The middle lamella typically contains about 30% of the total lignin in the lignocellulosic matrix; the remaining 70% is contained in the secondary cell wall (Young, 1986). Hemicellulose (Figure 4.3), is hydrogen-bonded to the outer surface of the cellulose microfibril (see "polyoses", Figure 8.3a). The secondary cell wall architectural detail and composite microstructure of wood are schematically illustrated in Figures 8.2 and 8.3 respectively. For prehydrolyzed wood, the hemicellulose fraction is selectively stripped from the lignocellulosic matrix. Details on the architecture, composite microstructure, and composition of the lignocellulosic matrix of wood are provided by Cote (1977), Thomas (1983), Parham and Gray (1984), Pettersen (1984b), and Young (1986).

As discussed earlier in chapter 5 (section III), the secondary cell wall of prehydrolyzed wood is microporous. Typically, for "prehydrolyzed mixed hardwood", the total micropore volume is about 0.7 mL microvoid/g lignocellulose, and the micropores range from 0 to 11 nm in diameter, with a mean diameter of about 2 nm (Grethlein, 1985). The micropores (microvoids) arise from imperfections in the lateral packing of the microstructural elements (Young, 1986). Global porosity

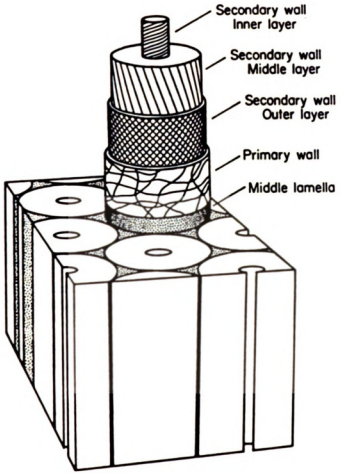


Figure 8.2. Exploded view of the secondary cell wall of the lignocellulosic matrix of wood. Reference: Young (1986).

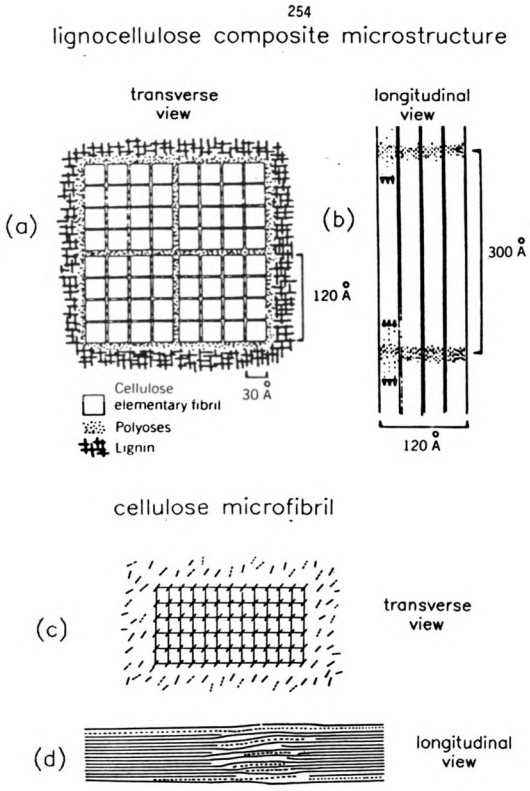


Figure 8.3. Lignocelluose composite microstructure. References: (a-b) Fengel and Wegener, (1984); (c-d) Young (1986).

(micropores + macropores) is about 3 mL/g. The bulk density of prehydrolyzed wood is about 0.3 g/cm^3. The volumetric properties of dry, prehydrolyzed wood are summarized in chapter 4, Table 4.6.

The secondary cell wall of prehydrolyzed wood is primarily cellulose, a hydrophilic, linear polymer of anhydroglucose (glucan) units joined by β-1,4-O-glycosidic linkages (see Figure 4.3). The linear cellulose chains are hydrogen-bonded in periodic and parallel array to form the paracrystalline cellulose microfibril, the basic structural unit of the secondary cell wall. The inter- and intra-molecular OH...OH hydrogen bonding network within the cellulose microfibril is schematically illustrated in Figure 8.4. Figure 8.4 does not show the hydrogen bond between hemiacetal oxygen O5 and hydroxyl group O3. The detailed conformation and structure of the hydrogen-bonding lattice within the cellulose microfibril are discussed by Blackwell (1980).

II. Micrographs of the HF-Reacted Lignocellulosic Matrix

In the attempt to shed some light on how adsorbed HF attacks the lignocellulosic matrix, cross-sections of the HF-reacted lignocellulosic matrix of wood at various extents of cellulose conversion were observed directly by light microscopy.

Sample micrographs of the cross-section of native and HF-reacted Bigtooth Aspen wood chips are given in Figures 8.5a to 8.5d. In micrographs (a) to (d), the water-soluble reaction products were washed out of the sample prior to

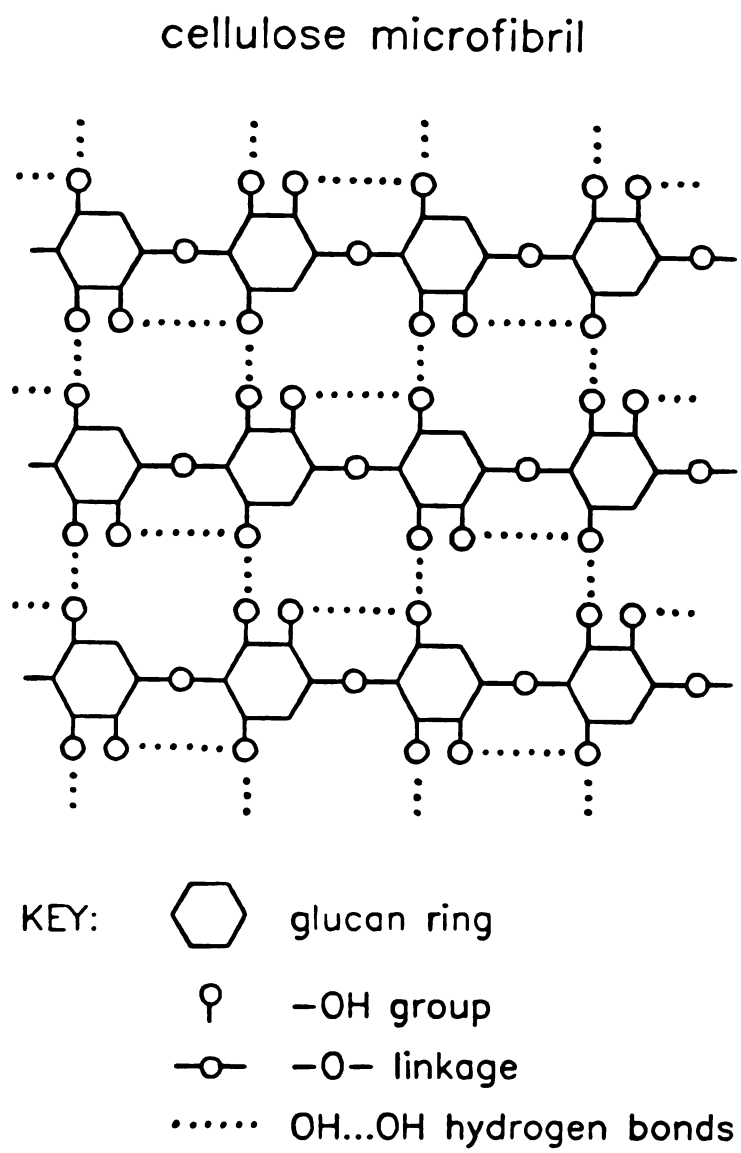


Figure 8.4. Two-dimensional schematic of the hydrogen-bonding network within the crystalline cellulose microfibril.

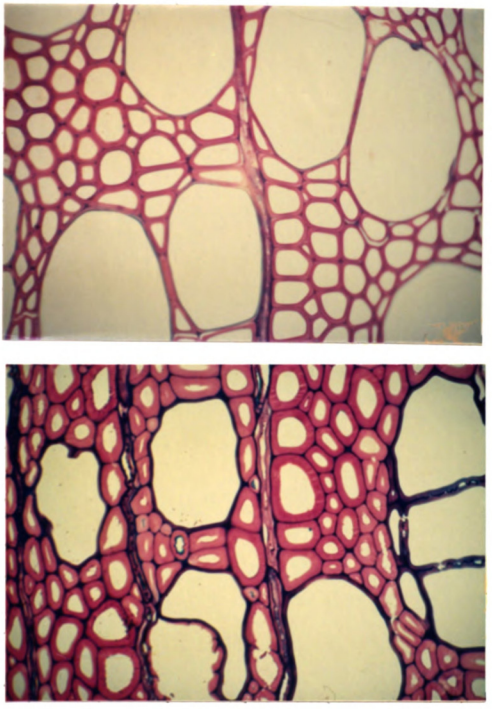


Figure 8.5. Light microphotographs (200 x) of the lignocellulosic matrix cross-section before and after reaction with HF vapor. HF-reacted wood chips were soaked in water prior to specimen preparation in order to remove water-soluble sugar products. Reaction conditions: 100% HF vapor at T_g = 50 °C (see Figure 6.5a). Reaction times: (a) 0 sec, unreacted wood; (b) 90 sec.

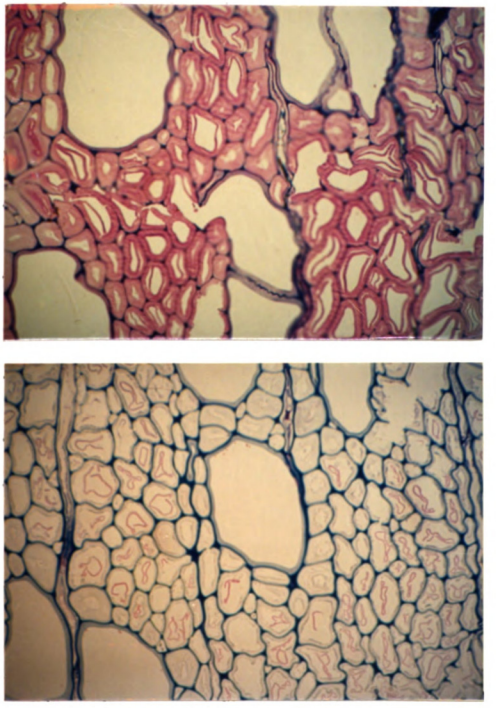


Figure 8.5 (cont'd.). (c) 120 sec; (d) 180 sec.

specimen preparation. Specimen preparation for light microscopy is detailed in chapter 4.

The micrographs in Figures 8.5a to 8.5d reveal that the secondary cell wall "swells" over the course of the reaction, indicating that adsorbed HF "solvates" the crystalline cellulose fibers. Most likely, adsorbed HF displaces OH...OH hydrogen bonds within the cellulose microfibril with stronger HO...HF hydrogen bonds. This "HF-solvation" of the cellulose microfibril disrupts the rigid hydrogen bonding network within the cellulose microfibril and unravels the HF-solvated cellulose chains away from the cellulose microfibril.

III. The Intrinsic Adsorption/Reaction Scheme

In this section, I propose an intrinsic adsorption/reaction scheme for the solvolysis of crystalline cellulose to glucosyl fluoride by anhydrous HF vapor. The intrinsic adsorption/reaction scheme physically models the adsorption of HF vapor onto the lignocellulosic matrix and the solvolytic cleavage of crystalline cellulose to glucosyl fluoride by the adsorbed HF.

A. Background and Cellulose Hydrolysis Chemistry

I begin by summarizing four observations of the gravimetric HF adsorption data and glucose yield vs. time data presented in chapters 5 and 6.

Observation 1. The equilibrium loading of HF on wood (θ_e) decreases with decreasing HF vapor partial pressure (P_{HF}) and increasing temperature (T_g) away from the normal boiling point of HF (19.54 °C) (see Figures 5.1a, 5.1b, and 5.8).

Therefore, HF vapor physically adsorbs onto the lignocellulosic matrix.

Observation 2. The overall glucose production rate (glucose yield vs. time profile) decreases with increasing HF vapor temperature at fixed HF partial pressure (see Figure 6.13). This behavior is the resolution of two opposing processes: 1) the intrinsic rate for cellulose solvolysis (i.e. the rate constant(s), k_i), which increases with increasing temperature by the Law of Arrhenius, and 2) the HF loading (θ_e) on the lignocellulosic matrix that the cellulose perceives for solvolysis (i.e. the HF concentration term), which decreases with increasing temperature, i. e., $T \uparrow \; k_i \uparrow \; \theta_e \downarrow$. Therefore, the thermodynamics of HF physical adsorption and the intrinsic kinetics of cellulose solvolysis work in opposing directions with increasing temperature, and this coupling determines the global dependence of glucose production rate on temperature.

Observation 3. The maximum average glucose yield is dependent on equilibrium HF loading and temperature (see Figures 6.14 and 6.15). For a 100% HF vapor stream at 1.0 atm and temperatures greater than 60 °C, the equilibrium HF loading (θ_e) is not sufficient to insure stoichiometric reaction with cellulose. The minimum HF loading on lignocellulose for complete solvolysis of cellulose corresponds to 4 moles of HF per 1 mole of glucan: 3 HF molecules for hydrogen bonding with each of the three -OH groups on glucan, and 1 HF molecule for formation of glucosyl fluoride by solvolytic cleavage of the ß-1,4-O-glycosidic linkage.

Observation 4. The glucose yield vs. time profile is sigmoidal whereas the gravimetric HF adsorption vs. time profile rapidly approaches the equilibrium HF

loading (compare Figure 6.13 with Figure 5.7). This behavior implies that the adsorption and reaction processes are sequential.

I will now summarize the established mechanisms for the hydronium-ion catalyzed hydrolysis of cellulose and the liquid-phase HF solvolysis of cellulose in order to rationalize a molecular basis for the solvolysis of crystalline cellulose to glucosyl fluoride by anhydrous HF vapor. The mechanism of hydronium ion-catalyzed hydrolysis of cellulose is discussed by Sharples (1957, 1958), Nelson (1960), Harris (1975), and Goldstein (1983). The mechanism of liquid-phase HF solvolysis of cellulose is discussed by Defaye et al. (1983) and Selke (1983).

For hydronium-ion catalyzed hydrolysis of the ß-1,4-O-glycosidic linkages of cellulose, flexure of the glucan ring to the half-chair conformation of the oxonium/carbonium ion intermediate is the rate-limiting step in the mechanism. Flexure of the glucan ring is further hampered by the rigid hydrogen-bonding network within the crystalline cellulose microfibril. Cleavage of the ß-1,4-O-glycosidic linkage is markedly preferred at the non-reducing end of the cellulose chain because the energy barrier for cellulose chain reorientation during flexure of the glucan ring to the half-chair conformation is at a minimum at this position.

For concentrated-acid cellulose hydrolysis, Goldstein (1983) further requires that

> "The rapid complete hydrolysis of cellulose at moderate temperatures depends on prior disruption of the crystalline structure of cellulose by lower energy processes of solution [solvation] or swelling. The glycosidic hydrolysis then proceeds rapidly at temperatures low enough to avoid degradation, making almost quantitative yields of glucose available. Decrystallization and hydrolysis may be accomplished by the use of concentrated acids, including hydrochloric,

> sulfuric, phosphoric, formic, hydrofluoric, and trifluoracetic. Minimum acid concentrations necessary for initiation of decrystallization are critical, because of the formation of various carbohydrate-acid complexes. In addition to acid-carbohyrate complexes some processes involve the formation of intermediate esters or halides which undergo hydrolysis by water to free sugars."

Defaye et al. (1983) proposed a mechanism for the liquid-phase HF solvolysis of cellulose to glucosyl fluoride consistent with the mechanism for hydronium-ion catalyzed hydrolysis of cellulose to glucose. Defaye's reaction mechanism for the HF-solvolysis of cellulose in liquid HF solution is schematically illustrated in Figure 2.1. In Defaye's mechanism, solid cellulose first dissolves in liquid HF. Once in HF solution, HF solvolytically cleaves the cellulose chain to glucosyl fluoride via an oxonium/carbonium ion intermediate.

In the subsequent formulation of the intrinsic adsorption/reaction scheme, I will assume that Defaye's mechanism for the liquid-phase HF-solvolysis of cellulose is correct and can be extended to the vapor-phase HF solvolysis of cellulose.

B. Formulation of the Intrinsic Adsorption/Reaction Scheme

Given Defaye's HF-solvolysis chemistry, Goldstein's discussion of concentrated-acid hydrolysis, micrographs of the HF-reacting lignocellulosic matrix, and the behavior of the reaction rate, glucose yield, and gravimetric HF adsorption data presented in chapters 5 and 6, I propose that the solvolysis of crystalline cellulose to glucosyl fluoride by anhydrous HF vapor proceeds by four sequential steps. The proposed four-step adsorption/reaction scheme is schematically illustrated in Figure 8.6a (steps 1 and 2) and Figure 8.6b (steps 3 and 4). The intrinsic adsorption/reaction scheme is summarized in Figure 8.7. All of the

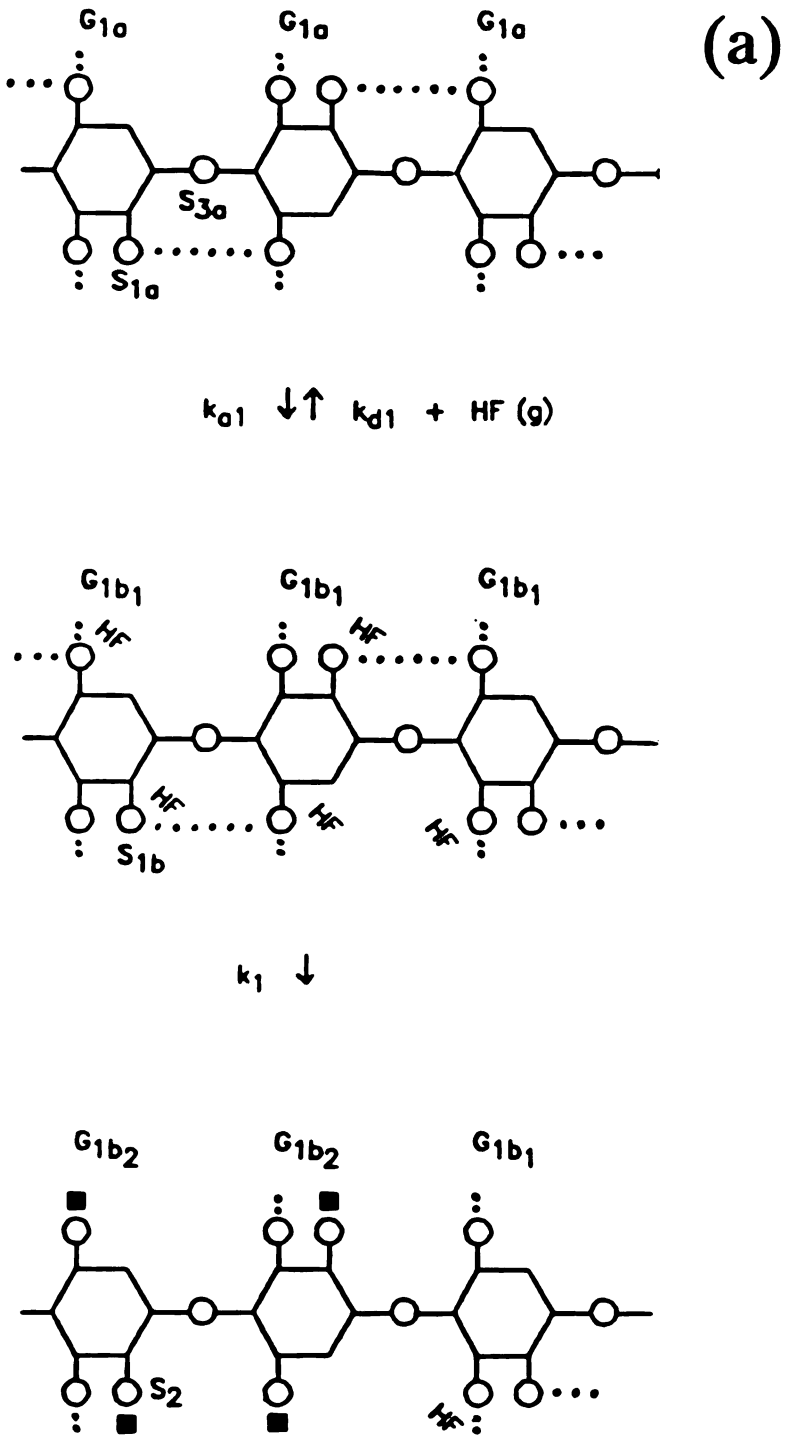


Figure 8.6. Schematic representation of the sequential adsorption and reaction processes presumed to occur during the vapor-phase HF solvolysis of crystalline cellulose. (a) HF-adsorption onto -OH sites and disruption of the hydrogen-bonded cellulose chains; (b) solvolytic cleavage of completely HF-complexed glucan units to glucosyl fluoride.

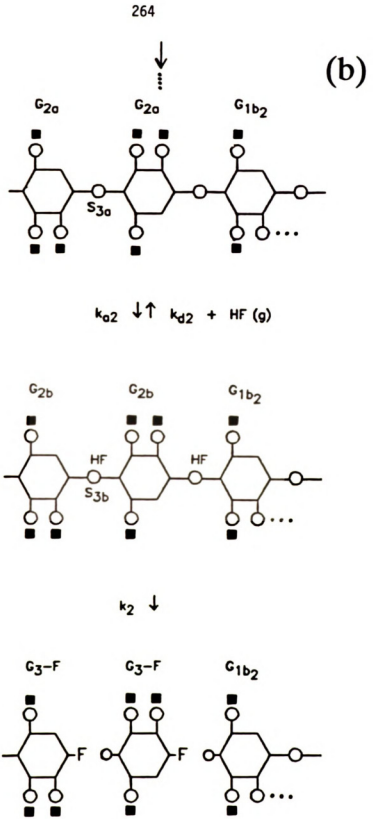


Figure 8.6 (cont'd.).

INTRINSIC ADSORPTION/REACTION SCHEME

Reaction	Process
1. $[S_{1a}] + HF\,(g) \underset{k_{d1}}{\overset{k_{o1}}{\rightleftarrows}} [S_{1b}\cdot HF]$	HF adsorption on OH groups (fast)
2. $[S_{1b}\cdot HF] \xrightarrow{k_1} [S_2\cdot HF]$	HF...HO complex (slow)
$[G_o] = [G_1]+[G_{2a}]+[G_{2b}]+[G_3-F]$	glucan balance
$[G_o] - [G_1] = f[S_2\cdot HF]$	HF–solvation of glucan units
3. $[G_{2a}] + HF\,(g) \underset{k_{d2}}{\overset{k_{o2}}{\rightleftarrows}} [G_{2b}\cdot HF]$	HF adsorption on –O– linkages (fast)
4. $[G_{2b}\cdot HF] \xrightarrow{k_2} [G_3-F]$	cleavage of –O– linkage (slow)

Figure 8.7. Summary of the intrinsic adsorption/reaction scheme proposed for the vapor-phase HF solvolysis of crystalline cellulose.

variables used in the formation of the intrinsic adsorption/reaction scheme are apparent from Figures 8.6a and 8.6b, or are defined in the List of Notation.

Step 1. HF vapor physically and reversibly adsorbs onto hydroxyl (-OH) groups of glucan units constituting cellulose chains bound in the crystalline cellulose microfibril:

$$[S_{1a}] + HF\ (g) \underset{k_{d1}}{\overset{k_{a1}}{\rightleftarrows}} [S_{1b}\cdot HF] \qquad [8\text{-}1]$$

In equation [8-1], $[S_{1a}]$ is the concentration of -OH groups on glucan that are not yet HF-adsorbed, and $[S_{1b}]$ is the concentration of -OH groups on glucan that are tentatively HF adsorbed. If the 100% HF vapor temperature is low enough (e.g. 20 °C to 40 °C at 1.0 atm), then multilayer HF adsorption and pore condensation of HF vapor into the microvoids of the secondary cell wall can also occur (see chapter 5, section III).

Step 2. The adsorbed HF "solvates" the -OH group on a given glucan unit within the hydrogen-bonded cellulose microfibril by displacing OH...OH hydrogen bonds with stronger HO...HF hydrogen bonds:

$$[S_{1b}\ HF] \xrightarrow{k_1} [S_2\cdot HF] \qquad [8\text{-}2]$$

In equation [8-2], $[S_2]$ is the concentration of -OH groups on glucan "complexed" with HF, and k_1 is the rate constant for displacement of the OH...OH hydrogen bond to the HF...HO hydrogen bond. The HO...HF hydrogen bond is stronger

than the OH...OH hydrogen bond (Morrison and Boyd, 1977), so that the HF molecule is tightly but reversibly complexed to the -OH adsorption site.

Eventually, all three -OH groups on a given glucan unit are complexed with HF. A glucan unit with each of its three -OH groups HF-complexed is called a "completely HF-complexed glucan unit". The concentration of completely HF-complexed glucan units is a stochastic function dependent on the total concentration of -OH groups on glucan HF-complexed:

$$[G_{2a}] + [G_{2b}] + [G_{3\text{-}F}] = f([S_2]) \qquad [8\text{-}3]$$

The functional dependence of the total concentration of completely HF-complexed glucan units ($[G_{2a}] + [G_{2b}] + [G_{3\text{-}F}]$) as a function of the total concentration of -OH sites HF-complexed ($[S_2]$) is derived in section IV (simplification 3) of this chapter.

Why is it necessary that all three -OH groups on a given glucan unit complex with HF before solvolytic cleavage of the ß-1,4-O-glycosidic linkage of that glucan unit can occur? When the adsorbed HF complexes with the -OH groups on glucan units constituting the cellulose chains, these "HF-solvated" cellulose chains break away from the rigid hydrogen bonding lattice of the crystalline cellulose microfibril, as shown in Figure 8.8 (compare to Figure 8.4). The completely HF-complexed glucan units within these "free", or HF-solvated cellulose chains are no longer rigidly pinned into the hydrogen bonding network of the paracrystalline cellulose microfibril. Thus, the chair conformation of the glucan ring of a completely HF-complexed glucan unit can now flex to the half-chair conformation

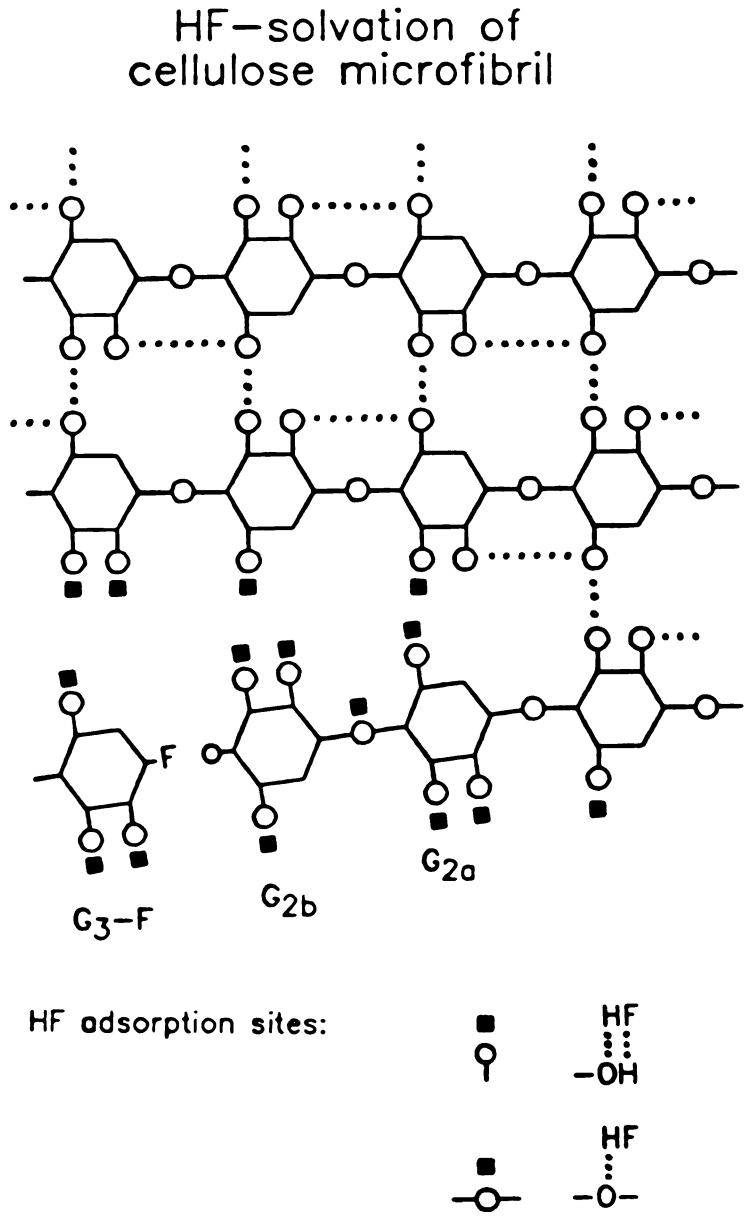


Figure 8.8. Composite illustration of the adsorption and reaction processes proposed to occur during the vapor-phase HF solvolysis of the cellulose microfibril.

of the oxonium/carbonium ion intermediate necessary for solvolytic cleavage of the ß-1,4-O-glycosidic linkage.

Step 3. HF vapor physically adsorbs onto the ß-1,4-O-glycosidic linkage (-O- linkage) joining two completely HF-complexed glucan units:

$$[G_{2a}] + HF\,(g) \underset{k_{d2}}{\overset{k_{a2}}{\rightleftarrows}} [G_{2b}\cdot HF] \qquad [8\text{-}4]$$

In equation [8-4], $[G_{2a}]$ is the concentration of completely HF-complexed glucan units in which the -O- linkage is not HF-adsorbed, and $[G_{2b}]$ is the concentration of completely HF-complexed glucan units in which the -O- linkage is HF-adsorbed.

Step 4. The adsorbed HF solvolytically cleaves the ß-1,4-O-glycosidic linkage at the non-reducing end of the HF-solvated cellulose chain, yielding α-D-glucosyl fluoride, which resides on the HF-reacting lignocellulosic matrix:

$$[G_{2b}\cdot HF] \xrightarrow{k_2} [G_3\text{-}F] \qquad [8\text{-}5]$$

In equation [8-4], $[G_{3\text{-}F}]$ is the concentration of glucosyl fluoride, and k_2 is the rate constant for solvolytic cleavage of the ß-1,4-O-glycosidic linkage of a completely HF-complexed glucan unit.

Although I assume that the solvolytic cleavage of the cellulose chain by adsorbed HF is markedly end-preferred (as is the case with hydronium-ion catalyzed cellulose hydrolysis), it is possible that in the early stages of the reaction, interior

random cleavage of interior ß-1,4-O-glycosidic linkages within the HF-solvated cellulose chain can also occur. In this case, the total number of glucosyl fluoride monomers released is a function of the total number of solvolytically cleaved ß-1,4-O-glycosidic linkages (see program CLEAVE2.BAS in Appendix D).

An attractive but complicated stochastic approach to modeling the kinetics of the chain-length dependent depolymerization of polymer chains is described by Montroll and Shimha (1940), Shimha (1941), Klein (1986), and Klein and McDermott (1986). Klein and McDermott's model (1986) is particularly attractive and in principle could be applied to the HF-solvolysis of the glucan polymer cellulose to the monomer glucosyl fluoride provided the rate constants for solvolytic cleavage of ß-1,4-O-glycosidic linkages at each position within the cellulose chain are known. However, this type of analysis is not attempted here and a single rate constant (k_2) for solvolytic cleavage of completely HF-complexed glucan units to glucosyl fluoride is assumed.

IV. Differential Material Balance and Rate Equations

A. Formulation of Rate Equations and Development of the Differential Material Balance and Kinetic Model

In this section, the rate equations that describe the unsteady-state, differential material balance of glucan and adsorbed HF within the HF-reacting lignocellulosic matrix are formulated from the intrinsic adsorption/reaction scheme developed in section III (see Figures 8.6a, 8.6b, 8.7, and 8.8).

The primary assumption I make in the formulation of the rate equations is that the rates for adsorption processes given by equations [8-1] and [8-4] are in near-equilibrium with respect to the rates for reaction processes given by equations [8-2] and [8-5]. This assumption, common in heterogeneous reaction kinetics, considerably simplifies the formulation of rate equations.

All variables presented in the subsequent development of the differential material balance and kinetic model are apparent from Figures 8.6a and 8.6b, or are defined in the List of Notation.

HF-Adsorption Site Balance. The HF-adsorption site balance on glucan is the sum of the -OH group HF-adsorption sites and the -O- glycosidic linkage HF-adsorption sites. The balance on -OH group HF-adsorption sites on glucan is

$$[S_o] = [S_1] + [S_2] \qquad [8\text{-}6]$$

$$[S_1] = [S_{1a}] + [S_{1b}] \qquad [8\text{-}7]$$

The balance on -O- linkage HF-adsorption sites on glucan is

$$[S_3] = [S_{3a}] + [S_{3b}] \qquad [8\text{-}8]$$

The total balance on glucan HF-adsorption sites is

$$[S_t] = [S_o] + [S_3] \qquad [8\text{-}9]$$

Differential -OH Group HF-adsorption Site Balance. Given equation [8-1], the rate equation for reversible adsorption of HF onto the -OH groups on glucan (see Figures 8.6a and 8.7) is

$$d[S_{1a}]/dt = 0 = -k_{a1}[S_{1a}]P_{HF} + k_{d1}[S_{1b}] \qquad [8\text{-}10]$$

where P_{HF} is the partial pressure of the HF vapor. A simplified form of equation [8-10] is

$$[S_{1a}] = K_1 P_{HF}/[S_{1b}],\ K_1 = k_{a1}/k_{d1} \qquad [8\text{-}11]$$

Given equation [8-2], the rate equation for the subsequent formation of the HO...HF complex is

$$d[S_{1b}]/dt = -k_1[S_{1b}] \qquad [8\text{-}12]$$

Equations [8-10] and [8-12] are now combined into one equation. First, insertion of equation [8-11] into equation [8-6] and solving for $[S_{1b}]$ yields

$$[S_{1b}] = K_1 P_{HF}[S_1]/(1 + K_1 P_{HF}) \qquad [8\text{-}13]$$

Second, the derivative of equation [8-6] with respect to time t is

$$d[S_1]/dt = d[S_{1a}]/dt + d[S_{1b}]/dt \qquad [8\text{-}14]$$

Finally, insertion of equation [8-13] into equation [8-12], and the subsequent insertion into equation [8-14] yields

$$d[S_1]/dt = -k_1\theta_1[S_1] \qquad [8\text{-}15]$$

where

$$\theta_1 = K_1 P_{HF}/(1 + K_1 P_{HF}) \qquad [8\text{-}16]$$

Equation [8-15] describes the overall rate of depletion of available -OH sites on glucan still within the crystalline cellulose microfibril. The variable θ_1 (equation [8-16]) is the potential equilibrium HF concentration on the -OH group HF-adsorption sites.

Differential Glucan Balance. Here, two rate equations are formulated. First, a rate equation is derived for the net rate of generation of completely HF-complexed glucan units, $d[G_2]/dt$. Second, a rate equation is derived for the

production rate of glucosyl fluoride, $d[G_{3\text{-}F}]/dt$.

In order to formulate these two rate equations, a glucan balance in the HF-reacting lignocellulosic matrix is performed. The overall balance on glucan within the HF-reacting cellulose microfibril is

$$[G_o] = [G_1] + [G_2] + [G_{3\text{-}F}] \qquad [8\text{-}17]$$

$$[G_1] = [G_{1a}] + [G_{1b}] \qquad [8\text{-}18]$$

$$[G_2] = [G_{2a}] + [G_{2b}] \qquad [8\text{-}19]$$

Differentiation of equation [8-17] with respect to reaction time t and solving for $d[G_2]/dt$ yields

$$d[G_2]/dt = -d[G_1]/dt - d[G_{3\text{-}F}]/dt \qquad [8\text{-}20]$$

The -OH group HF-adsorption site balance is now coupled to the glucan balance. Specifically, the total concentration of glucan units not yet completely HF-complexed, $[G_1]$, is related to the total concentration of -OH sites not yet HF-complexed, $[S_1]$, via

$$[G_o] - [G_1] = f([S_o] - [S_1]) \qquad [8\text{-}21]$$

Equation [8-21] is obtained by substituting equations [8-6], [8-17], and [8-19] into equation [8-3]. The derivative of equation [8-21] with respect to time t is

$$-d[G_1]/dt = df([S_o] - [S_1])/dt \qquad [8\text{-}22]$$

Substitution of equation [8-22] into equation [8-20] yields

$$d[G_2]/dt = df([S_o] - [S_1])/dt - d[G_{3\text{-}F}]/dt \qquad [8\text{-}23]$$

Upon inspection of equation [8-23], we see that a rate equation for $d[G_{3\text{-}F}]/dt$, the glucosyl fluoride production rate, is needed. The rate equation for $d[G_{3\text{-}F}]/dt$,

in terms of $[G_2]$, is derived here. Given equation [8-4], the rate equation for adsorption of HF onto the ß-1,4-O-glycosidic linkage (-O- linkage) of a completely HF-complexed glucan unit is (see Figures 8.6b and 8.7)

$$d[G_{2a}]/dt = 0 = -k_{a2}[G_{1a}]PHF + k_{d2}[G_{2b}] \quad [8\text{-}24]$$

A simplified form of equation [8-24] is

$$[G_{2a}] = K_2P_{HF}/[G_{2b}], \; K_2 = k_{a2}/k_{d2} \quad [8\text{-}25]$$

Given equation [8-5], the rate equation for the subsequent solvolytic cleavage of this HF-adsorbed -O- linkage is

$$d[G_{3\text{-}F}]/dt = k_2[G_{2b}] \quad [8\text{-}26]$$

Substitution of equation [8-25] into equation [8-19] and solving for $[G_{2b}]$ yields

$$[G_{2b}] = K_2P_{HF}[G_2]/(1 + K_2P_{HF}) \quad [8\text{-}27]$$

Substitution of equation [8-27] into equation [8-26] yields

$$d[G_{3\text{-}F}]/dt = k_2\theta_2[G_2] \quad [8\text{-}28]$$

where $$\theta_2 = K_2P_{HF}/(1 + K_2P_{HF}) \quad [8\text{-}29]$$

Equation [8-28] describes the production rate of glucosyl fluoride, $d[G_{3\text{-}F}]/dt$, as a function of $[G_2]$. The variable θ_2 (equation [8-29]) is the potential equilibrium HF concentration on the -O- linkage HF-adsorption sites.

Finally, insertion of equation [8-28] into equation [8-23] yields an relationship for $d[G_2]/dt$ in terms of $[G_2]$ and $[S_1]$:

$$d[G_2]/dt = df([S_o] - [S_1])/dt - k_2\theta_2[G_2] \quad [8\text{-}30]$$

The rate equations [8-15], [8-22], [8-30], and [8-28] specify the differential material balance on glucan within the HF-reacting lignocellulosic matrix in terms

of $[S_1]$, $[G_1]$, $[G_2]$, and $[G_3\text{-}F]$. These rate equations are summarized here:

$$d[S_1]/dt = -k_1\theta_1[S_1] \quad [8\text{-}15]$$

$$-d[G_1]/dt = df([S_o] - [S_1])/dt \quad [8\text{-}22]$$

$$d[G_2]/dt = df([S_o] - [S_1])/dt - k_2\theta_2[G_2] \quad [8\text{-}30]$$

$$d[G_{3\text{-}F}]/dt = k_2\theta_2[G_2] \quad [8\text{-}28]$$

The initial conditions for this set of rate equations are

$$t = 0: \quad [S_1] = [S_o]$$

$$[G_1] = [G_o]$$

$$[G_2] = 0$$

$$[G_{3\text{-}F}] = 0$$

Normalization of the Differential -OH Group HF-Adsorption Site Balance and the Differential Glucan Balance. The -OH group HF-adsorption site concentrations $[S_1]$, $[S_2]$ and glucan concentrations $[G_1]$, $[G_2]$, and $[G_{3\text{-}F}]$ within the HF-reacting lignocellulosic matrix are normalized by the following definitions:

$$Z_1 = [S_1]/[S_o] \quad [8\text{-}31] \qquad X_1 = [G_1]/[G_o] \quad [8\text{-}33]$$

$$Z_2 = [S_2]/[S_o] \quad [8\text{-}32] \qquad X2 = [G_2]/[G_o] \quad [8\text{-}34]$$

$$X3 = [G_3]/[G_o] \quad [8\text{-}35]$$

Please note that there are 3 -OH groups and 1 -O- linkage per glucan unit. Therefore, $[S_o] = 3\,[G_o]$, and $[S_t] = 4\,[G_o]$. Given definitions [8-31] and [8-32], and equation [8-6], the normalized -OH group HF-adsorption site balance is

$$1 = Z_1 + Z_2 \quad [8\text{-}36]$$

Given definitions [8-33] to [8-35], and equation [8-17], the normalized glucan unit balance is

$$1 = X_1 + X_2 + X_3 \qquad [8\text{-}37]$$

Given definitions [8-31] to [8-35], the normalized rate equations are

$$dZ_1 = -k_1\theta_1 Z_1 \qquad [8\text{-}38]$$

$$dX_1 = -df(1 - Z_1)/dt \qquad [8\text{-}39]$$

$$dX_2 = df(1 - Z_1)/dt - k_2\theta_2 X_2 \qquad [8\text{-}40]$$

$$dX_3 = k_2\theta_2 X_2 \qquad [8\text{-}41]$$

The initial conditions for normalized rate equations [8-38] to [8-41] are

$$t = 0: \quad Z_1 = 1$$

$$X_1 = 1$$

$$X_2 = 0$$

$$X_3 = 0$$

The major assumptions used in the development of rate equations [8-38] to [8-41] are summarized below:

* Defaye's (1983) mechanism for the HF-solvolysis of cellulose is correct
* The intrinsic adsorption/reaction scheme (Figures 8.6a, 8.6b, 8.7) is correct
* The adsorption rates are fast relative to reaction rates
* HF vapor physically adsorbs on -OH groups and -O- linkages of glucan
* All three -OH groups on a given glucan unit must be complexed with HF before solvolytic cleavage of the ß-1,4-O-glycosidic linkage of that glucan unit can occur
* Solvolytic cleavage of completely HF-complexed glucan units is markedly preferred at the nonreducing end of the HF-solvated cellulose chain and is represented by the single rate constant k_2

Equations [8-38] to [8-41] (and associated initial conditions) represent the differential material balance and kinetic model for glucan in the HF-reacting lignocellulosic matrix.

B. The Simplified Differential Material Balance and Kinetic Model

The differential material balance and kinetic model (equations [8-38] to [8-41]) cannot be integrated analytically or numerically, because several terms are not known explicitly. These terms are $df(1 - Z_1)/dt$, θ_1, and θ_2. In order to develop explicit functions for these terms, the differential material balance and kinetic model must be simplified. Additional assumptions and simplications are required so that the model predictions for glucosyl fluoride production can be compared to the glucose yield vs. time data presented in chapter 6.

Specifically, four assumptions/simplifications are incorporated into the differential material balance and kinetic model. This simplifed differential material balance and kinetic model can be integrated explicitly in order to predict the glucosyl fluoride production as a function of reaction time and HF vapor conditions. Futhermore, with the proper assumptions, glucosyl fluoride production can be quantified experimentally as the glucose yield in the water-soluble reaction products after posthydrolysis. Therefore, model predictions from the simplified differential material balance and kinetic model can be compared to glucose yield vs. time data, provided the HF vapor conditions are matched.

Simplification 1. The simplified differential material balance and kinetic model is valid for prehydrolyzed wood. There are four reasons why prehydrolyzed

(hemicellulose-free) wood, or lignocellulose, is an ideal substrate for comparing model predictions to data. First, the substrate is primarily crystalline cellulose (75%) and lignin (25%) and is not complicated by hemicellulose and extractives. Second, although prehydrolyzed wood is simple in composition, it still retains the native architecture and composite microstructure of native wood. Third, the glucosyl fluoride products stick to the intact, porous lignin framework. In contrast, pure cellulose "melts" to a glutinous drop. Finally, the mild-acid prehydrolysis used to selectively remove the hemicellulose from the lignocellulosic matrix "acid sharpens" the amorphous portion (ca. 10%; see Nelson, 1960) of native cellulose in wood to crystalline cellulose.

To summarize, prehydrolyzed wood retains all the structural features of native wood but is simple in composition. Therefore, glucose yield vs time data, gravimetric HF adsorption data, and particle temperature data from the vapor-phase HF solvolysis of prehydrolyzed wood most closely approximates the conditions under which model predictions are valid. Furthermore, this model system most closely approximates the real wood chip/HF vapor reaction system.

Simplification 2. Second, I assume that glucosyl fluoride production in the HF-reacting lignocellulose chip is quantified experimentally as the glucose yield in the water-soluble reaction products after posthydrolysis. Therefore, model predictions for glucosyl fluoride production vs. time compare directly to glucose yield vs. time data at the complimentary HF vapor conditions provided four conditions are met: 1) gas-phase mass-transfer resistances are minimized, 2) glucosyl fluoride is released

only from crystalline cellulose (not from amorphous cellulose or hemicellulose), 3) glucosyl fluoride does not form water-insoluble adducts with lignin, and 4) reversion oligomers are water-soluble and are recovered as glucose after dilute-acid posthydrolysis.

Simplification 3. Third, I assume that the adsorbed HF concentrations θ_1 and θ_2 on glucan unit -OH sites and -O- linkages (see equations [8-16] and [8-29]) can be approximated by the equilibrium HF loading (θ_e) on prehydrolyzed wood. The adsorbed HF concentrations θ_1 and θ_2 cannot be measured directly. However, the equilibrium HF loading θ_e on prehydrolyzed wood approximates the sum of the HF adsorbed on -OH sites and -O- linkages on glucan provided two conditions are satisfied.

Condition one requires that pore-condensation of HF vapor into the microvoids of the secondary cell wall is negligible. This condition is easily satisfied if the 100% HF vapor temperature (at 1.0 atm partial pressure) is above 50 °C.

Condition two requires that HF molecules adsorb selectively on -OH groups and -O- linkages of HF-reacting crystalline cellulose within the lignocellulosic matrix. Recall that prehydrolyzed wood is primarily crystalline cellulose (75%) and lignin (25%). The adsorption of HF on lignin is assumed negligible because 1) lignin is the minor component, with relatively few HF adsorption sites (see Table 5.1; 2) lignin is hydrophobic (Skaar, 1984); and 3) HF does not fluorinate lignin (Hardt and Lamport, 1982b). Therefore, HF molecules primarily adsorb on the -OH groups and -O- linkages of crystalline cellulose in prehydrolyzed wood, provided

pore-condensation is negligible.

If the adsorption site energies for θ_1 and θ_2 are approximately equal, then θ_1 and θ_2 in equations [8-38] to [8-41] can be approximated by θ_e on prehydrolyzed wood, provided the two afore-mentioned conditions are satisfied. Recall that the equilibrium HF loading on prehydrolyzed wood (θ_e) is estimated as a function of temperature (T) by equation [5-6], provided 100% HF vapor at 1.0 atm exists over the HF-reacting prehydrolyzed wood wafer. With this simplification (simplification 2), the rate equations [8-38] to [8-41] reduce to

$$dZ_1 = -k_1\theta_e Z_1 \qquad [8\text{-}42]$$

$$dX_1 = -df(1 - Z_1)/dt \qquad [8\text{-}43]$$

$$dX_2 = df(1 - Z_1)/dt - k_2\theta_e X_2 \qquad [8\text{-}44]$$

$$dX_3 = k_2\theta_e X_2 \qquad [8\text{-}45]$$

The equilibrium HF loading (θ_e) is normally evaluated at P_{HF} and T_g after the reaction is complete. However, θ_e in equations [8-38] to [8-41] can be thought of as an "adsorbed HF concentration potential" that is allowed to "float" with particle temperature (T) during the reaction. In other words, θ_e in equations [8-41] to [8-45] approximates the sum of the specific adsorbed HF concentration potentials θ_1 and θ_2, and is not to be confused with the equilibrium HF loading $\theta_e(P_{HF},T_g)$, or the gravimetric HF uptake, $\theta_{HF}(t)$ (see equation [8-50]).

The rate constants k_1 and k_2 must have units consistent with θ_e. For example, if θ_e is in units of g HF/g-wood, then k_1 will have units of g-wood/(g-HF sec). Estimation of the kinetic parameters posed by the differential material balance and

kinetic model is described in section IV of this chapter.

Simplification 4. Fourth, I assume that the fraction of completely HF-complexed glucan units $(1 - X_1)$ is a stochastic function of the fraction of HF-complexed -OH groups on glucan $(1 - Z_1)$. Recall that all three -OH groups on a given glucan unit within the cellulose microfibril must be complexed with HF before the β-1,4-O-glycosidic linkage of that glucan unit can be solvolytically cleaved. I propose that the liberation of completely HF-complexed glucan units is a perfectly random, stochastic process dependent on the number of HO...HF complexes. Therefore, the function (compare to equation [8-21])

$$(1 - X_1) = f(1 - Z_1) \qquad [8\text{-}46]$$

is approximated as a stochastic function. Once equation [8-46] is known explicitly, then $df(1-Z_1)/dt$ in equation [8-44] is known explicitly as well (see equation [8-49]).

The computer program CLEAVE1.BAS (see listing in Appendix D) stochastically calculates $(1 - X_1)$ as a function of $(1 - Z_1)$. Specifically, the program uses a random number generator $B_{i,j}$ (i = 1 to N glucan units, each with j = 1 to 3 -OH sites) to stochastically simulate the complexation of HF molecules with open -OH sites.

The algorithm of computer program CLEAVE1.BAS is overviewed here. Initially, all $B_{i,j}$ are set equal to zero. To start, a pair of (i,j) are randomly selected. If $B_{i,j} = 0$ (open -OH site), then $B_{i,j}$ is set equal to 1 (HF-complexed -OH site). The number of HF-complexed -OH sites is then incremented by one, and a new pair of (i,j) are randomly selected. If $B_{i,j} = 1$, then the -OH site at

position (i,j) is HF-complexed and a new pair of (i,j) are randomly reselected until $B_{i,j} = 0$. If $B_{i,1} = 1$, $B_{i,2} = 1$, and $B_{i,3} = 1$, then the glucan unit at position "i" on the glucan chain is completely HF-complexed. The number of completely HF-complexed glucan units is then incremented by one, and a new pair of (i,j) are selected. The procedure is repeated until all open -OH sites are HF-complexed.

The results of the stochastic simulation are shown in Figure 8.9. In Figure 8.9, $(1 - X_1)$ is the fraction of glucan units completely HF-complexed, and $(1 - Z_1)$ is the fraction of -OH sites on glucan HF-complexed. The values of $(1 - X_1)$ vs. $(1 - Z_1)$ given in Figure 8.9 were calculated for a cellulose chain of N = 1000 glucan units, averaged over five stochastic simulations, and then smoothed with the least-squares cubic polynomial

$$f(1 - Z_1) = b_o + b_1(1 - Z_1) + b_2(1 - Z_1)^2 + b_3(1 - Z_1)^3 \qquad [8\text{-}47]$$

where b_o, b_1, b_2, and b_3 are fitted constants (see Table 10.3 for numerical values of fitted constants b_o to b_3). Equation [8-47] is valid from $Z_1 = 0$ to $Z_1 = 1$.

Differentiation of equation [8-47] with respect to time yields

$$df(1 - Z_1)/dt = -dZ_1/dt\,[b_1 + 2b_2(1 - Z_1) + 3b_3(1 - Z_1)^2] \qquad [8\text{-}48]$$

Substitution of equation [8-42] into [8-48] yields an explicit relationship for $df(1-Z_1)/dt$ in terms of Z_1:

$$df(1 - Z_1)/dt = k_1\theta_e Z_1\,[b_1 + 2b_2(1 - Z_1) + 3b_3(1 - Z_1)^2] \qquad [8\text{-}49]$$

Equation [8-49] is then inserted into equation [8-44].

Equations [8-42] to [8-45], equation [8-49], and associated initial conditions constitute the simplified differential material balance and kinetic model. Integration

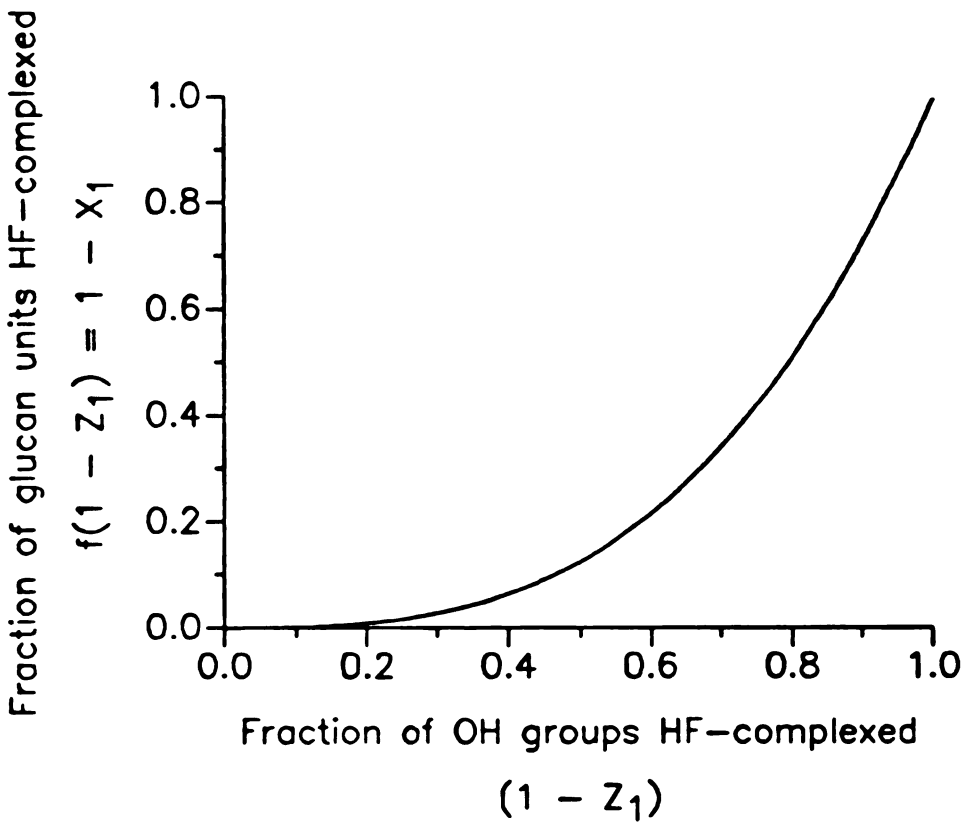


Figure 8.9. Fraction of glucan units completely HF-complexed, $(1 - Z_1)$, as a function of the total fraction of -OH groups on glucan HF-complexed, $f(1 - Z_1)$.

of this coupled set of first-order, nonlinear, differential equations with respect to time t predicts the normalized glucosyl fluoride production X_3 as a function of 1) reaction time t, 2) reaction temperature T (via k_1 and k_2), and 3) adsorbed HF concentration θ_e, which is in turn a function of reaction temperature (T) and HF vapor partial pressure (P_{HF}). Recall that glucosyl flouride production in the HF-reacting lignocellulose chip is quantified experimentally as the glucose yield in the water-soluble products after posthydrolysis.

Integration of the differential material balance and kinetic model equations [8-42] to [8-45], equation [8-49]) also predicts a sigmodial profile of the glucosyl fluoride production vs. time curve. Recall from chapter 6 that the profile of glucose yield vs. time data is also sigmoidal. The sigmoidal profile is a result of the sequential processes of 1) physical adsorption of HF vapor onto the lignocellulosic matrix, 2) HF-solvation of cellulose chains by adsorbed HF, and 3) solvolytic cleavage of HF-solvated cellulose chains to glucosyl fluoride.

The differential material balance and kinetic model also predicts the effect of temperature on the glucosyl fluoride production rate (glucose yield vs. time curve) by coupling the opposing dependencies of intrinsic rate constants k_1, k_2, and HF loading θ_e with temperature (i.e. T $\uparrow$, k_i $\uparrow$, θ_e $\downarrow$).

Gravimetric HF Adsorption vs. Reaction Time Profile. The total gravimetric adsorption vs. time profile is estimated by assuming that the gravimetric uptake of HF vapor onto the lignocellulosic matrix is the sum of two processes: 1) complexation of HF with -OH groups on glucan units (3 HF molecules per glucan

unit) by displacement of OH....OH hydrogen bonds with stronger HF...OH hydrogen bonds, and 2) consumption of HF to glucosyl fluoride by solvolytic cleavage of the ß-1,4,-O-glycosidic linkage (1 HF molecule per glucan unit). As discussed earlier, adsorption of HF onto hydrophobic lignin and pore-condensation of HF vapor into the microvoids of the secondary cell wall are assumed negligible. Given these assumptions, the gravimetric HF adsorption vs. time curve for prehydrolyzed wood (lignocellulose) is calculated by

$$\theta_{HF}(t) = \theta_e(T_g)\,[3(1 - Z_1) + X_3]/4 \qquad [8\text{-}50]$$

By neglecting the X_3 term, equation [8-50] reduces to

$$\theta_{HF}(t) = \theta_e(T_g)\,[1 - Z_1] \qquad [8\text{-}51]$$

The total rate of gravimetric uptake of HF vapor onto the lignocellulosic matrix of prehydrolyzed wood is

$$d\theta_{HF}(t)/dt = \theta_e(T_g)\,[3k_1\theta_e Z_1 + k_2\theta_e X_2]/4 \qquad [8\text{-}52]$$

Equation [8-52] is obtained by differentiation of equation [8-50] with respect to time t, followed by insertion of relationships for dZ_1/dt and dX_3/dt (equations [8-42] and [8-45]) into the differentiated equation. By neglecting the X_3 term, equation [8-52] reduces to

$$d\theta_{HF}(t)/dt = \theta_e(T_g)\,[k_1\theta_e Z_1] \qquad [8\text{-}53]$$

V. Kinetic Parameter Estimation

A. Overview

In this section, the kinetic parameters posed by the simplified differential material balance and kinetic model are estimated. The differential material balance and kinetic model has two rate constants, k_1 and k_2. The Arrhenius forms of the rate constants k_1 and k_2 are

$$k_1 = k_{1o} \exp[-E_1/R\ (1/T - 1/T_o)] \qquad [8\text{-}54]$$

$$k_2 = k_{2o} \exp[-E_2/R\ (1/T - 1/T_o)] \qquad [8\text{-}55]$$

where k_{1o} (g/g-sec) is the reference rate constant for k_1 at T_o, E_1(kcal/mol) is the activation energy for k_1, k_{2o} (g/g-sec) is the reference rate constant for k_2 at T_o, E_2 (kcal/mol) is the activation energy for k_2, and R is the thermodynamic constant (1.987 cal/mol). Therefore, four kinetic parameters must be estimated: k_{1o}, E_1, k_{2o}, E_2.

The parameter estimation scheme fits model predictions for the X_3 vs. t profile to the complimentary glucose yield vs. time data. The kinetic parameters posed by the model equations are adjusted until the sum of squared deviations between model predictions and data (i.e. the sum of squared residuals) is minimized. Therefore, the validity of the parameter estimates are limited by the validity of the model.

Recall from chapter 7 that the solvolysis of a single prehydrolyzed wood (lignocellulose) chip by anhydrous HF vapor is nonisothermal even under conditions where mass-transfer resistances are minimized. Therefore, k_1 and k_2 cannot be

estimated directly at a given HF vapor stream temperature T_g because k_1 and k_2 will vary with the particle temperature (T) via equations [8-54] and [8-55]. However, the kinetic parameters k_{1o}, E_1, k_{2o}, and E_2 can be estimated simultaneously from a single set of gravimetric HF adsorption and glucose yield vs. time data given the complimentary particle temperature vs. time data at the same HF vapor conditions.

For a "thin" lignocellulose chip (half-thickness L = 0.2 mm or 0.4 mm), I assume that intraparticle temperature gradients are small within the HF-reacting lignocellulose chip. With this assumption, the centerline particle temperature is essentially the particle temperature of the whole HF-reacting lignocellulose chip. As an aside note, this assumption is confirmed by model predictions for the particle temperature distribution in the HF-reacting lignocellulose chip (see chapter 10).

The kinetic parameters k_{1o}, E_1, k_{2o}, and E_2 are estimated by nonlinear, ordinary least-squares (OLS)/ Gauss minimization (Beck and Arnold, 1977). An iterative, nonlinear parameter estimation procedure is used because the differential material balance model equations are nonlinear with repsect to kinetic parameters E_1 and E_2. In principle, for a nonisthermal reaction, the kinetic parameters k_{1o}, E_1, k_{2o}, and E_2 can all be estimated simultaneously from a single set of glucose yield vs. time data and complimentary centerline particle temperature vs. time data. In practice, simultaneous estimation is not tractable because the "sensitivity equations" $\partial X_3/\partial k_{1o}$, $\partial X_3/\partial E_1$, $\partial X_3/\partial k_{2o}$, and $\partial X_3/\partial E_2$ are "nearly" linearly dependent. If the sensitivity equations are nearly linearly dependent, then

convergence to the least-squares criterion is difficult, if not impossible. Even if convergence is achieved, the near linear dependence of the sensitivity coefficient equations results in high correlation between parameter estimates (>0.9), which is in turn manifested unrealistically high standard error estimates. The difficulties inherent to simultaneous, nonlinear estimation of multiple parameters are discussed in detail by Beck and Arnold (1977).

B. Final Algorithm

In order to circumvent the least-squares convergence difficulties inherent to simultaneous estimation of k_{1o}, E_1, k_{2o}, and E_2, I finally developed a two-step, sequential parameter estimation approach. The first step (estimation scheme 1) estimates k_{1o} and E_1. The second step (estimation scheme 2) estimates k_{2o} and E_2. The complete parameter estimation algorithm is overviewed here. The major assumptions and restrictions placed on the data sets used for parameter estimation are

* Reaction of a 100% HF vapor stream with a single, dry prehydrolyzed wood chip
* Mass-transfer resistances to glucose yield vs. time data are minimized
* The centerline particle temperature of the of a "thin" HF-reacting lignocellulose chip is essentially the whole particle temperature
* Negligible error in the centerline particle temperature measurements (for parameter estimation purposes only)

Glucose yield vs. time data, gravimetric HF adsorption data, and particle temperature vs. time data from prehydrolyzed wood are used for parameter estimation, because as stated in section IV of this chapter, prehydrolyzed wood is

the model lignocellulose substrate selected comparison for of model to data.

The standard statistical assumptions in effect for ordinary least-squares (OLS) estimation are (see Beck and Arnold, 1977):

* additive measurement errors
* zero-mean (non-biased) measurement errors
* no error in independent variable (time)
* all weighting factors equal 1
* constant parameter vector
* no prior information

Estimation Scheme 1. First, k_{1o} and E_1 are estimated from a single set gravimetric HF adsorption vs. time data ($\theta_{HF,ex}$ vs. t) at a fixed set of 100% HF vapor conditions. This estimation scheme also requires complimentary centerline particle temperature vs. time data at the same set of 100% HF vapor conditions. Specifically, at the current fixed value for k_{1o}, E_1 is estimated by the iterative OLS/Gauss linearization equation

$$E_1^{k+1} = E_1^{k} + \frac{\sum [\partial\theta_{HF}(t_i)/\partial E_1 \cdot (\theta_{HF,ex}(t_i) - \theta_{HF}(t_i))]^{k}}{\sum[(\partial\theta_{HF}(t_i)/\partial E_1)^2]^{k}} \qquad [8\text{-}56]$$

where "k" is the iteration index. At the current, or k^{th} estimate of E_1, $\theta_{HF}(t)$ is calculated by equation [8-51]. In equation [8-51], Z_1 is calculated by 4th-order Runge-Kutta numerical integration of equation [8-42], given complimentary particle temperature vs. time data to drive $k_1(T)$ and $\theta_e(T)$. The sensitivity expression,

$\partial\theta_{HF}/\partial E_1$, given in equation [8-56] is calculated by 4th-order Runge-Kutta numerical integration of

$$\frac{\partial[d\theta_{HF}/dt]}{\partial E_1} = \frac{d[\partial\theta_{HF}/\partial E_1]}{dt} = -\frac{k_1}{R}[1/T - 1/T_o]\theta_e^2 Z_1 \qquad [8\text{-}57]$$

with respect to reaction time t. After numerical integration from t = 0 to t = t_f (the final time), the current estimate for E_1 is updated by equation [8-56] (Note: to start the estimation loop for E_1, an initial guess for E_1 is required). The iteration converges when

$$\frac{E_1^{k+1} - E_1^k}{E_1^{k+1}} < \text{tol (0.0001)} \qquad [8\text{-}58]$$

At the current fixed value for k_{1o}, the sum of squared residuals for estimation scheme 1 (s_1^2) is

$$s_1^2 = \sum [\theta_{HF,ex}(t_i) - \theta_{HF}(t_i)]^2 \qquad [8\text{-}59]$$

The algorithm is repeated with an incremented value of k_{1o} until the global sum of squared residuals (s_1^2) is minimized with respect to k_{1o}. The algorithm for estimation of k_{1o} and E_1 (estimation scheme 1) is carried out by computer program KINFIT1.BAS, which is listed in Appendix D. The errors introduced by numerical integration are assumed negligible.

Estimation Scheme 2. Once k_{1o} and E_1 are determined, k_{2o} and E_2 are estimated from a single set of normalized glucose yield vs. time data, $Y_{g,ex}(t_i)$, at

a fixed HF vapor set conditions. The normalized glucose yield is determined by

$$Y_{g,ex}(t_i) = Y_g(t_i)/Y_{g,max}$$

where $Y_{g,max}$ is the maximum average glucose yield obtained by experiment, e.g. for the vapor-phase HF solvolysis of prehydrolyzed Bigtooth Aspen wood, $Y_{g,max}$ = 0.78 g glucose/g-lignocellulose. This estimation scheme also requires complimentary centerline particle temperature vs. time data at the same set of HF vapor conditions. Specifically, at a fixed value for k_{2o}, E_2 is estimated by the iterative OLS/Gauss-linearization equation

$$E_2^{k+1} = E_2^k + \frac{\sum [\partial X_3(t_i)/\partial E_2 \, (Y_{g,ex}(t_i) - X_3(t_i))]^k}{\sum [(\partial X_3(t_i)/\partial E_2)^2]^k} \qquad [8\text{-}60]$$

where "k" is the iteration index. At the current, or k^{th} estimate for E_2, $X_3(t)$ is calculated via 4th-order Runge-Kutta integration of rate equations [8-42] to [8-45], given complimentary centerline particle temperature vs. time data to drive $k_1(T)$, $k_2(T)$ and $\theta_e(T)$. (Note: the OLS estimates of k_{1o} and E_1 obtained from estimation scheme 1 are used in estimation scheme 2). The sensitivity expression, $\partial X_3/\partial E_2$, given in equation [8-59] is calculated by 4th-order Runge-Kutta integration of

$$\frac{\partial[dX_3/dt]}{\partial E_2} = \frac{d[\partial X_3/\partial E_2]}{dt} = -\frac{k_2}{R}[1/T - 1/T_o]\theta_e X_2 \qquad [8\text{-}61]$$

with respect to time t. After numerical integration from t = 0 to t = t_f, the current estimate for E_2 is updated by equation [8-60]. (Note: to start the

estimation loop for E_2, an initial guess for E_2 is required). The iteration converges when

$$\frac{E_2^{k+1} - E_2^{k}}{E_2^{k+1}} < \text{tol (0.0001)} \qquad [8\text{-}62]$$

At the current fixed value for k_{2o}, the sum of squared residuals for estimation scheme 2 (s_2^2) is

$$s_2^2 = \sum [Y_{g,ex}(t_i) - X_3(t_i)]^2 \qquad [8\text{-}63]$$

The algorithm is repeated with an incremented value of k_{2o} until the minimum sum of squared residuals (s_2^2) is minimized with respect to k_{2o}. The algorithm for estimation of k_{2o} and E_2 (estimation scheme 2) is carried out by computer program KINFIT2.BAS, which is listed in Appendix D. The errors introduced by numerical integration are assumed negligible.

C. Final Parameter Estimates

The final parameter estimates for k_{1o}, E_1, k_{2o}, and E_2 are given in Table 8.1. Statistical information on the data sets used for parameter estimation are also given in Table 10.1.

Although the two-step parameter estimation scheme is convergent, the parameter estimates are probably inaccurate. A brief explanation of the problems inherent to parameter estimation schemes 1 and 2 is provided here. In Figure

Table 8.1. Estimation of kinetic parameters posed by the differential material balance and kinetic model (nonisothermal method).

Parameter	Estimation Scheme 1 [a]	Estimation Scheme 2 [b]
T_o	31 °C	52 °C
k_{∞}	0.009 g-wood/(g-HF sec)	0.039 g-wood/(g-sec)
E_1	10.2 kcal/mol	15.1 kcal/mol
n_1	18	14
s_1^2	$1.175\ 10^{-2}$ (g-HF/g-wood)^2	$4.393\ 10^{-3}$ (g glc/g wood)^2
RMS [c]	0.026 g HF/g-wood	0.018 g glc/g-wood
r_{12} [d]	0.99	0.99
t_f [e]	90 sec	240 sec

Notes:

[a] Data set selected for estimation scheme 1: $\theta_{HF}(t)$ vs. t, prehydrolyzed wood, 100% HF at 1.0 atm, T_g = 31 °C (see Figure 5.7).

[b] Data set selected for estimation scheme 2: Y_g vs. t, prehydrolyzed wood, 100% HF vapor at 1.0 atm, T_g = 52 °C (see Figure 6.13a).

[c] RMS is the root-mean square residual, defined by RMS = s_1^2/n.

[d] r_{12} is the correlation between parameters

[e] t_f is the final time of the portion of the data set selected for parameter estimation.

8.10a, the sum of squared residuals from estimation scheme 1 (s_1^2) is plotted as a function of k1o, and in Figure 8.10b, E_1 is plotted as a function of k_{1o}. In Figure 8.11a, the sum of squared residuals from estimation scheme 2 (s_2^2) is plotted as a function of k2o, and in Figure 8.11b, E_2 is plotted as a function of k_{2o}. Figures 8.10 and 8.11 show that estimates for E_1 and E_2 are very sensitive to small changes in k_{1o} and k_{2o} respectively. Further, a small change in the sum of squared residuals in estimation scheme 1 or estimation scheme 2 results in a fairly large change in the estimate for E_1 or E_2 respectively. The high correlation between parameters (r_{12} >0.9) for both pairs of parameters k_{1o}, E_1 and k_{2o}, E_2 (Table 8.1) also indicates that the parameter estimates may be inaccurate. Therefore, the kinetic parameter estimates given in Table 8.1 must be accepted with extreme caution. The standard error of each parameter estimate was not calculated because of the high correlation between parameter estimates.

Despite the inherent parameter estimation difficulties, the least-squares fit of the differential material balance and kinetic model to glucose yield vs. time data is excellent, as shown in Figure 8.12.

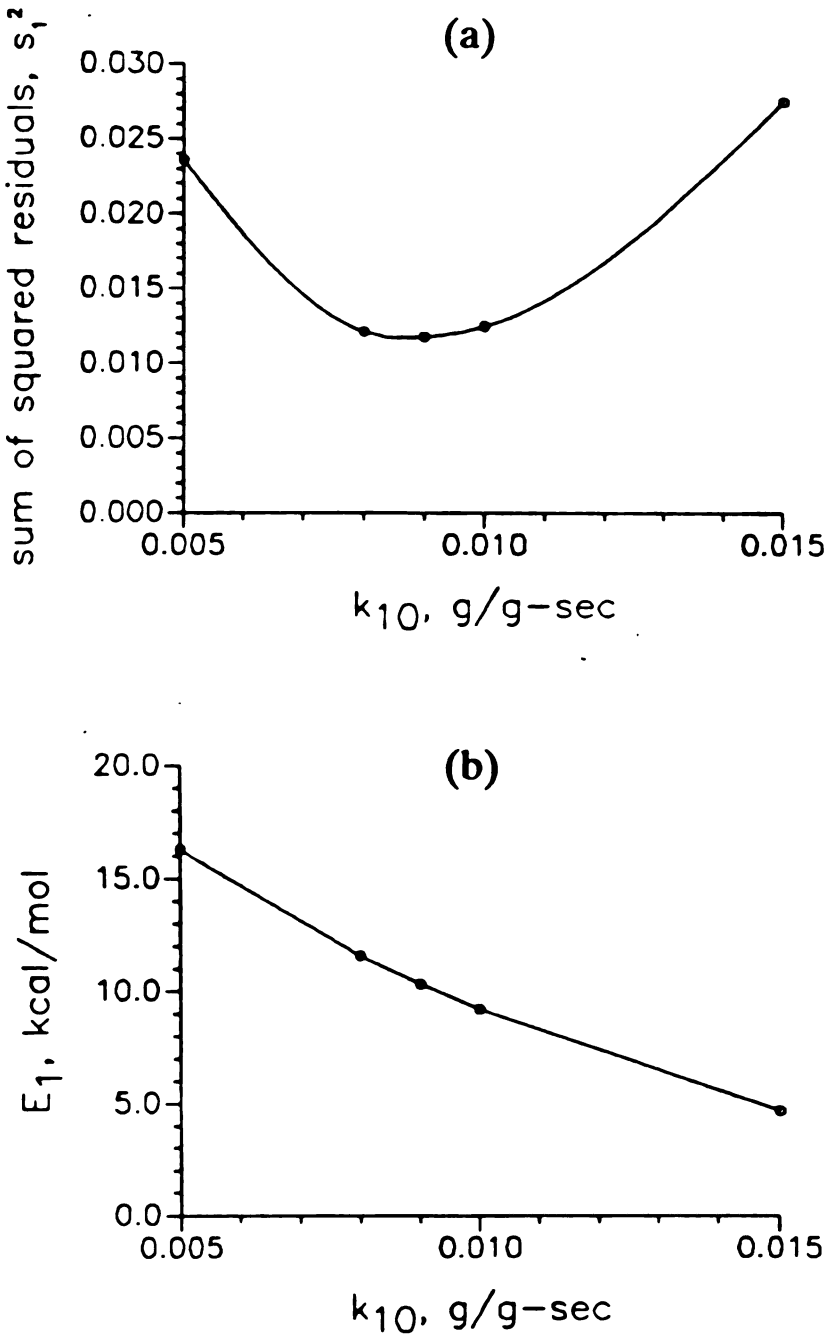


Figure 8.10. Parameter estimation scheme 1: minimization of the sum of squared residuals, s_1^2 (see Table 8.1). (a) s_1^2 vs. k_{1o}; (b) k_{1o} vs. E_1.

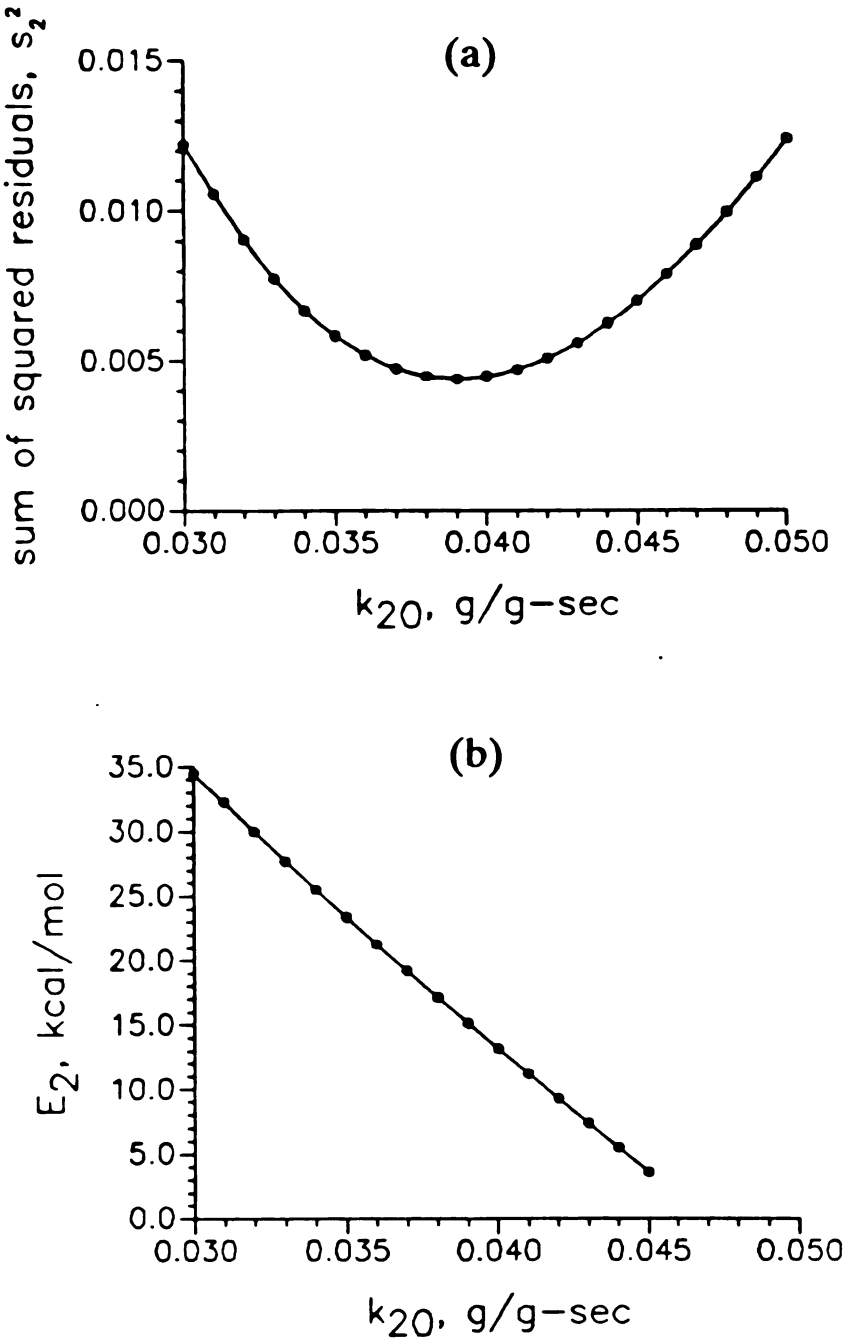


Figure 8.11. Parameter estimation scheme 2: minimization of the sum of squared residuals, s_2^2 (see Table 8.1). (a) s_2^2 vs. k_{2o}; (b) k_{2o} vs. E_2.

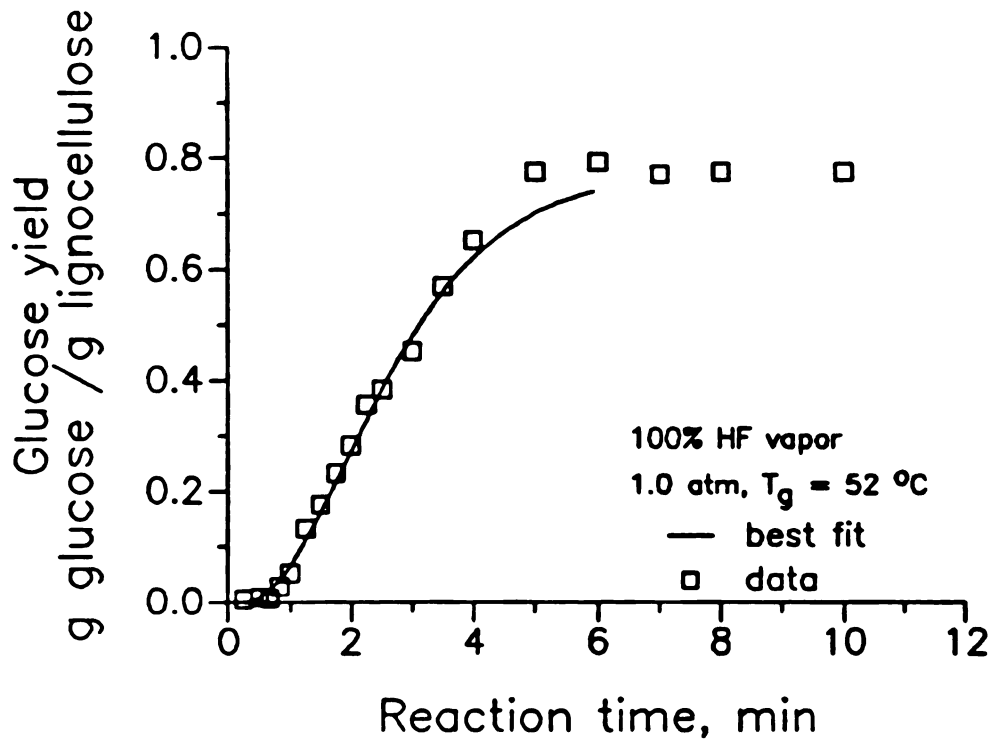


Figure 8.12. Least-squares fit of glucose yield vs. time data to parameter estimation scheme 2 (see kinetic parameter estimates in Table 8.1).

Preview of Chapters 9 and 10

In chapter 9, a differential energy balance and heat transport model for the vapor-phase HF solvolysis of lignocellulose is developed. This model predicts the temperature distribution in the HF-reacting lignocellulose chip as a function of reaction time, chip thickness, and HF vapor conditions. In chapter 10, the differential material balance and kinetic model is coupled to the differential energy balance and heat transport model. Model predictions for sugar product yield and particle temperature distribution in the HF-reacting lignocellulose chip as a function of reaction time and HF vapor conditions are compared to the complimentary experimental data.

Chapter 9. Model Development II: Energy Balance and Heat Transport Model

Introduction

The solvolysis of a single lignocellulose chip by anhydrous Hydrogen Fluoride (HF) vapor is an unsteady-state, noncatalytic, gas/solid reaction subject to both mass and heat transfer resistances. Recall from chapter 7 that even when external (film) and internal (intraparticle) mass-transfer resistances are minimized, heat-transfer resistances are still significant. The heat-transfer resistances and exothermic generation of energy causes the temperature within the HF-reacting lignocellulose chip to increase and then decrease over time. Since this transient particle temperature rise affects the reaction kinetics, a differential energy balance model for the HF-reacting lignocellulose chip must be coupled to the differential material balance and kinetic model developed in chapter 8. The combined material and energy balance model equations constitute a complete mathematical model for the solvolysis of a single lignocellulose chip by an anhydrous 100% HF vapor stream under conditions where gas-phase mass-transfer resistances are minimized.

In this chapter, I will develop a differential energy balance and heat transport model for the solvolysis of a single prehydrolyzed wood (lignocellulose) chip by a 100%, anhydrous HF vapor stream. The model assumes that gas-phase mass transfer resistances are minimized. This assumption implies that film and intraparticle HF vapor concentration gradients are negligible, so that the HF vapor

concentration near and within the HF-reacting lignocellulose chip is equal to the bulk HF vapor stream concentration. However, even in the absence of HF vapor concentration gradients, if intraparticle heat transfer resistances are present, then intraparticle temperature gradients will exist, and hence HF-adsorption and cellulose conversion gradients will exist within the solid phase of the HF-reacting lignocellulose chip. The assumption that heat transfer resistances are present even when mass-transfer resistances are not is reasonable considering the low thermal conductivity and high porosity of the lignocellulosic matrix.

The differential energy and heat transport model is valid for prehydrolyzed (hemicellulose-free) wood. As discussed in previous chapters, prehydrolyzed wood, or lignocellulose, is a model lignocellulosic substrate which possesses the native architecture and composite microstructure of wood but contains only two chemical components, crystalline cellulose (75%) and lignin (25%).

In sections I and II to follow, an unsteady-state energy balance on a differential volume element of the HF-reacting lignocellulose chip is formulated, and the associated boundary and initial conditions are stated. Simultaneous solution of the combined differential material and energy balance model equations is reserved for chapter 10.

I. The Modes of Energy Generation and Transport

The modes of unsteady-state energy generation and transport within a single HF-reacting lignocellulose chip are briefly overviewed here. Recall from chapter

7 that the transient particle temperature rise is largely dissipated before significant glucose yield is generated. Thus, energy is generated within the HF-reacting lignocellulose chip by the exothermic processes of 1) physical adsorption of HF vapor onto the lignocellulosic matrix and 2) HF-solvation of the crystalline cellulose microfibril by displacement of OH....OH hydrogen bonds with stronger HO...HF hydrogen bonds.

At the start of the reaction, HF vapor rapidly adsorbs on the lignocellulose chip, and energy is rapidly released to the HF-reacting lignocellulose chip by exothermic HF adsorption. Therefore, if any heat transfer resistances are present, then energy accumulates within the HF-reacting lignocellulose chip, and the particle temperature increases. This particle temperature rise is offset by two heat transport processes which work in series to dissipate energy to the surrounding HF vapor stream. First, heat generated within the HF-reacting lignocellulose chip is transported by Fourier conduction to the chip surface. Second, the heat flux transported to the particle surface is in turn transported from the hot particle surface to the cooler surrounding HF vapor stream by convection via Newton's Law of Cooling.

Near the end of the HF-adsorption stage of the reaction, the rate of HF adsorption decreases as the equilibrium HF loading is approached. Eventually, the rate of energy transported by conduction and convection is greater than the rate of energy generation by HF adsorption. At this point, the temperature distribution within the HF-reacting lignocellulose chip will decay slowly back to the surrounding

HF vapor temperature.

In summary, if heat transfer resistances are present, then the particle temperature will rise rapidly to a maximum temperature and then decay slowly back to the surrounding HF vapor stream temperature over time.

Internal heat transfer resistances result from Fourier heat conduction through the particle, and external heat transfer resistances result from convection of heat across the fluid film surrounding the particle. These heat transfer resistances create a temperature distribution within the HF-reacting lignocellulose chip which will vary both in position (x) and reaction time (t). Therefore, the differential energy and heat transport model is derived in terms of the dependent variable T(x,t), the local particle temperature within the HF-reacting lignocellulose chip.

II. Mathematical Formulation of the Differential Energy Balance and Heat Transport Model

I begin development of the differential energy balance and heat transport model by stating the following conditions and assumptions:

* Single, prehydrolyzed wood (lignocellulose) chip
* 100% anhydrous HF vapor stream at 1.0 atm
* The reaction is unsteady-state, noncatalytic, and generates solid glucosyl fluoride reaction products which reside on an intact lignin framework
* Film and intraparticle HF vapor concentration gradients are negligible
* No "edge effects": neglect heat loss from edges of HF-reacting wood chip

- "Thin slab" approximation
- Neglect enthalpy of HF vapor within the porous volume of HF-reacting lignocellulose chip
- Neglect consumption of energy by endothermic depolymerization of H-bonded HF oligomers in the vapor phase within the porous volume of the lignocellulose chip (i.e. "f" is close to 1).

Given the assumptions and conditions stated above, the unsteady-state energy balance on a differential volume element of the HF-reacting lignocellulose chip is stated qualitatively as

rate of energy into the volume element by Fourier heat conduction	-	rate of energy out of the volume element by Fourier heat conduction	+	
net rate of generation of energy within the volume element	=	rate of accumulation internal energy within the volume element		[9-1]

The HF-reacting lignocellulose chip is approximated as a thin slab with no edge effects so that the particle temperature profile is along the x-direction specified in Figure 8.1. Therefore, given equation [9-1], the unsteady-state energy balance on a differential volume element of the slab in the x direction at time t is

$$z^2\left(-k_e \frac{\partial T(x,\bar{t})}{\partial x}\right) - z^2\left(-k_e \frac{\partial T(x+\Delta x,\bar{t})}{\partial x}\right) + z^2\Delta x(-\Delta H_A(\theta_e))\rho_{LC} \frac{\partial \theta_{HF}(\bar{x},t)}{\partial t} + z^2\Delta x\,(-\Delta H_R)G_o\rho_{LC} \frac{\partial X_3(\bar{x},t)}{\partial t} = z^2\Delta x \frac{\partial[\rho E_u(\bar{x},t)]}{\partial t} \qquad [9\text{-}2]$$

where $E_u(x,t)$ is the local internal energy of the HF-reacting lignocellulose chip (cal/g-solid), G_o is the total glucan concentration in lignocellulose (mol/g-wood), $\Delta H_R(T)$ is the enthalpy of reaction for solvolytic cleavage of the ß-1,4-O-glycosidic linkages of HF-solvated cellulose (cal/mol glucan), $\Delta H_A(\theta_e)$ is the enthalpy of HF adsorption (cal/g HF-adsorbed), k_e is the local effective thermal conductivitiy of the HF-reacting lignocellulose chip (cal/cm-sec°C), t is the reaction time (sec or min), T(x,t) is the local particle temperature (°C), x is the position along the thickness axis of the lignocellulose chip (cm), z is the face length of the lignocellulose chip, ρ_{LC} is the bulk density of lignocellulose (g/cm^3 wood), and ρ is the overall density of the HF-reacting lignocellulose volume element (g/cm^3 solid). The variables are also defined in the List of Notation.

The differential energy balance is obtained by dividing equation [9-2] by Δx and taking the limit as Δx approaches zero. The result is

$$\frac{\partial[k_e\ \partial T(x,t)/\partial x]}{\partial x} + (-\Delta H_A(\theta_e))\rho_{LC}\frac{\partial \theta_{HF}(x,t)}{\partial t} + (-\Delta H_R)G_o\ \rho_{LC}\frac{\partial X_3(x,t)}{\partial t} = \frac{\partial[\rho E_u(x,t)]}{\partial t} \qquad [9\text{-}3]$$

The following five assumptions simplify equation [9-3] considerably. First, the Fourier conduction term in equation [9-3] reduces to

$$\frac{\partial[k_e\ \partial T/\partial x]}{\partial x} = k_e\frac{\partial^2 T}{\partial x^2} + \cancel{\frac{\partial k_e}{\partial x}\frac{\partial T}{\partial x}} \qquad [9\text{-}4]$$

by assuming the $\partial k_e/\partial x$ term is negligible. Second, it is assumed that the rate of heat generated by physical adsorption of HF onto the lignocellulosic matrix and HF-solvation of the crystalline cellulose microfibril is much larger in magnitude than the rate of heat generated by solvolytic cleavage of the ß-1,4-O-glycosidic linkage joining the glucan units. Therefore

$$(-\Delta H_A(\theta_e))\rho_{LC} \frac{\partial \theta_{HF}(x,t)}{\partial t} >> (-\Delta H_R)G_o\, \rho_{LC} \frac{\partial X_3(x,t)}{\partial t} \qquad [9\text{-}5]$$

Third, it is assumed that the internal energy within the HF-reacting lignocellulose chip (with respect to a reference temperature T_o) is the sum of the internal energies of the unreacted lignocellulose, glucosyl fluoride/lignin reaction products, and adsorbed HF. Therefore

$$\rho E_u = [\ \rho_{LC}C_{p,LC}(1 - X_3) + \rho_{LC}C_{p,G_3}\, X_3\ ]\ [T - T_o] + \rho_{LC}C_{p,HF,ads}\, \theta_{HF}(t)\ [T - T_o] \qquad [9\text{-}6]$$

where $C_{p,HF,ads}$ is the heat capacity of the adsorbed HF (cal/g-HF°C), and $C_{p,G3}$ is the heat capacity of the glucosyl fluoride/lignin solid reaction products (cal/g-solid°C). Fourth, it is assumed that the heat capacity of lignocellulose, $C_{p,LC}$ (cal/g-wood°C) is effectively equal to the heat capacity of the glucosyl fluoride/lignin reaction products, $C_{p,G3}$. The properties $C_{p,LC}$, $C_{p,HF,ads}$ and ρ_{LC} are evaluated

at the bulk HF vapor stream temperature T_g and do not vary significantly with T(x,t). Fifth, it is assumed that the heat of HF adsorption is much larger in magnitude than the specific heat of the adsorbed HF. Therefore

$$-\Delta H_A(\theta_e) \quad > \; > \quad C_{p,HF,ads}\,(T - T_o) \qquad [9\text{-}7]$$

By application of the third and fourth simplifying assumptions, the rate of accumulation of energy within the volume element is

$$\frac{\partial[\rho E_u(x,t)]}{\partial t} = \rho_{LC} C_{p,LC} \frac{\partial T(x,t)}{\partial t} + \rho_{LC} C_{p,HF,ads} \frac{\partial \theta_{HF}(x,t)}{\partial t} (T(x,t) - T_o) + \theta_{HF}(x,t) \frac{\partial T(x,t)}{\partial t} \qquad [9\text{-}8]$$

By inserting simplifying relationships [9-4], [9-5], [9-7] and [9-8] into equation [9-3] and rearranging, the differential heat balance is now in terms of the local particle temperature T(x,t):

$$k_e \frac{\partial^2 T(x,t)}{\partial x^2} + (-\Delta H_A(\theta_e))\rho_{LC} \frac{\partial \theta_{HF}(x,t)}{\partial t} = \rho_{LC}[C_{p,LC} + \theta_{HF}(x,t)\, C_{p,HF,ads}] \frac{\partial T(x,t)}{\partial t} \qquad [9\text{-}9]$$

In equation [9-9], the local gravimetric HF adsorption, $\theta_{HF}(x,t)$, and local rate of gravimetric HF adsorption, $\partial\theta_{HF}(x,t)/\partial t$, are respectively given by equations [8-51] and [8-53] at x and t.

An explicit relationship is now developed for the local thermal conductivity $k_e(x,t)$ of the HF-reacting lignocellulosic matrix. First, the effective thermal conductivity of the solid phase k_s is taken as the weight average of the unreacted lignocellulose, glucosyl fluoride/lignin reaction products, and adsorbed HF. Therefore

$$k_s = [(1 - X_3)\, k_{LC} + X_3\, k_{G_3}]\,[1 - w_{HF,ads}] + w_{HF,ads}\, k_{HF,ads} \qquad [9\text{-}10]$$

where k_{LC} is the thermal conductivity of solid lignocellulose, k_{G3} is the thermal conductivity of the solid glucosyl fluoride/lignin reaction products, $k_{HF,ads}$ is the thermal conductivity of the adsorbed HF (all thermal conductivities have units of cal/cm-sec^{o}C), and w_{HF} is the weight fraction of the HF adsorbed on lignocellulose. The properties k_{LC} and $k_{HF,ads}$ are evaluated at T_g, and do not vary significantly with T(x,t). At a given position x and time t, equation [9-10] is approximated by

$$k_s(x,t) = [1 - w_{HF}(x,t)]\, k_{LC} + w_{HF}(x,t)\, k_{HF,ads} \qquad [9\text{-}11]$$

The local weight fraction of the HF adsorbed on the HF-reacting lignocellulosic matrix, $w_{HF}(x,t)$, is given by

$$w_{HF}(x,t) = \frac{\theta_{HF}(x,t)}{1 + \theta_{HF}(x,t)} \qquad [9\text{-}12]$$

The HF-reacting lignocellulose chip is highly porous and so the local effective solid-phase thermal conductivity $k_s(x,t)$ must be corrected for the presence of HF vapor in the porous volume of the wood chip. A relationship for $k_e(x,t)$ developed by Smith (1981) for a porous catalyst pellet is appropriate

$$k_e(x,t) = k_s(x,t)\cdot[k_g/k_s(x,t)]^{(1 - \varepsilon)} \qquad [9\text{-}13]$$

where k_g is the thermal conductivity of the HF vapor (cal/cm-sec^{o}C, evaluated at T_g), and ϵ is the void fraction of the HF-reacting lignocellulosic matrix. Although the porosity of the HF-reacting lignocellulosic matrix is changing, for simplicity, ϵ is assumed constant and is evaluated for lignocellulose via equation [4-6].

The boundary and initial conditions for the differential energy balance (equation [9-9]) are now defined. At the particle centerline (x = L), the symmetry condition is valid. Therefore, the boundary condition at x = L is

$$\frac{\partial T(L,t)}{\partial x} = 0 \qquad [9\text{-}14]$$

At the particle surface (x = 0), the heat transported to the particle surface by Fourier conduction is in turn transported to the surrounding HF vapor steam by

convection via Newton's Law of Cooling. Therefore, the boundary condition at $x = 0$ is

$$\frac{\partial T(0,t)}{\partial x} = -\frac{h}{k_e}\,[T(0,t) - T_g] \qquad [9\text{-}15]$$

where "h" is the convective heat transfer coefficient (cal/cm^2-sec ^oC), and k_e is the local effective thermal conductivity of the particle surface, which is evaluated at T(0,t). At the start of the reaction, it is assumed that the lignocellulose chip is at the bulk HF vapor stream temperature (T_g). Therefore, the initial condition is

$$T(x,0) = T_g \qquad [9\text{-}16]$$

In equations [9-15] and [9-16], T_g is assumed constant.

In equation [9-15], the HF vapor stream convective heat transfer coefficient "h" is estimated by the correlation (Petersen, 1965)

$$Nu = 0.678\ Re^{0.5}\ Pr^{0.33} \qquad [9\text{-}17]$$

for laminar flow of HF vapor over the lignocellulose particle (slab). In equation [9-17], the Reynold's number (Re_z) for HF vapor flowing over the lignocellulose chip is

$$Re_z = G_{HF}\ z/2\ \mu_g \qquad [9\text{-}18]$$

The HF vapor stream Prandtl's number (Pr) is

$$Pr = \mu_g C_{p,g}/k_g \qquad [9\text{-}19]$$

and the HF vapor stream Nusselt's number (Nu) is

$$Nu = h\ z/2\ k_g \qquad [9\text{-}20]$$

In equations [9-18] to [9-20], G_{HF} is the superfacial mass velocity of the HF vapor stream (g HF/cm^2-min), and $C_{p,g}$, k_g, and μ_g are the heat capacity (cal/g^{o}C), thermal conductivity (cal/cm-sec^{o}C), and viscosity (g/cm-sec) of the 100% HF vapor stream respectively.

The complete differential energy balance and heat transport model for the solvolysis of a single lignocellulose chip by anhydrous HF vapor is specified by the differential energy balance [9-9], effective thermal conductivity relationships [9-11] through [9-13], boundary conditions [9-14], [9-15], and initial condition [9-16].

In chapter 10, the differential energy balance model is coupled to the differential material balance model developed in chapter 8. The combined differential material and energy balance model equations are solved simultaneously in order to predict the sugar product yield, particle temperature distribution, and energy release within a single HF-reacting lignocellulose chip as a function of reaction time, chip thickness, and HF vapor conditions.

Chapter 10. Model Predictions and Comparison to Experimental Data

Introduction

In this chapter, the differential material balance and kinetic model developed in chapter 8 is coupled to the differential energy balance and heat transport model developed in chapter 9. This combined model describes the solvolysis of a single prehydrolyzed wood (lignocellulose) chip by an anhydrous, 100% HF vapor stream under conditions where HF vapor concentration gradients are negligible.

This chapter is organized into four sections, labeled I to IV. In section I, the the differential material balance model equations are combined with the differential energy balance model equations. In section II, an algorithm is described for the numerical integration of the combined differential material and energy balance model equations over reaction time "t" and chip thickness position "x". In section III, model predictions for the global sugar product yield and temperature distribution within the HF-reacting lignocellulose chip as a function of reaction time, chip thickness, and 100% HF vapor conditions are compared directly to the complimentary experimental data. In section IV, the model is extended to predict the energy release and nonisothermal effectiveness factor in the HF-reacting lignocellulose chip as a function of reaction time, chip thickness, and 100% HF vapor conditions.

I. Combination of the Differential Material and Energy Balance Equations

In this section, I summarize the differential material and energy balance model equations and the major assumptions used to develop these equations.

I begin presentation of the combined differential material and energy balance model by summarizing the conditions and assumptions common to both the material and energy balance components of the model:

* Single, prehydrolyzed wood (lignocellulose) chip
* 100% anhydrous HF vapor stream at 1.0 atm
* The reaction is unsteady-state, noncatalytic, and generates solid glucosyl fluoride products which reside on an intact lignin framework
* Film and intraparticle HF vapor concentration gradients are negligible
* HF vapor physically adsorbs onto the lignocellulosic matrix
* Pore condensation of HF vapor into lignocellulose microvoids is negligible

The additional assumptions specific to the material and energy balance components of the model are listed after the model equations are presented.

Differential Material Balance and Kinetic Model. From chapter 8, the "simplified" differential material balance at reaction time "t" and position "x" within the HF-reacting lignocellulose chip is described by the following set of coupled, nonlinear, first-order differential equations

$$\partial Z_1(x,t)/\partial t = -k_1\theta_e Z_1(x,t) \qquad [10\text{-}1]$$

$$\partial X_1(x,t)/\partial t = -\partial f[1 - Z_1(x,t)]/\partial t \qquad [10\text{-}2]$$

$$\partial X_2(x,t)/\partial t = \partial f[1 - Z_1(x,t)]/\partial t - k_2\theta_e X_2(x,t) \qquad [10\text{-}3]$$

$$\partial X_3(x,t)/\partial t = k_2\theta_e X_2(x,t) \qquad [10\text{-}4]$$

where

$$f[1 - Z_1(x,t)] = b_o + b_1[1 - Z_1(x,t)] + b_2[1 - Z_1(x,t)]2 + b_3[1 - Z_1(x,t)]^3 \quad [10\text{-}5]$$

$$\partial f[1 - Z_1(x,t)]/\partial t = k_1\theta_e Z_1(x,t)\,(b_1 + 2b_2[1 - Z_1(x,t)] + 3b_3[1 - Z_1(x,t)]^2) \quad [10\text{-}6]$$

All variables in equations [10-1] to [10-6] are defined in chapter 8 and the List of Notation. Equations [10-1] to [10-4] have the initial conditions

$$Z_1(x,0) = 1$$

$$X_1(x,0) = 1$$

$$X_2(x,0) = 0$$

$$X_3(x,0) = 0$$

The local gravimetric HF adsorption, $\theta_{HF}(x,t)$, and local rate of gravimetric HF adsorption, $\partial\theta_{HF}(x,t)/\partial t$, at position "x" and time "t" are estimated by

$$\theta_{HF}(x,t) = \theta_e(T_g)\,(3[1 - Z_1(x,t)] + X_3(x,t))/4 \quad [10\text{-}7]$$

$$\partial\theta_{HF}(x,t)/\partial t = \theta_e(T_g)\,[3k_1\theta_e Z_1(x,t) + k_2\theta_e X_2(x,t)]/4 \quad [10\text{-}8]$$

Equations [10-7] and [10-8] are approximated by

$$\theta_{HF}(x,t) = \theta_e(T_g)\,[1 - Z_1(x,t)] \quad [10\text{-}9]$$

$$\partial\theta_{HF}(x,t)/\partial t = \theta_e(T_g)\,[k_1\theta_e Z_1(x,t)] \quad [10\text{-}10]$$

At position "x" and reaction time "t", rate constants k_1 and k_2 are explicit functions of the particle temperature distribution, T(x,t):

$$k_1 = k_{1o} \exp(-E_1/R \cdot [1/T(x,t) - 1/T_o]) \quad [10\text{-}11]$$

$$k_2 = k_{2o} \exp(-E_2/R \cdot [1/T(x,t) - 1/T_o]) \quad [10\text{-}12]$$

For 100% HF vapor at 1.0 atm, the local adsorbed HF concentration potential $\theta_e(x,t)$ is a function of the particle temperature T(x,t). Specifically, for prehydrolyzed wood, θ_e at T(x,t) is estimated by the correlation (see also equation [5-6])

$$\theta_e(x,t) = a_o + a_1 T(x,t) + a_2 T(x,t)^2 + a_3 T(x,t)^3 \quad [10\text{-}13]$$

The global glucosyl fluoride production in the HF-reacting lignocellulose chip is calculated by integration of of $X_3(x,t)$ over x at fixed t:

$$X_3(t) = \frac{1}{L} \int_0^L X_3(x,t)\, \partial x \quad [10\text{-}14]$$

Recall from chapter 4 that global glucosyl fluoride production is quantified experimentally as the glucose yield in the water-soluble reaction products after posthydrolysis. Recall from chapter 6 that at 100% HF vapor conditions of 1.0 atm and temperatures greater than 60 °C (refer to Figures 6.14 and 6.15), the equilibrium HF loading on prehydrolyzed wood is not sufficient to insure stoichiometric solvolysis with cellulose, and so the maximum glucose yield decreases. If the equilibrium HF loading on the HF-reacted lignocellulose chip is not sufficient to insure a stoichiometric solvolysis with cellulose, then the global glucose yield

$Y_g(t)$ is estimated by

$$Y_g(t) = X_3(t)\,[G_o]\,Y_o \qquad [10\text{-}15]$$

In equation [10-15], the stoichiometry factor, Y_o, is defined as

$$Y_o = \begin{cases} \theta_e/\theta_{min} \text{ if } \theta_e < \theta_{min} \\ 1 \text{ if } \theta_e \geq \theta_{min} \end{cases} \qquad [10\text{-}16]$$

where $\theta_{e,min}$ = 0.369 g HF/g prehydrolyzed wood (see equation [6-7]), and θ_e is estimated at T_g by equation [5-6].

The global gravimetric uptake of HF vapor onto a single HF-reacting lignocellulose is also calculated by integration of $\theta_{HF}(x,t)$ over x at fixed t:

$$\theta_{HF}(t) = \frac{1}{L}\int_0^L \theta_{HF}(x,t)\,\partial x \qquad [10\text{-}17]$$

The major conditions and assumptions imposed on the differential material balance and kinetic model (in addition to those already stated at the beginning of section I) are

* Intrinsic adsorption/reaction scheme given by Figure 8.7 is correct
* Adsorption rates are fast relative to reaction rates
* HF vapor physically adsorbs only onto -OH groups and -O- linkages on glucan
* Adsorption of HF vapor onto hydrophobic lignin is neglected
* All three OH groups on a given glucan unit must be complexed with HF before solvolytic cleavage of the ß-1,4-O-glycosidic linkage of that glucan unit can occur

* The number of glucan units completely HF-complexed is a stochastic function of the total number of -OH groups on glucan HF-complexed

* The "limiting stoichiometry" of adsorbed HF is described by equation [10-16]

* Glucosyl fluoride production in the HF-reacted lignocellulosic matrix is quantified experimentally as the glucose yield in the water-soluble reaction products after posthydrolysis

* The potential HF surface concentration on -OH groups and ß-1,4-O-glycosidic linkages of glucan (θ_1 and θ_2) is represented by θ_e

* Solvolytic cleavage of the ß-1,4-O-glycosidic linkage is preferred at the non-reducing end of the HF-solvated cellulose chain

* A single rate constant (k_2) describes solvolytic cleavage of HF-solvated cellulose chains to glucosyl fluoride, i.e. there are no chain-length dependent rate constants

* Glucosyl fluoride does not condense onto or form water-insoluble adducts with lignin

Differential Energy Balance and Heat Transport Model. From chapter 9, the "simplified" differential energy balance at reaction time "t" and position "x" within the HF-reacting lignocellulose chip in terms of the particle temperature distribution T(x,t) is described by the parabolic partial differential equation

$$k_e \frac{\partial^2 T(x,t)}{\partial x^2} + (-\Delta H_A(\theta_e))\rho_{LC} \frac{\partial \theta_{HF}(x,t)}{\partial t} = \rho_{LC}[C_{p,LC} + \theta_{HF}(x,t)\, C_{p,HF,ads}] \frac{\partial T(x,t)}{\partial t} \quad [10\text{-}18]$$

with boundary and initial conditions

$$\frac{\partial T(0,t)}{\partial x} = -\frac{h}{k_e}[T(0,t) - T_g] \quad [10\text{-}19]$$

$$\frac{\partial T(L,t)}{\partial x} = 0 \quad [10\text{-}20]$$

$$T(x,0) = T_g \quad [10\text{-}21]$$

The local heat of adsorption $\Delta H_A(\theta_e)$ and effective thermal conductivity k_e are implicit functions of T(x,t):

$$\Delta H_A[\theta_e(x,t)] = H_o \theta_e(x,t)^{-a} \quad [10\text{-}22]$$

$$k_e(x,t) = k_s(x,t)\,[k_g / k_s(x,t)]^{(1-\epsilon)} \quad [10\text{-}23]$$

where

$$k_s(x,t) = [1 - w_{HF}(x,t)]\, k_{LC} + w_{HF}(x,t)\, k_{HF,ads} \qquad [10\text{-}24]$$

$$w_{HF}(x,t) = \frac{\theta_{HF}(x,t)}{1 + \theta_{HF}(x,t)} \qquad [10\text{-}25]$$

All variables given in equations [10-18] to [10-25] are defined in chapter 9 and the List of Notation.

The major conditions and assumptions imposed on the differential energy balance and heat transport model (in addition to those already stated at the beginning of section I) are:

* "Thin slab" approximation: temperature distribution along x-direction only (thickness axis of lignocellulose chip)

* Neglect edge effects

* The overall volume change of the HF-reacting lignocellulose chip is negligible

* The rate of energy generated by physical adsorption of HF vapor onto the lignocellulosic matrix and HF-solvation of cellulose chains by adsorbed HF is much larger in magnitude then the rate of energy generated by solvolytic cleavage of ß-1,4-O-glycosidic linkages

* Neglect energy consumption by nonideal HF vapor as hydrogen-bonded HF oligomers depolymerize to HF monomers upon HF adsorption (i.e. f = 1)

* Heat capacity of lignocellulose is equivalent to the heat capacity of the glucosyl fluoride/lignin reaction products

* Heat capacity and density of the HF-reacting lignocellulosic matrix are evaluated at T_g and are not strongly dependent on particle temperature

* HF vapor stream temperature T_g is constant

The differential energy balance model is coupled directly to the differential material balance by equations [10-1], [10-9], and [10-10]. The differential material balance model is coupled implicitly to the differential energy balance model by T(x,t).

II. Numerical Solution Procedure

The differential material and energy balance model equations are nonlinear and cannot be integrated analytically. However, the model equations can be integrated numerically. In this section, I will overview the numerical solution procedure.

First, the particle temperature distribution T(x,t) is calculated by integrating the differential energy balance model equations and selected material balance model equations simultaneously over chip thickness position x and reaction time t. Specifically, the parabolic partial differential equation [10-18] is solved for T(x,t) by the Crank-Nicolson finite difference scheme (Carnahan et al., 1969) given boundary/initial conditions [10-19] to [10-21], and equations [10-22] to [10-25] for estimation of $\Delta H_A[\theta_e(x,t)]$ and $k_e(x,t)$. Simultaneously, at each node corresponding to T(x,t), $Z_1(x,t)$ is calculated by 4th-order Runge-Kutta integration of equation [10-1], given equations [10-11] and [10-13] for estimation of k_1 and θ_e at T(x,t). The local gravimetric uptake $\theta_{HF}(x,t)$ and local rate of gravimetric uptake $\partial\theta_{HF}(x,t)/\partial t$, which are components of differential energy balance equation [10-18], are then calculated from equations [10-9] and [10-10], given $Z_1(x,t)$. The numerical

solution procedure for the differential energy balance and heat transport model is carried out by computer program TDIST1.BAS, which is listed in Appendix D. In order to bring the calculated values for T(x,t) constant to 4 significant figures, a time step size (Δt) of 0.1 sec, and a position step size (Δx) of 0.002 cm or 0.004 cm are used.

Second, once T(x,t) is known, the differential material balance model equations are solved simultaneously over x and t. Specifically, $Z_1(x,t)$, $X_1(x,t)$, $X_2(x,t)$, and $X_3(x,t)$ at each node corresponding to T(x,t) are calculated by 4th-order Runge Kutta integration of differential material balance model equations [10-1] to [10-4] over time t, given equation [10-6] for calculation of $\partial f[1-Z_1(x,t)]/\partial t$, and equations [10-11] to [10-13] for estimation of k_1, k_2, and θ_e at T(x,t). At fixed t, the global glucosyl fluoride production $X_3(t)$ is then calculated by trapezoid-rule integration of $X_3(x,t)$ over chip thickness position x (equation [10-14]). The numerical solution procedure for the differential material balance and kinetic model is carried out by program TDIST2.BAS, which is listed in Appendix D. In order to bring the calculated value for $X_3(t)$ constant to four significant figures, a time step size (Δt) of 1 sec is used.

In summary, the particle temperature distribution T(x,t) is calculated by the Crank-Nicolson finite difference scheme via computer program TDIST1.BAS and stored. The calculated values for T(x,t) are then loaded by program TDIST2.BAS. At each node corresponding to T(x,t), the rate equations for $Z_1(x,t)$, $X_1(x,t)$, $X_2(x,t)$, and $X_3(x,t)$ are solved by 4th-order Runge-Kutta integration over time via

computer program TDIST2.BAS. The normalized, global glucosyl fluoride production, $X_3(t)$, is calculated by numerical integration of $X_3(x,t)$ over chip thickness position x at fixed t via program TDIST2.BAS and stored. Finally, the global glucose yield $Y_g(t)$ is calculated by equations [10-15] and [10-16].

III. Model Predictions and Comparison to Experimental Data

A. Comparison of Model to Data over a Limited Range of Process Variables

In this section, model predictions for the global sugar product yield and temperature distribution within the single HF-reacting lignocellulose chip are compared to the complimentary experimental data over a selected range of process variables.

The assumptions imposed on the differential material and and energy balance model equations restrict the range of process conditions where the model predictions are valid. To summarize, model predictions are valid only for the reaction of a single, dry prehydrolyzed wood (lignocellulose) chip with a 100% HF vapor stream at 1.0 atm under conditions where 1) external and internal mass transfer resistances are minimized, and 2) pore-condensation of HF vapor is negligible (e.g. $T_g > 50\ ^oC$ at 1.0 atm). The experimentally studied range of process conditions which fall within these restrictions are given in Table 10.1.

The process conditions selected for analysis are also summarized in Table 10.1. Model input parameters, including physical property constants, kinetic parameters, and HF adsorption parameters, are summarized in Tables 10.2 and 10.3.

Table 10.1. Range of process parameters selected for comparison of model to data.

Process Parameter	Variable	Range
Total system pressure	P_T	1.0 atm (fixed)
HF vapor partial pressure	P_{HF}	1.0 atm (fixed)
HF vapor stream temperature	T_s	52 °C, 60 °C, 68 °C
HF vapor flowrate	G_{HF}	0.42 g HF/cm^2-min
prehydrolyzed wood chip thickness to centerline	L	0.2 mm, 0.4 mm
prehydrolyzed wood chip face length	z	1.0 cm (fixed)
typical prehydrolyzed wood chip weight	m_{LC}	12.0 mg
reaction time	t	0 to 12 min

Table 10.2. Physical property input data for combined material and energy balance model.

Variable	T_g = 52°C	T_g = 60°C	T_g = 68°C	Units
$C_{p,LC}$	0.3	0.3	0.3	cal/g°C
k_{LC}	$2.0\ 10^{-4}$	$2.0\ 10^{-4}$	$2.0\ 10^{-4}$	cal/cm-sec°C
ρ_{LC}	0.3	0.3	0.3	g/cm^3
$C_{p,HF,ads}$	0.66	0.67	0.68	cal/g°C
$k_{HF,ads}$	0.0015	0.0016	0.0016	cal/cm-sec°C
$\rho_{HF,ads}$	0.9	0.86	0.80	g/cm^3
f	1.08	1.02	1.00	
$\theta_e(T_g)$	0.519	0.382	0.297	g HF/g-wood
Y_o	1.000	1.000	0.805	
$C_{p,g}$	3.5	1.3	0.6	cal/g°C
k_g	$5.0\ 10^{-4}$	$4.0\ 10^{-4}$	$3.0\ 10^{-4}$	cal/cm-sec°C
μ_g	$1.35\ 10^{-4}$	$1.40\ 10^{-4}$	$1.45\ 10^{-4}$	g/cm-sec
Pr	0.945	0.455	0.272	
G_{HF}	0.42	0.42	0.42	g HF/cm^2-min
Re_s	25.9	25.0	24.1	
Nu	3.32	5.22	2.16	
h	0.0034	0.0021	0.0013	cal/cm^2-sec°C

Table 10.3. Kinetic and adsorption parameters for combined material and energy balance model.

Parameter	Value & Units	Notes
k_{1o}	0.009 g/g-sec	T_o = 31 °C; see equation [10-11]
E_1	10.2 kcal/mol	
k_{2o}	0.039 g/g-sec	T_o = 52 °C; see equation [10-12]
E_2	15.1 kcal/mol	
a_o	5.440502	see equation [10-13]
a_1	-0.2024107	
a_2	$2.748926\ 10^{-3}$	
a_3	$-1.300829\ 10^{-5}$	
b_o	$-9.764\ 10^{-4}$	see equations [10-5], [10-6]
b_1	$7.522\ 10^{-3}$	
b_2	-0.02129	
b_3	1.0129	
H_o	-205.0 cal/g HF ads	see equation [10-22]
a	0.457	

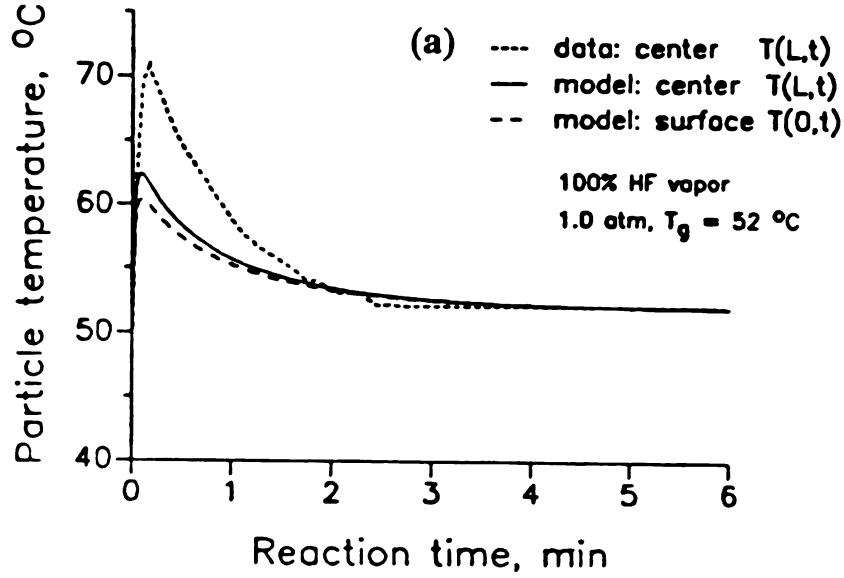
Computer modeling programs TDIST1.BAS and TDIST2.BAS calculated the temperature distribution, T(x,t), and global sugar yield, $Y_g(t)$, within a single, HF-reacting, prehydrolyzed wood chip as a function of reaction time "t" at a fixed 100% HF vapor stream temperature (T_g) and fixed flowrate (G_{HF}). Model input parameters are summarized in Tables 10.1, 10.2, and 10.3. The following model predictions are matched directly to the available experimental data. Specifically, the calculated T(L,t) (center) and T(0,t) (surface) profiles for a single, HF-reacting lignocellulose chip are compared to the complimentary particle temperature vs. time data at T_g = 52 °C, 60 °C, and 68 °C, in Figures 10.1a, 10.1b, and 10.1c respectively. Calculated $Y_g(t)$ profiles for a single, HF-reacting lignocellulose chip are compared to the complimentary glucose yield vs. data at T_g = 52 °C, 60 °C and 68 °C, in Figures 10.2a, 10.2b, and 10.3c respectively. The calculated T(x,t) profiles used in the calculation of $Y_g(t)$ in Figures 10.2a, 10.2b, and 10.2c are not shown.

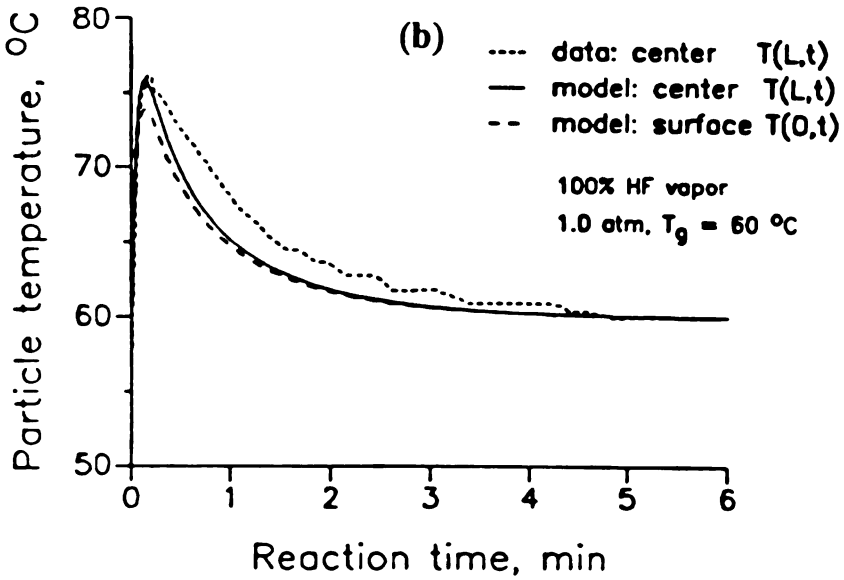
Complimentary model predictions for the global gravimetric uptake of 100% HF vapor onto a single, HF-reacting lignocellulose chip as a function of reaction time and 100% HF vapor stream temperatures (T_g) 52 °C, 60 °C, and 68 °C are presented in Figure 10.3. However, gravimetric HF adsorption vs. time data were not acquired at these HF vapor conditions.

In general, the agreement between model predictions and the available data is good. The model correctly predicts the following experimental observations:

1. The centerline particle temperature rapidly rises to a maximum temperature and then slowly decays back to the 100% HF vapor stream temperature over reaction time

Figure 10.1. Particle temperature vs. reaction time profiles for the solvolysis of a single prehydrolyzed wood (lignocellulose) chip by a 100% HF vapor stream at 1.0 atm: data and model predictions compared. (a) T_g = 52 °C; (b) T_g = 60 °C; (c) T_g = 68 °C. Notes: G_{HF} = 0.42 g HF/cm^2-min, L = 0.4 mm (see Tables 10.1 and 10.2 for detailed reaction conditions).


(a)
---- data: center T(L,t)
— model: center T(L,t)
-- model: surface T(0,t)
100% HF vapor
1.0 atm, T_g = 52 °C
Particle temperature, °C
70
60
50
40
0
1
2
3
4
5
6
Reaction time, min


(b)
---- data: center T(L,t)
— model: center T(L,t)
-- model: surface T(0,t)
100% HF vapor
1.0 atm, T_g = 60 °C
Particle temperature, °C
80
70
60
50
0
1
2
3
4
5
6
Reaction time, min

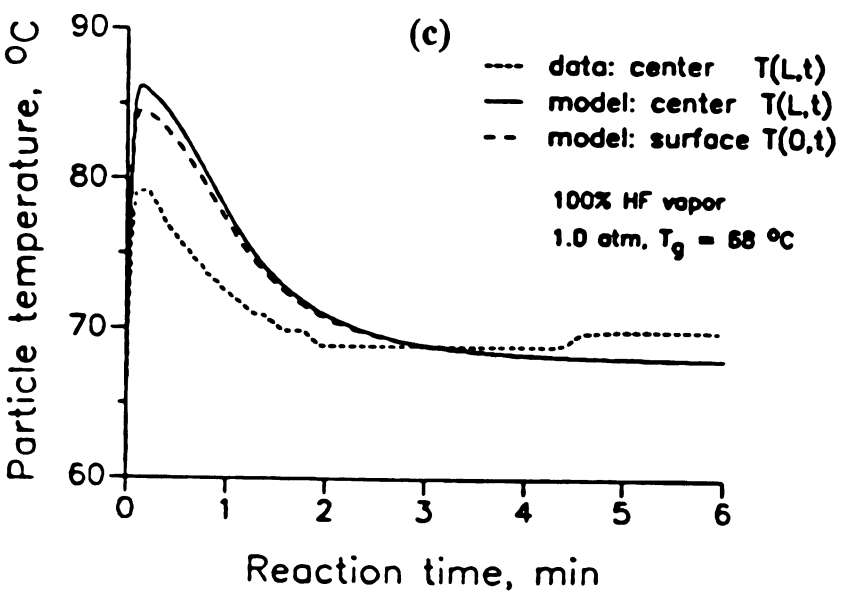
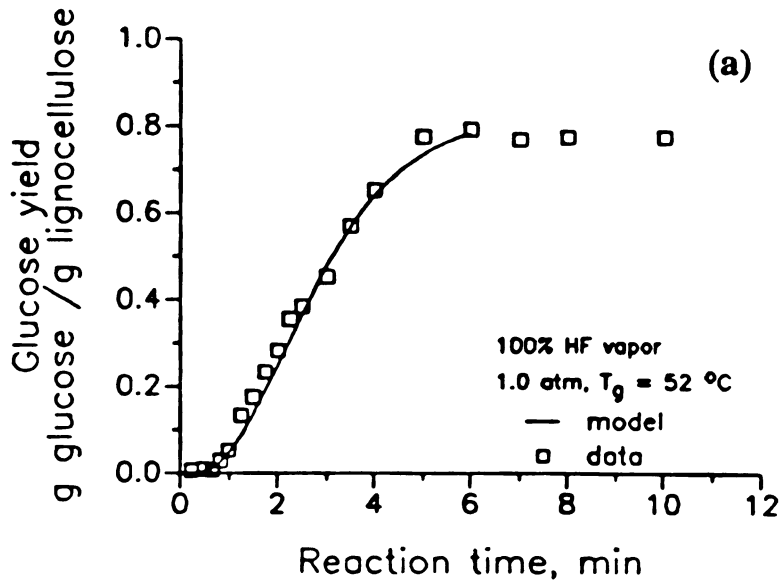
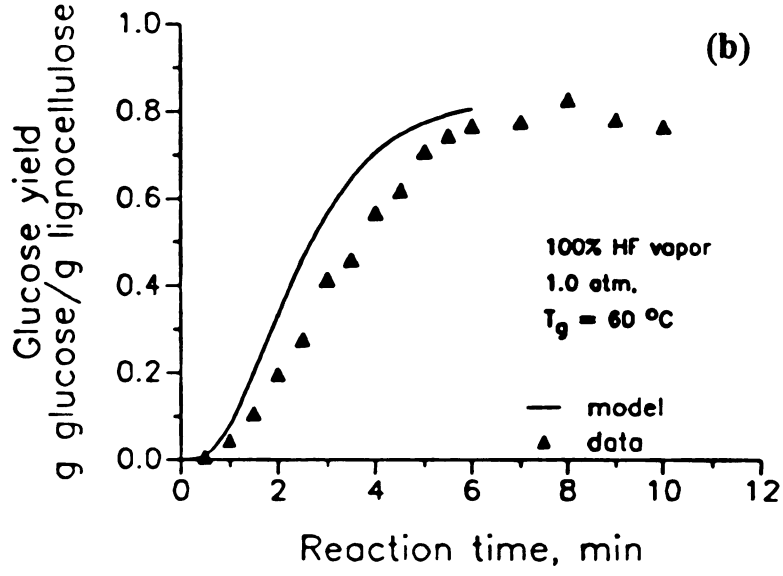
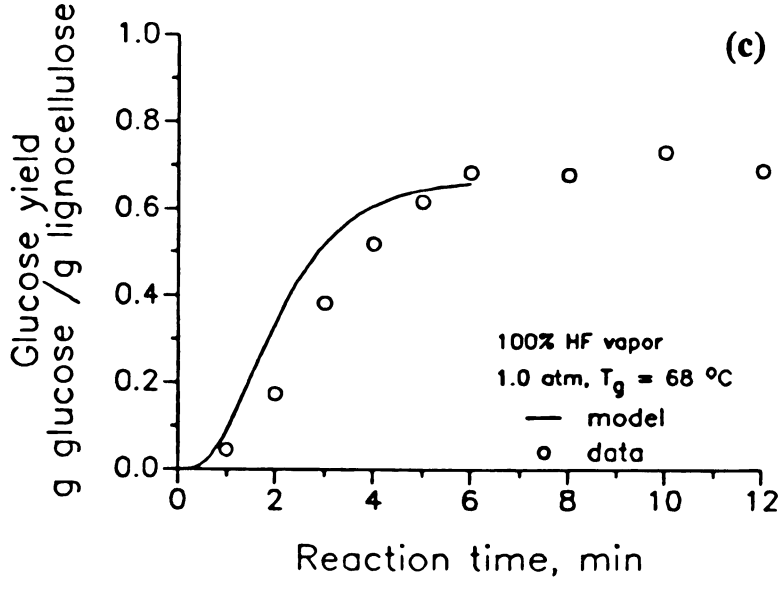

(c)
---- data: center T(L,t)
— model: center T(L,t)
-- model: surface T(0,t)
100% HF vapor
1.0 atm, T_g = 68 °C
Particle temperature, °C
90
80
70
60
0
1
2
3
4
5
6
Reaction time, min

Figure 10.2. Global glucose yield vs. reaction time profiles, $Y_g(t)$ vs. t, for the solvolysis of a single prehydrolyzed wood (lignocellulose) chip by a 100% HF vapor stream at 1.0 atm: data and model predictions compared. (a) T_g = 52 °C; (b) T_g = 60 °C; (c) T_g = 68 °C. Notes: G_{HF} = 0.42 g HF/cm^2-min, 2L = 0.4 mm (see Tables 10.1 and 10.2 for detailed reaction conditions).


(a)
Glucose yield
g glucose /g lignocellulose
1.0
0.8
0.6
0.4
0.2
0.0
0
2
4
6
8
10
12
Reaction time, min
100% HF vapor
1.0 atm, T_g = 52 °C
model
data


(b)
Glucose yield
g glucose/g lignocellulose
1.0
0.8
0.6
0.4
0.2
0.0
0
2
4
6
8
10
12
Reaction time, min
100% HF vapor
1.0 atm,
T_g = 60 °C
model
data


(c)
Glucose yield
g glucose /g lignocellulose
1.0
0.8
0.6
0.4
0.2
0.0
0
2
4
6
8
10
12
Reaction time, min
100% HF vapor
1.0 atm, T_g = 68 °C
model
data

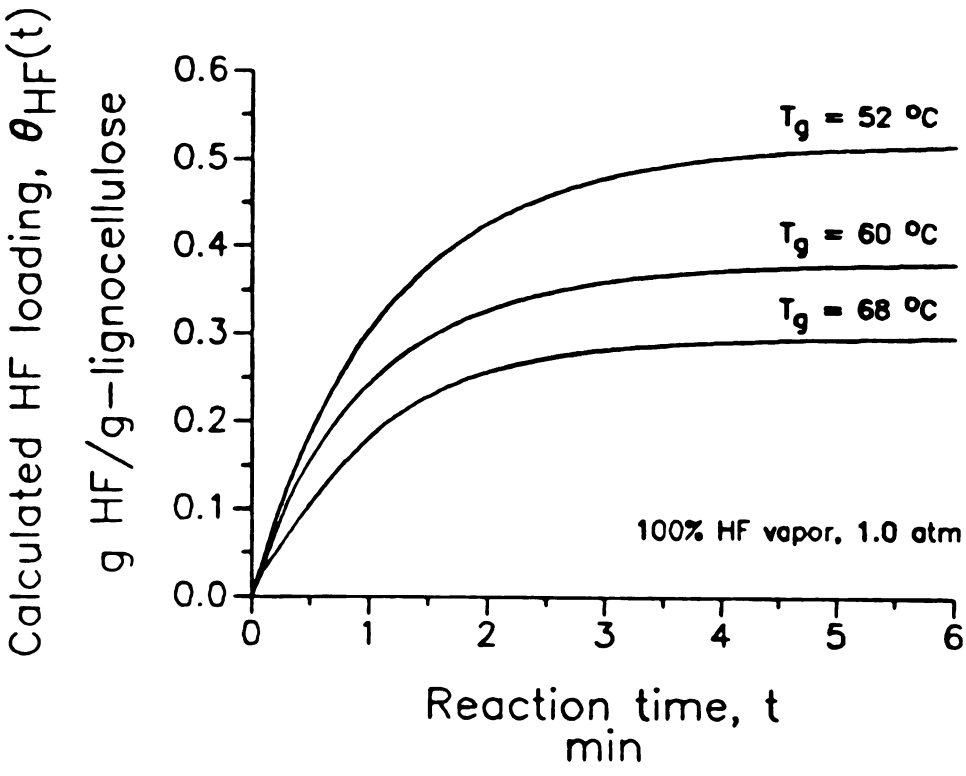


Figure 10.3. Model predictions for global gravimetric uptake of HF vapor onto a single, HF-reacting lignocellulose chip (2L = 0.4 mm), $\theta_{HF}(t)$, as a function of reaction time and 100% HF vapor temperature, T_g, at 1.0 atm. See Tables 10.1 and 10.2 for detailed reaction conditions.

2. The glucose yield vs. reaction time profile is sigmoidal

3. The global glucose production rate (the glucose yield vs. time profile) decreases with increasing HF vapor temperature at a fixed HF vapor partial pressure

Further, the model correctly predicts that heat transfer resistances are significant even when gas-phase mass-transfer resistances are minimized. Since the difference between the HF-reacting chip center temperature T(L,t) and surface temperature T(0,t) is small (usually less than 3 °C), external heat transfer resistances are dominant. However, for thicker lignocellulose chips, the intraparticle temperature gradients will be more significant.

As HF adsorbs onto the lignocellulose chip, the thermal properties of the HF-reacting lignocellulosic matrix change with time. The calculated effective thermal conductivity $k_e(L,t)$ and thermal diffusivity $\alpha_e(L,t)$ at the center of the HF-reacting lignocellulose chip at T_g = 60 °C are shown in Figures 10.4a and 10.4b respectively.

A detailed parametric sensitivity analysis was not performed. However, the model correctly predicts all the expected trends when the independent input variables are perturbed. For example, when the chip half-thickness "L" is increased, T(x,t) likewise increases, and the intraparticle temperature gradient along x is more significant. Also, when the film heat transfer coefficient "h" is increased, i.e., convective heat transfer from the particle surface to the surrounding HF vapor stream is improved, T(x,t) decreases.

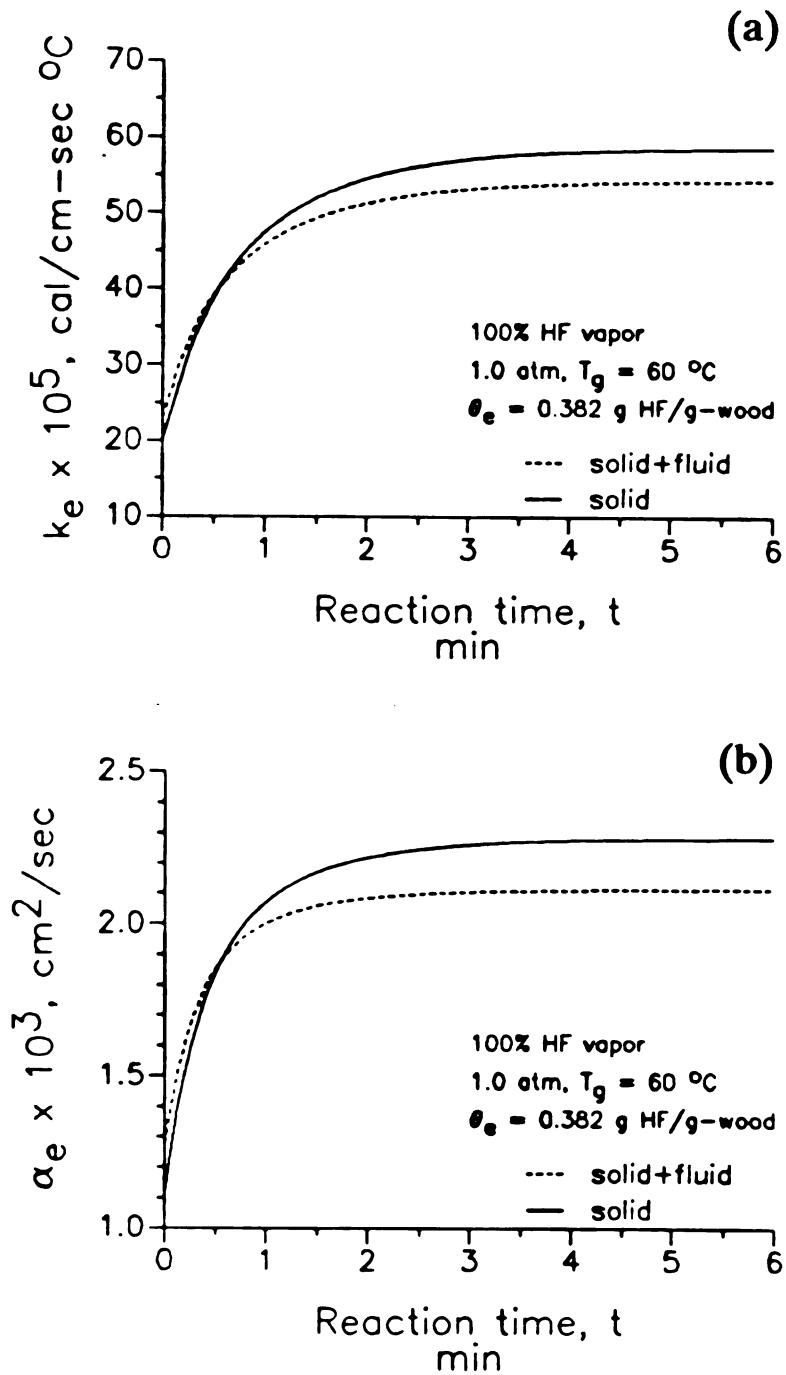


Figure 10.4. Thermal properties of the HF-reacting prehydrolyzed wood chip: model predictions for (a) the effective thermal conductivity, $k_e(L,t)$, and (b) the effective thermal diffusivity, $\alpha_e(L,t)$, at the chip centerline (2L = 0.4 mm). See Tables 10.1 and 10.2 for detailed reaction conditions at T_g = 60 °C.

B. A Discussion of the Differences Between Model Predictions and Data

I will now state the truisms of comparing model to data and offer some possible explanations for the differences between model predictions and data given in Figures 10.1 and 10.2.

In general, the agreement between model predictions and data is good. However, some discrepancies exist. By definition, a model is a simplified version of reality. Therefore, differences between model predictions and data are guaranteed to exist. In general, the source of the difference is due to failures in the model, failures in the experimental design, or both.

A detailed analysis of the differences between model and data ultimately requires that the assumptions used to develop and simplify the models be tested. Usually, the model assumptions which cannot be verified directly must be analyzed both experimentally and theoretically.

I will now discuss the two most prominent differences between model predictions and data. I will also point out possible limitations of the assumptions used in model development and experimental design.

Observation 1: model predictions for $X_3(t)$ are consistently higher than the complimentary glucose yield vs. time data at T_g = 60 °C and 68 °C. I offer three possible explanations for this difference between model predictions and data.

Explanation 1. The kinetic parameter estimates may be inaccurate, as cautioned in chapter 8. The validity of the kinetic parameter estimates is limited by the validity of the model and the experimental design.

Explanation 2. The differential material balance and kinetic model may be deficient in one or more respects. Given the complexity of the model and the many assumptions used in its development, model deficiences are hard to isolate, but I can think of two possiblities. First, the dependency of cellulose solvolysis rate on adsorbed HF concentration may be inaccurate, in particular, the assumption of letting adsorbed HF concentration potentials θ_1 and θ_2 be represented simply by the HF loading θ_e, and the subsequent assumption of letting $\theta_e(x,t)$ "float" with T(x,t). Recall that θ_1 and θ_2 cannot be separately determined by experiment. However, θ_e, which is measured experimentally, is the best approximation to adsorbed HF concentration potential that the cellulose perceives for solvolysis. Second, the rate constant k_2 for solvolytic cleavage of HF-solvated cellulose chains may be chain-length dependent, as discussed in chapter 8.

Explanation 3. The glucosyl fluoride yield in the HF-reacting lignocellulose chip is not quantified exactly as the glucose yield in the water-soluble reaction products after post hydrolysis. It is possible that unreacted ß-1,4 linked polyglucan fragments (D.P. 2 to 5), which are sparingly-soluble in water, are present in the water-soluble reaction products (D.P. > 5 are essentially insoluble). Since glucosyl fluoride production is quantified experimentally as glucose yield in the water-soluble reaction products after posthydrolysis, the presence of unreacted polyglucan fragments can affect the experimentally-determined reaction rate.

Observation 2: the calculated particle temperature vs. time profile T(L,t) is systematically diverging from the measured centerline particle temperature vs. time

profile as T_g increases from 52 °C to 68 °C. I offer four possible explanations for this discrepancy between model and data.

Explanation 1. The assumption of letting $T(x,0) = T_g$ is only approximately valid for particle temperature measurements, due to limitations on the experimental design. The lignocellulose chip temperature before reaction is usually lower than T_g, because as discussed in chapter 7, the lignocellulose chip must be inserted into the reactor from the outside. Therefore, the lignocellulose cannot be exactly preheated to the setpoint HF vapor stream temperature in the reactor. Further, once the sample access port is sealed, it takes approximately 15 seconds for the HF vapor stream temperature to stabilize around the T_g setpoint (see Figure 7.7). Therefore, T_g is not constant, although it is assumed so. Both of these effects will tend to lower the measured particle temperature as T_g increases. However, I did not attempt to incorporate $T_g(t)$ into the model calculation in order to bring model predictions for $T(L,t)$ closer to the measured particle temperature.

Explanation 2. The $-\Delta H_A(\theta_e)$ vs. θ_e correlation (equation [5-4]) may be inaccurate. Recall from chapter 5 that $\Delta H_A(\theta_e)$ at fixed θ_e was estimated by application of the Clausius-Clapeyron equation to equilibrium HF adsorption isotherm data; it was not measured by calorimetric measurement.

Explanation 3. The values for the film heat transfer coefficient "h" may be inaccurate. Recall from chapter 9 that "h" is estimated by a dimensionless Nusselt correlation (equation [9-17]); it is not measured directly. Further, the HF vapor property data used for estimating h, specifically, $C_{p,g}$, k_g, and μ_g vs. T_g (30 °C to

80 °C) at 1.0 atm, were sparse and possibly unreliable (see chapter 4).

Explanation 4. The effective thermal conductivity of the HF reacting lignocellulosic matrix was never measured directly; it was estimated by equations [10-21] to [10-23].

In conclusion, given the complexity of the combined material and energy balance model equations, and the many assumptions used to develop these equations, model deficiencies are hard to isolate, and some model assumptions are difficult to verify. In general, the difference between model and data are created by a variety of limitations, both experimental and theoretical. Analysis of these differences is further complicated by uncertainty of parameters estimated from the data, and the unreliablity or absence of the appropriate physical property data.

IV. Extended Model Predictions

In this section, I extend the differential energy balance and heat transport model to predict the energy release from a single HF-reacting lignocellulose chip. I also extend the differential material balance and kinetic model to predict the "nonisothermal effectiveness factor" under conditions where gas-phase mass-transfer resistances are minimized.

A. Energy Release

The release of energy from a single HF-reacting lignocellulose chip is calculated by integrating the heat flux from the chip face to the surrounding HF HF vapor stream over reaction time t. At time t, the differential heat flux q(t)

(cal/g-wood-sec) is calculated by

$$q(t) = h[T(0,t) - T_g] / (\rho_{LC} L) \quad [10\text{-}26]$$

In equation [10-26], the heat loss from the edges of the chip is neglected. All other assumptions for the differential energy balance and heat transport model are also assumed valid. At time t, the cumulative energy release Q(t) (cal/g-wood) is calculated by the integral

$$Q(t) = \frac{1}{\rho_{LC} L} \int_0^t h\,[T(0,t) - T_g]\,dx \quad [10\text{-}27]$$

Equation [10-27] is integrated numerically over time t by computer program TDIST3.BAS, which is listed in Appendix D. Values for T(0,t), the surface temperature of the HF-reacting lignocellulose chip, are needed as input.

Model calculations for Q(t) at T_g = 52 °C, 60 °C, and 68 °C are given in Table 10.4. Input parameters for calculation of Q(t) at each T_g are provided in Tables 10.1 to 10.3. Values for the calculated T(0,t) profile at each T_g were taken from Figures 10.1a, 10.1b, and 10.1c.

Also in Table 10.4, the isothermal energy release (Q_{iso}) is calculated by

$$Q_{iso} = \theta_e(T_g)\,(-\Delta H_A[\theta_e(T_g)]) \quad [10\text{-}28]$$

The calculated energy release Q(t) was not verified by direct calorimetric measurement. However, the energy release could be measured directly via differential scanning calorimetry (DSC), provided an HF-inert DSC cell is available.

Table 10.4. Model calculations for cumulative heat release.

T_g °C	θ_e [a] g HF/g	h cal/cm²-sec °C	Q(t) [b] cal/g-wood	$-\Delta H_A(\theta_e)$ [c] cal/g HF	Q_{iso} [d] cal/g-wood
52	0.519	0.0034	157	277	144
60	0.382	0.0021	141	318	122
68	0.297	0.0013	138	357	106

Notes:

[a] Calculated by equation [5-6].

[b] Calculated after t = 360 sec (6 min), given equation [10-28] and calculated T(0,t) values given in Figures 10.1a, 10.1b, and 10.1c.

[c] Calculated by equation [5-4].

[d] Calculated heat release for an isothermal particle (equation [10-28]).

B. Nonisothermal Effectiveness Factor

The nonisothermal effectiveness factor for sugar production within the HF-reacting ligocellulose chip under conditions where gas-phase mass-transfer resistances are minimized is defined as

$$\eta_1(t) = \frac{\frac{1}{L}\int_0^L X_3(x,t)\,\partial x}{X_3(t)\,|_{T_g}} \qquad [10\text{-}29]$$

Similarly, the nonisothermal effectiveness factor for gravimetric HF uptake is defined as

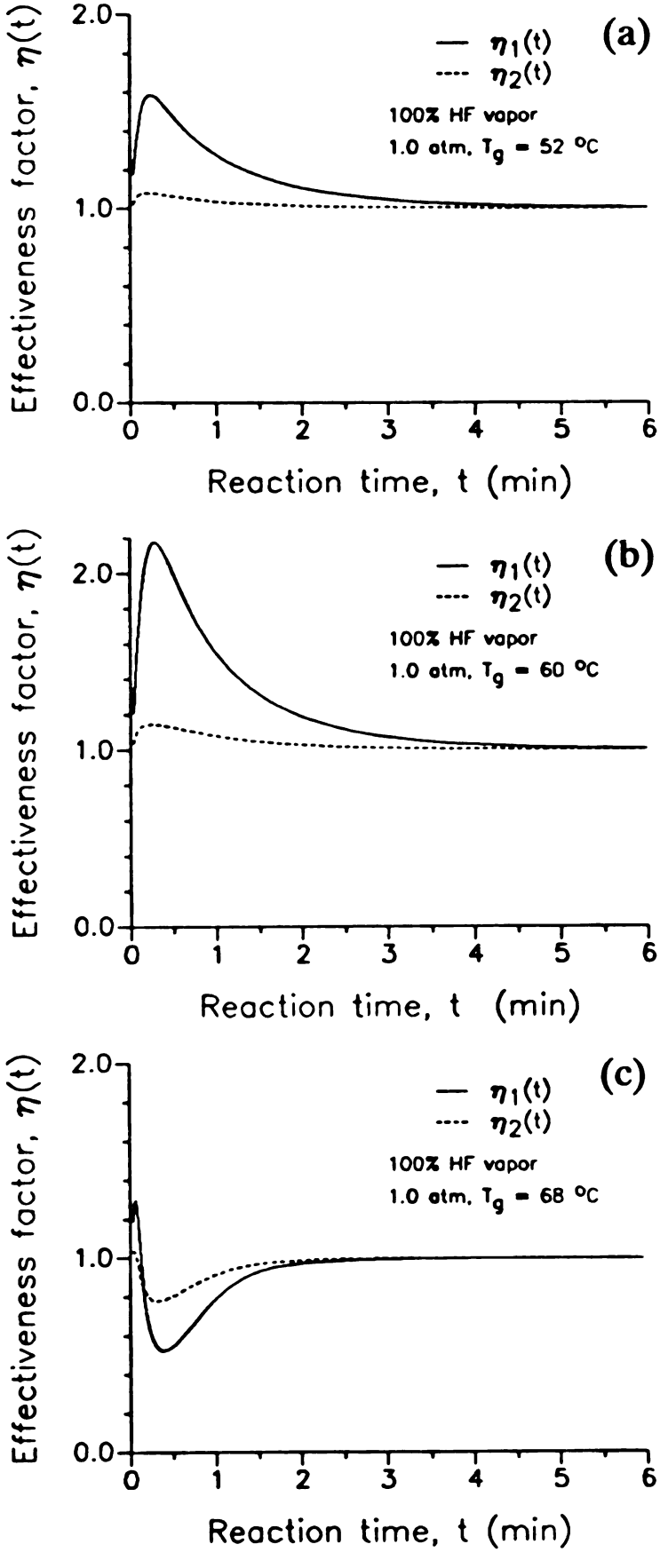
$$\eta_2(t) = \frac{\frac{1}{L}\int_0^L \theta_{HF}(x,t)\,\partial x}{\theta_{HF}(t)\,|_{T_g}} \qquad [10\text{-}30]$$

Since the solvolysis of a single lignocellulose chip by anhydrous HF vapor is unsteady state, the nonisothermal effectiveness factors $\eta_1(t)$ and $\eta_2(t)$ are functions of reaction time t.

The calculated nonisothermal effectiveness factors $\eta_1(t)$ and $\eta_2(t)$ at 100% HF vapor temperatures (T_g) of 52 °C, 60 °C, and 68 °C are shown in Figures 10.5a to 10.5c.

The nonisothermal effectiveness factor vs. time profile conveniently illustrates how the Arrhenius kinetics of cellulose solvolysis and the thermodynamics of HF physical adsorption oppose each other with increasing temperature, and how this

Figure 10.5. Model predictions for the nonisothermal effectiveness factor, $\eta(t)$, in the HF-reacting lignocellulose chip (2L = 0.4 mm) as a function of reaction time (t) and 100% HF vapor stream temperature (T_g). Note: gas-phase mass-transfer resistances are minimized; see Tables 10.1 and 10.2 for detailed reaction conditions.


(a)
— $\eta_1(t)$
---- $\eta_2(t)$
100% HF vapor
1.0 atm, T_g = 52 °C
Effectiveness factor, $\eta(t)$
2.0
1.0
0.0
0
1
2
3
4
5
6
Reaction time, t (min)
(b)
— $\eta_1(t)$
---- $\eta_2(t)$
100% HF vapor
1.0 atm, T_g = 60 °C
Effectiveness factor, $\eta(t)$
2.0
1.0
0.0
0
1
2
3
4
5
6
Reaction time, t (min)
(c)
— $\eta_1(t)$
---- $\eta_2(t)$
100% HF vapor
1.0 atm, T_g = 68 °C
Effectiveness factor, $\eta(t)$
2.0
1.0
0.0
0
1
2
3
4
5
6
Reaction time, t (min)

coupling determines the global dependence of glucose production rate with temperature. For example, if $\eta_1(t) < 1$, then adsorption is strongly influencing (limiting) the global rate of glucosyl fluoride (glucose) production. If $\eta_1(t) > 1$, then the intrinsic rate for cellulose solvolysis is strongly influencing the global rate of glucose production (i.e. cellulose solvolysis by adsorbed HF is becoming rate-controlling).

2546651

v.2
C.1

MICHIGAN STATE UNIVERSITY LIBRARIES
3 1293 00786 8213

LIBRARY
Michigan State
University

PLACE IN RETURN BOX to remove this checkout from your record.
TO AVOID FINES return on or before date due.

DATE DUE	DATE DUE	DATE DUE

MSU Is An Affirmative Action/Equal Opportunity Institution

c:\circ\datedue.pm3-p.1

SOLVOLYSIS OF A SINGLE LIGNOCELLUOSE PARTICLE BY ANHYDROUS HYDROGEN FLUORIDE VAPOR: REACTION RATE STUDIES, SUGAR YIELD STUDIES, AND DEVELOPMENT OF A DETAILED KINETIC AND HEAT TRANSPORT MODEL

VOLUME II

By

Gregory Lawrence Rorrer

A DISSERTATION

Submitted to
Michigan State University
in partial fulfillment of the requirements
for the degree of

DOCTOR OF PHILOSOPHY

Department of Chemical Engineering

1989

6043251

Chapter 11. Summary and Conclusions

In this chapter, the major results and conclusions of chapters 4 to chapter 10 are summarized. The significance of these results, and their applicability to process analysis and development, is then discussed. Finally, suggestions for future research are briefly overviewed.

Overview and Research Objectives

Biomass conversion processes produce useful chemical or fuels from renewable plant resources. This dissertation studied the "vapor-phase HF solvolysis of lignocellulose", a novel and potentially efficient biomass-conversion process which produces fermentable sugars and residual lignin from wood or agricultural residues. The fermentable sugars, glucose and xylose, are value-added chemical intermediates which can be fermented or catalytically processed to a spectum of useful chemical or liquid fuels, including, alcohols (e.g. ethanol, ketones, or organic acids.

The production of fermentable sugars and lignin by vapor-phase HF solvolysis of lignocellulose is carried out in several stages:

1. **HF-Adsorption and Reaction:**

* Diffusion of HF vapor into the lignocellulose particle
* Physical adsorption of HF vapor onto the lignocellulosic matrix
* Solvolysis of the glucan polymer cellulose to the monomer glucosyl fluoride by adsorbed HF

* Secondary reactions of glucosyl fluoride, including:

  In situ repolymerization (reversion) of glucosyl fluoride to water-soluble oligosaccharides and regeneration of HF

  In situ hydrolysis of glucosyl fluoride to glucose by water in the solid and regeneration of HF

2. HF-Desorption and Recycle:

Desorption of adsorbed HF by passing a hot, inert diluent gas over the HF-adsorbed/reacted solid; recycle of desorbed to a fresh charge of lignocellulose

3. Carbohydrate Recovery and Posthydrolysis:

* Separation of free sugars and sugar-oligomers from residual lignin

* Posthydrolysis of water-soluble sugar-oligomers to glucose

The vapor-phase HF solvolysis of lignocellulose is a promissing but largely unstudied biomass conversion technology. Chemical reaction engineering research is needed in three key areas of the overall process: HF-adsorption/reaction, sugar fluoride reversion/posthydrolysis, HF-desorption/recycle.

This dissertation focused on the adsorption/reaction stage of the process. Specifically, a chemical reaction engineering analysis was performed on the vapor-phase HF solvolysis of a single wood wafer under conditions where mass-transfer resistances were minimized.

This dissertation was organized into three major components: 1) experimental design (chapter 4); 2) expermental research program, including, HF-sorption, reaction rate, sugar yield, and particle temperature studies (chapters 5-7); and 3) reaction and transport modeling (chapters 8-10).

The specific research objectives of this dissertation are summarized below:

1. Document the technical feasibility of the vapor-phase HF solvolsyis of lignocellulose on a laboratory scale under carefully-controlled conditions

2. Study the adsorption and reaction processes using
   (a) gravimetric HF adsorption experiments
   (b) reaction rate and sugar yield experiments
   (c) particle temperature experiments

3. Determine maximum sugar yields and HF loading requirements

4. Develop a detailed kinetic and heat transport model

5. Provide a fundamental framework for bench- and pilot-scale process development studies

I. Summary of Major Results and Conclusions

The major results and conclusions, in the context of the afore-mentioned research objectives and the dissertation organization, are summarized next.

A. Technical Feasiblity

The technical feasibility of the vapor-phase HF solvolysis of lignocellulose for the production of fermentable sugars and residual lignin was verified on a laboratory scale under carefully-controlled conditions.

This laboratory-scale study documented that the vapor-phase HF solvolysis of lignocelulose offers:

1. **Rapid reaction rates at ambient reaction conditions.** For example, the reaction of a single wood wafer with an anhydrous HF vapor-stream at 1.0 atm and 30 ^{o}C was complete within 3 minutes.

2. **Production of solid-phase reaction products.** Sugar fluorides, reversion oligosaccharides reside on a porous, residual lignin matrix.

3. **Water soluble sugar-oligomer reaction products.** After vapor-phase HF solvolysis of a single wood wafer at the conditions described above, 78% of the original wood was rendered water soluble.

4. **High yields fermentable sugars after mild, dilute-acid posthydrolysis of the water-soluble reaction products.** Maximum glucose yields from Bigtooth Aspen wood averaged 0.52 g glucose/g-wood (85% of theoretical), and maximum xylose yields averaged 0.16 g xylose/g-wood (76% of theoretical). Maximum glucose yields from both prehydrolyzed (hemicellulose-free) wood and pure cellulose averaged 94% of theoretical.

Based on this benchmark laboratory-scale study, I conclude that the vapor phase HF solvolysis of lignocellulose offers high yields of fermentable sugars in short times at ambient processing conditions.

This vapor-phase HF solvolysis of lignocellulose also produces a residual lignin byproduct. However, in this dissertation, this residual "HF lignin" was not characterized. Furthermore, the suitablity of "HF lignin" as chemical feedstock was not evaluated.

Finally, this dissertation did not attempt a detailed technical evaluation on HF desorption and recovery. However, efficient and near 100% HF recovery / recycle is crucial to overall process technical feasibility and economics. Therefore, a detailed study of HF-desorption and recycle must be performed before the overall technical and economic feasiblity of the vapor-phase HF solvolysis can be evaluated and compared to other lignocellulose hydrolysis technologies.

B. Experimental Design and Research Program

The experimental reseach program focused on the adsorption and reaction processes of the vapor-phase HF solvolyis of a single lignocellulose chip via gravimetric HF adsorption experiments, reaction rate and sugar yield experiments, and particle temperature measurements.

Experimental Design (chapter 4). Four lignocellulosic substrates were considered in this dissertation: Bigtooth Aspen wood wafers, prehydrolyzed Bigtooth Aspen wood wafers, pure cellulose (filter paper) wafers, and filter paper/"milled-wood" lignin composite wafers.

The reaction of a single, dry lignocellulose wafer with an anhydrous HF vapor stream was studied with the aid of two carefully-controlled, milligram-scale, laboratory experiments. The gravimetric HF-adsorption experiment measured the HF loading on a single lignocellulose wafer as a function of time and HF vapor stream conditions. The vapor-phase HF solvolysis experiment measured sugar yield (cellulose conversion) and energy release (particle temperature) in the HF-reacting lignocellulose wafer as a function of reaction time and HF vapor conditions. Water-soluble reaction products were analyzed both before and after posthydrolysis by High-Performance Liquid Chromatography (HPLC). The glucosyl fluoride production and cellulose conversion was quantified experimentally as the glucose yield in the water-soluble reaction products after posthydrolysis.

In both experiments, experimental techniques were developed for handling HF vapor in a flow system. This information will be obviously valuable for the future

design and construction of bench- and pilot-scale reactors for the vapor-phase HF solvolysis of lignocellulose.

Gravimetric HF adsorption/desorption (chapter 5). The equilibrium HF loading on a single wood chip (g HF/g-wood) increased with increasing gas stream HF partial pressure (P_{HF}) and descreased with increasing gas stream temperature T_g) away from the normal boiling point of HF (19.54 °C).

In general, HF vapor phyiscally adsorbs onto lignocellulose. At low HF loadings, e.g. 0.4 g HF/g-wood (1.0 atm, 60 °C), HF adsorbs primarily on -OH groups on cellulose and hemicellulose, and HF is consumed by reaction to sugar fluorides. At high HF loadings, e.g. 1.5 g HF/g-wood (1.0 atm, 30 °C), multilayer adsorption and capillary condensation of HF vapor into lignocellulose micropores may also occur.

Reaction Rate Studies (chapter 6). When a single wood wafer (1.0 cm/side x 0.4 mm thick, 15 mg) was reacted with an anhydrous HF vapor stream at 1.0 atm, 30 °C, and 0.42 g HF/cm^2-min, maximum cellulose conversion was achieved within 3 minutes. At 50 °C, maximum cellulose conversion was achieved only after 6 minutes.

In general, The glucose yield vs. reaction time curve was sigmoidal. The overall glucose production rate increased with increasing gas-stream HF partial pressure (P_{HF}), but decreased with increasing gas-stream temperature (T_g).

The glucose production rate is dependent on the 1) unreacted glucan in lignocellulose, 2) HF loading on lignocellulose, and 3) reaction temperature. As the

temperature increases, the intrinsic rate constant for cellulose solvolysis increases, but the adsorbed HF on lignocellulose (θ_e) that the cellulose perceives for solvolysis decreases with increasing temperature, i.e., T ↑ k ↑ θ_e ↓. Thus, the Arrhenius kinetics of cellulose solvolysis and the thermodynamics of HF physical adsorption are coupled and work in opposing directions with increasing temperature. This coupling determines the overall decrease of glucose production rate with increasing temperature.

Maximum Glucose Yields and HF Loading Requirements (chapter 6). The HF adsorbed on lignocelluose was the stoichiometrically-limiting reagent. The minumum HF loading for complete solvolysis of cellulose in prehydrolyzed wood was about 0.4 g HF/g-lignocellulose. Lower HF loadings resulted in incomplete cellulose conversion and lowered glucose yields. Higher HF loadings did not affect the maximum glucose yield. A simple model was developed to predict maximum glucose yield as a function of 100% HF vapor temperature and HF loading.

Sugar Yield Comparisons (chapter 6). The solvolysis of a single lignocellulose wafer by anhydrous HF vapor at ambient conditions was rapid and resulted in a high yield of sugar fluorides, reversion sugar-oligomers, and residual lignin in solid form. After vapor-phase HF solvolysis, 78% of the total mass of the original wood wafer was rendered water soluble. A mild, dilute-acid posthydrolysis (e.g. 2 N TFA at 121 °C for 1 h) was required to convert the water-soluble sugar-oligomers to fermentable sugars.

After vapor-phase HF solvolysis and dilute-acid posthydrolysis of the water-soluble reaction products, high yields of fermentatable sugars were obtained: from Bigtooth Aspen wood, 0.52 g glucose/g-wood (85% of theoretical); from prehydrolyzed Bigtooth Aspen wood, 0.78 g glucose/g-lignocellulose (94% of theoretical); from filter paper, 93% of theoretical; and from filter paper/"milled-wood" lignin composite substrates, 94% of theoretical. The standard error (1 standard deviation) on the yield deteriminations was about +/- 2-3%.

In control experiments with the vapor-phase HF solvolysis of filter paper/MWL composite wafers of precisely known composition, HF-catalyzed condensation of sugar fluorides onto lignin was not observed. Glucose dehydration products, HMF and levoglucosan, were also not detected. However, residual carbohydrates (about 3% of the total potential glucan, 5% of total potential xylan) were recovered from the water-insoluble residue of the vapor-phase HF solvolysis of wood by a mild, dilute-acid hydrolysis. Therefore, if the whole HF-reacted solid is posthydrolyzed, then higher glucose yields are obtained.

Glucosyl Fluoride Reversion (chapter 6). During vapor-phase HF solvolysis of lignocellulose, glucosyl fluoride reaction products repolymerized to short-chain, water-soluble "reversion" oligosaccharides. The oligosaccharide distribution was measured by HPLC-oligosaccharide profiling of the water-soluble reaction products before posthydrolysis. Although the reaction of 100% HF vapor with pure cellulose was complete within 3 minutes, the oligosaccharide products took 12 minutes to settle down to an equilibrium product distribution. The extent of reversion

increased with increasing temperature. For the solvolysis of prehydrolyzed wood by 100% HF vapor at 30 °C, the equilibrium monomer yield before posthydrolysis was about 30% of the maximum theoretical, whereas at 52 °C, the equilibrium monomer yield before posthydrolysis was only 4-6% of theoretical.

Preliminary experiments showed that in situ methanolysis significantly shifted the reversion oligosaccharide product distribution back toward cellulose. When methanol-absorbed cellulose was reacted with 100% HF vapor at 30 °C, the equilibrium monomer yield before posthydrolysis was 60% of maximum theoretical, almost twice that for dry cellulose at the same conditions.

Particle Temperature Measurements (chapter 7). The centerline particle temperature of the HF-reacting lignocellulose rose rapidly to a maximum temperature (typically about 20 °C above the gas-stream temperature, T_g) and then slowly decayed back to T_g within 2 minutes. The particle temperature rise was largely dissipated before significant glucose yield was generated.

Apparently, heat transfer resistances are siginficant even when mass-transfer resistances are experimentally minimized. This is due to the high porousity and low thermal conductivity of the HF-reacting lignocellulosic matrix.

C. Modeling

Based on the behavior of the gravimetric HF adsorption data, the glucose yield vs. time data, and the particle temperature vs. time data, a detailed kinetic and heat transport model was developed. This model had two components: 1) the differential material balance and kinetic model, and 2) the differential material

balance and heat transport model. The combined model described HF-adsorption, cellulose solvolysis, energy release, and heat tranport processes within a single HF-reacting lignocellulose chip under conditions were mass-transfer resistances are minimized. The combined model required several constant input parameters, such as thermal properties of HF and lignocellulose, reaction rate constants, and heats of adsorption. These parameters were obtained from the literature or estimated from the data (heats of adsorption, chapter 5; kinetic parameters, chapter 8).

The combined, unsteady-state, differential material and energy balance model equations were solved by numerical solution techniques on computer. Computer model predictions for sugar product yield and particle temperature distribution in the HF-reacting lignocellulose chip as a function of reaction time and HF vapor stream conditions agreed quite well with the complimentary experimental data.

The detailed kinetic and heat transport model correctly predicted the following experimentally observed phenomena:

1. The rapid rise and slow decline of particle temperature over time
2. The sigmoidal profile of the glucose yield vs. time curve
3. The decrease in global glucose production rate with increasing 100% HF vapor temperature
4. The significance of heat transfer resistances even when gas-phase mass-transfer resistances are minimized

A fundamental limitation of the detailed kinetic and heat transport model was that it did not couple gas-phase film mass-transfer resistances and intraparticle

diffusion into the differential material balance equations. Therefore, the effect of mass-transfer resistances on model predictions for rates of sugar product yield and energy release could not be evaluated.

II. Significance

This dissertation described a benchmark study of the vapor-phase HF solvolysis of a single lignocellulose particle under carefully-controlled, laboratory-scale conditions.

The chemical reaction engineering analysis on the vapor-phase HF solvolysis of a single lignocellulose chip is of both practical and fundamental significance.

First, the process data verify and objectively document the technical feasibility of the vapor-phase HF solvolysis of lignocellulose. The process data and modeling are "intrinsic" and are thus independent of reactor or process configuration. Therefore, the data and modeling provide the benchmark analysis by which configurationally- dependent process data from a specific reactor or process can be meaningfully compared to process data from other reactors or processes. In addition, the process data provides valuable and concrete information that can be used to develop and guide bench and pilot-scale studies.

Second, the detailed kinetic and heat transport model can be extended to predict the effect of external and intraparticle mass-transport resistances in "big" wood chips during HF vapor/wood contacting and reaction. This extended model can then be coupled to noncatalytic gas/solid reactor models for HF vapor/wood contacting and reaction. These noncatalytic gas/solid reactor concepts might include

a packed-bed of HF-reacting wood chips in semibatch operation, or a fluidized bed of HF-reacting wood chips in continuous operation. Since these reactor models simulate process performance, reactor configurations can be screened by computational methods as opposed to empirical and expensive bench- or pilot-scale experimentation. By this computational screening procedure, only the most promissing reactor configurations will progress to the pilot-plant scale.

Finally, the research presented in this dissertation is of fundamental significance to the disciplines of chemical engineering and carbohydrate chemistry. The data and model describes the coupling of physical adsorption, reaction and heat transport in single, reacting particle. This analysis may be of fundamental interest to chemical reaction engineering, particularly in the area of unsteady-state, noncatalytic, gas/solid reactions within a single particle. Also unique to this research is the study of the reaction chemistry of anhydrous HF and carbohydrates in a highly-concentrated, solid-phase reaction medium.

III. Overview of Suggested Future Work

As mentioned earlier, the vapor-phase HF solvolysis of lignocellulose is a promissing but still largely unstuded biomass-conversion technology. Although this dissertation described a pioneering study which significantly advanced fundamental and practical knowledge in this area, the study was still very limited in scope. In general, research on the vapor-phase HF solvolysis of lignocellulose is still wide open. The researchers in this area should continue to be chemical engineers with a background in chemical reaction engineering, and chemists or biochemists with

interests in carbohydrate chemistry.

Some suggested avenues for future research, which are too numerous to describe in any detail, are listed next. Much of this suggested work is described in the relevant chapter of this dissertation. The specific projects are organized according to the three major research opportunities for chemical reaction engineering research: HF-adsorption/reaction, sugar fluoride reversion/ posthydrolysis, and HF-desorption/recovery. The rationale for research in each of these areas is described in chapter 3.

A. Single particle studies

HF-adsorption/reaction:

1. Continued external and intraparticle gas-phase mass-transfer experiments
2. Couple external and intraparticle gas-phase mass-transfer resistances to the detailed kinetic and heat transport model
3. Continued particle temperature measurements within "thick" chips
4. Direct measurement of heat release via Differential-Scanning Calorimetry
5. Continued unsteady-state gravimetric HF-adsorption experiments
6. Improved kinetic model, i.e. chain-length dependent rate constants for cellulose solvolysis
7. Improved kinetic parameter estimation schemes with model polysaccharides (e.g. cellobiose)
8. Gel-Permeation Chomatographic analysis of unreacted cellulose for analysis of the solvolytic chain-cleavage mechanism (e.g. random, end-preferred)
9. Experimental and computational analysis of HF vapor pore-condensation in cell-wall micropores and pore-size distribution measurements of the HF-reacted solid

Sugar fluoride reversion/posthydrolysis:

1. Glucosyl fluoride reversion experiments and development of sugar-oligomer analysis techniques, including, aqueous gel-permeation chromatography and Hakomori methylation for glycosidic linkage analysis

2. Kinetic model for glucosyl fluoride reversion and and sugar-oligomer equilibrium

3. Inhibition of glucosyl fluoride repolymerization by in situ hydrolysis, methanolysis, or other in situ reaction chemistries

4. Possible HF-catalyzed condensation of hemicellulose onto lignin or other hemicellulose degradation products

HF desorption:

1. Kinetics, mass transfer, and thermodynamics of HF desorption

2. Fluoride retention in the HF-desorbed solid

Other Studies:

1. Effect of substrate moisture content on HF-adsorption, reaction/rate sugar yield, sugar fluoride repolymerization, and HF-desorption

2. Residual lignin:
   (a) Physical and chemical characterization as a function of reaction conditions, e.g. solubility, Klason lignin, molecular weight profiling
   (b) Product utilization studies

3. HF vapor physical property estimation: HF-N_2 gas diffusivity

B. Process Development Studies

1. Couple single-particle models to heterogeneous reactor models for gas/solid contacting and reaction, e.g. packed bed, moving bed, fluidized bed

2. Perform reactor simulations to screen for promissing reactor concepts

3. Test the technical feasibility of the most promissing concept: construct bench-scale unit, perform parametric study, compare model simulations to process data.

A Concluding Comment

To summarize, although this research program was fundemental in scope, its goals were practical and were directed toward technical realization of an efficient process concept for the vapor-phase HF solvolysis of lignocellulose.

APPENDICES

APPENDIX A

LIST OF REFERENCES

LIST OF REFERENCES

Adamson, A. W. (1982). **Physical Chemistry of Surfaces**, 4th Edition. Wiley: New York.

Albersheim, P., Nevins, D. J., English, P. D., Karr, A. (1967). A method for the analysis of sugars in plant cell-wall polysaccharides by gas-liquid chromatography. **Carbohydrate Research, 5**, 340-345.

Allied Chemical Corporation (1978). **Hydrofluoric acid.** Industrial Chemicals Division, Morristown NJ, U.S.A.

Allied Chemical Corporation (1984). **First aid treatment for hydrofluoric acid burns.** Industrial Chemicals Division, Morristown, NJ, U.S.A.

American Society for Testing and Materials (ASTM) (1984). Standard method for preparation of extractive-free wood. Standard method #D1105-84.

Antonoplis, R. A., Blanch, H. W., Freitas, R. P., Sciamanna, A. F., and Wilke, C. R. (1983). Production of sugars from wood using high-pressure hydrogen chloride. **Biotechnology and Bioengineering, 25**, 2757-2773.

Baker, C. E. (1967). Thermal conductivities of gaseous HF, DF, and the equimolar HF-DF mixture. **Journal of Chemical Physics, 46**, 2846-2848.

Barnett, J. E. G. (1969). Acid and alkaline hydrolysis of glycopyranosyl fluorides. **Carbohydrate Research, 9**, 21-31.

Beck, J. V., and Arnold, K. J. (1977). **Parameter Estimation in Engineering and Science.** Wiley: New York, p. 334-418.

BeMiller, J. N. (1967). Acid-catalyzed hydrolysis of glycosides. **Advances in Carbohydrate Chemistry, 22**, 25-108.

Bentsen, T. and Kau, M. (1981). Solvolyse af halmcellulose ved hjaelp af fluorbrinte (meddelelser fra Bioteknisk Institut). **Afdeling for Bioteknologi, 1-4**, 4-11.

Bentsen, T. (1982). Hydrolysis of carbohydrates using a hydrogen fluoride pretreatment (meddelelser fram Bioteknisk Institut). **Afdeling for Bioteknologi, 3-4**, 40-42.

Bentsen, T. (1982). Hydrolysis of carbohydrates in straw using a hydrogen fluoride pretreatment. In: **Energy from Biomass: Second E. C. Conference**, A. Strub, P. Chartier, and G. Schleser, Eds. Applied Science Publishers: London, p. 1103-1105.

Bjorkman, A. (1956). Studies on finely divided wood. Part 1. Extraction of lignin with neutral solvents. **Svensk Papperstidning, 59**, 477-485.

Bjorkman, A., and Person, B. (1957a). Studies on finely divided wood. Part 2. The properties of lignins extracted with neutral solvents from hardwoods and softwoods. **Svensk Papperstidning, 60**, 158-169.

Bjorkman, A. (1957b). Studies on finely divided wood. Part 3. Extraction of lignin-carbohydrate complexes with neutral solvents. **Svensk Papperstidning, 60**, 245-251.

Bjorkman, A. (1957c). Studies on finely divided wood. Part 4. Some reactions of the lignin extracted by neutral solvents from Picea abies. **Svensk Papperstidning, 60**, 285-292.

Bjorkman, A. (1957d). Studies on finely divided wood. Part 5. The effect of milling. **Svensk Papperstidning, 60**, 329-335.

Blackwell, J. (1980). The structures of cellulose and chitin. In: **Biomolecular Structure, Conformation, Function, and Evolution, Vol. I: Diffraction and Related Studies**, R. Srinivasan, Ed. Pergamon Press: Oxford, p. 523-535.

Braker W., and Mossman A. L. (1971). Hydrogen fluoride. In: **Matheson Gas Data Book**. Matheson Gas Products, East Rutherford, NJ, U.S.A., p. 305-309.

Briegleb, G., and Strohmeier, W. (1953). Uber den assoziationszustand des fluorwasserstoffs im gaszustand II. **Zeitschrift fur Elektrochemie, 57**, 668-674.

Browning, B. L. (1971). Wood. In: **Encyclopedia of Polymer Science and Technology, Vol. 15**, p. 1-40.

Carnahan, B. A., Luther, H. A., and Wilkes, J. O. (1969). **Applied Numerical Methods**. Wiley: New York.

Clark, I. T. (1962). Determination of lignin by hydrofluoric acid. **TAPPI, 45**, 310-314.

Cooper, D., Douglas, M., Ali, O., Afrashtehfar, S., Ng, D., and Cooke, N. (1985). A low-pressure, low-temperature process for the conversion of wood to liquid fuels and chemicals using hydrogen iodide. In: **Fifth Canadian Bioenergy R&D Seminar**, S. Hasnain, Ed. Elsevier Applied Science: London, p. 455-459.

Costa, E. C., and Smith, J. M. (1971). Kinetics of noncatalytic, nonisothermal, gas-solid reactions: hydrofluorination of uranium dioxide. **AIChE Journal, 17,** 947-958.

Cote, W. A. (1977). Wood ultrastructure in relation to chemical composition. In: **Recent Advances in Phytochemistry, Vol. 11: The Structure, Synthesis, and Degradation of Wood**, F. A. Loewus, and V. C. Runeckles, Eds. Plenum Press: New York, p. 1-44.

Daniel, J. R. (1985). Cellulose, Structure and Properties. In: **Encyclopedia of Polymer Science and Technology, Vol. 3,** 2nd Edition, p. 90-123.

Defaye, J., Gadelle, A., and Pedersen, C. (1982). The behavior of cellulose, amylose, and xylan towards anhydrous hydrogen fluoride. **Carbohydrate Research, 110,** 217-227.

Defaye, J., Gadelle, A., Papadopoulos, J., and Pedersen, C. (1983). Hydrogen fluoride saccharification of cellulose and lignocellulosic materials. **Journal of Applied Polymer Science: Applied Polymer Symposium 37,** 653-670.

Denbigh, K. (1981). **The Principles of Chemical Equilibrium,** 4th Edition. Cambridge University Press: Cambridge, UK.

De Ruiter J. M., and Burns, J.C. (1986). Rapid determination of cell wall monosaccharides in flaccidgrass. **Journal of Agricultural and Food Chemistry, 34,** 780-785.

Downey, K. W., Selke, S. M., Hawley, M. C., and Lamport, D. T. A. (1983). HF solvolysis of wood for ethanol production: preliminary design, economics, and identification of needed research. In: **Proceedings of the Seventh International FPRS Industrial Wood Energy Forum** (Nashville , TN, Sept. 19-21, 1983).

Fanta, G. F., Abbott, T. P., Herman A. I., Burr, R. C., and Doane, W. M. (1984). Hydrolysis of wheat straw hemicellulose with trifluoroacetic acid. Fermentation of xylose with Pachysolen tannophilus. **Biotechology and Bioengineering, 26,** 1122-1125.

Fengel, D., Wegener, G., Heizmann, A., and Przyklenk, M. (1977). Trifluoressigsaure zur schnellen und schonenden hydrolyse von cellulose und anderen polysacchariden. **Holzforschung, 31,** 65-71.

Fengel, D., and Wegener, G. (1979). Hydrolysis of polysaccharides with trifluoroacetic acid and its application to rapid wood and pulp analysis. In: **Hydrolysis of Cellulose: Mechanisms of Enzymatic and Acid Catalysis,** R. D. Brown and L. Jurasek, Eds. American Chemical Society: Washington, D. C., p. 145-158.

Fengel, D., and Wegener, G. (1984). **Wood Chemistry, Ultrastructure, Reactions.** Walter de Gruyter: New York.

Finkel, A. J. (1973). Treatment of hydrogen fluoride burns. In: **Advances in Fluorine Chemistry, Vol. 7,** J. C. Tatlow et al. Eds. Butterworths Publishers: London, p. 199-203.

Frank, E. U., and Spalthoff, W. (1953). Das abnorme warmeleitvermogen gasformigen fluorwasserstoffs. **Naturwissenschaften, 40,** 580.

Franck, E. U., and Spalthoff, W. (1957). Fluorwasserstoff I. Spezifische warme, dampfdruck und dichte bis 300 C und 300 at. **Zeitschrift fur Elektrochemie, 61,** 348-357.

Frank, E. U., and Meyer, F. (1959). Fluorwasserstoff III. Spezifische warme und assoziation im gas bei neidrigem druck. **Zeitschrift fur Elektrochemie, 63,** 571-582.

Franz, R., Erckel, R., Reihm, T., and Woernle, R. (1982). Lignocellulose Saccharification by HF. In: **Energy From Biomass: Second E. C. Conference,** A. Strub, P. Chartier, and G. Schleser, Eds. Elsevier Applied Science Publishers: London, p. 873-878.

Franz, R., Fritsche-Lang, W., Deger, H.-M., Erckel, R., and Schlingmann, M. (1987). The behavior and derivatizations of carbohydrates in hydrogen fluoride. **Journal of Applied Polymer Science, 33,** 1291-1306.

Fredenhagen, K., and Cadenbach, G. (1933). Der Abbau Cellulose durch Fluorwasserstoff und ein neues Verfahren der Holzverzuckerung durch Hochkonzentrierten Fluorwasserstoff. **Agnewandte Chemie, 46,** 113-117.

Gall, J. F. (1980). Hydrogen fluoride. In: **Kirk-Othmer Encyclopedia of Chemical Technology, Vol. 10,** 3rd Edition, p. 733-753.

Gilrane, W. Personal communication. Wardrop, Inc., Winnepeg, Mannitoba, Canada. Jan. 29, 1988.

Glasser, W. G., Barnett, C., and Sano, Y. (1983). Classification of lignins with different genetic and industrial origins. **Journal of Applied Polymer Science: Applied Polymer Symposium 37**, 441-460.

Goldstein, I. S. (1983). Acid processes for cellulose hydrolysis and their mechanisms. In: **Wood and Agricultural Residues: Research on Use for Feed, Fuels, and Chemicals**, E. J. Soltes, Ed. Academic Press: New York, p. 315-328.

Gore, J. (1869). On hydrofluoric acid. **Journal of the American Chemical Society, 22**, 396-406.

Grethlein, H. E. (1985). The effect of pore size distribution on the rate of enzymatic hydrolysis of lignocellulosic substrates. **Bio/Technology, 3**, 155-160.

Hakomori, S. (1964). A rapid permethylation of glycolipid and polysaccharide catalyzed by methylsulfinyl carbanion in dimethyl sulfoxide. **Journal of Biochemistry, 55**, 205-207.

Hamilton, J. K., and Mitchell, R. L. (1965). Cellulose. **In: Encyclopedia of Polymer Science and Technology, Vol. 3**, p. 131-229.

Hardt, H., and Lamport, D. T. A. (1982a). Hydrogen fluoride saccharification of wood: lignin fluoride content, isolation of α-D-glucopyranosyl fluoride and posthydrolysis of reversion products. **Biotechnology and Bioengineering, 24**, 903-918.

Hardt, H., and Lamport, D. T. A. (1982b). Hydrogen fluoride saccharification of cellulose and xylan: isolation of α-D-glucopranosyl fluoride and α-D-xylospyranosyl fluoride intermediates, and 1,6-anhydro-ß-D-glucopyranose. **Phytochemistry, 21**, 2301-2303.

Harris, J. F. (1975). Acid hydrolysis and dehydration reactions for utilizing plant carbohydrates. **Journal of Applied Polymer Science: Applied Polymer Symposium 28**, 131-144.

Hawley, M. C., Selke, S. M., and Lamport, D. T. A. (1983). Comparison of hydrogen fluoride saccharification of lignocellulosic materials with other saccharification technologies. **Energy in Agriculture, 2**, 219-244.

Hawley, M. C., Downey, D. W., Selke, S. M., and Lamport, D. T. A. (1986). Hydrogen fluoride saccharification of lignocellulosic materials. In: **Cellulose: Structure, Modification, and Hydrolysis**, R. A. Young and R. M. Rowell, Eds. Wiley: New York, p. 297-321.

Heerema, J., Bollenback, G. N., and Linn, C. B. (1958). The catalyzed condensation of aromatic compounds with carbohydrates. 1-Deoxy-1,1-bis-(3,4-dimethylphenyl)-D-glucitol. **Journal of the American Chemical Society, 80,** 5555-5558.

Helferich, B., and Bottger, S. (1929). Die einwirkung von fluorwasserstoff auf cellulose. **Justus Liebiegs Annalen der Chemie, 476,** 150-170.

Helferich, B., Starker, A. and Peters, O. (1930). Die einwirkung von fluorwasserstoff auf starke. **Justus Liebiegs Annalen der Chemie, 482,** 183-188.

Helferich, B., and Peters, O. (1932). Einwirkung von fluorwasserstoff auf kohlenhydrate. **Justus Liebiegs Annalen der Chemie, 494,** 101-106.

Hu, J.-H., White, D., and Johnson, H. L. (1953). The heat capacity, heat of fusion and heat of vaporization of hydrogen fluoride. **Journal of the American Chemical Society, 75,** 1232-1236.

Husain, H. (1987). Acid for chips. **Bio-joule, 9,** 8-10.

I. G. Farbenindustrie AG (1932). Deutsches Reich Patentschrift 560535 (Oct. 5, 1932). Inventors: Fredenhagen, K., and Helferich, B.

I. G. Farbenindustrie AG (1933a). Deutsches Reich Patentschrift 577764 (June 3, 1933). Inventors: Fredenhagen, K., Helferich, B., and Koch, E.

I. G. Farbenindustrie AG (1933b). Deutsches Reich Patentschrift 585318 (Oct. 2, 1933). Inventors: Pfleiderer, G., and Koch, E.

Ishii, T., and Hiroi, T. (1986). Anhydrous hydrogen fluoride saccharification of lignocellulosic materials. I. Enzymic saccharification of pulp treated with anhydrous hydrogen fluoride. **Mokuzai Gakkaishi, 32,** 615-620.

Jarry, R. L., and Davis, W. (1953). The vapor pressure, association, and heat of vaporization of hydrogen fluoride. **Journal of Physical Chemistry, 57,** 600-604.

Johnson, G. K., Smith, P. N., and Hubbard, W. N. (1973). The enthalpies of solution and neutralization of HF (l); enthalpies of dilution and derived thermodynamic properties of HF (aq). **Journal of Chemical Thermodynamics, 5,** 793-809.

Kraska, K., and Micheel, F. (1976). Synthetische polysaccharide mit D-glucose und 3,6-anhydro-D-glucoseresten. **Carbohydrate Research, 49,** 195-199.

Lamport, D. T. A., Hardt, H., Smith, G., Morlok, S, Hawley, M. C., Chapman, R., and Selke, S. M. (1981). HF saccharification: the key to ethanol from wood?. In: **Energy from Biomass: First E. C. Conference,** W. Palz, P. Chartier, and D. O. Hall, Eds. Applied Science Publishers: London, p. 292-297.

Lenard, J. (1969). Reactions of proteins, carbohydrates, and related substances in liquid hydrogen fluoride. **Chemical Reviews, 69,** 625-638.

Long, R. W., Hildebrand, J. H., and Morrell, W. E. (1943). The polymerization of gaseous hydrogen and deuterium fluorides. **Journal of the American Chemical Society, 65,** 182-187.

Luers, H. (1937). Der heutige stand der holzverzuckerung. **Holz als Roh und Werkstoff, 1,** 35-40.

Luers, H. (1938). Das holzverzuckerungsverfahren mit fluorwasserstoff von Hoch und Bohunek. **Holz als Roh und Werkstoff, 1,** 342-344. See also: Meyerhofer, G., Bohunek, H., and Hoch, H. (1936). Osterreichisches Patentschrift 147494.

McDermott, J. B., and Klein, M. T. (1986). Chemical and probabilistic modeling of complex reactions: a lignin depolymerization example. **Chemical Engineering Science, 41,** 1053-1060.

McDermott, J. B. (1986). **Chemical and probabilistic modeling of complex reactions: a lignin depolymerization example.** Ph.D. Dissertation, University of Delaware.

Micheel, F. and Klemer, A. (1961). Glycosyl fluorides and azides. **Advances in Carbohydrate Chemistry, 16,** 85-103.

Mohring, W. M. (1987). **Gravimetric analysis of hydrogen fluoride vapor absorption by bigtooth aspen wood.** M. S. Thesis, Michigan State University.

Montroll, E. W., and Simha, R. (1940). Theory of depolymerization of long-chain molecules. **Journal of Chemical Physics, 8,** 721-727.

Morrison, R. T., and Boyd, R. N. (1977). **Organic Chemistry,** 3rd Edition. Allyn and Bacon: Boston.

Mort, A. J., and Parker, S. (1982). The use of anhydrous HF solvolysis in conversion of biomass to glucose. In: SERI Report SERI/232-1520.

Mort, A. J. (1983). An apparatus for safe and convenient handling of anhydrous, liquid hydrogen fluoride at controlled temperatures and reaction times. Application to the generation of oligosaccharides from polysaccharides. **Carbohydrate Research, 122,** 315-321.

Mort, A. J., Knirel, Y. A., Vinogradov, E. V. (1988). Application of anhydrous hydrogen fluoride for structural analysis of carbohydrates. **Journal Carbohydrate Chemistry** (in press).

Mort, A. J., Komalavilas, P., Rorrer, G. L., and Lamport, D. T. A. (1989). Anhydrous Hydrogen Fluoride and Cell Wall Analysis. In: **Modern Methods of Plant Analysis, Vol. 10: Plant Fibers,** H. F. Linskens and J. F. Jackson, Eds. Springer Verlag: Berlin-Heidelberg, p. 37-69.

Neely, W. B. (1960). Dextran: structure and synthesis. **Advances in Carbohydrate Chemistry, 15,** 341-369.

Nelson, M. L. (1960). Apparent activation energy of hydrolysis of some cellulosic materials. **Journal of Polymer Science, 63,** 351-371.

Ostrovski, C. M., Duckworth, H. E., and Aitken, J. C. (1984). Canertech's ethanol-from-cellulose program. In: **Fifth Canadian Bioenergy R&D Seminar,** S. Hasnain, Ed. Elsevier Applied Science: London, p. 478-482.

Ostrovski, C. M., Aitken, J. C., and Free, D. (1984). New developments in fuel ethanol production by gaseous anhydrous hydrofluoric acid hydrolysis of hardwood, Populus tremuloides. In: **Bio-Energy 1984 Proceedings, Vol. 3: Biomass Conversion** (Gothenburg Sweden, June 15-21, 1984), H. Egneous, and A. Ellegard, Eds.

Ostrovski, C. M., Aitken, J. C., and Hayes, R. D (1985). Hydrolysis of poplar wood using hydrofluoric acid for the production of fuel ethanol. In: **Proceedings from Energy from Biomass and Wastes IX** (Jan. 28 to Feb. 1, 1985, Buena Vista, FL), D. L. Klass, Ed. p. 895-913.

Papadopoulos, J. (1985). Acid hydrolysis for the conversion of cellulosic biomass to ethanol. In: **Proceedings of the E. C. Conference on Energy from Biomass.** Applied Science Publishers: London, p. 697-701.

Papadopoulos, J., and Defaye, J. (1986). Characterization of the lignin isolated from birch wood after extraction with hydrogen fluoride. **Journal of Wood Chemistry and Technology, 6,** 203-218.

Parham, R. A., and Gray, R. L. (1984). Formation and structure of wood. In: **The Chemistry of Solid Wood**, R. Rowell, Ed. American Chemical Society: Washington, D. C., p. 3-56.

Perry, R. H., and Chilton, C. H. (1973). **Chemical Engineer's Handbook**, 5th Edition. McGraw Hill: New York.

Pettersen R. C., Schwandt, V. H., and Effland, M. (1984a). An analysis of the wood sugar assay by HPLC: a comparison with paper chromatography. **Journal of Chromatographic Science, 22**, 478-484.

Pettersen, R. C. (1984b). The chemical composition of wood. In: **The Chemistry of Solid Wood**, R. Rowell, Ed. American Chemical Society: Washington, D. C., p. 57-126.

Petersen, E. E. (1965). **Chemical Reaction Analysis**. Prentice Hall: Englewood Cliffs, NJ, p. 129-167.

Posey, J. C. (1953). Report K-1063, Oak-Ridge Gaseous Diffusion Plant, Union Carbide Nuclear Co., Oak Ridge, TN.

Reffstrup, T., and Kau, M. (1985). Hydrogen fluoride aided hydrolysis of lignocellulosic biomass: development of a fast continuous process. In: **New Approaches to Research in Cereal Carbohydrates**, R. Hill, and L. Munck, Eds. Elsevier Applied Science Publishers: Amsterdam, p. 313-317.

Rogovin, Z. A., and Pogosov, Y. L. (1958). **Gidroliz. i. Lesokhim. Prom., 1**, 4-6 (**Chemical Abstracts, 52**, 8453i).

Rogovin, Z. A., and Pogosov, Y. L. (1959). The composition and structure of the products of cellulose hydrolysis and gluocose polycondensation under the action of concentrated hydrofluoric acid. **Nauch. Doklady Vysshei Shkoly, Khim i Khim. Tekhnol., 2**, 368-375 (**Chemical Abstracts, 53**, 22912h).

Sachs I. B., Clark I. T., and Pew J. C. (1963). Investigation of lignin distribution in the cell wall of certain woods. **Journal of Polymer Science: Part C, 2**, 203-212.

Sanger, M. P., and Lamport, D. T. A. (1983). A microapparatus for liquid hydrogen fluoride solvolysis: sugar and amino sugar composition of Erysiphe graminis and Triticum aestivum cell walls. **Analytical Biochemistry, 128**, 66-70.

Schaefer, C. A., and Thodos, G. (1959). Thermal conductivity of diatomic gases: liquid and gaseous states. **AIChE Journal, 5**, 367-372.

Selke, S. M., Hawley, M. C., Hardt, H., Lamport, D. T. A., Smith, G., and Smith, J. (1982). Chemicals from Wood via HF. **Industrial & Engineering Chemistry Product Research & Development, 21,** 11-16.

Selke, S. M., Hawley, M. C., and Lamport, D. T. A. (1983). Reaction rates for liquid phase hydrogen fluoride saccharification of wood. In: **Wood and Agricultural Residues: Research on Use for Feed, Fuels, and Chemicals,** E. J. Soltes, Ed. Academic Press: New York, p. 329-349.

Selke, S. M. (1983). **The kinetics of hydrogen fluoride saccharification of cellulose.** Ph.D. Dissertation, Michigan State University.

Sharkov, V. I., Bolotova, A. K., and Boiko, T. A. (1972). Wood hydrolysis by anhydrous hydrogen fluoride (translated from Russian). **Kompleks. Pererab. Rast. Syr'ya,** 39-49 (**Chemical Abstracts, 80,** 72199, 1974).

Sharples, A. (1957). The hydrolysis of cellulose and its relation to structure. **Transactions of the Faraday Society, 53,** 1003-1013.

Sharples, A. (1958). The hydrolysis of cellulose and its relation to structure. Part 2. **Transactions of the Faraday Society, 54,** 913-917.

Simha, R. (1941). Kinetics of degradation and size distribution of long chain polymers. **Journal of Applied Physics, 12,** 569-578.

Simons, J. H. (1950). Hydrogen fluoride. In: **Fluorine Chemistry,** J. H. Simons, Ed. Academic Press: New York, p. 225-259.

Skaar, C. (1984). Wood-water relationships. In: **The Chemistry of Solid Wood,** R. Rowell, Ed. American Chemical Society: Washington, D. C., p. 127-172.

Smith, D.F. (1958). Hydrogen fluoride polymer spectrum, hexamer and tetramer. **Journal of Chemical Physics, 28,** 1040-1056.

Smith, J. J, Lamport, D. T. A., Hawley, M. C., and Selke, S. M. (1983). Feasibility of using anhydrous hydrogen fluoride to "crack" cellulose. **Journal of Applied Polymer Science: Applied Polymer Symposium 37,** 641-651.

Smith, J. M. (1981). **Chemical Engineering Kinetics,** 3rd Edition. McGraw Hill: New York.

Spalthoff, W., and Franck, E. U. (1957). Fluorwasserstoff II. Die assoziation im gas bei hohen drucken. **Zeitschrift fur Elektrochemie,** 61, 993-1000.

Strohmeier, W., and Briegleb, G. (1953). Uber den assoziationszustand des HF im Gaszustand I. Neue experimentelle messungen. **Zeitschrift fur Elektrochemie, 57,** 662-667.

Timell, T. E. (1957). Carbohydrate composition of ten north american species of wood. **TAPPI, 40,** 568-572.

Vanderzee, C. E., and Rodenburg, W. W. (1970). Gas imperfections and excess thermodynamic properties of gaseous hydrogen fluoride. **Journal of Chemical Thermodynamics, 2,** 461-478.

Wegner, T. et al. (13 authors). (1984). Wood. In: **Kirk-Othmer Encyclopedia of Chemical Technology, Vol. 24,** p. 579-611.

Wright, J. D., and Power, A. J. (1985). Concentrated halogen acid hydrolysis processes for alcohol fuel production. **Biotechnology and Bioengineering Symposium 15,** 511-532.

Wright, J. D, and Power, A. J. (1986). Comparative technical evaluation of acid hydrolysis processes for conversion of cellulose to ethanol. SERI Report SERI/TP-232-2957.

Young, R. A. (1986). Structure, swelling, and bonding of cellulose fibers. In: **Cellulose: Structure, Modification, and Hydrolysis,** R. A. Young and R. M. Rowell, Eds. Wiley: New York, p. 91-198.

Yu, E. K. C., Deschatelets, L., Levitin, N, and Saddler, J. N. (1984). Production of 2,3-butanediol from HF-hydrolyzed apsen wood. **Biotechnology Letters, 6,** 611-614.

APPENDIX B

HF SACCHARIFICATION BIBLIOGRAPHY

HF SACCHARIFICATION BIBIOGRAPHY

Provided here is a list of all available literature references for the "HF saccharification" of cellulose or lignocellulose. This list includes laboratory-scale investigations and process-development studies. References for the vapor-phase HF solvolysis of lignocellulose are marked with an asterisk (*). This list is specific to the HF-solvolysis of cellulose or lignocellulose and does not include all of the available literature on the reactions of anhydrous HF with sugars, short-chain natural oligosaccharides, or sugar derivatives.

Bentsen, T. and Kau, M. (1981). Solvolyse af halmcellulose ved hjaelp af fluorbrinte (meddelelser fra Bioteknisk Institut). **Afdeling for Bioteknologi, 1-4,** 4-11.

* Bentsen, T. (1982). Hydrolysis of carbohydrates using a hydrogen fluoride pretreatment (meddelelser fram Bioteknisk Institut). **Afdeling for Bioteknologi, 3-4,** 40-42.

* Bentsen, T. (1982). Hydrolysis of carbohydrates in straw using a hydrogen fluoride pretreatment. In: **Energy from Biomass: Second E. C. Conference,** A. Strub, P. Chartier, and G. Schleser, Eds. Applied Science Publishers: London, p. 1103-1105.

Clark, I. T. (1962). Determination of lignin by hydrofluoric acid. **TAPPI, 45,** 310-314.

Defaye, J., Gadelle, A., and Pedersen, C. (1982). The Behavior of cellulose, amylose, and xylan towards anhydrous hydrogen fluoride. **Carbohydrate Research, 110,** 217-227.

Defaye, J., Gadelle, A., Papadopoulos, J., and Pedersen, C. (1983). Hydrogen fluoride saccharification of cellulose and lignocellulosic materials. **Journal of Applied Polymer Science: Applied Polymer Symposium 37,** 653-670.

* Franz, R., Erckel, R., Reihm, T., and Woernle, R. (1982). Lignocellulose Saccharification by HF. In: **Energy From Biomass: Second E. C. Conference,** A. Strub, P. Chartier, and G. Schleser, Eds. Elsevier Applied Science Publishers: London, p. 873-878.

* Franz, R., Fritsche-Lang, W., Deger, H.-M., Erckel, R., and Schlingmann, M. (1987). The behavior and derivatizations of carbohydrates in hydrogen fluoride. **Journal of Applied Polymer Science, 33,** 1291-1306.

* Fredenhagen, K., and Cadenbach, G. (1933). Der Abbau Cellulose durch Fluorwasserstoff und ein neues Verfahren der Holzverzuckerung durch Hochkonzentrierten Fluorwasserstoff. **Agnewandte Chemie, 46,** 113-117.

Gore, J. (1869). On hydrofluoric acid. **Journal of the American Chemical Society, 22,** 396-406.

Hardt, H., and Lamport, D. T. A. (1982a). Hydrogen fluoride saccharification of wood: lignin fluoride content, isolation of α-D-glucopyranosyl fluoride and posthydrolysis of reversion products. **Biotechnology and Bioengineering, 24,** 903-918.

Hardt, H., and Lamport, D. T. A. (1982b). Hydrogen fluoride saccharification of cellulose and xylan: isolation of α-D-glucopranosyl fluoride and α-D-xylospyranosyl fluoride intermediates, and 1,6-anhydro-ß-D-glucopyranose. **Phytochemistry, 21,** 2301-2303.

Hawley, M. C., Selke, S. M., and Lamport, D. T. A. (1983). Comparison of hydrogen fluoride saccharification of lignocellulosic materials with other saccharification technologies. **Energy in Agriculture, 2,** 219-244.

Hawley, M. C., Downey, D. W., Selke, S. M., and Lamport, D. T. A. (1986). Hydrogen fluoride saccharification of lignocellulosic materials. In: **Cellulose: Structure, Modification, and Hydrolysis,** R. A. Young and R. M. Rowell, Eds. Wiley: New York, p. 297-321.

Helferich, B., and Bottger, S. (1929). Die einwirkung von fluorwasserstoff auf cellulose. **Justus Liebiegs Annalen der Chemie, 476,** 150-170.

Helferich, B., Starker, A. and Peters, O. (1930). Die einwirkung von fluorwasserstoff auf starke. **Justus Liebiegs Annalen der Chemie, 482,** 183-188.

Helferich, B., and Peters, O. (1932). Einwirkung von fluorwasserstoff auf kohlenhydrate. **Justus Liebiegs Annalen der Chemie, 494,** 101-106.

* Husain, H. (1987). Acid for chips. **Bio-joule, 9,** 8-10.

* I. G. Farbenindustrie AG (1932). Deutsches Reich Patentschrift 560535 (Oct. 5, 1932). Inventors: Fredenhagen, K., and Helferich, B.

* I. G. Farbenindustrie AG (1933). Deutsches Reich Patentschrift 577764 (June 3, 1933). Inventors: Fredenhagen, K., Helferich, B., and Koch, E.

* I. G. Farbenindustrie AG (1933). Deutsches Reich Patentschrift 585318 (Oct. 2, 1933). Inventors: Pfleiderer, G., and Koch, E.

Ishii, T., and Hiroi, T. (1986). Anhydrous hydrogen fluoride saccharification of lignocellulosic materials. I. Enzymic saccharification of pulp treated with anhydrous hydrogen fluoride. **Mokuzai Gakkaishi, 32,** 615-620.

Lamport, D. T. A., Hardt, H., Smith, G., Morlok, S, Hawley, M. C., Chapman, R., and Selke, S. M. (1981). HF saccharification: the key to ethanol from wood?. In: **Energy from Biomass: First E. C. Conference,** W. Palz, P. Chartier, and D. O. Hall, Eds. Applied Science Publishers: London, p. 292-297.

* Luers, H. (1937). Der heutige stand der holzverzuckerung. **Holz als Roh und Werkstoff, 1,** 35-40.

* Luers, H. (1938). Das holzverzuckerungsverfahren mit fluorwasserstoff von Hoch und Bohunek. **Holz als Roh und Werkstoff, 1,** 342-344. See also: Meyerhofer, G., Bohunek, H., and Hoch, H. (1936). Osterreichisches Patentschrift 147494.

Mort, A. J., and Parker, S. (1982). The use of anhydrous HF solvolysis in conversion of biomass to glucose. In: SERI Report SERI/232-1520.

* Mohring, W. M. (1987). **Gravimetric analysis of hydrogen fluoride vapor absorption by bigtooth aspen wood.** M. S. Thesis, Michigan State University.

* Mohring, W. M., and Hawley, M. C. (1989). Gravimetric analysis of hydrogen fluoride vapor absorption by bigtooth aspen wood. **Industrial and Engineering Chemistry Research, 28,** 237-243.

Murray, W. D. (1984a). Hydrogen fluoride solvolysis of aspen wood chips. In: **Proceedings of the Fifth Canadian Bioenergy R & D Seminar,** S. Hasnain, Ed. Elsevier Applied Science: London, p. 255-256.

Murray, W. D., Asther, M. (1984b). Ethanol fermentation of hexose and pentose wood sugars produced by hydrogen fluoride solvolysis of aspen chips. **Biotechnology Letters, 6,** 323-326.

* Ostrovski, C. M., Duckworth, H. E., and Aitken, J. C. (1984). Canertech's ethanol-from-cellulose program. In: **Fifth Canadian Bioenergy R&D Seminar,** S. Hasnain, Ed. Elsevier Applied Science: London, p. 478-482.

* Ostrovski, C. M., Aitken, J. C., and Free, D. (1984). New developments in fuel ethanol production by gaseous anhydrous hydrofluoric acid hydrolysis of hardwood, Populus tremuloides. In: **Bio-Energy 1984 Proceedings, Vol. 3: Biomass Conversion** (Gothenburg Sweden, June 15-21, 1984), H. Egneous, and A. Ellegard, Eds.

* Ostrovski, C. M., Aitken, J. C., and Hayes, R. D (1985). Hydrolysis of poplar wood using hydrofluoric acid for the production of fuel ethanol. In: **Proceedings from Energy from Biomass and Wastes IX** (Jan. 28 to Feb. 1, 1985, Buena Vista, FL), D. L. Klass, Ed. p. 895-913.

Papadopoulos, J. (1985). Acid hydrolysis for the conversion of cellulosic biomass to ethanol. In: **Proceedings of the E. C. Conference on Energy from Biomass.** Applied Science Publishers: London, p. 697-701.

Papadopoulos, J., and Defaye, J. (1986). Characterization of the lignin isolated from birch wood after extraction with hydrogen fluoride. **Journal of Wood Chemistry and Technology, 6,** 203-218.

* Reffstrup, T., and Kau, M. (1985). Hydrogen fluoride aided hydrolysis of lignocellulosic biomass: development of a fast continuous process. In: **New Approaches to Research in Cereal Carbohydrates,** R. Hill, and L. Munck, Eds. Elsevier Applied Science Publishers: Amsterdam, p. 313-317.

Rogovin, Z. A., and Pogosov, Y. L. (1958). **Gidroliz. i. Lesokhim. Prom., 1,** 4-6 (**Chemical Abstracts, 52,** 8453i).

Rogovin, Z. A., and Pogosov, Y. L. (1959). The composition and structure of the products of cellulose hydrolysis and gluocose polycondensation under the action of concentrated hydrofluoric acid. **Nauch. Doklady Vysshei Shkoly, Khim i Khim. Tekhnol., 2,** 368-371 (**Chemical Abstracts, 53,** 22912h).

* Rorrer, G. L., Hawley, M. C., and Lamport, D. T. A. (1986). Reaction rates for gas-phase hydrogen fluoride saccharification of wood. **Industrial and Engineering Chemistry Product Research and Development, 25,** 589-595.

* Rorrer, G. L., Hawley, M. C., and Lamport, D. T. A. (1987). Solvolysis of wood and pure cellulose by anhydrous hydrogen fluoride vapor. **Biomass, 12,** 227-246.

* Rorrer, G. L., Mohring, W. R., Hawley, M. C., and Lamport, D. T. A. (1988). Adsorption and reaction processes of the solvolysis of wood and pure cellulose by anhydrous hydrogen fluoride vapor. **Energy and Fuels, 2,** 556-566.

* Rorrer, G. L., Hawley, M. C., and Lamport, D. T. A. (1988). A detailed kinetic and heat transport model for the hydrolysis of lignocellulose by anhydrous hydrogen fluoride vapor. **Chemical Engineering Science, 43,** 1831-1836.

* Rorrer, G. L., Hawley, M. C., Dey, P. M., and Lamport, D. T. A. (1989). Anhydrous hydrogen fluoride as a potent reagent for the solvolysis of polysaccharides and deglycosylation of glycoproteins. In: **Methods in Plant Biochemistry, Vol. I: Carbohydrates**, P. M. Dey, Ed. Academic Press: London (in press).

Saddler, J. N., Yu, E. K. C., Mes-Hartree, M., Levitin, N., and Brownell, H. H. (1985). The fractionation of lignocellulosic substrates by steam explosion and the subsequent conversion of the various components to sugars, fuels, and chemicals. In: **Proceedings of the E. C. Conference on Energy from Biomass.** Applied Science Publishers: London, p. 978-981.

Sanger, M. P., and Lamport, D. T. A. (1983). A microapparatus for liquid hydrogen fluoride solvolysis: sugar and amino sugar composition of Erysiphe graminis and Triticum aestivum cell walls. **Analytical Biochemistry, 128,** 66-70.

Selke, S. M., Hawley, M. C., Hardt, H., Lamport, D. T. A., Smith, G., and Smith, J. (1982). Chemicals from Wood via HF. **Industrial & Engineering Chemistry Product Research & Development, 21,** 11-16.

Selke, S. M., Hawley, M. C., and Lamport, D. T. A. (1983). Reaction rates for liquid phase hydrogen fluoride saccharification of wood. In: **Wood and Agricultural Residues: Research on Use for Feed, Fuels, and Chemicals,** E. J. Soltes, Ed. Academic Press: New York, p. 329-349.

Selke, S. M. (1983). **The kinetics of hydrogen fluoride saccharification of cellulose.** Ph.D. Dissertation, Michigan State University.

* Sharkov, V. I., Bolotova, A. K., and Boiko, T. A. (1972). Wood hydrolysis by anhydrous hydrogen fluoride (translated from Russian). **Kompleks. Pererab. Rast. Syr'ya,** 39-49.

Smith, J. J, Lamport, D. T. A., Hawley, M. C., and Selke, S. M. (1983). Feasibility of using anhydrous hydrogen fluoride to "crack" cellulose. **Journal of Applied Polymer Science: Applied Polymer Symposium 37,** 641-651.

Wright, J. D., and Power, A. J. (1985). Concentrated halogen acid hydrolysis processes for alcohol fuel production. **Biotechnology and Bioengineering Symposium 15,** 511-532.

Yu, E. K. C., Deschatelets, L., Levitin, N, and Saddler, J. N. (1984). Production of 2,3-butanediol from HF-hydrolyzed apsen wood. **Biotechnology Letters, 6,** 611-614.

APPENDIX C

HF SAFETY

HF SAFETY: TOXICITY, HANDLING PROCEDURES, AND FIRST-AID

Purpose: Document "HF safety" in the laboratory. Summarize toxicity data, procedures and precautions for handling HF, and first-aid in the event of HF exposure via inhalation, eye contact, or skin contact.

I. Toxicity

Table C-1. HF toxicity.

Concentration	Exposure	Symptoms and Toxicity
gas, 3 ppm	inhalation	TLV ceiling
gas, 50 ppm	inhalation	Delayed pulmonary edema. Possibly fatal if not professionally treated.
gas, 100%	inhalation	Sharp, penetrating odor. Coughing, choking, chest tightness, cyanosis. Burning and swelling of tissues of nose and throat. Prolonged exposure: pulmonary edema. Fatal if not immediately and professionally treated.
gas or liquid, any conc.	eye	Burns eye tissue, resulting in permanent damage or blindness if not immediately professionally treated. Damage dependent on severity of exposure and effectiveness of first aid.
gas or liquid, > 50 wt. % HF	skin	Immediate and acute burning sensation of affected tissue. White discoloration of skin. Deeply penetrates and dissolves skin tissue; reacts with calcium in bone. If not treated, permanent damage, disablity, or death will result. Damage dependent on severity of exposure and effectiveness of first aid.
20 - 50% HF	skin	Burn symptoms delayed 1 to 8 hrs.
< 20% HF	skin	Burn symptoms delayed up to 24 hrs.

II. HF Handling: Precautions and Procedures

A. Protective Garments...always wear

1. Lab coat: long sleeve, full-length
2. Gloves: full length (14-19 in), Viton
3. Full face shield

B. HF Cylinders

1. Store HF cylinders in fume hood , whether full, partially full, or empty. Make sure fume hood is on and functioning properly, i.e., hood door shut down to proper working height, air intake at rated face velocity (e.g. 100 fpm).

2. Label all HF cylinders: DOT approved label, stating Anhydrous Hydrogen Fluoride (liquid), source (Matheson), cylinder ID#, size, tare weight HF, date received.

3. Support all HF cylinders on cylinder stand or support.

4. Keep primary HF cylinder valve closed and capped for any HF cylinder not connected to an HF apparatus.

5. Connect a secondary, manual-control valve (Matheson, Monel, model 55-A) to any HF cylinder connected to an HF apparatus.

6. Never expose HF cylinder surface to temperatures higher than 125 °F.

C. HF-Wetted Apparatus

1. Contain HF-wetted apparatus and all HF-wetted parts or equipment within properly-functioning fume hood.

2. Handle all HF-wetted apparatus, parts, and equipment with gloves.

3. Rinse all HF-wetted parts with sodium bicarbonate solution (ca. 10 g/L) before removing from hood.

4. All HF-wetted parts must be constructed of HF-resistant non-permeable materials such as Monel and Teflon.

5. Leak-check all lines before exposure to HF.

6. Flush HF lines with nitrogen following exposure to HF.

D. Experiments with HF

1. Perform all experiment using HF in properly-functioning fume hood.

2. Notify personnel in the laboratory that you will be performing an experiment using HF. Make sure personnel are trained in emergency and first-aid procedures (cf. section III) in case of accident.

3. Put up sign on fume hood sash labeled "CAUTION! Experiment using HF in progress!" prior to performing an experiment using HF.

4. Wear protective garments (section II.A) when performing experiments using HF.

5. Avoid any procedure which exposes anhydrous HF liquid or vapor to fume-hood atmosphere.

E. Calcium Carbonate (or Calcium Oxide) Trap

1. Keep an accounting of the amount of HF introduced into the trap. Make sure enough unreacted calcium carbonate or oxide is in the trap to neutralize the inlet HF to calcium fluoride.

2. Dispose of reacted calcium carbonate or calcium oxide in sealed, approved solid-waste container. Empty trap outdoors...wear breathing mask, gloves, and goggles.

3. Never contact acids with trap waste. Calcium fluoride in trap waste can react with the acid and regenerate HF!

III. Emergency and First-Aid Procedures

A. HF Vapor Leakage to Laboratory Atmosphere (e.g. outside of fume hood)

1. Evacuate all personnel in the laboratory.

2. Let trained personnel wearing full-length protective clothing and self-contained breathing apparatus re-enter the contaminated area and attempt to stop the HF vapor leak.

3. Do not re-enter laboratory until HF concentration in laboratory atmosphere is determined to be less than 3 ppm via HF Gas Detection System.

B. Liquid HF Spills

1. Small spills (< 2 ml) within fume hood: pipette 5 to 10 ml 6 N ammonium hydroxide solution onto HF puddle to neutralize HF....close hood door completely and let evaporate.

C. Emergency Equipment...located conveniently near fume hood

1. Large sink

2. Safety shower

3. Eye-wash station

4. Self-contained breathing apparatus with canister for HF

5. Oxygen mask and tank

D. Emergency First-Aid -- direct exposure to anhydrous HF

1. Inhalation

a. Victim: leave contaminated area to fresh air. Personnel: if necessary, put on self-contained breathing apparatus and assist victim out of contaminated area and into fresh air.

b. Keep victim warm and lying down...remove HF-contaminated clothing.

c. Immediately contact health care professional trained in HF exposure. If victim is not breathing, give artifical respiration.

e. If victim is breathing difficultly with symptoms given in section I, give 100% oxygen via oxygen mask to counteract pulonary edama.

f. Transport victim to hospital for professional treatment.

2. Eye Contact

   a. Immediately flush eyes with cold tap water for 15 to 30 min. Keep eyelids open to prevent spasms of the eyelid.

   b. Contact health-care professional trained in treating HF exposure.

   c. Transport victim to hospital for professional treatment.

3. Skin Contact

   a. Wash burn area with cold, running tap water for at least 15 min.

   b. Contact health care professional trained in treating HF exposure.

   c. Apply compress to burn area saturated with ICED 0.13 wt % aqueous ZEPHIRAN chloride solution (1:750 v/v , or 1:127 v/v for 17% ZEPHIRAN chloride stock solution) for 1 to 4 hr.

      notes:

      i) If 0.13 wt ZEPHIRIN chloride solution is not available, ICED saturated solution of EPSON salts (magnesium chloride) can be substituted.

      ii) If compress is not avialable, immerse burn area directly into solution.

      iii) Do not contact ZEPHIRIN chloride solution with eye.

   d. If directed by health care professional, apply calcium gluconate (20 wt % in glycerol) antidote to burn area.

   e. Transport victim to hospital for professional follow-up treatment.

4. Ingestion

   a. Drink several glasses of water to dilute HF in stomach, followed by 2 glasses of milk or 2 oz of "milk of magnesia" to neutralize HF.

   b. Contact health-care professional trained in treating HF exposure.

   c. Transport to hospital for professional treatment.

APPENDIX D

COMPUTER PROGRAMS

COMPUTER PROGRAMS

All computer programs were written in the Micrsoft BASIC programming language for an IMB-compatible personal computer. Each computer program and its chapter reference are listed below.

Program	chapter
DATA1.BAS	4
RK.BAS	5
DATA2.BAS	7
DATA3.BAS	7
RAWTSK2.BAS	7
CLEAVE1.BAS	8
CLEAVE2.BAS	8
KINFIT1.BAS	8
KINFIT2.BAS	8
TDIST1.BAS	10
TDIST2.BAS	10
TDIST3.BAS	10

The listing of each computer program (in the order above) is provided next.

```
10 REM ************************************************************************
20 REM **                                                                    **
30 REM **                          PROGRAM DATA1.BAS                         **
40 REM **                CREATED 10/17/87 BY GREGORY L. RORRER               **
50 REM **                                                                    **
60 REM **  This program processes the raw data file obtained from Mohring's  **
70 REM **  (1987) gravimetric HF adsorption apparatus computer data          **
80 REM **  acquistion system.  Specifically, the program loads in the raw    **
90 REM **  sample weight readings, HF and N2 mass flowmeter readings, and    **
100 REM *  reactor gas-stream temperature readings as a function of run       **
110 REM *  time.  The program will then retrieve a portion of the file and   **
120 REM *  and resquence the run time to the desired reaction or experiment  **
130 REM *  time.  The program will calculate the HF loading ( e.g. g HF/     **
140 REM *  g-wood) from the HF-adsorbed sample weight data, given the        **
150 REM *  initial weight of the wood chip.  The program will also average   **
160 REM *  the HF loading and gas-stream temperature over time within the    **
170 REM *  upper and lower time limits of the retrieved portion of the file. **
180 REM *  Finally, the program will store the resequenced HF loading vs.    **
190 REM *  time profile and gas-stream temperature vs. time profile into     **
200 REM *  a processed data file.                                           **
210 REM *                                                                   **
220 REM ************************************************************************
230 CLS
240 REM
250 REM *****  DECLARE ARRAY VARIABLES  *****
260 REM
270 DIM T(2000),T1(2000),WS(2000),WHF(2000),TEMP(2000)
280 REM
290 REM *****  LOAD RAW DATA FILE FROM MOHRING'S (1987) HF GRAVIMETRIC  *****
300 REM *****  COMPUTER DATA ACQUISITION SYSTEM                         *****
310 REM
320 INPUT"INPUT DATA FILE NAME:  ",FILE1$
330 PRINT
340 PRINT"READING DATA....."
350 J=0
```

```
360 OPEN "I",1,FILE1$
370 INPUT #1, RUNDATE
380 INPUT #1, JUNK
390 INPUT #1, NDATA
400 REM
410 REM *****          UNITS FOR INPUT VARIABLES                    *****
420 REM *****  T (sec), WS (mg), N2 (slpm), HF (slpm), TEMP ('F)   *****
430 REM
440 J=J+1
450 IF J=NDATA THEN GOTO 490
460 INPUT #1, T(J),WS(J),N2,HF,TEMP(J)
470 TEMP(J)=(TEMP(J)-32)/1.8  'convert degrees F to degrees C
480 GOTO 440
490 CLOSE
500 NDATA=J
510 REM
520 REM *****  RETRIEVE DESIRED PORTION OF RAW DATA FILE  *****
530 REM
540 PRINT
550 PRINT"SELECT TIME WINDOW:"
560 INPUT"ENTER LOWER, UPPER TIME LIMITS (in sec): ",TMIN,TMAX
570 PRINT
580 PRINT"SEACHING DATA...."
590 PRINT
600 FOR J=1 TO NDATA
610 IF T(J-1)>TMIN THEN GOTO 630
620 IF T(J)>TMIN THEN J1=J-1
630 IF T(J)>TMAX THEN J2=J
640 IF T(J)>TMAX THEN GOTO 660
650 NEXT J
660 INPUT"INITIAL SAMPLE WEIGHT (mg) = ",WO
670 INPUT"TOTAL WEIGHT CORRECTION (mg) = ",WC
680 PRINT
690 PRINT"DISPLAY DATA IN TIME WINDOW:"
700 PRINT
```

```
710 PRINT
720 PRINT"ELAPSED TIME (sec)  RUN TIME (sec)  g HF/g wood":PRINT
730 PRINT
740 K=0
750 SUMWHF=0
760 SUMTEMP=0
770 FOR J=J1 TO J2
780 K=K+1
790 T1(J)=T(J)-T(J1) 'resequence run time to reaction or experiment time
800 WHF(J)=(WS(J)-WO-WC)/WO  'convert sample weight to HF loading (g HF/g-wood)
810 PRINT USING"  ######              #######          ###.####";T(J),T1(J),WHF(J
)
820 REM
830 REM *****  AVERAGE HF LOADING AND GAS-STREAM TEMPERATURE OVER  *****
840 REM *****  THE RETIEVED TIME INTERVAL                          *****
850 REM
860 SUMWHF=SUMWHF+WHF(J)
870 SUMTEMP=SUMTEMP+TEMP(J)
880 NEXT J
890 PRINT
900 AVEWHF=SUMWHF/K
910 AVETEMP=SUMTEMP/K
920 PRINT"AVERAGE HF ADSORBED (g HF/g wood) = ";AVEWHF;" IN TIME"
930 PRINT"WINDOW OF ";T(J1);" sec TO ";T(J2);" sec "
940 PRINT
950 PRINT"AVERAGE HF VAPOR TEMPERATURE ('C) = ";AVETEMP;" IN TIME"
960 PRINT"WINDOW OF ";T(J1);" sec TO ";T(J2);" sec "
970 PRINT
980 PRINT"DO YOU WANT TO STORE THE DATA IN THE TIME WINDOW OF"
990 PRINT T(J1);" sec TO ";T(J2);" sec IN A PERMANENT FILE?"
1000 INPUT" (1=YES, 2=NO)",OPT2
1010 IF OPT2=1 THEN GOTO 1090
1020 OPT1=0
1030 IF OPT2=2 THEN INPUT"DO YOU WANT TO EXIT THIS PROGRAM (1=YES, 2=NO)";OPT1
1040 IF OPT1=1 THEN END ELSE GOTO 540
1050 REM
```

```
1060 REM *****  STORE PROCESSED HF LOADING AND GAS-STREAM TEMPERATURE VS.  *****
1070 REM *****  INTO PERMANENT FILES                                       *****
1080 REM
1090 INPUT"FILE NAME HF FOR ADSORPTION/DESORPTION VS. TIME DATA: ",FILE2$
1100 OPEN "O",1,FILE2$
1110 FOR J=J1 TO J2
1120 PRINT #1, T1(J)/60, WHF(J)
1130 NEXT J
1140 CLOSE
1150 INPUT"FILE NAME HF FOR VAPOR TEMPERATURE VS. TIME DATA: ",FILE3$
1160 OPEN "O",1,FILE3$
1170 FOR J=J1 TO J2
1180 PRINT #1, T1(J)/60, TEMP(J)
1190 NEXT J
1200 CLOSE
1210 OPT2=2
1220 GOTO 1030
1230 END
```

```
10 REM ************************************************************************
20 REM **                                                                    **
30 REM **                          PROGRAM RK.BAS                            **
40 REM **                                                                    **
50 REM **              CREATED 12/27/88 BY GREGORY L. RORRER                 **
60 REM **                                                                    **
70 REM **  This program calculates the pore-condensation radius, rk, in      **
80 REM **  condensation of nonideal HF vapor into the secondary cell wall    **
90 REM **  microporous volume of wood.                                       **
100 REM *                                                                    **
110 REM ************************************************************************
120 CLS
130 REM
140 REM *****  DECLARE ARRAY VARIABLES  *****
150 REM
160 DIM P(350),F(350),F1(350) ,X(5)
170 REM
180 REM *****  INPUT NONIDEAL HF VAPOR CONDITIONS  *****
190 REM
200 INPUT"Enter the HF gas temperature, Tg ( C) = ",TG
210 INPUT"Enter the nonideal HF gas partial pressure, PHF'(atm) = ",PHF
220 T=TG+273
230 REM
240 REM ****  CALCULATE EQUILIBRIUM CONSTANT FOR HF VAPOR ASSOCATION *****
250 REM
260 K=10^(8910/T-43.65)
270 REM
280 REM ****  CALCULATE HF VAPOR PRESSURE AND LIQUID SURFACE TENSION *****
290 REM
300 PO=(10^(7.37-1315/T))/760 ' atm  -- HF vapor pressure at Tg
310 GAM=40.7*(1-T/503.2)^1.72 ' g/cm-sec^2 -- HF liquid surface tension
320 VHF=20 ' cm^3/mol HF --  molar volume of HF liquid
330 R = 8.314 'J/mol K  --  thermodynamic gas constant
340 REM
350 REM ****  CALCULATE FUGASITY COEFFICIENT FOR NONIDEAL HF VAPOR *****
```

```
360 REM
370 REM
380 REM *****  GENERATE VALUES FOR  PHF'(atm)  vs. f  *****
390 REM
400 F(0)=1
410 P(0)=(5^5*(F(0)-1)/(K*(6-F(0))^6))^.2/760
420 FOR I=1 TO 3000
430 F(I)=1+I*.001 ' f -- nonideal HF vapor association factor
440 P(I)=(5^5*(F(I)-1)/(K*(6-F(I))^6))^.2/760 ' PHF' in atm
450 F1(I)=(1/F(I)-1)/P(I)
460 NEXT I
470 FOR J=1 TO 2
480 REM
490 REM *****  TRAPEZOID RULE INTEGRATION OF (1/f - 1)/PHF' vs. PHF' *****
500 REM
510 IF J=1 THEN P1=PHF
520 IF J=2 THEN P1=PO
530 SUM1=0
540 FOR I=1 TO 3000
550 IF P(I)>P1 THEN P2=P(I)
560 IF P(I)>P1 THEN P(I)=P1
570 IF P(I)=P1 THEN F(I)=F(I-1)+(P1-P(I-1))/(P2-P(I-1))*(F(I)-F(I-1))
580 IF P(I)=P1 THEN F1(I)=(1/F(I)-1)/P(I)
590 SUM1=SUM1+(F1(I)+F1(I-1))/2*(P(I)-P(I-1))
600 IF P(I)=P1 THEN GOTO 620
610 NEXT I
620 X(J)=EXP(SUM1)
630 NEXT J
640 REM
650 REM *****  CALCULATE FUGASITY  ******
660 REM
670 FHF=X(1)*PHF
680 FO=X(2)*PO
690 CLS
700 REM
```

```
710 REM *****  SUMMARIZE THERMODYNAMIC CALCULATIONS  *****
720 REM
730 PRINT"THERMODYNAMIC PARAMETERS:":PRINT
740 PRINT"HF GAS TEMPERATURE = ";TG;" C"
750 PRINT"NONIDEAL HF GAS PARTIAL PRESSURE = ";PHF;" atm"
760 PRINT"HF VAPOR PRESSURE AT ";TG;" C = ";PO;" atm"
770 PRINT"FUGASITY COEFF. AT ";PHF;" atm  = ";X(1)
780 PRINT"FUGASITY COEFF. AT ";PO;" atm = ";X(2)
790 PRINT
800 PRINT
810 REM
820 REM *****  CALCULATE PORE-CONDENSATION RADIUS rk  *****
830 REM
840 PRINT"PORE-CONDENSATION RADIUS:"
850 PRINT
860 RK=-2*VHF*GAM/(R*T*LOG(FHF/FO))*10 ' rk in angstroms
870 RKI=-2*VHF*GAM/(R*T*LOG(PHF/PO))*10
880 PRINT"rk (non ideal HF gas) = ";RK;" A"
890 PRINT"rk (ideal HF gas) = ";RKI;" A"
900 PRINT
910 END
```

```
10 REM ************************************************************************
20 REM **                                                                    **
30 REM **                          PROGRAM DATA2.BAS                         **
40 REM **                  CREATED 10/4/87 BY GREGORY L. RORRER              **
50 REM **                                                                    **
60 REM **  This program performs three data processing functions.  First,    **
70 REM **  a sequential ASCII data file (units=mV) is loaded from a 5.25 in. **
80 REM **  floppy disk.  (Note:  this data was originally acquired by an     **
90 REM **  Omega 660 digital thermometer (1 mV/1'C analog output) interfaced **
100 REM *  to an IBM-9000 benchtop computer (CSOS operating system) via      **
110 REM *  "CAPS".  The raw data file processed under the "CAPS" software    **
120 REM *  was then reprocessed to a sequential ASCII data file (units=mV)   **
130 REM *  on CSOS operating system by the program RAWTSK2.BAS.  This file   **
140 REM *  was downloaded to the MS/DOS 3.2 operating system via PROCOMM).   **
150 REM *  Second, the sequential mV data file is converted to a temperature **
160 REM *  ('C) vs. time (min) data file.  Third,  a desired portion of the  **
170 REM *  temperature ('C) vs. time (min) data file is retreived and then   **
180 REM *  resequenced so that the first point is at time = 0 min.  This     **
190 REM *  portion of the file is stored as a permanent file if desired.     **
200 REM *                                                                    **
210 REM ************************************************************************
220 CLS
230 REM
240 REM ***** DECLARE ARRAY VARIABLES *****
250 REM
260 DIM T(4000),T1(1000),MV(4000),TEMP(4000)
270 REM
280 REM ***** LOAD RAW SEQUENTIAL DATA FILE (units=mV) *****
290 REM
300 PRINT
310 INPUT"INPUT DATA FILE NAME:  ",FILE1$
320 REM INPUT"RUN TIME (min):  ",RUNTIME
330 PRINT
340 PRINT"READING DATA....."
350 J=0
```

```
360 OPEN "I",1,FILE1$
370 REM
380 INPUT #1, RUNTIME
390 INPUT #1, PTS
400 DT=RUNTIME/PTS
410 PRINT"RUNTIME = ";RUNTIME;" min"
420 PRINT"DATA PTS = ";PTS
430 PRINT"TIME INCREMENT = ";DT;" min"
440 J=J+1
450 INPUT #1, MV(J)
460 REM PRINT J, MV(J)
470 IF MV(J)=999 THEN GOTO 490 'end of file flag
480 GOTO 440
490 CLOSE
500 NDATA=J-1
510 REM
520 REM ***** CONVERT SEQUENTIAL mV DATA FILE TO TEMP ('C) VS. TIME (min) *****
530 REM ***** DATA FILE.  SORT OUT ANY ZERO'S (0) UNINTENTIONALLY ADDED   *****
540 REM ***** TO THE FILE AS THE RESULT OF CSOS/MS-DOS DOWNLOADING        *****
550 REM
560 FOR J=1 TO NDATA
570 IF MV(J)= 0 THEN GOTO  620
580 I=I+1
590 TEMP(I)=MV(J) '1 mV = 1 'C
600 T(I)=I*DT
610 PRINT I,T(I),TEMP(I)
620 NEXT J
630 REM
640 REM ***** RETRIEVE DESIRED PORTION OF TEMP ('C) VS. TIME (min) ARRAY  *****
650 REM ***** RESEQUENCE THIS PORTION OF THE FILE SO THAT THE FIRST DATA  *****
660 REM ***** POINT IS AT TIME=0 min                                      *****
670 REM
680 PRINT
690 PRINT "SELECT TIME WINDOW:  "
700 INPUT"ENTER LOWER, UPPER TIME LIMITS (in min): ",TMIN,TMAX
```

```
710 PRINT
720 PRINT"SEACHING DATA...."
730 FOR J=1 TO I
740 IF T(J-1)>TMIN THEN GOTO 760
750 IF T(J)>TMIN THEN J1=J-1
760 IF T(J)>TMAX THEN J2=J
770 IF T(J)>TMAX THEN GOTO 800
780 NEXT J
790 PRINT
800 PRINT"DISPLAY DATA IN TIME WINDOW:"
810 PRINT
820 PRINT"ELAPSED TIME (min)  RUN TIME (min)    TEMP ('C)":PRINT
830 K=0
840 FOR J=J1 TO J2
850 K=K+1
860 T1(K)=T(J)-T(J1)
870 PRINT USING"    ###.##             ###.##          ###.##";T(J),T1(K),TEMP(J)
880 NEXT J
890 REM
900 REM ***** STORE RETRIEVED PORTION OF FILE INTO RESEQUENCED TEMP ('C)  *****
910 REM ***** VS. TIME (sec) PERMANENT FILE (IF DESIRED)                  *****
920 REM
930 PRINT
940 PRINT" DO YOU WANT TO STORE THE DATA IN THE TIME WINDOW OF"
950 PRINT T(J1);" min TO ";T(J2);" min IN A PERMANENT FILE?"
960 INPUT" (1=YES, 2=NO)",OPT2
970 IF OPT2=1 THEN GOTO 1010
980 OPT1=0
990 IF OPT2=2 THEN INPUT" DO YOU WANT TO EXIT THIS PROGRAM (1=YES, 2=NO)";OPT1
1000 IF OPT1=1 THEN END ELSE GOTO 690
1010 INPUT" ENTER PERMANENT FILE NAME: ",FILE2$
1020 K=0
1030 OPEN "O",1,FILE2$
1040 FOR J=J1 TO J2
1050 K=K+1
```

```
1060 PRINT #1, T1(K)*60, TEMP(J)
1070 NEXT J
1080 CLOSE
1090 OPT2=2
1100 GOTO 990
1110 END
```

```
10 REM ************************************************************************
20 REM **                                                                    **
30 REM **                          PROGRAM DATA3.BAS                         **
40 REM **                CREATED 11/13/87 BY GREGORY L. RORRER               **
50 REM **                                                                    **
60 REM **  This program reprocesses a temperature ('C) vs. time (sec) data   **
70 REM **  originally processed by DATA2.BAS.  This program performs two     **
80 REM **  functions.  First, the temperature points are corrected for mV    **
90 REM **  offset (a linear function of the true mV) created by the IBM-9000 **
100 REM *  "CAPS" software.  Second, the corrected temperature data is       **
110 REM *  "smoothed"  by a moving-average procedure.  The temperature data  **
120 REM *   must be smoothed because the output resolution on the Omega 660  **
130 REM *   digital thermometer is about 0.5 mV/ 'C.                         **
140 REM *                                                                    **
150 REM ************************************************************************
160 CLS
170 REM
180 REM ***** DECLARE ARRAY VARIABLES ******
190 REM
200 DIM T(1000),TEMP(1000),T1(1000),TEMP1(1000),TEMP2(1000)
210 REM
220 REM ***** LOAD TEMP ('C) VS. TIME (sec) DATA FILE ORIGINALLY *****
230 REM ***** PROCESSED BY DATA2.BAS                              *****
240 REM
250 PRINT
260 INPUT"INPUT DATA FILE NAME:  ",FILE1$
270 PRINT
280 PRINT"READING DATA..."
290 PRINT:PRINT
300 OPEN "I",1,FILE1$
310 IF EOF(1) THEN GOTO 360
320 J=J+1
330 INPUT #1,T(J),TEMP(J)
340 REM PRINT T(J),TEMP(J)
350 GOTO 310
```

```
360 CLOSE
370 NDATA=J
380 REM
390 REM ***** LOAD PARAMETERS FOR TEMP DATA SMOOTHING *****
400 REM
410 INPUT"ENTER TIME  INCREMENT (in sec) FOR MOVING AVERAGE: ",NMA
420 INPUT"ENTER TIME OFFSET (in sec) BEFORE START OF MOVING AVERAGE:  ",K
430 INPUT"ENTER OUTPUT FILE NAME:  ",FILE2$
440 PRINT:PRINT
450 REM
460 REM ***** CORRECT TEMP DATA FOR "CAPS" mV LINEAR VOLTAGE OFFSET *****
470 REM
480 M=.04905
490 B=-.76 'mV
500 OPEN "O",1,FILE2$
510 FOR I=1 TO K
520 T1(I)=T(I)/60
530 TEMP1(I)=(TEMP(I)-B)/(M+1)
540 PRINT #1,T1(I),TEMP1(I)
550 PRINT T1(I),TEMP1(I)
560 NEXT I
570 REM
580 REM ***** PERFORM TEMP DATA SMOOTHING *****
590 REM
600 FOR I=K+1 TO NDATA
610 T1(I)=T(I)/60
620 TEMP1(I)=(TEMP(I)-B)/(M+1)
630 NEXT I
640 FOR I=K+1 TO NDATA
650 TEMPSUM=0
660 FOR J=I-NMA/2 TO I+NMA/2
670 TEMPSUM=TEMPSUM+TEMP1(J)
680 IF T1(J)=0 THEN GOTO 770
690 NEXT J
700 TEMP2(I)=TEMPSUM/(NMA+1)
```

```
710 REM
720 REM ***** WRITE SMOOTHED TEMP ('C) VS. TIME (min) DATA TO PERMANENT FILE **
730 REM
740 PRINT #1,USING"##.###    ###.#";T1(I),TEMP2(I)
750 PRINT USING"##.###    ###.#    ###.#"; T1(I),TEMP1(I),TEMP2(I)
760 NEXT I
770 CLOSE
780 END
```

```
10 REM PROGRAM RAWTSK2.BAS CREATED 10/3/87 BY GREGORY L RORRER
20 REM ADAPTED FROM CAPS UPDATE RELEASE 1.3 PAGE 45
30 REM THIS PROGRAM CONVERTS CAP .RAW DATA FILES TO ASCII
40 REM FILES THAT CAN BE READ BY BASIC ON THE CSOS OPERATING
50 REM SYSTEM.  CAPS STORES VOLTAGE VS TIME DATA SEQUENTIALLY
60 REM IN EQUAL TIME INCREMENTS. EACH VOLTAGE POINT IS STORED
70 REM AS 32 BINARY BITS.  AN "SREAD" I/O  ROUTINE IS USED TO
80 REM READ IN THIS CAPS DATA.  THE FOUR BYTE INTEGER IS CONVERTED
90 REM TO A REAL NUMBER.
100 DIM INBUF%(256),READING(8000),T(8000),MV(8000)
110 CNT%=0
120 CLS
130 PRINT:PRINT:PRINT
140 INPUT"ENTER CAPS RAW DATA FILE NAME (NAME.RAW):   ";FILE$
150 PRINT
160 INPUT"ENTER RUNTIME (MIN) = ";RUNTIME
170 PRINT
180 PRINT"READING DATA..."
190 OPEN FILE$ AS FILE #1
200 INC=1
210 REM OUTER LOOP READS FILE UNTIL EOF IS ENCOUNTERED
220 REM INCREASE LOOP TARGET IF FILE IS LARGER THAN 128 SECTORS
230 REM SIZE OF READING ARRAY MAY HAVE TO BE INCREASED ALSO
240 FOR I=1 TO 256
250 CALL SREAD(1,INBUF%(1),256.,0,0,I)
260 REM INNER LOOP DOES THE CONVERSION
270 FOR K=1 TO 127 STEP 2
280 MSW=65536*INBUF%(K)
290 T%=INBUF%(K+1)
300 IF T%<0 THEN LSW=65535-ABS(T%) ELSE LSW=T%
310 CNT%=CNT%+1
320 READING(CNT%)=LSW+MSW
330 IF READING(CNT%) < 0 THEN GOTO 360
340 NEXT K
350 NEXT I
```

```
360 CLOSE #1
370 REM THE CONVERTED CAPS VOLTAGE DATA IS NOW IN MICROVOLTS PLUS
380 REM A 6000 MICROVOLT OFFSET.
390 REM THIS VOLTAGE DATA IS STORED SEQUENTIALLY IN EQUAL TIME
400 REM INCREMENTS. CONVERT THIS CAPS VOLTAGE DATA TO MILLIVOLT
410 REM VS TIME DATA IN THE ARRAY T,MV
420 REM THE FIRST READING IS THE RUNTIME
430 REM RUNTIME=READING(1) (NOTE:  THE RUNTIME IS ENTERED MANUALLY)
440 PRINT:PRINT:PRINT"RUNTIME = ";RUNTIME;" MIN"
450 REM DT=TIME INCREMENT
470 PTS=CNT%-2
480 DT=RUNTIME/PTS
490 PRINT:PRINT
500 FOR I=2 TO PTS+1
510 T(I-1)=(I-1)*DT
520 MV(I-1)=(READING(I+1)-6000)/1000
530 PRINT I-1, T(I-1),MV(I-1)
540 NEXT I
550 REM OPTION FOR SAVING CONVERTED ASCII FILE OF MILLIVOLT VS TIME
560 REM DATA
570 PRINT
580 PRINT"DO YOU WANT TO SAVE THE MILLIVOLT VS TIME (MIN) ASCII DATA"
590 INPUT"FILE IN A PERMANENT FILE (1=YES, 2=NO):  ";OPT1
600 IF OPT1=2 THEN END
610 INPUT"OUTPUT FILE NAME:  ";FILE2$
620 OPEN FILE2$ FOR OUTPUT AS FILE #1
630 PRINT #1,RUNTIME
640 PRINT #1,PTS
650 FOR I=1 TO PTS
660 PRINT #1, MV(I)
670 NEXT I
680 PRINT #1,999
690 CLOSE #1
700 END
```

```
10 REM ************************************************************************
20 REM **                                                                    **
30 REM **                        PROGRAM CLEAVE1.BAS                         **
40 REM **                 CREATED 3/18/88 BY GREGORY L. RORRER               **
50 REM **                                                                    **
60 REM **  This program stochastically simulates the complexation of HF      **
70 REM **  with available OH groups on the "n" glucan units which constitute **
80 REM **  a single cellulose chain.  On a normalized basis, the fraction of **
90 REM **  OH groups complexed with HF can be equated with (1-Z1).           **
100 REM *  If all 3 OH groups on a given glucan unit are complexed with HF,  **
110 REM *  then on a normalized basis, the fraction of completely HF-        **
120 REM *  complexed glucan units can be equated with f(1-Z1)=1-X1           **
130 REM *                                                                   **
140 REM ************************************************************************
150 CLS
160 REM
170 REM ***** SET RANDOM NUMBER GENERATOR *****
180 REM
190 RANDOMIZE
200 PRINT
210 REM
220 REM ***** DECLARE ARRAY VARIABLES *****
230 REM
240 DIM B(1000,3),X1(3000),Y1(3000),Z1(3000),Y1P(100),X1P(100)
250 REM
260 REM ***** INITIALIZE STOCHASTIC SIMULATION *****
270 REM
280 INPUT"enter number of glucan units in cellulose chain:  ", N
290 PRINT
300 X=0
310 Y=0
320 L=0
330 REM
340 REM ***** BEGIN STOCHASTIC SIMULATION *****
350 REM
```

```
360 I=INT(RND*N+1) 'I=1 to N glucan units constituting a single cellulose chain
370 J=INT(RND*3+1) 'J=1 to 3 OH groups on each glucan unit (3*N total HF
380 REM             adsorption sites)
390 REM
400 REM ***** SEARCH FOR OPEN OH GROUPS (ADSORPTION SITES) *****
410 REM
420 IF B(I,J)=1 THEN L=L+1
430 IF L=(N+2)*3 THEN GOTO 700
440 IF B(I,J)=1 THEN GOTO 360
450 IF B(I,J)=0 THEN B(I,J)=1
460 X=X+1 'tally of HF-complexed OH groups
470 PRINT X,I,J
480 REM
490 REM ***** SEARCH FOR GLUCAN UNITS NOT YET COMPLETELY HF-COMPLEXED ***
500 REM
510 IF B(I,1)=1 THEN GOTO 520 ELSE GOTO 320
520 IF B(I,2)=1 THEN GOTO 530 ELSE GOTO 320
530 IF B(I,3)=1 THEN Y=Y+1 'tally of glucan units with all 3 of its OH
540 REM                    groups HF-complexed
550 IF B(I,3)=0 THEN GOTO 320
560 PRINT
570 PRINT Y,I
580 PRINT
590 X1(X)=X 'remember sequence of X
600 Y1(X)=Y 'remember sequence of Y as a function of X
610 Z1(X)=I
620 REM
630 REM ***** DETERMINE THE POSITION OF THE GLUCAN CHAIN WHERE THE *****
640 REM ***** FIRST GLUCAN UNIT IS COMPLETELY HF-COMPLEXED (ALL 3  *****
650 REM ***** OH GROUPS HF-COMPLEXED)                              *****
660 REM
670 IF Y=1 THEN N1=X
680 IF Y=1 THEN N2=I
690 GOTO 320
700 PRINT:PRINT:PRINT
```

```
710 CLS
720 PRINT"N = ";N" glucan units"
730 PRINT
740 PRINT"-OH groups      liberated    glucan units'  "
750 PRINT"HF complexed      number       position"
760 PRINT
770 FOR I=1 TO N*3
780 IF X1(I)>0 THEN PRINT USING"   #####          #####      #####    ";X1(I),Y1(
I),Z1(I)
790 IF Z1(I)=1 THEN YI=Y1(I)
800 IF Z1(I)=1 THEN XI=X1(I)
810 NEXT I
820 PRINT:PRINT
830 PRINT"position of first glucan unit with all 3 -OH groups complexed= ";N2
840 PRINT"hydroxyl group number at this position = ";N1
850 PRINT"number of glucan units liberated when n=1 glucan unit liberated = ";YI
860 PRINT"hydroxyl group number at this position = ";XI
870 PRINT:PRINT
880 REM
890 REM ***** FINAL f(1-Z1)=1-X1 OUTPUT CONTROL *****
900 REM
910 INC=10
920 NP=INT(N/INC)
930 K=1
940 REM PRINT K/N,N1/(N*3)
950 REM
960 REM ***** NORMALIZE X1 AND Y1 *****
970 REM
980 FOR I=1 TO N*3
990 IF Y1(I)=INC*K THEN Y1P(K)=Y1(I)/N 'equivalent to f(1-Z1)=1-X1
1000 IF Y1(I)=INC*K THEN X1P(K)=X1(I)/(N*3) 'equivalent to (1-Z1)
1010 IF Y1(I)=INC*K THEN K=K+1
1020 NEXT I
1030 FOR K=1 TO NP
1040 PRINT X1P(K),Y1P(K)
1050 NEXT K
1060 PRINT
1070 END
```

```
10 REM ************************************************************************
20 REM **                                                                    **
30 REM **                        PROGRAM CLEAVE2.BAS                         **
40 REM **                 CREATED 1/5/89 BY GREGORY L. RORRER                **
50 REM **                                                                    **
60 REM **  This program calculates the number of monomer units released as   **
70 REM **  as a function of the number of bonds cleaved for a linear         **
80 REM **  polymer chain undergoing perfectly random depolymerization.       **
90 REM **                                                                    **
100 REM ************************************************************************
110 REM
120 REM ***** DECLARE ARRAY VARIABLES *****
130 REM
140 DIM X(1000),X1(1000),X1P(1000),Y(1000),YP(1000)
150 REM
160 REM ***** INITIALIZE STOCHASTIC SIMULATION *****
170 REM
180 N=100 'number of monomer units in the linear polymer chain
190 B=0
200 M=0
210 J=1
220 IP=10
230 L=1
240 X(N+1)=1 'the reducing end of the chain
250 REM
260 REM ***** SET RANDOM NUMBER GENERATOR *****
270 REM
280 RANDOMIZE
290 REM
300 REM ***** BEGIN STOCHASTIC SIMULATION *****
310 REM
320 REM
330 REM ***** SEARCH FOR UNCLEAVED BONDS JOINING MONOMER UNITS *****
340 REM
350 I=INT(RND*N+1) 'I=1 TO N monomer units in the polymer chain
```

```
360 IF X(I)=1 THEN GOTO 350
370 IF X(I)=0 THEN B=B+1    ' B is the current number of bonds cleaved
380 IF X(I)=0 THEN X(I)=1   ' X(I) is position of the bond on the polymer chain
390 REM
400 REM ***** SEARCH FOR MONOMER UNITS RELEASED IN POLYMER CHAIN *****
410 REM ***** AT THE THE CURRENT TOTAL NUMBER OF BONDS CLEAVED   *****
420 M=0
430 FOR I=1 TO N
440 IF  X(I)=1 AND X(I+1)=1 THEN M=M+1   ' M is the current number of monomer
450 NEXT I                               ' units released (bonds at both ends
460 REM                                  ' of a given monomer unit are cleaved)
470 REM
480 REM ***** NORMALIZE AND STORE M VS. B *****
490 REM
500 X1(J)=B/N
510 Y(J)=M/N
520 REM PRINT X1(J),Y(J)
530 IF J=L*IP THEN X1P(L)=X1(J)
540 IF J=L*IP THEN YP(L)=Y(J)
550 IF J=L*IP THEN PRINT X1P(L),YP(L)
560 IF J=L*IP THEN L=L+1
570 J=J+1
580 IF B=N THEN GOTO 600
590 GOTO 350
600 END
```

```
10 REM ************************************************************************
20 REM **                                                                    **
30 REM **                        PROGRAM KINFIT1.BAS                         **
40 REM **                 CREATED 12/9/87 BY GREGORY L. RORRER               **
50 REM **                                                                    **
60 REM **  This program estimates the reference rate constant k10 and        **
70 REM **  activation energy E1 given  1) HF loading vs. reaction time t     **
80 REM **  data, and 2) complimentary centerline particle temperature vs.     **
90 REM **  time (T(L,t)) data, via the nonlinear OLS-Gauss minimization      **
100 REM *  scheme.  Specifically, the ordinary least-squares estimate of     **
110 REM *  E1 is calculated at fixed k10.  The HF loading vs. t data is      **
120 REM *  subjected to the estimation scheme.  The calculated values for    **
130 REM *  the HF loading (i.e. ETA(I)) are determined by 4th order Runge-   **
140 REM *  Kutta integration of the HF-adsorption component of the kinetic   **
150 REM *  model given the current estimates for k10 and E1.  The final      **
160 REM *  least-squares estimates for of K10 and E1 are determined when     **
170 REM *  the global sum of squares as a function of the estimate of k10    **
180 REM *  is minimized.                                                     **
190 REM *                                                                    **
200 REM ************************************************************************
210 CLS
220 REM
230 REM ***** DECLARE ARRAY VARIABLES *****
240 REM
250 DIM TI1(200),THETA(200),TI2(200),T(200),T1(200),ETA(200),ETAI(200),SC2(200),
SCI2(200),E(200)
260 REM
270 REM ***** INTEGRATION AND PARAMETER ESTIMATION CONTROL PARAMETERS *****
280 REM
290 TIF=95 'sec, final time for data set
300 TOL=.0001
310 DT=1! 'sec, numerical integration step size
320 REM
330 REM ***** HF LOADING (g HF/g prehydrolzed wood) vs. t  DATA *****
340 REM
350 PRINT:INPUT"ENTER HF LOADING VS. TIME DATA FILE:  ",FILE1$
```

```
360 PRINT
370 J=0 'initial point (0,0) given in HF loading vs. time input file
380 OPEN "I",1,FILE1$
390 INPUT #1, TI1(J),THETA(J)  'TI1(J) in min, THETA(J) in g HF/g wood
400 IF TI1(J)*60>TIF THEN GOTO 440
410 PRINT USING"###.#   #.###";TI1(J)*60,THETA(J) 'convert min to sec
420 J=J+1
430 GOTO 390
440 CLOSE
450 NDATA=J-1
460 REM
470 REM ***** LOAD COMPLIMENTARY T(L,t) DATA *****
480 REM
490 PRINT:INPUT"ENTER COMPLIMENTARY T(L,t) DATA FILE:  ",FILE2$
500 INPUT"ENTER HF VAPOR STREAM TEMPERATURE ('C):  ",TG
510 T0=TG+273 'convert 'C to 'K
520 J=0
530 PRINT
540 OPEN "I",1,FILE2$
550 INPUT #1,TI2(J),T(J)  'TI2(J) in min, T(J) in 'C
560 PRINT USING"###.#    ###.##";TI2(J)*60,T(J) 'convert min to sec
570 T1(J)=T(J)+273 'convert degrees C to degrees K
580 IF TI2(J)*60 >TIF THEN GOTO 610
590 J=J+1
600 GOTO 550
610 CLOSE
620 NCALC=J
630 REM
640 REM ***** LOAD INITIAL GUESS FOR k10 AND E1 *****
650 REM
660 PRINT:INPUT"ENTER INITIAL GUESS FOR k10 (in g/g-sec):  ",B1S
670 INPUT"ENTER INITIAL GUESS FOR E1 (in kcal/mol):  ",B2S
680 REM
690 REM ***** HF ADSORPTION PARAMETERS *****
700 REM
```

```
710 R=1.987 'cal/mol
720 AO=5.440502  'AO...A3 empirical constants for calculating
730 A1=-.2024107 'AE (g HF/g prehydrolyzed wood) as a function of T (in 'C)
740 A2=2.748926E-03
750 A3=-1.300829E-05
760 REM
770 REM *****  BEGIN ALGORITHM  *****
780 REM
790 B1=B1S
800 B2=B2S
810 K=0 'initial point (0,0) given in HF loading vs. time input file
820 REM
830 REM ***** 4th ORDER RUNGE KUTTA INTEGRATION OF Z1 *****
840 REM
850 REM
860 REM ***** INITIAL VALUE FOR Z1 *****
870 REM
880 Z1=1!
890 PRINT
900 FOR I=0 TO NCALC
910 PRINT USING"###  ##.#  #.###  #.###   #.##########";I*DT,T(I),Z1,ETA(I),SC2(I
)
920 K1=B1*EXP(-B2*(1/T1(I)-1/T0)*1000/R)
930 AE=AO+A1*T(I)+A2*T(I)^2+A3*T(I)^3
940 AEG=AO+A1*TG+A2*TG^2+A3*TG^3
950 F11=-K1*AE*Z1
960 F12=-K1*AE*(Z1+.5*DT*F11)
970 F13=-K1*AE*(Z1+.5*DT*F12)
980 F14=-K1*AE*(Z1+DT*F13)
990 IF I*DT>TI1(K)*60+.1*DT THEN ETAI(K)=ETA(I-1)
1000 IF I*DT>TI1(K)*60+.1*DT THEN SCI2(K)=SC2(I-1)
1010 IF I*DT>TI1(K)*60+.1*DT THEN PRINT USING"###                #.###   #.######
##";TI1(K)*60,ETAI(K),SCI2(K)
1020 IF I*DT>TI1(K)*60+.1*DT THEN K=K+1
1030 SC2(I+1)=SC2(I)+DT*(-K1*1000/R*(1/T1(I)-1/T0)*AEG*AE*Z1)
1040 Z1=Z1+DT*(F11+2*F12+2*F13+F14)/6
1050 ETA(I+1)=AEG*(1-Z1)
```

```
1060 NEXT I
1070 REM
1080 REM ***** NONLINEAR OLS-GAUSS ESTIMATION OF B2 GIVEN B1 (E1 given k1O)  ***
1090 REM
1100 C2SUM=0
1110 H2SUM=0
1120 SUMSQ=0
1130 PRINT:PRINT
1140 FOR I=0 TO NDATA
1150 E(I)=THETA(I)-ETAI(I)
1160 PRINT USING"###.#   #.####  #.####  #.####";TI1(I)*60,THETA(I),ETAI(I),E(I)
1170 C2SUM=C2SUM+SCI2(I)*SCI2(I)
1180 H2SUM=H2SUM+SCI2(I)*E(I)
1190 SUMSQ=SUMSQ+E(I)^2
1200 NEXT I
1210 C22=C2SUM
1220 H2=H2SUM
1230 B2S=B2+H2/C22
1240 REM
1250 REM ***** CONVERGENCE CHECK FOR LEAST-SQUARES ESTIMATE OF E1 GIVEN k1O ***
1260 REM
1270 TESTB2=ABS((B2S-B2)/B2)
1280 PRINT:PRINT:PRINT
1290 PRINT B2S,B2,TESTB2,SUMSQ
1300 PRINT:PRINT:PRINT
1310 IF TESTB2>TOL THEN GOTO 790
1320 REM
1330 REM ***** PRINT OUT LEAST-SQUARES ESTIMATE OF E1 GIVEN K1O *****
1340 REM
1350 K1O=B1S
1360 E1=B2S
1370 PRINT"FOR k1O = ";K1O;" g/g-sec"
1380 PRINT"E1 = ";E1; " kcal/mol"
1390 PRINT"SUM OF SQUARED RESIDUALS (s^2) = ";SUMSQ
1400 PRINT"n = ";NDATA
```

```
1410 PRINT
1420 REM
1430 REM ***** INCREMENT K1O AND CALCULATE A NEW LEAST-SQUARES       *****
1440 REM ***** ESTIMATE FOR E1 UNTIL THE GLOBAL MINIMUM SUM OF      *****
1450 REM ***** IS ACHIEVED                                          *****
1460 REM
1470 B1S=K1O+.001
1480 IF B1S>.015 THEN END
1490 B2S=E1
1500 GOTO 790
1510 END
```

```
10 REM ************************************************************************
20 REM **                                                                    **
30 REM **                      PROGRAM KINFIT2.BAS                           **
40 REM **              CREATED 3/31/88 BY GREGORY L. RORRER                  **
50 REM **                                                                    **
60 REM **  This program estimates the reference rate constant k20 and        **
70 REM **  activation energy E2 given  1) k10 and E1 estimated via           **
80 REM **  KINFIT1.BAS, 2)  normalized glucose yield vs. time (Yg vs. t)     **
90 REM **  data, and 3) complimentary centerline particle temperature vs.    **
100 REM *  time (T(L,t)) data, via the nonlinear OLS-Gauss minimization      **
110 REM *  scheme.  Specifically,  the ordinary least-squares estimate of    **
120 REM *  E2 is calculated at fixed k20.  The normalized Yg vs. t data are  **
130 REM *  subjected to the estimation scheme.  The predicted values for Yg  **
140 REM *  (i.e. X3) are calculated by 4th-order Runge-Kutta integration of  **
150 REM *  the kinetic model given the current estimates for k20 and E2. The **
160 REM *  final least-squares estimates of k20 and E2 are determined when   **
170 REM *  global sum of squares as a function of the estimate of k20 is     **
180 REM *  minimized.                                                        **
190 REM *                                                                   **
200 REM ************************************************************************
210 CLS
220 REM
230 REM ***** DECLARE ARRAY VARIABLES *****
240 REM
250 DIM TI1(400),Y(400),TI2(400),T(400),T1(400),ETA(400),ETAI(400),E(400)  ,SC2(4
00),SCI2(400)
260 REM
270 REM ***** INTEGRATION AND PARAMETER ESTIMATION CONTROL PARAMETERS *****
280 REM
290 TIF=240 'sec, final time for data set
300 TOL=.001
310 DT=1 'sec, numerical integration step size
320 REM
330 REM ***** LOAD NORMALIZED Yg vs. t DATA *****
340 REM
350 PRINT:INPUT"ENTER NORMALIZED Yg vs. t DATA FILE:  ",FILE1$
```

```
360 PRINT
370 J=1
380 OPEN "I",1,FILE1$
390 INPUT #1,THETA 'equilibrium loading at Tg  (g HF/g prehydrolyzed wood)
400 INPUT #1, Y(J),TI1(J)
410 IF TI1(J)>TIF THEN GOTO 450
420 PRINT USING"###.#   #.###";TI1(J),Y(J)
430 J=J+1
440 GOTO 400
450 CLOSE
460 NDATA=J-1
470 REM
480 REM ***** LOAD COMPLIMENTARY T(L,t) DATA *****
490 REM
500 PRINT:INPUT"ENTER COMPLIMENTARY T(L,t) DATA FILE:  ",FILE2$
510 INPUT"ENTER HF VAPOR STREAM TEMPERATURE (Tg in 'C):  ",TG
520 T0=TG+273 ' convert 'C to 'K
530 J=0
540 PRINT
550 OPEN "I",1,FILE2$
560 INPUT #1,TI2(J),T(J)
570 REM PRINT USING"###.#    ###.##";TI2(J)*60,T(J) 'convert min to sec
580 T1(J)=T(J)+273 'convert 'C to  'K
590 IF TI2(J)*60>TIF THEN GOTO 620
600 J=J+1
610 GOTO 560
620 CLOSE
630 NCALC=J
640 REM
650 REM ***** LOAD INITIAL GUESS FOR k20 AND E2 *****
660 REM
670 PRINT:INPUT"ENTER INITIAL GUESS FOR k20 (in g/g-sec):  ",B1S
680 INPUT"ENTER INITIAL GUESS FOR E2 (in kcal/mol):  ",B2S
690 REM
700 REM ***** LOAD KNOWN KINETIC AND HF-ADSORPTION PARAMETERS *****
```

```
710 REM
720 R=1.987 ' cal/mol
730 K1O=8.999999E-03 ' g/g-sec at 31 C
740 E1=10.2 'kcal/mol
750 AO=5.440502  'AO...A3 empirical constants for calculating
760 A1=-.2024107 'AE (g HF/g prehydrolyzed wood) as a function of T (in 'C)
770 A2=2.748926E-03
780 A3=-1.300829E-05
790 CO=-.0009764 'CO...C3 empirical constants for calculating f(1-Z1)=1-X1
800 C1=.007522   'as a function of Z1
810 C2=-.02129
820 C3=1.0129
830 REM
840 REM *****  BEGIN ALGORITHM  *****
850 REM
860 B1=B1S
870 B2=B2S
880 K=1
890 REM
900 REM ***** 4th ORDER RUNGE-KUTTA INTEGRATION OF Z1, X1, X2, X3 *****
910 REM
920 REM
930 REM ***** INITIAL VALUES FOR Z1, X1, X2, X3 *****
940 REM
950 X1=1!
960 Z1=1
970 X2=0
980 X3=0
990 ETA(0)=0
1000 PRINT
1010 FOR I=0 TO NCALC
1020 K2=B1*EXP(-B2*(1/T1(I)-1/T0)*1000/R)
1030 K1=K1O*EXP(-E1*(1/T1(I)-1/304)*1000/R)
1040 AE=AO+A1*T(I)+A2*T(I)^2+A3*T(I)^3
1050 F=CO+C1*(1-Z1)+C2*(1-Z1)^2+C3*(1-Z1)^3
```

```
1060 DF=C1+2*C2*(1-Z1)+3*C3*(1-Z1)^2
1070 F11=-K1*AE*Z1
1080 F12=-K1*AE*(Z1+.5*DT*F11)
1090 F13=-K1*AE*(Z1+.5*DT*F12)
1100 F14=-K1*AE*(Z1+DT*F13)
1110 F21=K1*AE*Z1*DF-K2*AE*X2
1120 F22=K1*AE*Z1*DF-K2*AE*(X2+.5*DT*F21)
1130 F23=K1*AE*Z1*DF-K2*AE*(X2+.5*DT*F22)
1140 F24=K1*AE*Z1*DF-K2*AE*(X2+DT*F23)
1150 F31=K2*AE*X2
1160 IF I*DT>TI1(K)+.1*DT THEN ETAI(K)=ETA(I-1)
1170 IF I*DT>TI1(K)+.1*DT THEN SCI2(K)=SC2(I-1)
1180 IF I*DT>TI1(K)+.1*DT THEN GOTO 1200
1190 IF (I+1)*DT>TI1(K)+.1*DT THEN PRINT USING"###.#  ##.#  #.#####   #.#####
#.#####   #.#####   #.#####";I*DT,T(I),Z1,X1,X2,X3,X1+X2+X3
1200 IF I*DT>TI1(K)+.1*DT THEN K=K+1
1210 SC2(I+1)=SC2(I)+DT*(-K2*1000/R*(1/T1(I)-1/T0)*AE*X2)
1220 X1=1-F
1230 Z1=Z1+DT*(F11+2*F12+2*F13+F14)/6
1240 X2=X2+DT*(F21+2*F22+2*F23+F24)/6
1250 X3=X3+DT*F31
1260 ETA(I+1)=X3
1270 NEXT I
1280 REM
1290 REM ***** NONLINEAR OLS-GAUSS ESTIMATION OF B2 GIVEN B1 (E2 given k20) **
1300 REM
1310 C2SUM=0
1320 H2SUM=0
1330 SUMSQ=0
1340 PRINT
1350 FOR I=1 TO NDATA
1360 E(I)=Y(I)-ETAI(I)
1370 PRINT USING"###.#   #.####  #.####  #.####";TI1(I),Y(I),ETAI(I),E(I)
1380 C2SUM=C2SUM+SCI2(I)*SCI2(I)
1390 H2SUM=H2SUM+SCI2(I)*E(I)
1400 SUMSQ=SUMSQ+E(I)^2
```

```
1410 NEXT I
1420 C2=C2SUM
1430 H2=H2SUM
1440 B2S=B2+H2/C2
1450 REM
1460 REM ***** CONVERGENCE CHECK FOR LEAST-SQUARES ESTIMATE OF E2 GIVEN K2O ***
1470 REM
1480 TESTB2=(B2S-B2)/B2
1490 PRINT
1500 PRINT B2S,B2,TESTB2,SUMSQ
1510 PRINT
1520 IF ABS(TESTB2)>TOL THEN GOTO 860
1530 REM
1540 REM ***** PRINT OUT LEAST-SQUARES ESTIMATE OF E2 GIVEN K2O *****
1550 REM
1560 K2O=B1S
1570 E2=B2S
1580 PRINT"FOR k2O = ";K2O; "g/g-sec"
1590 PRINT"E2 = ";E2; " kcal/mol"
1600 PRINT"SUM OF SQUARED RESIDUALS (s^2) = ";SUMSQ
1610 PRINT"n = ";NDATA
1620 PRINT
1630 REM
1640 REM ***** INCREMENT K2O AND CALCULATE A NEW LEAST-SQUARES      *****
1650 REM ***** ESTIMATE FOR E2 UNTIL THE GLOBAL MINIMUM SUM OF      *****
1660 REM ***** SQUARES IS ACHIEVED                                  *****
1670 REM
1680 B1S=K2O+.001
1690 IF B1S>.05 THEN END
1700 B2S=E2
1710 GOTO 860
1720 END
```

```
10 REM ************************************************************************
20 REM **                                                                    **
30 REM **                        PROGRAM TDIST1.BAS                          **
40 REM **                  CREATED 12/9/87 BY GREGORY L. RORRER              **
50 REM **                                                                    **
60 REM **  This program solves the differential energy balance and heat      **
70 REM **  transport model developed in chapter 9.  The particle temperature **
80 REM **  distribution T(x,t) in a single HF-reacting lignocellulose chip   **
90 REM **  is calculated by the Crank-Nicolson finite difference scheme for  **
100 REM *  parabolic partial differential equations.                         **
110 REM *                                                                    **
120 REM ************************************************************************
130 REM
140 CLS
150 REM ***** DECLARE ARRAY VARIABLES *****
160 REM
170 DIM K1(20),HA(20),KS(20),KE(20),AE(20),AD(20),WHF(20),RA(20),Z1(20)
180 DIM ALPHA (20), BETA(20)
190 DIM A(20),B(20),C(20),D(20),Q(20),P(20)
200 DIM T(20),TEMP(20,400),TIP(400)
210 REM
220 REM ***** NUMERICAL INTEGRATION CONTROL PARAMETERS *****
230 REM
240 DT=.1' sec, time integration step size
250 L=.04'cm
260 N=10'number of nodes in x direction
270 DX=L/N 'distance between nodes
280 LAM=DT/DX^2
290 TIF=360 'sec, final integration time
300 IP=1! 'sec, time interval for saving T(x,t)
310 NP=(TIF/IP)
320 FOR K=1 TO NP
330 TIP(K)=K*IP ', IP=1, save T(x,t) every 1.0 sec
340 NEXT K
350 K=1
```

```
360 REM
370 REM ***** KINETIC AND HF ADSORPTION PARAMETERS *****
380 REM
390 K1O=8.999999E-03'g/g-sec at 31  C
400 E1=10.2'kcal/mol
410 R=1.987 'cal/mol
420 AO=5.440502  'AO...A3 empirical constants for calculating
430 A1=-.2024107 'AE (g HF/g prehydrolyzed wood) as a function of T (in  C)
440 A2=2.748926E-03
450 A3=-1.300829E-05
460 REM
470 REM ***** LIGNOCELLULOSE PHYSICAL PROPERTIES *****
480 REM
490 PLC=.3 'g/cm^3
500 CPLC=.3 'cal/g C
510 KLC=.0002'cal/cm sec C
520 EPSILON=1-PLC/1.5 ' density of lignocellulose (no void) = 1.5 g/cm^3
530 REM
540 REM ***** ADSORBED HF PHYSICAL PROPERTIES *****
550 REM
560 PHF=.9 'g/cm^3 at 60 C
570 CPHF=.67 'cal/g C at 60 C
580 KHF=.0016 'cal/cm sec C (for water at 60 C)
590 REM
600 REM ***** BULK HF VAPOR STREAM PHYSICAL PROPERTIES *****
610 REM
620 H=.0021'cal/cm^2 sec C for 100% HF vapor at 1.0 atm, 60 C, 0.42 g/cm^2-min
630 KHFG=.0004 'cal/cm sec C  for 100% HF vapor at 1.0 atm, 60 C
640 REM
650 REM ***** INITIALIZE TEMPERATURE DISTRIBUTION *****
660 REM
670 TG=60 'C
680 YO=1 'no stoichiometric limit on cellulose conversion by adsorbed HF
690 FOR I=0 TO N
700 T(I)=TG
```

```
710 Z1(I)=1!
720 NEXT I
730 J=0
740 REM
750 REM ***** BEGIN CRANK-NICOLSON FINITE DIFFERENCE SCHEME *****
760 REM
770 TI=J*DT
780 PRINT USING "###.#      ###.###  ###.###  ###.###  ###.###  ###.### ###.###"
;TI,T(O),T(2),T(4),T(6),T(8),T(10)
790 REM
800 REM ***** STEP 1.  CALCULATE ALPHA(I) AND BETA(I) *****
810 REM
820 AEG=AO+A1*TG+A2*TG^2+A3*TG^3
830 FOR I=0 TO N
840 AD(I)=AEG*(1-Z1(I))
850 AE(I)=AO+A1*T(I)+A2*T(I)^2+A3*T(I)^3
860 K1(I)=K1O*EXP(-E1*(1/(T(I)+273)-1/304)*1000/R)
870 RA(I)=AEG*AE(I)*K1(I)*Z1(I)
880 HA(I)=205*AE(I)^(-.457)
890 WHF(I)=AD(I)/(1+AD(I))
900 KS(I)=(1-WHF(I))*KLC+WHF(I)*KHF
910 KE(I)=KS(I)*(KHFG/KS(I))^(1-EPSILON)
920 ALPHA(I)=KE(I)/(PLC*CPLC+AD(I)*PLC*CPHF)
930 BETA(I)=PLC*HA(I)*RA(I)/(PLC*CPLC+AD(I)*PLC*CPHF)
940 REM
950 REM ***** STEP 2.  4th ORDER RUNGE-KUTTA INTEGRATION OF Z1(I) *****
960 REM *****          OVER J (i.e, Z1(x,t) over reaction time t) *****
970 REM
980 F11=-K1(I)*AE(I)*Z1(I)
990 F12=-K1(I)*AE(I)*(Z1(I)+.5*DT*F11)
1000 F13=-K1(I)*AE(I)*(Z1(I)+.5*DT*F12)
1010 F14=-K1(I)*AE(I)*(Z1(I)+DT*F13)
1020 Z1(I)=Z1(I)+DT*(F11+2*F12+2*F13+F14)/6
1030 REM
1040 REM ***** STEP 3.  CALCULATE TEMPERATURE DISTRIBUTION T(x,t) AT FIXED t ***
1050 REM *****          (i.e., T(I,J) at fixed J)                              ***
```

```
1060 REM
1070 REM ***** FINITE DIFFERENCE EQUATIONS:  x=0, I=0 (particle surface) *****
1080 REM
1090 IF I>0 THEN GOTO 1210
1100 G=H/KE(0)
1110 A(0)=0
1120 B(0)=1+LAM*ALPHA(0)*(1+DX*G)
1130 C(0)=-LAM*ALPHA(0)
1140 D(0)=BETA(0)*DT+LAM*ALPHA(0)*T(1)+(1-LAM*ALPHA(0)*(1+DX*G))*T(0)+2*LAM*ALPH
A(0)*DX*G*TG
1150 Q(0)=B(0)
1160 P(0)=D(0)/Q(0)
1170 REM
1180 REM ***** FINITE DIFFERENCE EQUATIONS:  0<x<L, 0<I<N (interior nodes) *****
1190 REM
1200 IF I=0 THEN GOTO 1380
1210 IF I=N THEN GOTO 1320
1220 A(I)=-LAM*ALPHA(I)
1230 B(I)=2*(1+LAM*ALPHA(I))
1240 C(I)=-LAM*ALPHA(I)
1250 D(I)=2*BETA(I)*DT+LAM*ALPHA(I)*T(I-1)+2*(1-LAM*ALPHA(I))*T(I)+LAM*ALPHA(I)*
T(I+1)
1260 Q(I)=B(I)-A(I)*C(I-1)/Q(I-1)
1270 P(I)=(D(I)-A(I)*P(I-1))/Q(I)
1280 REM
1290 REM ***** FINITE DIFFERENCE EQUATIONS:  x=L, I=N (particle center) *****
1300 REM
1310 IF I<N THEN GOTO 1380
1320 A(N)=-LAM*ALPHA(N)
1330 B(N)=1+LAM*ALPHA(N)
1340 C(N)=0
1350 D(N)=BETA(N)*DT+LAM*ALPHA(I)*T(N-1)+(1-LAM*ALPHA(N))*T(N)
1360 Q(N)=B(N)-A(N)*C(N-1)/Q(N-1)
1370 P(N)=(D(N)-A(N)*P(N-1))/Q(N)
1380 NEXT I
1390 REM
1400 REM ***** GAUSSIAN ELIMINATION TO SOLVE TRIDIAGONAL MATRIX *****
```

```
1410 REM
1420 T(N)=P(N)
1430 IF (J+1)*DT=TIP(K) THEN TEMP(N,K)=T(N)
1440 FOR I=N-1 TO 0 STEP -1
1450 T(I)=P(I)-C(I)*T(I+1)/Q(I)
1460 IF I=0 THEN T(0)=(D(0)-C(0)*T(1))/B(0)
1470 IF (J+1)*DT=TIP(K) THEN TEMP(I,K)=T(I)
1480 NEXT I
1490 IF (J+1)*DT=TIP(K) THEN K=K+1
1500 J=J+1
1510 IF TI<TIF THEN GOTO 770
1520 REM
1530 REM ***** END CRANK-NICOLSON FINITE DIFFERENCE SCHEME *****
1540 REM
1550 REM
1560 REM ***** STORE T(x,t) OUTPUT IN PERMANENT FILE *****
1570 REM
1580 PRINT:INPUT"ENTER FILENAME FOR T(x,t) OUTPUT:  ",TEMPFILE$
1590 OPEN "O",1,TEMPFILE$
1600 FOR K=1 TO NP
1610 FOR I=0 TO N
1620 PRINT #1,TEMP(I,K)
1630 NEXT I
1640 NEXT K
1650 CLOSE
1660 END
```

```
10 REM ************************************************************************
20 REM **                                                                    **
30 REM **                        PROGRAM TDIST2.BAS                          **
40 REM **                CREATED 12/9/87 BY GREGORY L. RORRER                **
50 REM **                                                                    **
60 REM **  This program solves the differential material balance and kinetic **
70 REM **  model developed in chapter 8.  Specifically, the conversion and   **
80 REM **  and yield profiles  Z1(x,t), X1(x,t), X2(x,t), and X3(x,t) are    **
90 REM **  calculated by 4th-order Runge-Kutta numerial integration given    **
100 REM *  a T(x,t) input  file to drive the reaction kinetics.  The T(x,t)   **
110 REM *  input file is the numerial solution of the differential energy    **
120 REM *  energy balance and heat transport model.  T(x,t) is calculated by **
130 REM *  program TDIST1.BAS via the Crank-Nicolson Method.                 **
140 REM *  This program also calculates the global X3(t) vs. t profile by    **
150 REM *  trapezoid rule integration of X3(x,t) over x at fixed t.          **
160 REM *                                                                    **
170 REM ************************************************************************
180 REM
190 CLS
200 REM ***** DECLARE ARRAY VARIABLES *****
210 REM
220 DIM T(20,400),Z1(20),X1(20),X2(20),X3(20),XM3(400)
230 REM
240 REM ***** INTEGRATION CONTROL PARAMETERS *****
250 REM
260 N=10 'number of nodes in x direction
270 M=360 ' number of time steps stored in T(x,t) input file
280 L=.02 'cm, slab thickness
290 DT=1! 'sec, time integration step size
300 DX=L/N
310 TIF=360 'sec, final integration time
320 REM
330 REM ***** LOAD T(x,t) FROM COMPLIMENTARY TDIST1.BAS OUTPUT *****
340 REM
350 INPUT"ENTER T(x,t) FILENAME:  ",TEMPFILE$
```

```
360 INPUT"ENTER Tg (in 'C):  ",TG
370 OPEN "I",1,TEMPFILE$
380 FOR J=1 TO M
390 FOR I=0 TO N
400 INPUT #1,T(I,J)
410 NEXT I
420 NEXT J
430 CLOSE
440 REM
450 REM ***** KINETIC AND HF ADSORPTION PARAMETERS *****
460 REM
470 YO=1! 'no stoichiometric limit on cellulose conversion by adsorbed HF
480 K1O=8.999999E-03'g/g-sec at 31 C
490 K2O=.039 'g/g-sec at 52 C
500 E1=10.2'kcal/mol
510 E2=15.1 'kcal/mol
520 R=1.987 ' cal/mol
530 AO=5.44052  'AO...A3 empirical constants for calculating
540 A1=-.202417 'AE (g HF/g prehydrolyzed wood) as a function of T (in  C)
550 A2=2.748926E-03
560 A3=-1.300829E-05
570 BO=-.0009764 'BO...B3  empirical constants for calculating
580 B1=.007522   'f(1-Z1)=1-X1 as a function of Z1
590 B2=-.02129
600 B3=1.0129
610 REM
620 REM  ***** INITIALIZE TEMPERATURE AND CONVERSION PROFILES *****
630 REM
640 FOR I=0 TO N
650 T(I,0)=TG
660 Z1(I)=1!
670 X1(I)=1!
680 X2(I)=0
690 X3(I)=0
700 NEXT I
```

```
710 REM
720 REM ***** 4th ORDER RUNGE-KUTTA INTEGRATION OF Z1(I),X2(I),AND X3(I) *****
730 REM ***** IN EACH NODE I OF T(I,J)                                    *****
740 REM ***** TRAPEZOID-RULE NUMERICAL INTEGRATION OF X3(I) OVER I       *****
750 REM
760 J=0
770 XM3SUM=0
780 T1=J*DT
790 PRINT:PRINT"time = ";T1;" sec":PRINT
800 FOR I=0 TO N-1
810 XM3SUM=XM3SUM+(X3(I+1)+X3(I))/2
820 NEXT I
830 FOR I=0 TO N
840 K1=K1O*EXP(-E1*(1/(T(I,J)+273)-1/304)*1000/R)
850 K2=K2O*EXP(-E2*(1/(T(I,J)+273)-1/325)*1000/R)
860 AE=AO+A1*T(I,J)+A2*T(I,J)^2+A3*T(I,J)^3
870 F=BO+B1*(1-Z1(I))+B2*(1-Z1(I))^2+B3*(1-Z1(I))^3
880 DF=B1+2*B2*(1-Z1(I))+3*B3*(1-Z1(I))^2
890 F11=-K1*AE*Z1(I)
900 F12=-K1*AE*(Z1(I)+.5*DT*F11)
910 F13=-K1*AE*(Z1(I)+.5*DT*F12)
920 F14=-K1*AE*(Z1(I)+DT*F13)
930 F21=K1*AE*Z1(I)*DF-K2*AE*X2(I)
940 F22=K1*AE*Z1(I)*DF-K2*AE*(X2(I)+.5*DT*F21)
950 F23=K1*AE*Z1(I)*DF-K2*AE*(X2(I)+.5*DT*F22)
960 F24=K1*AE*Z1(I)*DF-K2*AE*(X2(I)+DT*F23)
970 F31=K2*AE*X2(I)
980 PRINT USING "###.##   #.#####   #.#####   #.#####   #.#####";T(I,J),Z1(I),X1
(I),X2(I),X3(I)
990 Z1(I)=Z1(I)+DT*(F11+2*F12+2*F13+F14)/6
1000 X1(I)=1-F
1010 X2(I)=X2(I)+DT*(F21+2*F22+2*F23+F24)/6
1020 X3(I)=X3(I)+DT*F31
1030 NEXT I
1040 XM3(J)=XM3SUM/N
1050 PRINT:PRINT"global glucose yield = ";XM3(J)
```

```
1060 J=J+1
1070 IF J*DT<TIF THEN GOTO 770
1080 REM
1090 REM ***** STORE GLOBAL X3 vs t OUTPUT, AND T(L,t), T(0,t) OUTPUTS *****
1100 REM
1110 PRINT
1120 PRINT:INPUT"ENTER GLOBAL GLUCOSE YIELD VS TIME OUTPUT FILENAME:  ",FILE1$
1130 OPEN "O",1,FILE1$
1140 FOR J=0 TO TIF
1150 PRINT #1,J*DT/60, XM3(J)*.83*YO 'convert normalized glucose yield to
1160 REM                                  g glucose/g prehydrolyzed wood
1170 NEXT J
1180 CLOSE
1190 INPUT"ENTER T(L,t) OUTPUT FILENAME:  ",FILE2$
1200 OPEN "O",1,FILE2$
1210 FOR J=0 TO TIF
1220 PRINT #1,J*DT/60, T(N,J)
1230 NEXT J
1240 CLOSE
1250 INPUT"ENTER T(0,t) OUTPUT FILENAME:  ",FILE3$
1260 OPEN "O",1,FILE3$
1270 FOR J=0 TO TIF
1280 PRINT #1,J*DT/60,T(0,J)
1290 NEXT J
1300 CLOSE
1310 END
```

```
10 REM ************************************************************************
20 REM **                                                                    **
30 REM **                        PROGRAM TDIST3.BAS                          **
40 REM **                  CREATED 5/31/88 BY GREGORY L. RORRER              **
50 REM **                                                                    **
60 REM **  This program calculates the cumulative energy release Q1(t) from  **
70 REM **  a single HF-reacting lignocellulose chip by integrating the       **
80 REM **  energy flux from the particle surface to the surrounding HF       **
90 REM **  HF vapor stream via Newton's Law of Cooling, given T(0,t) and     **
100 REM *  heat transfer coefficient "h" as input.  This program then        **
110 REM *  compares Q1(t) to Q2(t), the cumulative energy generated within   **
120 REM *  the HF-reacting lignocellulose chip.                              **
130 REM *                                                                   **
140 REM ************************************************************************
150 CLS
160 REM
170 REM ***** DECLARE ARRAY VARIABLES *****
180 REM
190 DIM T(400),TR(400),Z1(400),AD(400),DQ1(400),DQ2(400),Q1(400),Q2(400)
200 REM
210 REM ***** LOAD T(0,t) INPUT FILE *****
220 REM
230 N=360
240 DT=1! 'sec
250 INPUT"ENTER PARTICLE TEMPERATURE VS. TIME DATA FILE: ",TEMPFILE1$
260 OPEN "I",1,TEMPFILE1$
270 FOR I=0 TO N
280 INPUT #1,T(I),TR(I)
290 T(I)=T(I)*60
300 NEXT I
310 CLOSE
320 REM
330 REM ***** HF VAPOR STREAM PROPERTIES *****
340 REM
350 INPUT"ENTER HF VAPOR STREAM TEMPERATURE (in C): ",TG
```

```
360 H=.0021 'cal/cm^2 sec C   100% HF vapor at 1.0 atm and Tg = 60 C
370 REM
380 REM ***** LIGNOCELLULOSE VOLUMETRIC PROPERTIES *****
390 REM
400 Z=1! ' cm
410 L=.04 'cm
420 PLC=.3 'g/cm^3
430 SLC=Z^2
440 VLC=SLC*L
450 MLC=VLC*PLC
460 REM
470 REM ***** KINETIC AND HF ADSORPTION PARAMETERS *****
480 REM
490 R=1.987 ' cal/mol
500 K1O=8.999999E-03' g/g-sec at 31 C
510 E1=10.2'kcal/mol
520 AO=5.440502
530 A1=-.2024107
540 A2=2.748926E-03
550 A3=-1.300829E-05
560 AEG=AO+A1*TG+A2*TG^2+A3*TG^3
570 PRINT:PRINT:PRINT
580 Z1(0)=1
590 DQ1(0)=0
600 DQ2(0)=0
610 Q1(0)=0
620 Q2(0)=0
630 FOR I=0 TO N
640 REM
650 REM ***** CALCULATE dQ1(t)/dt and dQ2(t)/dt *****
660 REM
670 K1=K1O*EXP(-E1*(1/(TR(I)+273)-1/304)*1000/R)
680 AE=AO+A1*TR(I)+A2*TR(I)^2+A3*TR(I)^3
690 HA=205*(AE^-.457) 'cal/g HF ads
700 C11=-K1*AE*Z1(I)
```

```
710 C12=-K1*AE*(Z1(I)+.5*DT*C11)
720 C13=-K1*AE*(Z1(I)+.5*DT*C12)
730 C14=-K1*AE*(Z1(I)+DT*C13)
740 C21=MLC*HA*K1*AEG*AE*Z1(I)
750 C22=MLC*HA*K1*AEG*AE*(Z1(I)+.5*DT*C21)
760 C23=MLC*HA*K1*AEG*AE*(Z1(I)+.5*DT*C22)
770 C24=MLC*HA*K1*AEG*AE*(Z1(I)+DT*C23)
780 DQ1(I)=H*(TR(I)-TG)*SLC/(VLC*PLC)
790 DQ2(I)=(C21+2*C22+2*C23+C24)/(6*MLC)
800 Z1(I+1)=Z1(I)+DT*(C11+2*C12+2*C13+C14)/6
810 AD(I)=AEG*(1-Z1(I))
820 REM
830 REM ***** INTEGRATE dQ1(t)/dt AND dQ2(t)/dt OVER t *****
840 REM
850 IF I>0 THEN Q1(I)=Q1(I-1)+DT/2*(DQ1(I-1)+DQ1(I))
860 Q2(I+1)=Q2(I)+DT*DQ2(I)
870 PRINT USING"###   ###.###   #.#####   #.#####   ###.#####   ###.#####";I*DT,
 TR(I),Z1(I),AD(I),Q1(I),Q2(I)
880 NEXT I
890 PRINT:PRINT
900 REM
910 REM ***** STORE HEAT RELEASE OUTPUTS IN PERMANENT FILE *****
920 REM
930 INPUT"DO YOU WANT TO STORE THE OUTPUT (1=YES,2=NO):   ",OPT1
940 IF OPT1=2 THEN END
950 PRINT
960 INPUT"ENTER Q1(t) vs. t DATA FILE NAME:  ",FILE1$
970 OPEN "O",1,FILE1$
980 FOR I=0 TO N
990 PRINT #1, T(I)/60,Q1(I)
1000 NEXT I
1010 CLOSE
1020 INPUT"ENTER Q2(t) vs. t DATA FILE NAME:  ",FILE2$
1030 OPEN "O",1,FILE2$
1040 FOR I=0 TO N
1050 PRINT #1, T(I)/60,Q2(I)
```

```
1060 NEXT I
1070 CLOSE
1080 INPUT"ENTER dQ1(t)/dt vs. t DATA FILE NAME:  ",FILE3$
1090 OPEN "O",1,FILE3$
1100 FOR I=0 TO N
1110 PRINT #1, T(I)/60,DQ1(I)
1120 NEXT I
1130 CLOSE
1140 INPUT"ENTER dQ2(t)/dt vs. t DATA FILE NAME:  ",FILE4$
1150 OPEN "O",1,FILE4$
1160 FOR I=0 TO N
1170 PRINT #1, T(I)/60,DQ2(I)
1180 NEXT I
1190 CLOSE
1200 END
```

MICHIGAN STATE UNIV. LIBRARIES
31293007868213